Hybrid discontinuous Galerkin methods coupled with hybrid explicit/implicit schemes for the unsteady Maxwell's equations

Georges Nehmetallah

UNIVERSITÉ CÔTE D'AZUR

ÉCOLE DOCTORALE
SCIENCES FONDAMENTALES ET APPLIQUÉES

THÈSE DE DOCTORAT

Méthodes Galerkin discontinues hybrides couplées à des schémas de type explicite/implicite pour les équations de Maxwell instationnaires

Hybrid discontinuous Galerkin methods coupled with hybrid explicit/implicit schemes for the unsteady Maxwell's equations

Georges Nehmetallah

Inria Sophia Antipolis

Présentée en vue de l'obtention du grade de docteur en mathématiques appliquées	**Devant le jury, composé de :**
d'Université Côte d'Azur	Xavier Antoine, Rapporteur, Professeur, Université de Lorraine
Dirigée par : Stéphane Descombes	Julien Diaz, Rapporteur, Directeur de recherche, Centre INRIA Bordeaux-Sud-Ouest
Co-encadrée par : Stéphane Lanteri	Mihai Bostan, Examinateur, Professeur, Aix-Marseille Université
Soutenue le : 14/12/2020	Stella Krell, Examinateur, Maître de conférence, Université Côte d'Azur
	Stéphane Descombes, Directeur de thèse, Professeur, Université Côte d'Azur
	Stéphane Lanteri, Co-directeur de thèse, Directeur de recherche, INRIA Sophia Antipolis

Méthodes Galerkin discontinues hybrides couplées à des schémas de type explicite/implicite pour les équations de Maxwell instationnaires

---

Résumé

Dans cette thèse, nous étudions et développons différentes familles de schémas d'intégration en temps combinés avec une méthode Galerkin disontinue hybride (GDH) en espace pour les équations de Maxwell. Après avoir passé en revue les méthodes GDH pour l'équation de Poisson, les équations de Maxwell en domaine fréquentiel et les équations de Maxwell en domaine temporel avec une discrétisation temporelle totalement implicite dans la première partie, nous construisons une méthode GDH totalement explicite en temps pour les équations de Maxwell en 3D en domaine temporel dans la deuxième partie. Cette méthode est précise avec un ordre élevé en espace et en temps et peut être vue comme une généralisation d'un schéma GD classique basé sur des flux décentrés. En particulier, elle coïncide avec ce schéma pour un choix particulier du paramètre de stabilisation introduit dans la définition des traces numériques dans le cadre GDH. Nous présentons des résultats numériques visant à évaluer ses propriétés de convergence. Nous proposons ensuite une nouvelle technique de post-traitement pour cette dernière méthode que nous couplons avec un schéma de Runge-Kutta explicite. Le champ électromagnétique post-traité converge plus vite d'un ordre que la solution non post-traitée en norme $H(curl)$. L'approche proposée est locale, c'esr-à-dire que la solution améliorée est calculée indépendamment dans chaque cellule du maillage, et à chaque pas de temps nécessaire. En conséquence, son calcul n'est pas coûteux, surtout si la région d'intérêt est localisée, soit dans le temps, soit dans l'espace. Nous présentons plusieurs expériences numériques mettant en évidence les propriétés de superconvergence du champs électromagnétique post-traité. Dans la dernière partie, nous proposons une méthodologie pour construire des méthodes hybrides explicites/implicites (IMEX) pour les équations de Maxwell. Nous présentons ces méthodes IMEX obtenues en séparant la formulation semi-discrète en parties grossières et fines, puis en appliquant trois schémas en temps différents, d'ordre allant de 1 à 3. Nous présentons des résultats numériques montrant que nos méthodes sont efficaces en terme de précision et en terme de temps de calcul. Nous choisissons des cas où les maillages localement raffinés sont indispensables pour la précision de la solution approchée : un domaine en forme de L où la solution présente une singularité, un domaine hétérogène avec un variation importante de la vitesse de l'onde et un dispositif de cristaux photoniques où les sphères en silicium sont très proches les unes des autres.

Mots clés: Maxwell, HDG, IMEX, post traitement

Hybrid discontinuous Galerkin methods coupled with hybrid explicit/implicit schemes for the unsteady Maxwell's equations

Abstract

In this thesis, we study and develop different families of time integration schemes combined with a hybrid discontinuous Galerkin (HDG) discretization in space for Maxwell's equations. After presenting a review of HDG methods for Poisson equation, time-harmonic Maxwell's equations and for the time-domain Maxwell's equations with a fully implicit time discretization in the first part, we construct a fully explicit HDGTD method for the 3D time-domain Maxwell's equations in the second part. This HDGTD method is high order accurate in both space and time and can be seen as a generalization of the classical DGTD scheme based on upwind fluxes. In particular, it coincides with the latter scheme for a particular choice of the stabilization parameter introduced in the definition of numerical traces in the HDG framework. We provide numerical results aiming at assessing its numerical convergence properties. Then we propose a novel postprocessing technique for the latter method that we couple with an explicit Runge-Kutta time-marching scheme. The postprocessed electromagnetic field converges one order faster than the unpostprocessed solution in the $H(curl)$-norm. The proposed approach is local, in the sense that the enhanced solution is computed independently in each cell of the computational mesh, and at each time step of interest. As a result, it is inexpensive to compute, especially if the region of interest is localized, either in time or space. We present several numerical experiments that highlight the superconvergence properties of the postprocessed electromagnetic fields. Pursuing our aim, we propose a methodology to construct hybrid explicit/implicit (IMEX) HDGTD methods for Maxwell's equations in the last part. We present the IMEX HDGTD methods obtained from dividing the semi-discrete formulation into coarse and fine parts and then applying three different IMEX time-marching of three different orders (less or equal to 3). We present numerical results for various test cases. An L shape domain where we have a singularity in the solution, a heterogeneous domain where we have an important variation of the wave speed, and a crystal photonic device where the spheres made of silicium are too close to each other. In these cases, the locally refined meshes are a must for the accuracy of the approximated solution and the obtained numerical results demonstrate that our methods are efficient in terms of accuracy and CPU time metrics.

Key words: Maxwell, HDG, IMEX, postprocessing

Contents

List of Figures

List of Tables

1

Introduction

1.1 Physical context

A system of mathematical models can describe a wide variety of phenomena, which can be physical, biological, economic, demographic, geological for example. There is a considerable number of models, from different families, sometimes established well before the birth of the first computers. Some are stochastic, *e.g.* with consideration of randomness, while others are deterministic, *e.g.* in the form of ordinary differential equations (ODE) or a system of partial differential equations (PDE). Those models can be used to simulate realistic phenomena, which can thus play a predictive or explicative role. The study and exploitation of these models have always been essential for engineers. The importance of numerical modeling has become a more significant challenge with the increase in computer system capabilities, and in particular, with the advent of parallel computers. This was particularly the case for electromagnetism.

The physicist James Clerk Maxwell (Fig. 1.1) laid the foundations of modern electromagnetism in 1865 in [1]. For the first time, he formulated the classical theory of electromagnetism by bringing together electricity, magnetism, and light as various manifestations of the same phenomenon. Maxwell's equations have been studied for many decades, for different purposes. As for most of the computational models, computational electromagnetism can be used for validation and prototyping in a goal-oriented engineering setup. We can find electromagnetism applications everywhere. Many of those are part of our daily life, such as wireless communications, electromagnetic braking, optical fibers, medical imaging, magnetic lift train, induction charging of batteries, or even in our computer's hard drives. The full wave Maxwell's equations can be formulated in two settings: the time-domain (TD) and the frequency-domain (FD) formulations. Several numerical methods have been devised to solve both formulations. As often in numerical modeling, the choice of a method is driven by the application. In the context of this thesis we are mainly concerned with the time-domain formulation.

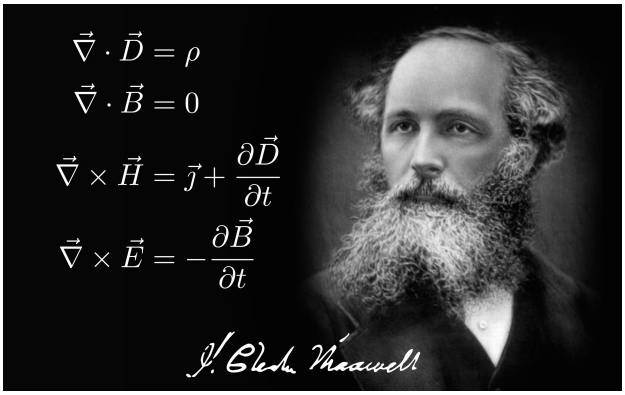

Figure 1.1 | James Clerk Maxwell's equations.

1.2 Numerical context

The Finite Difference Time-Domain (FDTD) method introduced by K.S. Yee in 1966 [2] is a widely used approach for solving the system of time-domain Maxwell equations. The main reasons for the popularity of this method are its ease of implementation and its computational efficiency. However, to achieve the latter properties, the FDTD relies on a cartesian structured discretization of the computational domain [3]. When the underlying physics involves complex geometrical features and curvilinear interfaces and boundaries, the structured grid becomes a significant limitation, which is manageable but makes the method more complex. Being naturally constructed for unstructured grids, the Finite Element Method (FEM) is well suited for the numerical solution of PDEs in complex geometries [4]. Although initially developed for elliptic equations, FEM have been further extended to hyperbolic equations. In the time-domain and for the classic FEM, one generally needs to solve the sparse linear system associated to the mass matrix at each time-step, which makes the method very expensive and rarely used in practice. The Finite Volume method (FVM) relies on the evaluation of integrals over volume elements and facets of the mesh. This allows great geometrical flexibility, which is required for most electromagnetic problems [5]. However, this method lends itself to a piecewise constant approximation of the field and is thus facing accuracy issues. During the last twenty years, numerical methods formulated on unstructured meshes have drawn a lot of attention in computational electromagnetics with the aim of dealing with irregularly shaped structures and heterogeneous media. In particular, the discontinuous Galerkin time-domain (DGTD) method has progressively emerged as a viable alternative to the methods mentioned so far since it integrates advantages of both the finite volume time domain (FVTD) method and the finite element time domain (FETD) method. Like FVTD, the numerical flux is used to exchange information between neighboring elements, thus all operations of DGTD are local and easily parallelizable. Similar to FETD, DGTD employs unstructured mesh and is capable of high order accuracy if the high order hierarchical basis function is adopted. Such a DGTD method has been recently designed at Inria in the Nachos project-team for the simulation of nanoscale light/matter interaction problems. In this doctoral thesis project, we propose to study an alternative method, which is high order accurate in space and time and well suited to the use of locally refined unstructured grids. In particular, we aim at devising a method that allows to reduce the number of globally coupled degrees of freedom in this context, when using a fully implicit time integration scheme, and when combined with a hybrid implicit/explicit time

scheme it deals efficiently with the drastic restriction of the time step in this context, when using a fully explicit time integration scheme. For that purpose, we will consider a particular form of the DG method that has been recently introduced for the numerical treatment of model time-domain electromagnetics problems. This particular DG formulation is referred to as the Hybridized Discontinuous Galerkin (HDG) method.

1.3 Generalities about the DGTD method

During the last ten years, the DGTD method has progressively emerged as a viable alternative to well established FDTD (Finite Difference Time-Domain) [6] and FETD (Finite Element Time-Domain) [7] methods for the numerical simulation of electromagnetic wave propagation problems in the time-domain.

The DGTD method can be considered as a finite element method where the continuity constraint at an element interface is released. While it keeps almost all the advantages of the finite element method (large spectrum of applications, complex geometries, etc.), the DGTD method has other nice properties which explain the renewed interest it gains in various domains in scientific computing:

- It is naturally adapted to a high order approximation of the unknown field. Moreover, one may increase the degree of the approximation in the whole mesh as easily as for spectral methods but, with a DGTD method, this can also be done locally *i.e.* at the mesh cell level. In most cases, the approximation relies on a polynomial interpolation method but the method also offers the flexibility of applying local approximation strategies that best fit to the intrinsic features of the modeled physical phenomena.
- When the discretization in space is coupled to an explicit time integration method, the DG method leads to a block diagonal mass matrix independently of the form of the local approximation (e.g the type of polynomial interpolation). This is a striking difference with classical, continuous FETD formulations. Moreover, the mass matrix is diagonal if an orthogonal basis is chosen.
- It easily handles complex meshes. The grid may be a classical conforming finite element mesh, a non-conforming one or even a hybrid mesh made of various elements (tetrahedra, prisms, hexahedra, etc.). The DGTD method has been proven to work well with highly locally refined meshes. This property makes the DGTD method particularly well suited to the design of a hp-adaptive solution strategy (*i.e.* where the characteristic mesh size h and the interpolation degree p changes locally wherever it is needed).
- It is flexible with regards to the choice of the time stepping scheme. One may combine the discontinuous Galerkin spatial discretization with any global or local explicit time integration scheme, or even implicit, provided the resulting scheme is stable.
- It is naturally adapted to parallel computing. As long as an explicit time integration scheme is used, the DGTD method is easily parallelized. Moreover, the compact nature of method is in favor of high computation to communication ratio especially when the interpolation order is increased.

As in a classical finite element framework, a discontinuous Galerkin formulation relies on a weak form of the continuous problem at hand. However, due to the discontinuity of the global approximation, this variational formulation has to be defined at the element level. Then, a degree of

freedom in the design of a discontinuous Galerkin scheme stems from the approximation of the boundary integral term resulting from the application of an integration by parts to the element-wise variational form. In the spirit of finite volume methods, the approximation of this boundary integral term calls for a numerical flux function which can be based on either a centered scheme or an upwind scheme, or a blend of these two schemes.

Figure 1.2 | Boris Grigoryevich Galerkin.

1.4 DGTD methods for time-domain electromagnetics

In the early 2000's, DGTD methods for time-domain electromagnetics have been studied by a few groups of researchers, most of then from the applied mathematics community. One of the most significant contributions is due to Hesthaven and Warburton [8] in the form of a high order nodal DGTD method formulated on unstructured simplicial meshes. The proposed formulation is based on an upwind numerical flux, nodal basis expansions on a triangle (2D case) and a tetrahedron (3D case) and a Runge-Kutta time stepping scheme. In [9], Kakbian et al. describe a rather similar approach. More precisely, the authors develop a parallel, unstructured, high order DGTD method based on simple monomial polynomials for spatial discretization, an upwind numerical flux and a fourth-order Runge-Kutta scheme for time marching. The method has been implemented with hexahedral and tetrahedral meshes. A high order DGTD method based on a strong stability preserving Runge-Kutta time scheme has been studied by Chen et al. [10]. The authors also present post-processing techniques that can double the convergence order. A locally divergence-free DGTD method is formulated and studied by Cockburn et al. in [11]. In the same period, a high order nodal DGTD method formulated on unstructured simplicial meshes has also been proposed by Fezoui et al. [12]. However, contrary to the DGTD methods discussed in [8] and [9], the method proposed in [12] is non-dissipative thanks to a combination of a centered numerical flux with a second-order leap-frog time stepping scheme. The DGTD method has then been progressively considered and extended to increasingly more complex modeling situations by groups of researchers in the applied electromagnetics and electrical engineering communities for a wide variety of applications related to aeronautics, defense, semiconductor device fabrication, etc. [13]-[14]-[15]-[16]-[17]-[18]-[19] to

cite a few. More recently, the method has also been adopted and further developed by researchers in the nano-optics domain [20]-[21]-[22]-[23]. A full review of the nowadays numerous applications of DGTD methods would certainly require more than a simple paragraph. Also worth to note, the DGTD method has been implement in commercial software such HFSS-TD (the time-domain version of the well-known HFSS software used for antenna design) [24].

1.5 Explicit versus implicit DGTD methods

From the above discussion, it is clear that the DGTD method is nowadays a very popular numerical method in the computational electromagnetics community. The works mentioned so far are mostly concerned with time explicit DGTD methods relying on the use of a single global time step computed so as to insure the stability of the simulation. It is however well known that when combined with an explicit time integration method and in the presence of an unstructured locally refine mesh, a high order DGTD method suffers from a severe time step size restriction. A possible alternative to overcome this limitation is to use smaller time steps, given by a local stability criterion, precisely where the smallest elements are located. The local character of a DG formulation is a very attractive feature for the development of explicit local time stepping schemes. Such techniques have been developed for the second order wave equation discretized in space by a DG method [25]-[26]. In [27], a second order symplectic local time stepping DGTD method is proposed for Maxwell's equations in a non-conducting medium, based on the Störmer-Verlet method. Grote and Mitkova derived local time-stepping methods of arbitrarily high accuracy for Maxwell's equations from the standard leap-frog scheme [28]. In [29], Taube et al. also proposed an arbitrary high order local time-stepping method based on ADER DG approach for Maxwell's equation. An alternative approach that has been considered in [30]-[31] is to use a hybrid explicit-implicit (or locally implicit) time integration strategy. Such a strategy relies on a component splitting deduced from a partitioning of the mesh cells in two sets respectively gathering coarse and fine elements. In these works, a second order explicit leap-frog scheme is combined with a second order implicit Crank-Nicolson scheme in the framework of a non-dissipative (centered flux based) DG discretization in space. At each time step, a large linear system must be solved whose structure is partly diagonal (for those rows of the system associated to the explicit unknowns) and partly sparse (for those rows of the system associated to the implicit unknowns). The computational efficiency of this locally implicit DGTD method depends on the size of the set of fine elements that directly influences the size of the sparse part of the matrix system. Therefore, an approach for reducing the size of the subsystem of globally coupled (i.e. implicit) unknowns is worth considering if one wants to solve very large-scale problems.

A particularly appealing solution in this context is given by the concept of hybridizable discontinuous Galerkin (HDG) method. The HDG method has been first introduced by Cockbrun et al. in [32] for a model elliptic problem and has been subsequently developed for a variety of PDE systems in continuum mechanics [33]. The essential ingredients of a HDG method are:

1. a local Galerkin projection of the underlying system of PDEs at the element level onto spaces of polynomials to parametrize the numerical solution in terms of the numerical trace,

2. a judicious choice of the numerical flux to provide stability and consistency,

3. a global jump condition that enforces the continuity of the numerical flux to arrive at a global weak formulation in terms of the numerical trace.

HDG methods are fully implicit, high order accurate and endowed with several unique features which distinguish them from other DG methods. Most importantly, they reduce the globally coupled unknowns to the approximate trace of the solution on element boundaries, thereby leading to a significant reduction in the number of degrees of freedom. HDG methods for the system of time-harmonic Maxwell equations have been proposed in [34]-[35]-[36].

1.6 Contributions and thesis outline

The remaining of this manuscript is structured as follows:

- Chapter 2 presents the HDG method that has been studied on different equations and published in previous works. The advantages of using HDG methods over those of DG methods for Poisson equations are presented in section 2.3. Section 2.4 first elaborates the formulation and the main principles of the HDG method for 3D time-harmonic Maxwell's equations. Then, to better understand how it works, we are going to present all the details for the implementation of this method. We describe in section 2.5 the formulation of the fully implicit HDG method for 3D time-domain Maxwell's equations, a proof for the semi-discrete stability, the well-posedness of the local solver, the existence and the uniqueness of the solution, a proof for the unconditional stability of the HDGTD method combined with the Crank-Nicholson time integration and finally some numerical results showing that the HDG method outperforms the DG method both in the memory requirement and CPU time metrics.

- In chapter 3 we describe the fully explicit high order accurate HDG method for the 3D time-domain Maxwell's equations. Our work is published in [37].

  - Our starting point for section 3.2 is the same HDGTD global formulation (2.43) mentioned in chapter 2 for the time-domain Maxwell's equations. Since we are applying an explicit time scheme on the mentioned formulation, we will obtain a direct relation between all the variables at the same time step with the help of the conservativity equation. So we are going then to reformulate the numerical fluxes in terms of the variables inside the two neighboring elements (3.2)-(3.3), and inject them in the local problem to obtain a DG method with generalized upwind fluxes. In other words, this method coincides with the classical upwind flux-based DG method for a particular choice of the stabilization parameter τ in the HDG numerical traces.
  - In section 3.3 we present first the formulation obtained in the last section with some bilinears forms, and then we are going to find the electromagnetic energy in terms of these bilinears forms so we can proceed for the stability proofs. Theorem 4 shows that the energy function $\mathcal{E}_h(.)$ decreases in time, so we have a semi-discrete stability for the scheme. Lemma 2 leads us to proposition 1 where we are going to show that under a 4/3 CFL condition, $i.e$ $\Delta t \leq ch^{\frac{4}{3}}$, the explicit HDGTD scheme with a RK2 discretization in time is stable in finite time.
  - Section 3.4 describes, step by step, through the spatial discretization of Maxwell's equations by the proposed hybridizable discontinuous Galerkin method. Then, Low-Storage Runge Kutta (LSRK) time integration is proposed in section 3.4.3 as a fully explicit time integration to complete the discretization.
  - Finally, in section 3.5 we assess numerically the influence of the parameter τ on the fully explicit HDG scheme and we will present the numerical solution of Maxwell's equations

in the case of propagation of a standing wave in a cubic PEC cavity, propagation of a plane wave in a homogeneous domain and scattering of a plane wave by a dielectric sphere. We also see that this method is high order accurate and leads us to an optimal convergence order. All the numerical results are simulated in the framework of the DIOGENeS software suite (section 3.5.1). It was very important to understand how it works since he treats the DG method for Maxwell's equations and in this chapter the method proposed is a generalized one. So we updated all the routines treating the numerical fluxes on the interior faces, also on the perfectly metallic boundary and the absorbing boundary faces.

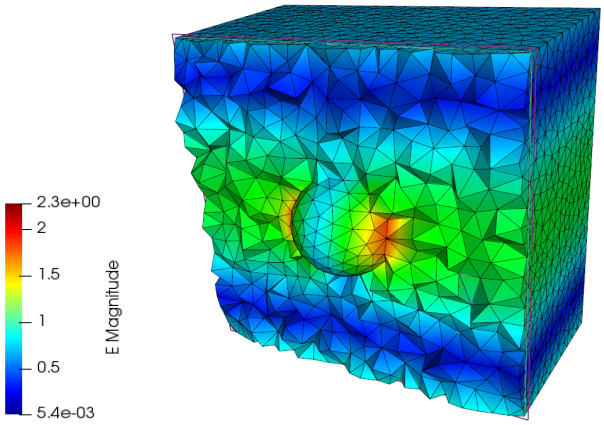

Figure 1.3 | 3D simulation for the magnitude of the electric field at a fixed time with $\mathbb{P}_4$ elements with the explicit HDGTD discretization for Maxwell's equations.

- Chapter 4 aims at showing that the fully explicit HDG method for the 3D time-domain Maxwell's equations presented in chapter 3 is amenable to local postprocessing to obtain a superconvergence property with a rate $k+1$, if $k \geq 1$ is the interpolation order, in the $H(curl)$-norm instead of k. Our novel postprocessing is inspired by two recent works, namely, a postprocessing for an explicit HDG discretization of the 2D acoustic wave equation [38], and a postprocessing for a HDG discretization of the 3D time-harmonic Maxwell's equations [39].

  - Section 4.2 presents the previous work done in [39] for the local postprocessing technique of a HDG discretization for the 3D time-harmonic Maxwell's equations. We recall the definition of the postprocessed solution and present numerical results for the cubic cavity test case in which the postprocessed solutions converge with an order $k+1$, in the $H(curl)$-norm instead of k.
  - Section 4.3 describes our novel postprocessing done for the first time in the context of time-domain Maxwell's equations. First we define our postprocessing technique that hinges on element-wise finite-element saddle-point problems. Then, we show that there exists a unique solution for the postprocessed variables in Theorem 5. Second, we write all the details needed to obtain the space discretization of this postprocessing method in 4.3.4.
  - Finally, in section 4.4 the superconvergence property is validated with the same numerical cases considered in chapter 3. Where, in the case of propagation of a standing wave

in a cubic PEC cavity, we will show in Figures 4.1 and 4.2 the behavior of the error for the original and postprocessed discrete solutions with respect to time on a fixed mesh. The postprocessed solution is about 10 times more accurate than the original one, while it is 5 times more accurate in the case of the propagation of a plane wave in a homogeneous domain (Figures 4.3 and 4.4). We submitted our work in the computational and applied mathematics (COAM) journal. Tables 4.2 and 4.3 present in more detail our results on a series of meshes and for different polynomial degrees. We see that in each case, the curl of the postprocessed solution converges with the expected order, namely $k+1$. And finally, scattering of a plane wave by a dielectric sphere does not have an analytical solution, so we will compute a reference solution with $\mathbb{P}_4$ elements on a fine mesh. We will assess the impact of our novel postprocessing by considering a set of evaluation points where we compute the relative errors between the reference solution and the solution before and after postprocessing. Table 4.4 shows that error after postprocessing is less than the error before postprocessing for all the evaluation points that we have selected. All the numerical results were simulated on the DIOGENeS software suite. We added different routines to obtain these numerical results. First, on the calculation of the $H(curl)$ error and then on the definition of all the elementary matrices mentioned in the implementation section 4.3.4 leading us to find the new approximated solution locally in space and time. And finally on all the different routines needed for the comparison between the solutions before and after postprocessing.

- Chapter 5 presents the ultimate goal of this thesis which is elaborating a hybrid implicit/explicit (IMEX) HDG method for Maxwell's equations. We consider hybridized discontinuous Galerkin time-domain (HDGTD) methods and propose efficient time integration methods when using non-uniform (locally refined) meshes. However, locally refined meshes lead to severe stability constraints when considering fully explicit time integration methods in combination with high order HDG spatial discretization. If relatively few refined elements are present in the grid, this time step restriction can be removed by blending an implicit and an explicit (IMEX) time-integration schemes where only the degrees of freedom associated with small elements are treated implicitly. This approach requires the solve of a linear system at each time step, but the size of this system is limited, since it only corresponds to the finest regions of the space grids where the implicit scheme is applied.

  - Section 5.2 presents the first step towards elaborating the IMEX HDG method, which is writing the semi-discrete formulation of the HDG method in terms of coarse and fine elements of the mesh. Then, we will introduce some notations to obtain a compact expression of the semi-discrete HDG global weak formulation. Later on in this section, we will usher some preliminary results, as Lemmas 3-4 and Corollary 4.1 to find some upperbounds leading us to the stability analysis studied later on in this chapter.
  - In section 5.3, we will first give a quick overview on Runge-Kutta and IMEX Runge-Kutta methods and show the way they are applied on the semi discrete HDG discretization 5.3.1. Then we will consider three different hybrid implicit-explicit (IMEX) HDG methods, which are based on the following time schemes: the first order Euler implicit-explicit method in 5.3.2, a second order implicit-explicit Runge-Kutta method in 5.3.2, and third order implicit-explicit SSP-LDIRK3 method, which is a mix between the explicit strong stability preserving and the L-stable diagonally implicit Runge-Kutta methods in 5.3.2. With the help of Lemmas 3-4 and Corollary 4.1, theorems 6-7 show

that for $\Delta t \leq \eta h^2_{\mathcal{T}_h^{CO}}$ ($\mathcal{T}_h^{CO}$ is the coarse part of the mesh), the totally discrete hybrid implicit-explicit Euler HDG and implicit-explicit Runge-Kutta 2 scheme are stable in the sense that for all $n \in \mathbb{N}$, there exists $\beta > 0$ (independent of h and Δt) such that $\mathcal{E}_h^n \leq e^{\beta T}\mathcal{E}_h^0$.

- Finally, we present numerical results for four different numerical cases to assess the convergence and accuracy of the method and to show her importance in terms of the gain obtained for the CPU time, in the cases where the locally refined meshes is a must for the accuracy of the approximated solution in section 5.4.
  In order to validate and study the numerical convergence of the proposed IMEX HDG methods, we first consider in 5.4.1 the propagation of an eigenmode in a source-free closed cavity with perfectly metallic walls while considering a uniform mesh. It is clear that in the case of uniform meshes, we have $h_{\mathcal{T}_h^{CO}} = h$. The goal of this section is just to validate the hybrid implicit/explicit HDGTD scheme without seeing the gain this method is designed for. While considering an arbitrary fine region, tables 5.3-5.4-5.7 present in more detail our results on a series of meshes and for the correspondent polynomial degree, in the sense that for a time scheme of order k, it is sufficient to consider a $k-1$ polynomial degree.
  In 5.4.2 we consider a model problem for which an analytical solution is available and that consists in the propagation of a standing wave in a PEC disc sector. The solution presents a singularity at the origin, as shown on the bottom image of Fig. 5.14. Therefore, it is necessary to locally refine the mesh in this region to preserve the convergence of the HDG scheme, see Fig. 5.15, 5.16, 5.17 and 5.18. For a mesh consisted of 28.75% fine elements and a ratio of almost 31 between $h_{\mathcal{T}_h^{CO}}$ and h (Fig.5.20) and without losing any accuracy (Fig. 5.22), Tab. 5.8 shows that the third order IMEX HDGTD scheme outperforms the third order fully explicit and implicit HDGTD schemes on CPU time metrics.
  Then, in 5.4.3 we will consider the propagation of an eigenmode in a source-free closed cavity with $\varepsilon = \varepsilon(\mathbf{x})$. In this case we have an important change in the velocity of the wave between two different parts of the mesh corresponding to two different permittivities. To better catch the information of the wave, we have to increase the number of elements per wave length in the region where the velocity of the wave is higher. For this reason the locally refined mesh (Fig. 5.24 on the right) is a must in this case (Fig. 5.27). For a mesh constituted of 82.66% fine elements and a ratio of almost 13.6 between $h_{\mathcal{T}_h^{CO}}$ and h, Tab. 5.9 shows that the second order IMEX HDGTD scheme outperforms the second order fully explicit HDGTD scheme and implicit HDGTD schemes on CPU time metrics. Note that in this case, the percentage on the fine elements is very high, so the global HDG matrix we are inverting at each time step will have a very few modifications between IMEX and fully implicit scheme. Therefore, the CPU time metrics will lightly change for these two time schemes.
  Finally in 5.4.4, we will consider a prototype problem of a photonic crystal structure in the emerging nanophotonics area [40]. The photonic crystal type represents a nanostructuring device encapsulated in a square which is composed of cylindrical holes made of silicium enclosed by a silica device (Fig.5.30). We use absorbing boundary conditions with an incident plane wave. First we will test our third order fully explicit HDGTD scheme. The simulation is presented in Fig.5.32. Then , we will consider the same problem but with a smaller distance between the holes (Fig. 5.33) to test our third

order IMEX HDGTD scheme. For a mesh constituted of 8.3% fine elements and a ratio of almost 3 between $h_{\mathcal{T}_h^{CO}}$ and h, Tab. 5.10 shows that our third order IMEX HDGTD scheme outperform both of the fully explicit and implicit HDGTD schemes on computational time while preserving the same accuracy (Fig. 5.38).
All the numerical results are simulated by our MATLAB code designed for the HDGTD method for 2D Maxwell's equations.

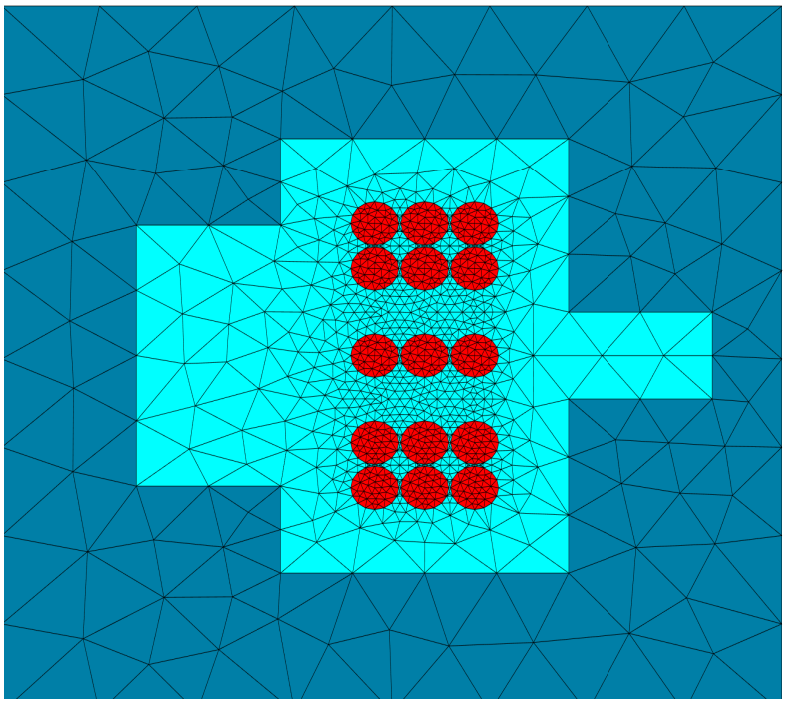

Figure 1.4 | A Locally refined mesh for the photonic crystal device, while the holes are very close to each others.

- Annex contains our conference paper on the fully explicit HDGTD method for Maxwell's equations [37] and our submitted paper on a postprocessing technique for a discontinuous Galerkin discretization of time-dependent Maxwell's equations.

2

The HDG method

2.1 Introduction

In recent years, hybrid (hybridized or hybridizable) discontinuous Galerkin (HDG) methods have been investigated and applied to various problems. The usual discontinuous Galerkin (DG) method utilizes two types of numerical fluxes to deal with the discontinuity of an approximate solution u_h on inter-element boundaries. In the HDG method, a numerical trace $\hat{u}_h$ is introduced to approximate the trace of a solution besides u_h, which is a new unknown and may be called the hybrid unknown. The number of degrees of freedom (DOF) of the DG method is much larger than that of a continuous finite element method. By static condensation, that is, eliminating the element unknown u_h by the hybrid unknown $\hat{u}_h$, we obtain a discretized equation in terms of $\hat{u}_h$ only. As a result, the number of DOF of the HDG method can be considerably reduced, which is the main advantage of the HDG method over the DG method. We note that the HDG method has remarkable features besides the above advantage, such as superconvergence properties and various connections with other numerical methods (nonconforming and mixed finite element methods, etc). The HDG method was firstly introduced by Cockburn et al. [32], in which the hybridization of the local discontinuous Galerkin (LDG) method (cf. [41]) is successful to unify the formulations of various hybrid methods. An overview of various HDG methods is already provided in [32], and we refer to it as for an overview of the main achievements with such methods. This chapter is organized as follow: The HDG method for the Poisson equation (section 2.3), for Maxwell's equations in frequency-domain (section 2.4) and for Maxwell's equations in time-domain while using a fully implicit time integration (section 2.5) .

2.2 Notations

We consider a partition $\mathcal{T}_h$ of a Lipschitz polyhedral $\Omega \subset \mathbb{R}^n (n = 2, 3)$ into a set of triangles or tetraedra. Each non-empty intersection of two elements K^+ and K^- is called a face. We denote by $\mathcal{F}_h$ the set of all faces of $\mathcal{T}_h$. Note that $\partial\mathcal{T}_h$ represents all the faces ∂K for all $K \in \mathcal{T}_h$. As a result, an interior face shared by two elements appears twice in $\partial\mathcal{T}_h$, unlike of $\mathcal{F}_h$ where this face is counted once. For an interface $F \in \mathcal{F}_h^I$, $F = \overline{K}^+ \cap \overline{K}^-$. If $\boldsymbol{v} : \Omega \to \mathbb{R}^3$ is a function admitting

well-defined traces on F, $\boldsymbol{v}^{\pm}$ denote the traces of $\boldsymbol{v}$ on F from the interior of $K^{\pm}$. On this interior face, we define mean values $\{\cdot\}$ and jumps $[\![\cdot]\!]$ as

$$\begin{cases} \{\boldsymbol{v}\}_F = \dfrac{1}{2}(\boldsymbol{v}^+ + \boldsymbol{v}^-), \\ [\![\boldsymbol{v}]\!]_F = \boldsymbol{n}^+ \times \boldsymbol{v}^+ + \boldsymbol{n}^- \times \boldsymbol{v}^-, \end{cases}$$

where the unit outward normal vector to K is denoted by $\boldsymbol{n}^{\pm}$. For the boundary faces these expressions are modified as

$$\begin{cases} \{\boldsymbol{v}\}_F = \boldsymbol{v}^+, \\ [\![\boldsymbol{v}]\!]_F = \boldsymbol{n}^+ \times \boldsymbol{v}^+, \end{cases}$$

since we assume $\boldsymbol{v}$ is single-valued on the boundaries. In the following, we introduce the discontinuous finite element spaces and some basic operations on these spaces for later use. Let $\mathbb{P}_k(K)$ denotes the space of polynomial functions of degree at most k on the element $K \in \mathcal{T}_h$. The discontinuous finite element space is as usual defined as

$$\boldsymbol{V}_h^m = \left\{ \boldsymbol{v} \in \left[L^2(\Omega)\right]^m \text{ such that } \boldsymbol{v}|_K \in [\mathbb{P}_k(K)]^m, \quad \forall K \in \mathcal{T}_h \right\}, \tag{2.1}$$

where $L^2(\Omega)$ is the space of square integrable functions on the domain Ω and $m \in \{1, 2, 3\}$. The functions in $\boldsymbol{V}_h^m$ are continuous inside each element and discontinuous across the interfaces between elements. In addition, we introduce two traced finite element spaces, $\boldsymbol{M}_h^m$ and $\boldsymbol{M}_h^{t,m}$, where

$$\boldsymbol{M}_h^m = \left\{ \eta \in [L^2(\mathcal{F}_h)]^m \text{ such that } \eta|_F \in [\mathbb{P}_k(F)]^m, \quad \forall F \in \mathcal{F}_h \right\}, \tag{2.2}$$

and

$$\boldsymbol{M}_h^{t,m} = \left\{ \boldsymbol{\eta} \in \left[L^2(\mathcal{F}_h)\right]^m \text{ such that } \boldsymbol{\eta}|_F \in [\mathbb{P}_f(F)]^m \text{ and } (\boldsymbol{\eta} \cdot \boldsymbol{n})|_F = 0, \quad \forall F \in \mathcal{F}_h \right\}. \tag{2.3}$$

Let us define D as a domain in $\mathbb{R}^3$. For two vectorial functions $\boldsymbol{u}$ and $\boldsymbol{v}$ in $\left[L^2(D)\right]^3$, we denote $(\boldsymbol{u}, \boldsymbol{v})_D = \displaystyle\int_D \boldsymbol{u} \cdot \boldsymbol{v} \, \mathrm{d}\boldsymbol{x}$, and we denote $< \boldsymbol{u}, \boldsymbol{v} >_F = \displaystyle\int_F \boldsymbol{u} \cdot \boldsymbol{v} \, \mathrm{d}s$ if F is a two-dimensional face.
Note that in chapter 5, the computational mesh $\mathcal{T}_h$ is split into two parts that we denote by $\mathcal{T}_h^{CO}$ and $\mathcal{T}_h^{FI}$, where $\mathcal{T}_h^{FI}$ is the fine part which contains all the small elements of the mesh, and $\mathcal{T}_h^{CO}$ is the coarse part, and contains all the remaining elements, we denote by $h_{\mathcal{T}_h^{CO}} = \min\limits_{K \in \mathcal{T}_h^{CO}} h_K$.
Accordingly, for the mesh we have

$$\begin{aligned}
(\cdot,\cdot)_{\mathcal{T}_h} &= \sum_{K \in \mathcal{T}_h} (\cdot,\cdot)_K, & \langle \cdot,\cdot \rangle_{\partial \mathcal{T}_h} &= \sum_{K \in \mathcal{T}_h} \langle \cdot,\cdot \rangle_{\partial K}, \\
\langle \cdot,\cdot \rangle_{\mathcal{F}_h} &= \sum_{F \in \mathcal{F}_h} \langle \cdot,\cdot \rangle_F, & \langle \cdot,\cdot \rangle_{\Gamma_a} &= \sum_{F \in \mathcal{F}_h \cap \Gamma_a} \langle \cdot,\cdot \rangle_F. \\
(\cdot,\cdot)_{\mathcal{T}_h^{FI}} &= \sum_{K \in \mathcal{T}_h^{FI}} (\cdot,\cdot)_K, & \langle \cdot,\cdot \rangle_{\partial \mathcal{T}_h^{FI}} &= \sum_{K \in \mathcal{T}_h^{FI}} \langle \cdot,\cdot \rangle_{\partial K}, \\
(\cdot,\cdot)_{\mathcal{T}_h^{CO}} &= \sum_{K \in \mathcal{T}_h^{CO}} (\cdot,\cdot)_K, & \langle \cdot,\cdot \rangle_{\partial \mathcal{T}_h^{CO}} &= \sum_{K \in \mathcal{T}_h^{CO}} \langle \cdot,\cdot \rangle_{\partial K}.
\end{aligned}$$

We set,

$$\boldsymbol{v}^t = -\boldsymbol{n} \times (\boldsymbol{n} \times \boldsymbol{v}), \quad \boldsymbol{v}^n = \boldsymbol{n}\,(\boldsymbol{n} \cdot \boldsymbol{v}),$$

where $\boldsymbol{v}^t$ and $\boldsymbol{v}^n$ are the tangential and normal components of $\boldsymbol{v}$ such as $\boldsymbol{v} = \boldsymbol{v}^t + \boldsymbol{v}^n$.
Note that $\boldsymbol{M}_h^{t,3}$ consists of vector-valued functions whose normal component is zero on any face $F \in \mathcal{F}_h$. Thus, an element of $\boldsymbol{M}_h^{t,3}$ can be characterized by two tangential vectors on the faces: if $\mathbf{t}_1^F$ and $\mathbf{t}_2^F$ denote independent tangent vectors on F, the restriction of $\eta \in \boldsymbol{M}_h^{t,3}$ on F can be written as

$$\eta|_F = \eta_1^F \mathbf{t}_1^F + \eta_2^F \mathbf{t}_2^F,$$

where $\eta_1^F \in \mathbb{P}_f(F)$ and $\eta_2^F \in \mathbb{P}_f(F)$ are real-valued polynomials of degree at most f on F. Thus, the vector-valued function $\eta \in \boldsymbol{M}_h^{t,3}$ is characterized by two scalar functions η_1 and η_2.
For a given $K \in \mathcal{T}_h$ and $F \in \mathcal{F}_h$ we denote by h_K and h_F their diameter, $\rho_K = \min\limits_{1 \le i \le 4} \rho_i$, ρ_i being the diameter of the circle inscribed in the triangle formed by the three vertices $(a_j)_{j \neq i}$ and $h = \min\limits_{K \in \mathcal{T}_h} h_K$. We consider a shape-regular and a quasi-uniform mesh, i.e

$$\forall h, \forall K \in \mathcal{T}_h, \exists \eta > 0\,;\ \frac{h_K}{\rho_K} < \eta \quad (\,\text{shape regular}\,),$$

and

$$\exists \eta > 0; \forall K, K' \in \mathcal{T}_h, h_K \le \eta h_{K'} \quad (\,\text{quasi uniform}\,).$$

We recall the following definitions of Sobolev spaces,

Sobolev spaces

$$\begin{aligned}
H^1(\Omega) &= \left\{ f \in L^2(\Omega); \quad \nabla f \in L^2(\Omega) \right\}, \\
H_0^1(\Omega) &= \left\{ f \in H^1(\Omega); \quad \gamma_0(f) = 0 \right\}, \\
H^{div}(\Omega) &= \left\{ \boldsymbol{f} \in \left[L^2(\Omega) \right]^n ; \boldsymbol{\nabla} \cdot \boldsymbol{f} \in L^2(\Omega) \right\}, \\
H^{curl}(\Omega) &= \left\{ f \in L^2(\Omega); \quad \nabla \times f \in L^2(\Omega) \right\}, \\
L_0^2(\mathcal{F}_h) &= \left\{ f \in L^2(\mathcal{F}_h); \quad f = 0 \,\text{on}\, \partial\Omega \right\}.
\end{aligned} \tag{2.4}$$

With, γ_0 is the usual continuous trace operator for Sobolev spaces.

2.3 From DG to HDG for Poisson equation

In this section, we will review the DG method on a simple example, show the importance of changing from DG to HDG discretization in terms of how the HDG method will reduce the number of globally coupled DoFs without entering in details. The reader is referred to [32] to see the proof in this case.

2.3.1 Problem statement

Let $\Omega \subset \mathbb{R}^n (n = 2, 3)$ be a bounded domain and $f \in L^2(\Omega)$ be a given function. We consider the Poisson equation with homogeneous boundary condition,

Poisson equation

$$\begin{aligned} -\Delta u &= f, \text{ in } \Omega, \\ u &= 0, \text{ on } \partial\Omega. \end{aligned} \tag{2.5}$$

We first rewrite the problem as a first-order system,

First-order Poisson equation

$$\begin{aligned} \boldsymbol{\sigma} &= \boldsymbol{\nabla} u, \text{ in } \Omega, \\ -\nabla \cdot \boldsymbol{\sigma} &= f \quad , \text{ in } \Omega, \\ u &= 0 \quad , \text{ on } \partial\Omega. \end{aligned} \tag{2.6}$$

2.3.2 Weak formulation

It is now possible to write the weak formulation of problem (2.6) in the cell K. By taking the L^2 scalar product of each term in the first two equations with the test functions $\boldsymbol{v}_1$ and v_2 respectively, one obtains the following variational problem:

Find $(\boldsymbol{\sigma}, u) \in H^{div}(\Omega) \times H_0^1(\Omega)$ such that $\forall (\boldsymbol{v}_1, v_2) \in H^{div}(\Omega) \times H_0^1(\Omega)$

$$\begin{cases} \displaystyle\int_K \boldsymbol{\sigma} \cdot \boldsymbol{v}_1 - \int_K \boldsymbol{\nabla} u \cdot \boldsymbol{v}_1 = 0, \\ \displaystyle -\int_K \boldsymbol{\nabla} \cdot \boldsymbol{\sigma}\, v_2 - \int_K f\, v_2 = 0. \end{cases} \tag{2.7}$$

Note that if $\boldsymbol{\sigma}$ does not belong to $H^{div}(\Omega)$ then $\boldsymbol{\nabla} \cdot \boldsymbol{\sigma}$ is not a $L^2(\Omega)$ function and the first term of the second equation of (2.7) is not defined as well . Integrating by parts the two equations of (2.7) gives

$$\begin{cases} \displaystyle\int_K \boldsymbol{\sigma} \cdot \boldsymbol{v}_1 + \int_K u\, \boldsymbol{\nabla} \cdot \boldsymbol{v}_1 - \int_{\partial K} u\, \boldsymbol{n} \cdot \boldsymbol{v}_1 = 0, \\ \displaystyle\int_K \boldsymbol{\sigma} \cdot \boldsymbol{\nabla} v_2 - \int_K f\, v_2 - \int_{\partial K} \boldsymbol{\sigma} \cdot \boldsymbol{n}\; v_2 = 0. \end{cases} \tag{2.8}$$

Hence, after summing over all the elements K in $\mathcal{T}_h$ we obtain

Weak formulation

$$\begin{cases} (\boldsymbol{\sigma}, \boldsymbol{v}_1)_{\mathcal{T}_h} + (u, \boldsymbol{\nabla} \cdot \boldsymbol{v}_1)_{\mathcal{T}_h} - \langle u, \boldsymbol{n} \cdot \boldsymbol{v}_1 \rangle_{\partial \mathcal{T}_h} = 0 \quad \forall \boldsymbol{v}_1 \in H^{div}(\Omega), \\ (\boldsymbol{\sigma}, \boldsymbol{\nabla} v_2)_{\mathcal{T}_h} - (f, v_2)_{\mathcal{T}_h} - \langle \boldsymbol{\sigma} \cdot \boldsymbol{n}, v_2 \rangle_{\partial \mathcal{T}_h} = 0 \quad \forall \boldsymbol{v}_2 \in H_0^1(\Omega). \end{cases} \tag{2.9}$$

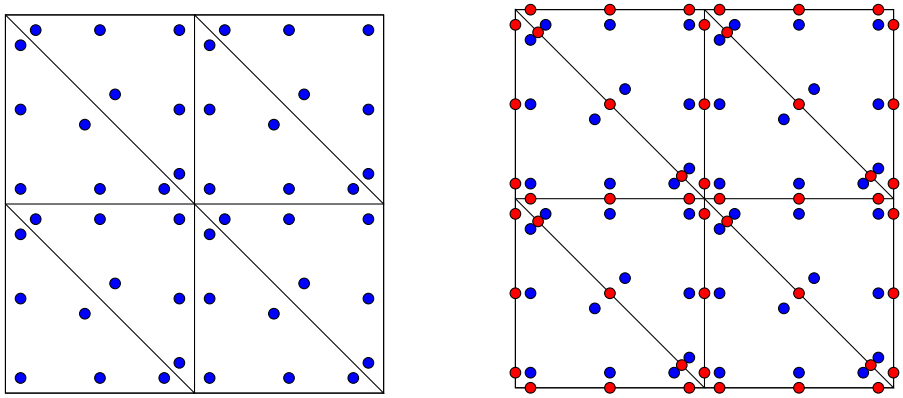

Figure 2.1 | DoFs for the DG and HDG method with a P_2 interpolation.

2.3.3 DG global formulation

Following the classical DG approach, approximate solutions $(\boldsymbol{\sigma}_h, u_h)$, are seeked in the space $\boldsymbol{V}_h^1 \times \boldsymbol{V}_h^2$ satisfying for all K in $\mathcal{T}_h$,

DG formulation

$$\begin{cases} (\boldsymbol{\sigma}_h, \boldsymbol{v}_1)_K + (u_h, \boldsymbol{\nabla} \cdot \boldsymbol{v}_1)_K - \langle \hat{u}_h, \boldsymbol{n} \cdot \boldsymbol{v}_1 \rangle_{\partial K} = 0, \ \forall \boldsymbol{v}_1 \in \boldsymbol{V}_h^2, \\ (\boldsymbol{\sigma}_h, \boldsymbol{\nabla} v_2)_K - (f, v_2)_K - \langle \hat{\boldsymbol{\sigma}}_h \cdot \boldsymbol{n}, v_2 \rangle_{\partial K} = 0, \ \forall v_2 \in \boldsymbol{V}_h^1. \end{cases} \tag{2.10}$$

where the numerical fluxes $\hat{\boldsymbol{\sigma}}_h$ and $\hat{u}_h$ are approximations to $\boldsymbol{\sigma} = \boldsymbol{\nabla} u$ and to u, respectively, on the boundary of K. To complete the formulation of a DG method we must express the numerical fluxes $\hat{\boldsymbol{\sigma}}_h$ and $\hat{u}_h$ in terms of $\boldsymbol{\sigma}_h$ and u_h. The choice of the numerical fluxes is a crucial step, as it can affect the stability and the accuracy of the method. Consider,

$$\hat{u}_h = \{u_h\} + \alpha [\![\boldsymbol{\sigma}_h]\!] \quad \text{and} \quad \hat{\boldsymbol{\sigma}}_h = \{\boldsymbol{\sigma}_h\} + \alpha [\![u_h]\!], \tag{2.11}$$

where $\alpha = 0$ corresponds to a centered flux, $\alpha = 1$ to an upwind flux. We can easily see from (2.10) and (2.11) that, we have to solve a large global problem containing a large number of DoFs since an important number of the DoFs are coupled (the blue dots in figure (2.1) (left)). Here comes the concept of hybridizable discontinuous Galerkin (HDG) method in solving the problem by reducing the number of the globally coupled unknowns to the approximate trace of the solution on element boundaries, thereby leading to a significant reduction in the degrees of freedom (the red dots in figure (2.1) (right)) and then we can find locally the solution of the element unknowns.

2.3.4 Derivation of the HDG scheme

To hybridize the DG method presented in (2.10), we have to consider the numerical flux $\hat{u}_h$ as a new variable λ_h, so now the new approximate solutions $(\boldsymbol{\sigma}_h, u_h, \lambda_h)$ are seeked in $\boldsymbol{V}_h^2 \times \boldsymbol{V}_h^1 \times \boldsymbol{M}_h^{t,1}$ such that

HDG formulation

$$\begin{cases} (\boldsymbol{\sigma}_h, \boldsymbol{v}_1)_{\mathcal{T}_h} + (u_h, \boldsymbol{\nabla} \cdot \boldsymbol{v}_1)_{\mathcal{T}_h} - \langle \lambda_h, \boldsymbol{n} \cdot \boldsymbol{v}_1 \rangle_{\partial \mathcal{T}_h} = 0, \ \forall \boldsymbol{v}_1 \in \boldsymbol{V}_h^2, \\ (\boldsymbol{\sigma}_h, \boldsymbol{\nabla} v_2)_{\mathcal{T}_h} - (f, v_2)_{\mathcal{T}_h} - \langle \hat{\boldsymbol{\sigma}}_h \cdot \boldsymbol{n}, v_2 \rangle_{\partial \mathcal{T}_h} = 0, \ \forall v_2 \in \boldsymbol{V}_h^1, \\ \langle \hat{\boldsymbol{\sigma}}_h \cdot \boldsymbol{n}, \eta \rangle_{\partial \mathcal{T}_h} = 0, \ \forall \eta \in \boldsymbol{M}_h^{t,1}. \end{cases} \tag{2.12}$$

while,

Numerical fluxes

$$\hat{\boldsymbol{\sigma}}_h \cdot \boldsymbol{n} = \boldsymbol{\sigma}_h \cdot \boldsymbol{n} + \tau \left(\hat{u}_h - u_h \right) \quad \text{on } \partial K. \tag{2.13}$$

The idea here is to create a global problem, that only depends on the degrees of freedom of λ_h, from the third equation of (2.12) and the local form of the first two equations, and then deduce locally u_h and $\boldsymbol{\sigma}_h$.

2.4 HDG method for 3D time-harmonic Maxwell's equations

2.4.1 Problem statement

In this section, we will focus on devising a HDG method for the Maxwell's equations in frequency-domain [42]-[34]. The time-harmonic Maxwell's equations in a bounded domain $\Omega \subset \mathbb{R}^3$ is considered as

Time-harmonic Maxwell's equations

$$\begin{cases} i\omega\varepsilon_r \boldsymbol{E} - \mathbf{curl}\, \boldsymbol{H} = -\boldsymbol{J}, \ \text{in } \Omega, \\ i\omega\mu_r \boldsymbol{H} + \mathbf{curl}\, \boldsymbol{E} = 0, \ \text{in } \Omega. \end{cases} \tag{2.14}$$

where i is the imaginary unit, ω is the angular frequency, ε_r and μ_r are the relative permittivity and permeability. $\boldsymbol{J}$ is a known current density, $\boldsymbol{E}$ and $\boldsymbol{H}$ are the electric and magnetic fields. The boundary of Ω is defined as $\partial\Omega = \Gamma_m \cup \Gamma_a$ with $\Gamma_m \cap \Gamma_a = \emptyset$. The boundary conditions are choosen as

Boundary conditions

$$\begin{cases} \boldsymbol{n} \times \boldsymbol{E} = 0, \ \text{on } \Gamma_m, \\ \boldsymbol{n} \times \boldsymbol{E} + \boldsymbol{n} \times (\boldsymbol{n} \times \boldsymbol{H}) = \boldsymbol{n} \times \boldsymbol{E}^{\text{inc}} + \boldsymbol{n} \times (\boldsymbol{n} \times \boldsymbol{H}^{\text{inc}}), \\ \qquad = \boldsymbol{g}^{\text{inc}}, \ \text{on } \Gamma_a. \end{cases} \tag{2.15}$$

Here $\boldsymbol{n}$ denotes the unit outward normal to $\partial\Omega$ and $(\boldsymbol{E}^{\text{inc}}, \boldsymbol{H}^{\text{inc}})$ a given incident field. The first boundary condition is often referred as a metallic boundary condition and is applied on a perfectly conducting surface. The second relation is an absorbing boundary condition and takes here the form of the Silver-Müller condition. It is applied on a surface corresponding to an artificial truncature of a theoretically unbounded propagation domain.

2.4.2 Global formulation

Following the classical DG approach, approximate solutions $(\boldsymbol{E}_h,\boldsymbol{H}_h)$, are seeked in the space $\boldsymbol{V}_h^3 \times \boldsymbol{V}_h^3$ satisfying for all K in $\mathcal{T}_h$

$$\begin{cases} (i\omega\varepsilon_r \boldsymbol{E}_h, \boldsymbol{v})_K - (\mathbf{curl}\, \boldsymbol{H}_h, \boldsymbol{v})_K = 0, \ \forall \boldsymbol{v} \in \boldsymbol{V}_h^3, \\ (i\omega\mu_r \boldsymbol{H}_h, \boldsymbol{v})_K + (\mathbf{curl}\, \boldsymbol{E}_h, \boldsymbol{v})_K = 0, \ \forall \boldsymbol{v} \in \boldsymbol{V}_h^3. \end{cases} \tag{2.16}$$

Applying Green's formula, on both equations of (2.16) introduces boundary terms which are replaced by numerical traces $\hat{\boldsymbol{E}}_h$ and $\hat{\boldsymbol{H}}_h$ in order to ensure the connection between element-wise solutions and global consistency of the discretization. This leads to the formulation

$$\begin{cases} (i\omega\varepsilon_r \boldsymbol{E}_h, \boldsymbol{v})_K - (\boldsymbol{H}_h, \mathbf{curl}\, \boldsymbol{v})_K + \left\langle \hat{\boldsymbol{H}}_h, \boldsymbol{n} \times \boldsymbol{v} \right\rangle_{\partial K} = 0, \ \forall \boldsymbol{v} \in \boldsymbol{V}_h^3, \\ (i\omega\mu_r \boldsymbol{H}_h, \boldsymbol{v})_K + (\boldsymbol{E}_h, \mathbf{curl}\, \boldsymbol{v})_K - \left\langle \hat{\boldsymbol{E}}_h, \boldsymbol{n} \times \boldsymbol{v} \right\rangle_{\partial K} = 0, \ \forall \boldsymbol{v} \in \boldsymbol{V}_h^3. \end{cases} \tag{2.17}$$

It is straightforward to verify that $\boldsymbol{n} \times \boldsymbol{v} = \boldsymbol{n} \times \boldsymbol{v}^t$ and $< \boldsymbol{H}, \boldsymbol{n} \times \boldsymbol{v} >= - < \boldsymbol{n} \times \boldsymbol{H}, \boldsymbol{v} >$. Therefore, using numerical traces defined in terms of the tangential components $\hat{\boldsymbol{H}}_h^t$ and $\hat{\boldsymbol{E}}_h^t$, we can rewrite (2.17) as

$$\begin{cases} (i\omega\varepsilon_r \boldsymbol{E}_h, \boldsymbol{v})_K - (\boldsymbol{H}_h, \mathbf{curl}\, \boldsymbol{v})_K + \left\langle \hat{\boldsymbol{H}}_h^t, \boldsymbol{n} \times \boldsymbol{v} \right\rangle_{\partial K} = 0, \ \forall \boldsymbol{v} \in \boldsymbol{V}_h^3, \\ (i\omega\mu_r \boldsymbol{H}_h, \boldsymbol{v})_K + (\boldsymbol{E}_h, \mathbf{curl}\, \boldsymbol{v})_K - \left\langle \hat{\boldsymbol{E}}_h^t, \boldsymbol{n} \times \boldsymbol{v} \right\rangle_{\partial K} = 0, \ \forall \boldsymbol{v} \in \boldsymbol{V}_h^3. \end{cases} \tag{2.18}$$

The hybrid variable $\boldsymbol{\Lambda}_h$ introduced in the setting of a HDG method [32] is here defined for all the interfaces of $\mathcal{F}_h$ as

$$\boldsymbol{\Lambda}_h := \hat{\boldsymbol{H}}_h^t, \quad \forall F \in \mathcal{F}_h. \tag{2.19}$$

We want to determine the fields $\hat{\boldsymbol{H}}_h^t$ and $\hat{\boldsymbol{E}}_h^t$ in each element K of $\mathcal{T}_h$ by solving system (2.18) and assuming that $\boldsymbol{\Lambda}_h$ is known on all the faces of an element K. We consider a numerical trace $\hat{\boldsymbol{E}}_h^t$ for all K given by

$$\hat{\boldsymbol{E}}_h^t = \boldsymbol{E}_h^t + \tau_K \boldsymbol{n} \times (\boldsymbol{\Lambda}_h - \boldsymbol{H}_h^t) \text{ on } \partial K, \tag{2.20}$$

where τ_K is a local stabilization parameter which is assumed to be strictly positive. We recall that $\boldsymbol{n} \times \boldsymbol{H}_h^t = \boldsymbol{n} \times \boldsymbol{H}_h$.

Remark 1. In a classical DG method the traces of the local fields $\boldsymbol{E}_h$ and $\boldsymbol{H}_h$ between neighboring elements are defined as

$$\hat{\boldsymbol{E}}_h = \{\boldsymbol{E}_h\} + \alpha_H [\![\boldsymbol{H}_h]\!] \text{ and } \hat{\boldsymbol{H}}_h = \{\boldsymbol{H}_h\} + \alpha_E [\![\boldsymbol{E}_h]\!],$$

where α_H and α_E are positive penalty parameters.

Remark 2. Following the HDG approach, when the hybrid variable $\boldsymbol{\Lambda}_h$ is known for all the faces of the element K, the electromagnetic field can be determined by solving the local system (2.18) using (2.19) and (2.20).

For the sake of simplicity, we denote by $\boldsymbol{g}^{\text{inc}}$ the L^2 projection of $\boldsymbol{g}^{\text{inc}}$ on $\boldsymbol{M}_h$. Summing the contributions of (2.18) over all the elements and enforcing the continuity of the tangential component of $\hat{\boldsymbol{E}}_h$, we can formulate a problem which is to find $(\boldsymbol{E}_h, \boldsymbol{H}_h, \boldsymbol{\Lambda}_h) \in \boldsymbol{V}_h^3 \times \boldsymbol{V}_h^3 \times \boldsymbol{M}_h^{t,3}$ such that

HDG formulation 1

$$\begin{cases} (\mathrm{i}\omega\varepsilon_r \boldsymbol{E}_h, \boldsymbol{v})_{\mathcal{T}_h} - (\boldsymbol{H}_h, \mathbf{curl}\, \boldsymbol{v})_{\mathcal{T}_h} + \langle \boldsymbol{\Lambda}_h, \boldsymbol{n} \times \boldsymbol{v} \rangle_{\partial\mathcal{T}_h} = 0, \ \forall \boldsymbol{v} \in \boldsymbol{V}_h^3, \\ (\mathrm{i}\omega\mu_r \boldsymbol{H}_h, \boldsymbol{v})_{\mathcal{T}_h} + (\boldsymbol{E}_h, \mathbf{curl}\, \boldsymbol{v})_{\mathcal{T}_h} - \left\langle \hat{\boldsymbol{E}}_h^t, \boldsymbol{n} \times \boldsymbol{v} \right\rangle_{\partial\mathcal{T}_h} = 0, \ \forall \boldsymbol{v} \in \boldsymbol{V}_h^3, \\ \left\langle [\![\hat{\boldsymbol{E}}_h]\!], \boldsymbol{\eta} \right\rangle_{\mathcal{F}_h} - \langle \boldsymbol{\Lambda}_h, \boldsymbol{\eta} \rangle_{\Gamma_a} - \left\langle \boldsymbol{g}^{\text{inc}}, \boldsymbol{\eta} \right\rangle_{\Gamma_a} = 0, \ \forall \boldsymbol{\eta} \in \boldsymbol{M}_h. \end{cases} \tag{2.21}$$

Where the last equation is called the conservativity condition with which we ask the tangential component of $\hat{\boldsymbol{E}}_h$ to be weakly continuous across any interface between two neighboring elements. With the definition (2.20) of $\hat{\boldsymbol{E}}_h^t$, we employ again a Green formula with the second equation of (2.21), in order to get the following formulation,

HDG formulation 2

$$\begin{cases} (\mathrm{i}\omega\varepsilon_r \boldsymbol{E}_h, \boldsymbol{v})_{\mathcal{T}_h} - (\boldsymbol{H}_h, \mathbf{curl}\, \boldsymbol{v})_{\mathcal{T}_h} + \langle \boldsymbol{\Lambda}_h, \boldsymbol{n} \times \boldsymbol{v} \rangle_{\partial\mathcal{T}_h} = 0, \ \forall \boldsymbol{v} \in \boldsymbol{V}_h^3, \\ (\mathrm{i}\omega\mu_r \boldsymbol{H}_h, \boldsymbol{v})_{\mathcal{T}_h} + (\mathbf{curl}\, \boldsymbol{E}_h, \boldsymbol{v})_{\mathcal{T}_h} + \langle \tau \boldsymbol{n} \times (\boldsymbol{H}_h - \boldsymbol{\Lambda}_h), \boldsymbol{n} \times \boldsymbol{v} \rangle_{\partial\mathcal{T}_h} = 0, \ \forall \boldsymbol{v} \in \boldsymbol{V}_h^3, \\ \langle \boldsymbol{n} \times \boldsymbol{E}_h, \boldsymbol{\eta} \rangle_{\partial\mathcal{T}_h} + \left\langle \tau \left(\boldsymbol{H}_h^t - \boldsymbol{\Lambda}_h \right), \boldsymbol{\eta} \right\rangle_{\partial\mathcal{T}_h} - \langle \boldsymbol{\Lambda}_h, \boldsymbol{\eta} \rangle_{\Gamma_a} = \left\langle \boldsymbol{g}^{\text{inc}}, \boldsymbol{\eta} \right\rangle_{\Gamma_a}, \ \forall \boldsymbol{\eta} \in \boldsymbol{M}_h^{t,3}. \end{cases} \tag{2.22}$$

Note that we have used

$$\boldsymbol{n} \times \boldsymbol{v}^t = \boldsymbol{n} \times \boldsymbol{v} \text{ and } \boldsymbol{n} \times (\boldsymbol{n} \times \boldsymbol{v}^t) = -\boldsymbol{v}^t \tag{2.23}$$

to obtain (2.22). Indeed, the last relation of (2.21) together with the definition (2.20) of $\hat{\boldsymbol{E}}_h^t$ yields

$$\left\langle \boldsymbol{n} \times \boldsymbol{E}_h^t, \boldsymbol{\eta} \right\rangle_{\partial\mathcal{T}_h} + \left\langle \tau \boldsymbol{n} \times \left(\boldsymbol{n} \times \left(\boldsymbol{H}_h^t - \boldsymbol{\Lambda}_h \right) \right), \boldsymbol{\eta} \right\rangle_{\partial\mathcal{T}_h} - \langle \boldsymbol{\Lambda}_h, \boldsymbol{\eta} \rangle_{\Gamma_a} = \left\langle \boldsymbol{g}^{\text{inc}}, \boldsymbol{\eta} \right\rangle_{\Gamma_a},$$

which can be written, using (2.23)

$$\langle \boldsymbol{n} \times \boldsymbol{E}_h, \boldsymbol{\eta} \rangle_{\partial\mathcal{T}_h} + \left\langle \tau \left(\boldsymbol{H}_h^t - \boldsymbol{\Lambda}_h \right), \boldsymbol{\eta} \right\rangle_{\partial\mathcal{T}_h} - \langle \boldsymbol{\Lambda}_h, \boldsymbol{\eta} \rangle_{\Gamma_a} = \left\langle \boldsymbol{g}^{\text{inc}}, \boldsymbol{\eta} \right\rangle_{\Gamma_a}.$$

Moreover, we note that the last relation of (2.21) for a boundary face F on Γ_a is equivalent to,using the fact that $[\![\hat{\boldsymbol{E}}_h^t]\!] = \boldsymbol{n} \times \hat{\boldsymbol{E}}_h^t$,

$$\left\langle \boldsymbol{n} \times \hat{\boldsymbol{E}}_h^t, \boldsymbol{\eta} \right\rangle_{\mathcal{F}_h} - \left\langle \hat{\boldsymbol{H}}_h^t, \boldsymbol{\eta} \right\rangle_{\Gamma_a} = \left\langle \boldsymbol{g}^{\text{inc}}, \boldsymbol{\eta} \right\rangle_{\Gamma_a},$$

that is,

$$\left\langle \left(\boldsymbol{n} \times \hat{\boldsymbol{E}}_h + \boldsymbol{n} \times \left(\boldsymbol{n} \times \hat{\boldsymbol{H}}_h \right), \boldsymbol{\eta} \right) \right\rangle_F = \left\langle \boldsymbol{g}^{\text{inc}}, \boldsymbol{\eta} \right\rangle_F$$

which is nothing else than the Silver-Müller boundary condition in (2.15) with the numerical traces $\hat{\boldsymbol{E}}_h$ and $\hat{\boldsymbol{H}}_h$.

2.4.3 Main principles of the HDG method

The main principles of the HDG method can be summarized as

1. The DoFs (Degrees of Freedoms) of the hybrid variable are determined by solving a global linear system (from the discretization of the conservation condition) supported by the interfaces of $\mathcal{F}_h$;
2. The DoFs of the electromagnetic field in each element are evaluated by solving local linear systems, more exactly for the DoFs of $(\boldsymbol{E}_h, \boldsymbol{H}_h)$ in the considered element.

2.4.4 Implementation

In this section, we will present all the details elaborating the HDG method for the time-harmonic Maxwell's equations.

Discretization of the local equations

Let $\mathcal{T}_h$ be the set of all K_e with $e \in \{1, \cdots, |\mathcal{T}_h|\}$, and let N_K^e be the number of degrees of freedom in element K_e. We denote by $\sigma(e,l)$ the face number l in the element K_e with $l \in \{1, \cdots, |\nu_e|\}$ and ν_e is the set of indices of all neighboring elements to the element K_e. Let $N_F^{\sigma(e,l)}$ be the number of DoFs in the face ∂K_e^l. We define the restricted fields $\boldsymbol{E}^e = \boldsymbol{E}_{h|_{K_e}} = \begin{pmatrix} E_x^e \\ E_y^e \\ E_z^e \end{pmatrix}$, $\boldsymbol{H}^e = \boldsymbol{H}_{h|_{K_e}} = \begin{pmatrix} H_x^e \\ H_y^e \\ H_z^e \end{pmatrix}$ and $\boldsymbol{\Lambda}^{\sigma(e,l)} = \boldsymbol{\Lambda}_{h|_{\partial K_e^l}} = \begin{pmatrix} \Lambda_{\boldsymbol{u}}^{\sigma(e,l)} \\ \Lambda_{\boldsymbol{w}}^{\sigma(e,l)} \end{pmatrix}$, while the vector $(\boldsymbol{u}, \boldsymbol{w})^T$ constitute the basis of the face ∂K_e^l with $\boldsymbol{u} = \begin{pmatrix} u_x^{\sigma(e,l)} \\ u_y^{\sigma(e,l)} \\ u_z^{\sigma(e,l)} \end{pmatrix}$ and $\boldsymbol{w} = \begin{pmatrix} w_x^{\sigma(e,l)} \\ w_y^{\sigma(e,l)} \\ w_z^{\sigma(e,l)} \end{pmatrix}$. We will now develop the first equation of (2.22) in order to exhibit the local matrices characterizing the HDG scheme. Let $(\varphi_k^e)_{1 \le k \le N_K^e}$ and $\left(\psi_p^{\sigma(e,l)}\right)_{1 \le p \le N_F^{\sigma(e,l)}}$ be the set of scalar basis functions defined in K_e and ∂K_e^l respectively. First by setting $\boldsymbol{v} = \boldsymbol{\varphi}_{xk}^e = \begin{pmatrix} \varphi_k^e \\ 0 \\ 0 \end{pmatrix}$ for $1 \le k \le N_K^e$ in the first equation of (2.22) becomes

$$\begin{aligned} &\int_{K_e} i\omega\varepsilon E_x^e \varphi_k^e - \int_{K_e} \left(H_y^e \partial_z \varphi_k^e - H_z^e \partial_y \varphi_k^e \right) + \\ &\sum_{l=1}^{|\nu_e|} \int_{\partial K_e^l} \left(\Lambda_{\boldsymbol{u}}^{\sigma(e,l)} \boldsymbol{u} + \Lambda_{\boldsymbol{w}}^{\sigma(e,l)} \boldsymbol{w} \right) \cdot \left(0, n_z^{\sigma(e,l)} \varphi_k^e, -n_y^{\sigma(e,l)} \varphi_k^e \right)^T = 0. \end{aligned} \tag{2.24}$$

Note that we obtain N_K^e equations of the form (2.24), one for each value of k. The different terms appearing in (2.24) can be developed as follows.

- **Mass matrix.** Assuming that ε_r is constant on every K_e, we obtain

$$\begin{aligned}\int_{K_e} i\omega\varepsilon_r E_x^e \varphi_k^e &= i\omega\varepsilon_r \int_{K_e} \sum_{l=1}^{N_K^e} E_x^e[l]\varphi_l^e\varphi_k^e \\ &= i\omega\varepsilon_r \sum_{l=1}^{N_K^e} E_x^e[l] \int_{K_e} \varphi_l^e\varphi_k^e \\ &= i\omega\varepsilon_r \left(\mathbb{M}^e \underline{E}_x^e\right)_k, \ 1 \le k \le N_K^e,\end{aligned} \tag{2.25}$$

where $\mathbb{M}^e$ is the mass matrix, of dimension $N_K^e \times N_K^e$

$$\mathbb{M}^e = \left(\int_{K_e} \varphi_l^e\varphi_k^e\right)_{1\le l,k\le N_k^e},$$

and assuming that the vector of all the degrees of freedom of $\boldsymbol{E}$ in K_e has been ordered as

$$\underline{\boldsymbol{E}}^e = \begin{pmatrix}\underline{E}_x^e \\ \underline{E}_y^e \\ \underline{E}_z^e\end{pmatrix} = \begin{pmatrix}\left(E_x^e[l]\right)_{1\le l\le N_K^e}^T \\ \left(E_y^e[l]\right)_{1\le l\le N_K^e}^T \\ \left(E_z^e[l]\right)_{1\le l\le N_K^e}^T\end{pmatrix}.$$

- **Stiffness matrix.**

$$\begin{aligned}\int_{K_e} H_y^e\partial_z\varphi_k^e - H_z^e\partial_y\varphi_k^e &= \int_{K_e} \sum_{l=1}^{N_K^e} \left(H_y^e[l]\varphi_l^e\ \partial_z\varphi_k^e - H_z^e[l]\varphi_l^e\ \partial_y\varphi_k^e\right) \\ &= \sum_{l=1}^{N_K^e} H_y^e[l] \int_{K_i} \varphi_l^e\ \partial_z\varphi_k^e - \sum_{l=1}^{N_K^e} H_z^e[l] \int_{K_i} \varphi_l^e\ \partial_y\varphi_k^e \\ &= \left(\mathbb{D}_z^e\underline{H}_y^e - \mathbb{D}_y^e\underline{H}_z^e\right)_k, \ 1 \le k \le N_K^e.\end{aligned} \tag{2.26}$$

Here, the stiffness matrices were introduced

$$\left(\mathbb{D}_\xi^e\right) = \left(\int_{K_e} \varphi_l^e\ \partial_\xi\,\varphi_k^e\right)_{1\le l,k\le N_K^e} \qquad \text{for } \xi \in \{x,y,z\},$$

and

$$\underline{\boldsymbol{H}}^e = \begin{pmatrix}\underline{H}_x^e \\ \underline{H}_y^e \\ \underline{H}_z^e\end{pmatrix} = \begin{pmatrix}\left(H_x^e[l]\right)_{1\le l\le N_K^e}^T \\ \left(H_y^e[l]\right)_{1\le l\le N_K^e}^T \\ \left(H_z^e[l]\right)_{1\le l\le N_K^e}^T\end{pmatrix}.$$

- **Flux matrix.**

$$
\begin{aligned}
&\sum_{l=1}^{|\nu_e|} \int_{\partial K_e^l} \left(\Lambda_{\boldsymbol{u}}^{\sigma(e,l)} \boldsymbol{u} + \Lambda_{\boldsymbol{w}}^{\sigma(e,l)} \boldsymbol{w}\right) \cdot \left(0, n_z^{\sigma(e,l)} \varphi_k^e, -n_y^{\sigma(e,l)} \varphi_k^e\right)^T \\
=&\sum_{l=1}^{|\nu_e|} \int_{\partial K_e^l} \Big[\Lambda_{\boldsymbol{u}}^{\sigma(e,l)} n_z^{\sigma(e,l)} u_y \varphi_k^e - \Lambda_{\boldsymbol{u}}^{\sigma(e,l)} n_y^{\sigma(e,l)} u_z \varphi_k^e \\
&\qquad + \Lambda_{\boldsymbol{w}}^{\sigma(e,l)} n_z^{\sigma(e,l)} w_y \varphi_k^e - \Lambda_{\boldsymbol{w}}^{\sigma(e,l)} n_y^{\sigma(e,l)} w_z \varphi_k^e\Big] \\
=&\sum_{l=1}^{|\nu_e|} \int_{\partial K_e^l} \Bigg[n_z^{\sigma(e,l)} u_y \sum_{i=1}^{N_F^{\sigma(e,l)}} \Lambda_{\boldsymbol{u}}^{\sigma(e,l)}[i] \psi_i^{(e,l)} \varphi_k^e - n_y^{\sigma(e,l)} u_z \sum_{i=1}^{N_F^{\sigma(e,l)}} \Lambda_{\boldsymbol{u}}^{\sigma(e,l)}[i] \psi_i^{(e,l)} \varphi_k^e \\
&\qquad + n_z^{\sigma(e,l)} w_y \sum_{i=1}^{N_F^{\sigma(e,l)}} \Lambda_{\boldsymbol{w}}^{\sigma(e,l)}[i] \psi_i^{(e,l)} \varphi_k^e - n_y^{\sigma(e,l)} w_z \sum_{i=1}^{N_F^{\sigma(e,l)}} \Lambda_{\boldsymbol{w}}^{\sigma(e,l)}[i] \psi_i^{(e,l)} \varphi_k^e\Bigg] \qquad (2.27) \\
=&\sum_{l=1}^{|\nu_e|} \Bigg[\left(n_z^{\sigma(e,l)} u_y - n_y^{\sigma(e,l)} u_z\right) \sum_{i=1}^{N_F^{\sigma(e,l)}} \Lambda_{\boldsymbol{u}}^{\sigma(e,l)}[i] \int_{\partial K_e^l} \psi_i^{(e,l)} \varphi_k^e \\
&\qquad + \left(n_z^{\sigma(e,l)} w_y - n_y^{\sigma(e,l)} w_z\right) \sum_{i=1}^{N_F^{\sigma(e,l)}} \Lambda_{\boldsymbol{w}}^{\sigma(e,l)}[i] \int_{\partial K_e^l} \psi_i^{(e,l)} \varphi_k^e\Bigg] \\
=&\sum_{l=1}^{|\nu_e|} \Bigg[\left(n_z^{\sigma(e,l)} u_y - n_y^{\sigma(e,l)} u_z\right) \left(\mathbb{F}^{(e,l)} \underline{\Lambda}_{\boldsymbol{u}}^{\sigma(e,l)}\right)_k \\
&\qquad + \left(n_z^{\sigma(e,l)} w_y - n_y^{\sigma(e,l)} w_z\right) \left(\mathbb{F}^{(e,l)} \underline{\Lambda}_{\boldsymbol{w}}^{\sigma(e,l)}\right)_k\Bigg], \quad 1 \le k \le N_K^e,
\end{aligned}
$$

where $\mathbb{F}^{(e,l)}$ is the flux matrix, of dimension $N_K^e \times N_F^{\sigma(e,l)}$

$$
\mathbb{F}^{(e,l)} = \left(\int_{\partial K_e^l} \varphi_i^e \psi_j^{\sigma(e,l)}\right)_{1 \le i \le N_e^K,\, 1 \le j \le N_F^{\sigma(e,l)}}.
$$

By setting $\boldsymbol{v} = \boldsymbol{\varphi}_{yk}^e = \begin{pmatrix} 0 \\ \varphi_k^e \\ 0 \end{pmatrix}$ and then $\boldsymbol{v} = \boldsymbol{\varphi}_{zk}^e = \begin{pmatrix} 0 \\ 0 \\ \varphi_k^e \end{pmatrix}$ for $1 \le k \le N_K^e$, in the first equation of (2.22) and following the same procedure for the second equation of (2.22), the discretization of the local equations can be written as,

$$
\begin{cases}
\mathrm{i}\omega\varepsilon_r\mathbb{M}^e\underline{E}_x^e - \mathbb{D}_z^e\underline{H}_y^e + \mathbb{D}_y^e\underline{H}_z^e + \displaystyle\sum_{l=1}^{|\nu_e|}\Big[\Big(n_z^{(e,l)}u_y^{\sigma(e,l)} - n_y^{(e,l)}u_z^{\sigma(e,l)}\Big)\mathbb{F}^{(e,l)}\underline{\Lambda}_{\boldsymbol{u}}^{\sigma(e,l)} \\
\qquad + \Big(n_z^{(e,l)}w_y^{\sigma(e,l)} - n_y^{(e,l)}w_z^{\sigma(e,l)}\Big)\mathbb{F}^{(e,l)}\underline{\Lambda}_{\boldsymbol{w}}^{\sigma(e,l)}\Big] = 0, \\
\mathrm{i}\omega\varepsilon_r\mathbb{M}^e\underline{E}_y^e + \mathbb{D}_z^e\underline{H}_x^e - \mathbb{D}_x^e\underline{H}_z^e + \displaystyle\sum_{l=1}^{|\nu_e|}\Big[\Big(n_x^{(e,l)}u_z^{\sigma(e,l)} - n_z^{(e,l)}u_x^{\sigma(e,l)}\Big)\mathbb{F}^{(e,l)}\underline{\Lambda}_{\boldsymbol{u}}^{\sigma(e,l)} \\
\qquad + \Big(n_x^{(e,l)}w_z^{\sigma(e,l)} - n_z^{(e,l)}w_x^{\sigma(e,l)}\Big)\mathbb{F}^{(e,l)}\underline{\Lambda}_{\boldsymbol{w}}^{\sigma(e,l)}\Big] = 0, \\
\mathrm{i}\omega\varepsilon_r\mathbb{M}^e\underline{E}_z^e - \mathbb{D}_y^e\underline{H}_x^e + \mathbb{D}_x^e\underline{H}_y^e + \displaystyle\sum_{l=1}^{|\nu_e|}\Big[\Big(n_y^{(e,l)}u_x^{\sigma(e,l)} - n_x^{(e,l)}u_y^{\sigma(e,l)}\Big)\mathbb{F}^{(e,l)}\underline{\Lambda}_{\boldsymbol{u}}^{\sigma(e,l)} \\
\qquad + \Big(n_y^{(e,l)}w_x^{\sigma(e,l)} - n_x^{(e,l)}w_y^{\sigma(e,l)}\Big)\mathbb{F}^{(e,l)}\underline{\Lambda}_{\boldsymbol{w}}^{\sigma(e,l)}\Big] = 0, \\
\mathrm{i}\omega\mu_r\mathbb{M}^e\underline{H}_x^e - (\mathbb{D}_z^e)^T\underline{E}_y^e + (\mathbb{D}_y^e)^T\underline{E}_z^e - \displaystyle\sum_{l=1}^{|\nu_e|}\tau^{(e,l)}\Big(u_x^{\sigma(e,l)}\mathbb{F}^{(e,l)}\underline{\Lambda}_{\boldsymbol{u}}^{\sigma(e,l)} + w_x^{\sigma(e,l)}\mathbb{F}^{(e,l)}\underline{\Lambda}_{\boldsymbol{w}}^{\sigma(e,l)}\Big) \\
\qquad + \displaystyle\sum_{l=1}^{|\nu_e|}\tau^{(e,l)}\Big[\Big(1-(n_x^{(e,l)})^2\Big)\mathbb{E}^{(e,l)}\underline{H}_x^e - n_x^{(e,l)}n_y^{(e,l)}\mathbb{E}^{(e,l)}\underline{H}_y^e - n_x^{(e,l)}n_z^{(e,l)}\mathbb{E}^{(e,l)}\underline{H}_z^e\Big] = 0, \\
\mathrm{i}\omega\mu_r\mathbb{M}^e\underline{H}_y^e + (\mathbb{D}_z^e)^T\underline{E}_x^e - (\mathbb{D}_x^e)^T\underline{E}_z^e - \displaystyle\sum_{l=1}^{|\nu_e|}\tau^{(e,l)}\Big(u_y^{\sigma(e,l)}\mathbb{F}^{(e,l)}\underline{\Lambda}_{\boldsymbol{u}}^{\sigma(e,l)} + w_y^{\sigma(e,l)}\mathbb{F}^{(e,l)}\underline{\Lambda}_{\boldsymbol{w}}^{\sigma(e,l)}\Big) \\
\qquad + \displaystyle\sum_{l=1}^{|\nu_e|}\tau^{(e,l)}\Big[\Big(1-(n_y^{(e,l)})^2\Big)\mathbb{E}^{(e,l)}\underline{H}_y^e - n_x^{(e,l)}n_y^{(e,l)}\mathbb{E}^{(e,l)}\underline{H}_x^e - n_y^{(e,l)}n_z^{(e,l)}\mathbb{E}^{(e,l)}\underline{H}_z^e\Big] = 0, \\
\mathrm{i}\omega\mu_r\mathbb{M}^e\underline{H}_z^e - (\mathbb{D}_y^e)^T\underline{E}_x^e + (\mathbb{D}_x^e)^T\underline{E}_y^e - \displaystyle\sum_{l=1}^{|\nu_e|}\tau^{(e,l)}\Big(u_z^{\sigma(e,l)}\mathbb{F}^{(e,l)}\underline{\Lambda}_{\boldsymbol{u}}^{\sigma(e,l)} + w_z^{\sigma(e,l)}\mathbb{F}^{(e,l)}\underline{\Lambda}_{\boldsymbol{w}}^{\sigma(e,l)}\Big) \\
\qquad + \displaystyle\sum_{l=1}^{|\nu_e|}\tau^{(e,l)}\Big[\Big(1-(n_z^{(e,l)})^2\Big)\mathbb{E}^{(e,l)}\underline{H}_z^e - n_x^{(e,l)}n_z^{(e,l)}\mathbb{E}^{(e,l)}\underline{H}_x^e - n_y^{(e,l)}n_z^{(e,l)}\mathbb{E}^{(e,l)}\underline{H}_y^e\Big] = 0,
\end{cases}
\tag{2.28}
$$

Where

$$
\mathbb{E}^{(e,l)} = \left(\int_{\partial K_e^l}\varphi_i^e\varphi_j^e\right)_{1\le i,j\le N_K^e},
$$

Now we can write the local linear system associated to the element K_e as

$$
\mathbb{A}^e\begin{bmatrix}\underline{E}_x^e\\ \underline{E}_y^e\\ \underline{E}_z^e\\ \underline{H}_x^e\\ \underline{H}_y^e\\ \underline{H}_z^e\end{bmatrix} + \sum_{l=1}^{|\nu_e|}\mathbb{C}^{(e,l)}\begin{bmatrix}\underline{\Lambda}_{\boldsymbol{u}}^{\sigma(e,l)}\\ \underline{\Lambda}_{\boldsymbol{w}}^{\sigma(e,l)}\end{bmatrix} = 0,
\tag{2.29}
$$

where

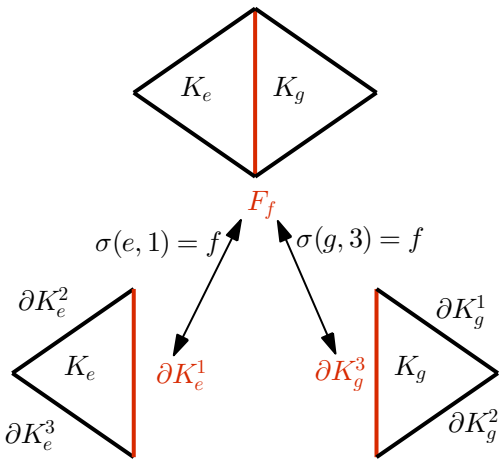

Figure 2.2 | Illustration presenting the notation of the faces

- $\mathbb{A}^e$ matrix of size $6N_K^e \times 6N_K^e$, defined by

$$\mathbb{A}^e = \begin{bmatrix} \mathrm{i}\omega\varepsilon_r\mathbb{M}^e & 0 & 0 & 0 & -\mathbb{D}_z^e & \mathbb{D}_y^e \\ 0 & \mathrm{i}\omega\varepsilon_r\mathbb{M}^e & 0 & \mathbb{D}_z^e & 0 & -\mathbb{D}_x^e \\ 0 & 0 & \mathrm{i}\omega\varepsilon_r\mathbb{M}^e & -\mathbb{D}_y^e & \mathbb{D}_x^e & 0 \\ 0 & -\left[\mathbb{D}_z^e\right]^T & \left[\mathbb{D}_y^e\right]^T & \mathrm{i}\omega\mu_r\mathbb{M}^e + \mathbb{E}_x^e & -\mathbb{E}_{xy}^e & -\mathbb{E}_{xz}^e \\ \left[\mathbb{D}_z^e\right]^T & 0 & -\left[\mathbb{D}_x^e\right]^T & -\mathbb{E}_{xy}^e & \mathrm{i}\omega\mu_r\mathbb{M}^e + \mathbb{E}_y^e & -\mathbb{E}_{yz}^e \\ -\left[\mathbb{D}_y^e\right]^T & \left[\mathbb{D}_x^e\right]^T & 0 & -\mathbb{E}_{xz}^e & -\mathbb{E}_{yz}^e & \mathrm{i}\omega\mu_r\mathbb{M}^e + \mathbb{E}_z^e \end{bmatrix},$$

with

$$\begin{cases} \mathbb{E}_\xi^e = \displaystyle\sum_{l=1}^{|\nu_e|} \tau^{(e,l)}((1-(n_\xi^{(e,l)})^2))\mathbb{E}^{(e,l)}, \\ \mathbb{E}_{\xi\zeta}^e = \displaystyle\sum_{l=1}^{|\nu_e|} \tau^{(e,l)} n_\xi^{(e,l)} n_\zeta^{(e,l)} \mathbb{E}^{(e,l)}, \end{cases} \qquad \xi, \zeta \in \{x, y, z\},$$

- $\mathbb{C}^{(e,l)}$ matrix of size $6N_K^e \times 2N_F^{\sigma(e,l)}$, defined by

$$\mathbb{C}^{(e,l)} = \begin{bmatrix} (n_z^{(e,l)} u_y^{\sigma(e,l)} - n_y^{(e,l)} u_z^{\sigma(e,l)})\mathbb{F}^{(e,l)} & (n_z^{(e,l)} w_y^{\sigma(e,l)} - n_y^{(e,l)} w_z^{\sigma(e,l)})\mathbb{F}^{(e,l)} \\ (n_x^{(e,l)} u_z^{\sigma(e,l)} - n_z^{(e,l)} u_x^{\sigma(e,l)})\mathbb{F}^{(e,l)} & (n_x^{(e,l)} w_z^{\sigma(e,l)} - n_z^{(e,l)} w_x^{\sigma(e,l)})\mathbb{F}^{(e,l)} \\ (n_y^{(e,l)} u_x^{\sigma(e,l)} - n_x^{(e,l)} u_y^{\sigma(e,l)})\mathbb{F}^{(e,l)} & (n_y^{(e,l)} w_x^{\sigma(e,l)} - n_x^{(e,l)} w_y^{\sigma(e,l)})\mathbb{F}^{(e,l)} \\ -\tau^{(e,l)} u_x^{\sigma(e,l)} \mathbb{F}^{(e,l)} & -\tau^{(e,l)} w_x^{\sigma(e,l)} \mathbb{F}^{(e,l)} \\ -\tau^{(e,l)} u_y^{\sigma(e,l)} \mathbb{F}^{(e,l)} & -\tau^{(e,l)} w_y^{\sigma(e,l)} \mathbb{F}^{(e,l)} \\ -\tau^{(e,l)} u_z^{\sigma(e,l)} \mathbb{F}^{(e,l)} & -\tau^{(e,l)} w_z^{\sigma(e,l)} \mathbb{F}^{(e,l)} \end{bmatrix}.$$

Discretisation of the global problem for Λ

Let $F_f \in \mathcal{F}_h^I$, the conservativity condition for F_f and for all $\boldsymbol{\eta} \in \boldsymbol{M}_h^{t,3}$

$$\begin{aligned} &\langle \boldsymbol{n} \times \boldsymbol{E}_h, \boldsymbol{\eta} \rangle_{\partial K_e^l} - \tau^{(e,l)} \langle \boldsymbol{n} \times (\boldsymbol{n} \times \boldsymbol{H}_h), \boldsymbol{\eta} \rangle_{\partial K_e^l} - \tau^{(e,l)} \langle \boldsymbol{\Lambda}_h, \boldsymbol{\eta} \rangle_{\partial K_e^l} \\ &+ \langle \boldsymbol{n} \times \boldsymbol{E}_h, \boldsymbol{\eta} \rangle_{\partial K_g^k} - \tau^{(g,k)} \langle \boldsymbol{n} \times (\boldsymbol{n} \times \boldsymbol{H}_h), \boldsymbol{\eta} \rangle_{\partial K_g^k} - \tau^{(g,k)} \langle \boldsymbol{\Lambda}_h, \boldsymbol{\eta} \rangle_{\partial K_g^k} = 0. \end{aligned} \tag{2.30}$$

For a boundary face $F_f \in \Gamma_a$, the conservativity condition for all $\boldsymbol{\eta} \in \boldsymbol{M}_h^{t,3}$

$$\langle \boldsymbol{n} \times \boldsymbol{E}_h, \boldsymbol{\eta} \rangle_{\partial K_e^l} - \tau^{(e,l)} \langle \boldsymbol{n} \times (\boldsymbol{n} \times \boldsymbol{H}_h), \boldsymbol{\eta} \rangle_{\partial K_e^l} - (1 + \tau^{(e,l)}) \langle \boldsymbol{\Lambda}_h, \boldsymbol{\eta} \rangle_{\partial K_e^l} = \langle \boldsymbol{g}^{inc}, \boldsymbol{\eta} \rangle_{\partial K_e^l} \tag{2.31}$$

For (2.30) we have

$$\begin{cases} \left(n_z^{(e,l)} u_y^{\sigma(e,l)} - n_y^{(e,l)} u_z^{\sigma(e,l)}\right) \left[\mathbb{F}^{(e,l)}\right]^T \underline{E}_x^e + \left(n_x^{(e,l)} u_z^{\sigma(e,l)} - n_z^{(e,l)} u_x^{\sigma(e,l)}\right) \left[\mathbb{F}^{(e,l)}\right]^T \underline{E}_y^e \\ + \left(n_z^{(e,l)} u_y^{\sigma(e,l)} - n_y^{(e,l)} u_z^{\sigma(e,l)}\right) \left[\mathbb{F}^{(e,l)}\right]^T \underline{E}_z^e + \tau^{(e,l)} u_x^{\sigma(e,l)} \left[\mathbb{F}^{(e,l)}\right]^T \underline{H}_x^e + \tau^{(e,l)} u_y^{\sigma(e,l)} \left[\mathbb{F}^{(e,l)}\right]^T \underline{H}_y^e \\ + \tau^{(e,l)} u_z^{\sigma(e,l)} \left[\mathbb{F}^{(e,l)}\right]^T \underline{H}_z^e - \tau^{(e,l)} \mathbb{G}^{(e,l)} \underline{\Lambda}_{\boldsymbol{u}}^{\sigma(e,l)} - \tau^{(e,l)} \left(\boldsymbol{u}^{\sigma(e,l)} \cdot \boldsymbol{w}^{\sigma(e,l)}\right) \mathbb{G}^{(e,l)} \underline{\Lambda}_{\boldsymbol{w}}^{\sigma(e,l)} + R_{\boldsymbol{u}}^{(g,k)} = 0, \\ \\ \left(n_z^{(e,l)} w_y^{\sigma(e,l)} - n_y^{(e,l)} w_z^{\sigma(e,l)}\right) \left[\mathbb{F}^{(e,l)}\right]^T \underline{E}_x^e + \left(n_x^{(e,l)} w_z^{\sigma(e,l)} - n_z^{(e,l)} w_x^{\sigma(e,l)}\right) \left[\mathbb{F}^{(e,l)}\right]^T \underline{E}_y^e \\ + \left(n_z^{(e,l)} w_y^{\sigma(e,l)} - n_y^{(e,l)} w_z^{\sigma(e,l)}\right) \left[\mathbb{F}^{(e,l)}\right]^T \underline{E}_z^e + \tau^{(e,l)} w_x^{\sigma(e,l)} \left[\mathbb{F}^{(e,l)}\right]^T \underline{H}_x^e + \tau^{(e,l)} w_y^{\sigma(e,l)} \left[\mathbb{F}^{(e,l)}\right]^T \underline{H}_y^e \\ + \tau^{(e,l)} w_z^{\sigma(e,l)} \left[\mathbb{F}^{(e,l)}\right]^T \underline{H}_z^e - \tau^{(e,l)} \left(\boldsymbol{u}^{\sigma(e,l)} \cdot \boldsymbol{w}^{\sigma(e,l)}\right) \mathbb{G}^{(e,l)} \underline{\Lambda}_{\boldsymbol{u}}^{\sigma(e,l)} - \tau^{(e,l)} \mathbb{G}^{(e,l)} \underline{\Lambda}_{\boldsymbol{w}}^{\sigma(e,l)} + R_{\boldsymbol{w}}^{(g,k)} = 0, \end{cases} \tag{2.32}$$

where

$$\mathbb{G}^{(e,l)} = \left(\int_{\partial K_e^l} \psi_i^{\sigma(e,l)} \psi_j^{\sigma(e,l)} \right)_{1 \le i,j \le N_F^{\sigma(e,l)}},$$

For (2.31) we have

$$\begin{cases} \left(n_z^{(e,l)} u_y^{\sigma(e,l)} - n_y^{(e,l)} u_z^{\sigma(e,l)}\right) \left[\mathbb{F}^{(e,l)}\right]^T \underline{E}_x^e + \left(n_x^{(e,l)} u_z^{\sigma(e,l)} - n_z^{(e,l)} u_x^{\sigma(e,l)}\right) \left[\mathbb{F}^{(e,l)}\right]^T \underline{E}_y^e \\ + \left(n_z^{(e,l)} u_y^{\sigma(e,l)} - n_y^{(e,l)} u_z^{\sigma(e,l)}\right) \left[\mathbb{F}^{(e,l)}\right]^T \underline{E}_z^e + \tau_x^{(e,l)} \left[\mathbb{F}^{(e,l)}\right]^T \underline{H}_x^e + \tau^{(e,l)} u_y^{\sigma(e,l)} \left[\mathbb{F}^{(e,l)}\right]^T \underline{H}_y^e \\ + \tau^{(e,l)} u_z^{\sigma(e,l)} \left[\mathbb{F}^{(e,l)}\right]^T \underline{H}_z^e - \left(1 + \tau^{(e,l)}\right) \mathbb{G}^{(e,l)} \underline{\Lambda}_{\boldsymbol{u}}^{\sigma(e,l)} - \left(1 + \tau^{(e,l)}\right) \left(\boldsymbol{u}^{\sigma(e,l)} \cdot \boldsymbol{w}^{\sigma(e,l)}\right) \mathbb{G}^{(e,l)} \underline{\Lambda}_{\boldsymbol{w}}^{\sigma(e,l)} \\ = \mathbb{G}^{(e,l)} \underline{\boldsymbol{g}}_{\boldsymbol{u}}^{\mathrm{inc},\sigma(e,l)}, \\ \\ \left(n_z^{(e,l)} w_y^{\sigma(e,l)} - n_y^{(e,l)} w_z^{\sigma(e,l)}\right) \left[\mathbb{F}^{(e,l)}\right]^T \underline{E}_x^e + \left(n_x^{(e,l)} w_z^{\sigma(e,l)} - n_z^{(e,l)} w_x^{\sigma(e,l)}\right) \left[\mathbb{F}^{(e,l)}\right]^T \underline{E}_y^e \\ + \left(n_z^{(e,l)} w_y^{\sigma(e,l)} - n_y^{(e,l)} w_z^{\sigma(e,l)}\right) \left[\mathbb{F}^{(e,l)}\right]^T \underline{E}_z^e + \tau^{(e,l)} w_x^{\sigma(e,l)} \left[\mathbb{F}^{(e,l)}\right]^T \underline{H}_x^e + \tau^{(e,l)} w_y^{\sigma(e,l)} \left[\mathbb{F}^{(e,l)}\right]^T \underline{H}_y^e \\ + \tau^{(e,l)} w_z^{\sigma(e,l)} \left[\mathbb{F}^{(e,l)}\right]^T \underline{H}_z^e - \left(1 + \tau^{(e,l)}\right) \left(\boldsymbol{u}^{\sigma(e,l)} \cdot \boldsymbol{w}^{\sigma(e,l)}\right) \mathbb{G}^{(e,l)} \underline{\Lambda}_{\boldsymbol{u}}^{\sigma(e,l)} - \left(1 + \tau^{(e,l)}\right) \mathbb{G}^{(e,l)} \underline{\Lambda}_{\boldsymbol{w}}^{\sigma(e,l)} \\ = \mathbb{G}^{(e,l)} \underline{\boldsymbol{g}}_{\boldsymbol{w}}^{\mathrm{inc},\sigma(e,l)}, \end{cases} \tag{2.33}$$

with

$$\underline{\boldsymbol{g}}_{\boldsymbol{\nu}}^{\mathrm{inc},\sigma(e,l)} = \left[\underline{\boldsymbol{g}}_{\boldsymbol{\nu}}^{\mathrm{inc},\sigma(e,l)}[1], \cdots, \underline{\boldsymbol{g}}_{\boldsymbol{\nu}}^{\mathrm{inc},\sigma(e,l)}[N_F^{\sigma(e,l)}] \right]^T, \ \boldsymbol{\nu} \in \{\boldsymbol{u}, \boldsymbol{w}\}.$$

We define a matrix $\mathcal{A}_{HDG}^e$ of size

$$\sum_{l=1}^{|\nu_e|} 2N_F^{\sigma(e,l)} \times \sum_{f=1}^{|\mathcal{F}_h|} 2N_F^f,$$

such that

$$\mathcal{A}_{HDG}^e \, \underline{\Lambda} = \left[\underline{\Lambda}^{\sigma(e,1)}, \cdots, \underline{\Lambda}^{\sigma(e,|\nu_e|)} \right]^T.$$

Adding all equations involving interior faces (2.32) and every boundary face (2.33) element-by-element we have

$$\sum_{e=1}^{|\mathcal{T}_h|} [\mathcal{A}^e_{HDG}]^T \left(\mathbb{B}^e \underline{W}^e + \mathbb{G}^e \mathcal{A}^e_{HDG} \underline{\Lambda}\right) = \sum_{e=1}^{|\mathcal{T}_h|} [\mathcal{A}^e_{HDG}]^T \underline{\boldsymbol{g}}^e, \tag{2.34}$$

where

- $\underline{W}^e$ the column vector of size $6N_K^e$, defined by $\underline{W}^e = \left[\underline{E}^e_x, \underline{E}^e_y, \underline{E}^e_z, \underline{H}^e_x, \underline{H}^e_y, \underline{H}^e_z\right]^T$,
- $\mathbb{B}^e$ the matrix of size $\sum_{l=1}^{|\nu_e|} 2N_F^{\sigma(e,l)} \times 6N_K^e$, defined by

  $\mathbb{B}^e =$

$$\begin{bmatrix} \mathbb{F}^{(e,1)}_{zy,u} & \mathbb{F}^{(e,1)}_{xz,u} & \mathbb{F}^{(e,1)}_{yx,u} & \tau^{(e,1)} u_x^{\sigma(e,1)} \left[\mathbb{F}^{(e,1)}\right]^T & \tau^{(e,1)} u_y^{\sigma(e,1)} \left[\mathbb{F}^{(e,1)}\right]^T & \tau^{(e,1)} u_z^{\sigma(e,1)} \left[\mathbb{F}^{(e,1)}\right]^T \\ \mathbb{F}^{(e,1)}_{zy,w} & \mathbb{F}^{(e,1)}_{xz,w} & \mathbb{F}^{(e,1)}_{yx,w} & \tau^{(e,1)} w_x^{\sigma(e,1)} \left[\mathbb{F}^{(e,1)}\right]^T & \tau^{(e,1)} w_y^{\sigma(e,1)} \left[\mathbb{F}^{(e,1)}\right]^T & \tau^{(e,1)} w_z^{\sigma(e,1)} \left[\mathbb{F}^{(e,1)}\right]^T \\ \mathbb{F}^{(e,2)}_{zy,u} & \mathbb{F}^{(e,2)}_{xz,u} & \mathbb{F}^{(e,2)}_{yx,u} & \tau^{(e,2)} u_x^{\sigma(e,2)} \left[\mathbb{F}^{(e,2)}\right]^T & \tau^{(e,2)} u_y^{\sigma(e,2)} \left[\mathbb{F}^{(e,2)}\right]^T & \tau^{(e,2)} u_z^{\sigma(e,2)} \left[\mathbb{F}^{(e,2)}\right]^T \\ \cdots & \cdots & \cdots & \cdots & \cdots & \cdots \\ \mathbb{F}^{(e,|\nu_e|)}_{zy,w} & \mathbb{F}^{(e,|\nu_e|)}_{xz,w} & \mathbb{F}^{(e,|\nu_e|)}_{yx,w} & \tau^{(e,|\nu_e|)} w_x^{\sigma(e,|\nu_e|)} \left[\mathbb{F}^{(e,|\nu_e|)}\right]^T & \tau^{(e,|\nu_e|)} w_y^{\sigma(e,|\nu_e|)} \left[\mathbb{F}^{(e,|\nu_e|)}\right]^T & \tau^{(e,|\nu_e|)} w_z^{\sigma(e,|\nu_e|)} \left[\mathbb{F}^{(e,|\nu_e|)}\right]^T \end{bmatrix},$$

  with

$$\mathbb{F}^{(e,l)}_{\xi\zeta,\nu} = \left(n_\xi^{(e,l)} \nu_\zeta^{\sigma(e,l)} - n_\zeta^{(e,l)} \nu_\xi^{\sigma(e,l)}\right) \left[\mathbb{F}^{(e,l)}\right]^T, \ l = 1, \cdots, |\nu_e|, \ \xi, \zeta \in \{x, y, z\}, \ \nu \in \{u, w\},$$

- $\mathbb{G}^e$ the matrix of size $\sum_{l=1}^{|\nu_e|} 2N_F^{\sigma(e,l)} \times \sum_{l=1}^{|\nu_e|} 2N_F^{\sigma(e,l)}$, defined by

$$\mathbb{G}^e = \begin{bmatrix} -\kappa^{(e,1)}\mathbb{G}^{(e,1)} & -\kappa^{(e,1)}(\boldsymbol{u}^{\sigma(e,1)} \cdot \boldsymbol{w}^{\sigma(e,1)})\mathbb{G}^{(e,1)} & \cdots & 0 \\ -\kappa^{(e,1)}(\boldsymbol{u}^{\sigma(e,1)} \cdot \boldsymbol{w}^{\sigma(e,1)})\mathbb{G}^{(e,1)} & -\kappa^{(e,1)}\mathbb{G}^{(e,1)} & \cdots & 0 \\ \cdots & \cdots & \cdots & \cdots \\ 0 & 0 & \cdots & -\kappa^{(e,|\nu_e|)}(\boldsymbol{u}^{\sigma(e,|\nu_e|)} \cdot \boldsymbol{w}^{\sigma(e,|\nu_e|)})\mathbb{G}^{(e,|\nu_e|)} \\ 0 & 0 & \cdots & -\kappa^{(e,|\nu_e|)}\mathbb{G}^{(e,|\nu_e|)} \end{bmatrix},$$

  with

$$\kappa^{(e,l)} = \begin{cases} \tau^{(e,l)}, \text{ if the face } F_{\sigma(e,l)} \in \mathcal{F}_h \setminus \Gamma_a, \\ 1 + \tau^{(e,l)}, \text{ if the face } F_{\sigma(e,l)} \in \mathcal{F}_h^B \cap \Gamma_a, \end{cases} \quad l = 1, \cdots, |\nu_e|,$$

- $\underline{\boldsymbol{g}}^e$ the column vector of size $\sum_{l=1}^{|\nu_e|} 2N_F^{\sigma(e,l)}$, defined by

$$\underline{\boldsymbol{g}}^e = \left[\underline{\boldsymbol{g}}^{\sigma(e,1)}, \cdots, \underline{\boldsymbol{g}}^{\sigma(e,|\nu_e|)}\right]^T \text{ with } \underline{\boldsymbol{g}}^{\sigma(e,l)} = \left[\underline{\boldsymbol{g}}_{\boldsymbol{u}}^{\sigma(e,l)}, \underline{\boldsymbol{g}}_{\boldsymbol{w}}^{\sigma(e,l)}\right]^T, l = 1, \cdots, |\nu_e|,$$

  where

$$\underline{\boldsymbol{g}}^{\sigma(e,l)} = \begin{cases} \mathbb{G}^{(e,l)} \underline{\boldsymbol{g}}_{\boldsymbol{u}}^{\sigma(e,l)} \\ \mathbb{G}^{(e,l)} \underline{\boldsymbol{g}}_{\boldsymbol{w}}^{\sigma(e,l)} \end{cases} \text{ and } \underline{\boldsymbol{g}}_{\boldsymbol{\nu}}^{\sigma(e,l)} = \begin{cases} 0 & \text{if } F_{\sigma(e,l)} \in \mathcal{F}_h \setminus \Gamma_a \\ \underline{\boldsymbol{g}}_{\boldsymbol{\nu}}^{\text{inc},\sigma(e,l)} & \text{if } F_{\sigma(e,l)} \in \mathcal{F}_h^B \cap \Gamma_a \end{cases} \quad \boldsymbol{\nu} \in \{\boldsymbol{u}, \boldsymbol{w}\}.$$

Now we can rewrite the equation for the local solver (2.29) as

$$\mathbb{A}^e \underline{W}^e + \mathbb{C}^e \mathcal{A}^e_{HDG} \underline{\Lambda} = 0, \tag{2.35}$$

where $\mathbb{C}^e$ is the matrix of size $6N_K^e \times \sum_{l=1}^{|\nu_e|} N_F^{\sigma(e,l)}$, defined by $\mathbb{C}^e = \left[\mathbb{C}^{(e,1)} \quad \cdots \quad \mathbb{C}^{(e,|\nu_e|)}\right]$.
Finally we substitute $\underline{W}^e$ by the solution of the local system (2.35) in to obtain (2.34)

$$\left[\sum_{e=1}^{|\mathcal{T}_h|} \left[\mathcal{A}_{HDG}^e\right]^T \left(-\mathbb{B}^e \left[\mathbb{A}^e\right]^{-1} \mathbb{C}^e + \mathbb{G}^e\right) \mathcal{A}_{HDG}^e\right] \underline{\Lambda} = \sum_{e=1}^{|\mathcal{T}_h|} \left[\mathcal{A}_{HDG}^e\right]^T \underline{\boldsymbol{g}}^e.$$

Thus we write the following linear system for the global trace $\underline{\Lambda}$

$$\mathbb{K}\underline{\Lambda} = \underline{\boldsymbol{g}}, \tag{2.36}$$

where

- $\mathbb{K}$ the matrix of size $\sum_{f=1}^{|\mathcal{F}_h|} 2N_F^f \times \sum_{f=1}^{|\mathcal{F}_h|} 2N_F^f$, defined by

$$\mathbb{K} = \sum_{e=1}^{|\mathcal{T}_h|} \left[\mathcal{A}_{HDG}^e\right]^T \mathbb{K}^e \mathcal{A}_{HDG}^e = \sum_{e=1}^{|\mathcal{T}_h|} \left[\mathcal{A}_{HDG}^e\right]^T \left(\mathbb{G}^e - \mathbb{B}^e \left[\mathbb{A}^e\right]^{-1} \mathbb{C}^e\right) \mathcal{A}_{HDG}^e,$$

- $\underline{\boldsymbol{g}}$ the column vector $\sum_{f=1}^{|\mathcal{F}_h|} 2N_F^f$, defined by $\underline{\boldsymbol{g}} = \sum_{e=1}^{|\mathcal{T}_h|} \left[\mathcal{A}_{HDG}^e\right]^T \underline{\boldsymbol{g}}^e$.

2.5 HDG method for the 3D time-domain Maxwell's equations with a fully implicit time discretization

2.5.1 Introduction

In this section, we are considering the 3D time-domain Maxwell's equations with a hybrid discontinuous Galerkin (HDG) space discretization where we have to choose a specific time discretization to obtain the fully discrete scheme. The interest of HDGTD methods with respect to those of DGTD, turns out with an implicit time integration. This is what has been done in [43] whose results are recalled in this section. We rewrote the proofs of that paper with some clarifications, then we elaborate all the details in the implementation of the fully discrete scheme with a Cranck-Nicholson time integration and finally rewrote the same test case used in this paper to show the interest of using the HDG method compared to a classical DG discretization. Note that the definitions of the hybrid variable and numerical trace are exactly those adopted in the context of the formulation of HDG methods for the 3D time-harmonic Maxwell equations 2.4.

2.5.2 Problem statement

We consider the system of 3D time-domain Maxwell's equations on a bounded polyhedral domain $\Omega \subset \mathbb{R}^3$

Time-domain Maxwell's equations

$$\begin{cases} \varepsilon \partial_t \boldsymbol{E} - \mathbf{curl}\, \boldsymbol{H} = -\boldsymbol{J}, \text{ in } \Omega \times [0,T], \\ \mu \partial_t \boldsymbol{H} + \mathbf{curl}\, \boldsymbol{E} = 0, \text{ in } \Omega \times [0,T], \end{cases} \tag{2.37}$$

where the symbol ∂_t denotes a time derivate, $\boldsymbol{J}$ the current density, T a final time, $\boldsymbol{E}(\boldsymbol{x},t)$ and $\boldsymbol{H}(\boldsymbol{x},t)$ are the electric and magnetic fields. The relative dielectric permittivity ε and the relative magnetic permeability μ are varying in space, time-invariant and both strictly positive functions. The boundary of Ω is defined as $\partial\Omega = \Gamma_m \cup \Gamma_a$ with $\Gamma_m \cap \Gamma_a = \emptyset$. The boundary conditions are the same as in the frequency-domain (2.15).

Boundary conditions

$$\begin{cases} \boldsymbol{n} \times \boldsymbol{E} = 0, \text{ on } \Gamma_m \times [0,T], \\ \boldsymbol{n} \times \boldsymbol{E} + \boldsymbol{n} \times (\boldsymbol{n} \times \boldsymbol{H}) = \boldsymbol{n} \times \boldsymbol{E}^{\text{inc}} + \boldsymbol{n} \times (\boldsymbol{n} \times \boldsymbol{H}^{\text{inc}}) \\ \qquad\qquad\qquad\qquad\qquad\qquad = \boldsymbol{g}^{\text{inc}}, \text{ on } \Gamma_a \times [0,T]. \end{cases}$$

Here $\boldsymbol{n}$ denotes the unit outward normal to $\partial\Omega$ and $(\boldsymbol{E}^{\text{inc}}, \boldsymbol{H}^{\text{inc}})$ a given incident field. The first boundary condition is often referred as a metallic boundary condition and is applied on a perfectly conducting surface. The second relation is an absorbing boundary condition and takes here the form of the Silver-Müller condition. It is applied on a surface corresponding to an artificial truncature of a theoretically unbounded propagation domain. Finally, the system is supplemented with initial conditions: $\boldsymbol{E}_0(\boldsymbol{x}) = \boldsymbol{E}(\boldsymbol{x},0)$ and $\boldsymbol{H}_0(\boldsymbol{x}) = \boldsymbol{H}(\boldsymbol{x},0)$. For sake of simplicity, we omit the volume source term $\boldsymbol{J}$ in what follows.

2.5.3 Global formulation

Following the classical DG approach, approximate solutions $(\boldsymbol{E}_h, \boldsymbol{H}_h)$, for all $t \in [0,T]$, are seeked in the space $\boldsymbol{V}_h^3 \times \boldsymbol{V}_h^3$ satisfying for all K in $\mathcal{T}_h$

$$\begin{cases} (\varepsilon \partial_t \boldsymbol{E}_h, \boldsymbol{v})_K - (\mathbf{curl}\, \boldsymbol{H}_h, \boldsymbol{v})_K = 0, \ \forall \boldsymbol{v} \in \boldsymbol{V}_h^3, \\ (\mu \partial_t \boldsymbol{H}_h, \boldsymbol{v})_K + (\mathbf{curl}\, \boldsymbol{E}_h, \boldsymbol{v})_K = 0, \ \forall \boldsymbol{v} \in \boldsymbol{V}_h^3. \end{cases} \tag{2.38}$$

Applying Green's formula, on both equations of (2.38) introduces boundary terms which are replaced by numerical traces $\hat{\boldsymbol{E}}_h$ and $\hat{\boldsymbol{H}}_h$ in order to ensure the connection between element-wise solutions and global consistency of the discretization. This leads to the formulation for all $t \in [0,T]$

$$\begin{cases} (\varepsilon \partial_t \boldsymbol{E}_h, \boldsymbol{v})_K - (\boldsymbol{H}_h, \mathbf{curl}\, \boldsymbol{v})_K + \left\langle \hat{\boldsymbol{H}}_h, \boldsymbol{n} \times \boldsymbol{v} \right\rangle_{\partial K} = 0, \ \forall \boldsymbol{v} \in \boldsymbol{V}_h^3, \\ (\mu \partial_t \boldsymbol{H}_h, \boldsymbol{v})_K + (\boldsymbol{E}_h, \mathbf{curl}\, \boldsymbol{v})_K - \left\langle \hat{\boldsymbol{E}}_h, \boldsymbol{n} \times \boldsymbol{v} \right\rangle_{\partial K} = 0, \ \forall \boldsymbol{v} \in \boldsymbol{V}_h^3. \end{cases} \tag{2.39}$$

It is straightforward to verify that $\boldsymbol{n} \times \boldsymbol{v} = \boldsymbol{n} \times \boldsymbol{v}^t$ and $< \boldsymbol{H}, \boldsymbol{n} \times \boldsymbol{v} >= - < \boldsymbol{n} \times \boldsymbol{H}, \boldsymbol{v} >$. Therefore, using numerical traces defined in terms of the tangential components $\hat{\boldsymbol{H}}_h^t$ and $\hat{\boldsymbol{E}}_h^t$, we can rewrite

(2.39) as

$$\begin{cases} (\varepsilon\partial_t \boldsymbol{E}_h, \boldsymbol{v})_K - (\boldsymbol{H}_h, \mathbf{curl}\,\boldsymbol{v})_K + \left\langle \hat{\boldsymbol{H}}_h^t, \boldsymbol{n}\times\boldsymbol{v}\right\rangle_{\partial K} = 0,\ \forall \boldsymbol{v}\in \boldsymbol{V}_h^3, \\ (\mu\partial_t \boldsymbol{H}_h, \boldsymbol{v})_K + (\boldsymbol{E}_h, \mathbf{curl}\,\boldsymbol{v})_K - \left\langle \hat{\boldsymbol{E}}_h^t, \boldsymbol{n}\times\boldsymbol{v}\right\rangle_{\partial K} = 0,\ \forall \boldsymbol{v}\in \boldsymbol{V}_h^3. \end{cases} \tag{2.40}$$

The hybrid variable $\boldsymbol{\Lambda}_h$ is here defined for all the interfaces of $\mathcal{F}_h$ as

$$\boldsymbol{\Lambda}_h := \hat{\boldsymbol{H}}_h^t, \quad \forall F\in\mathcal{F}_h. \tag{2.41}$$

We want to determine the fields $\hat{\boldsymbol{H}}_h^t$ and $\hat{\boldsymbol{E}}_h^t$ in each element K of $\mathcal{T}_h$ by solving system (2.40) and assuming that $\boldsymbol{\Lambda}_h$ is known on all the faces of an element K. We consider a numerical trace $\hat{\boldsymbol{E}}_h^t$ for all K given by

$$\hat{\boldsymbol{E}}_h^t = \boldsymbol{E}_h^t + \tau_K \boldsymbol{n}\times(\boldsymbol{\Lambda}_h - \boldsymbol{H}_h^t) \text{ on } \partial K, \tag{2.42}$$

where τ_K is a local stabilization parameter which is assumed to be strictly positive. We recall that $\boldsymbol{n}\times\boldsymbol{H}_h^t = \boldsymbol{n}\times\boldsymbol{H}_h$. Note that the definitions of the hybrid variable (2.41) and numerical trace (2.42) are exactly those adopted in the context of the formulation of HDG methods for the 3D time-harmonic Maxwell equations 2.4. Summing the contributions of (2.40) over all the elements and enforcing the continuity of the tangential component of $\hat{\boldsymbol{E}}_h$, we can formulate a problem which is to find $(\boldsymbol{E}_h, \boldsymbol{H}_h, \boldsymbol{\Lambda}_h)\in \boldsymbol{V}_h^3\times\boldsymbol{V}_h^3\times\boldsymbol{M}_h^{t,3}$ such that for all t in $[0,T]$

HDG formulation 1

$$\begin{aligned} (\varepsilon\partial_t \boldsymbol{E}_h, \boldsymbol{v})_{\mathcal{T}_h} - (\boldsymbol{H}_h, \mathbf{curl}\,\boldsymbol{v})_{\mathcal{T}_h} + \langle \boldsymbol{\Lambda}_h, \boldsymbol{n}\times\boldsymbol{v}\rangle_{\partial\mathcal{T}_h} &= 0,\ \forall \boldsymbol{v}\in\boldsymbol{V}_h^3, \\ (\mu\partial_t \boldsymbol{H}_h, \boldsymbol{v})_{\mathcal{T}_h} + (\boldsymbol{E}_h, \mathbf{curl}\,\boldsymbol{v})_{\mathcal{T}_h} - \left\langle \hat{\boldsymbol{E}}_h^t, \boldsymbol{n}\times\boldsymbol{v}\right\rangle_{\partial\mathcal{T}_h} &= 0,\ \forall \boldsymbol{v}\in\boldsymbol{V}_h^3, \\ \left\langle [\![\hat{\boldsymbol{E}}_h]\!], \boldsymbol{\eta}\right\rangle_{\mathcal{F}_h} - \langle \boldsymbol{\Lambda}_h, \boldsymbol{\eta}\rangle_{\Gamma_a} - \langle \boldsymbol{g}^{\text{inc}}, \boldsymbol{\eta}\rangle_{\Gamma_a} &= 0,\ \forall \boldsymbol{\eta}\in\boldsymbol{M}_h^{t,3}, \end{aligned} \tag{2.43}$$

where the last equation is called the conservativity condition with which we ask the tangential component of $\hat{\boldsymbol{E}}_h$ to be weakly continuous across any interface between two neighboring elements. With the definition of the numerical trace (2.42) and after applying a Green formula on the second equation of (2.43), we can get for all t $\in [0,T]$

HDG formulation 2

$$\begin{cases} (\varepsilon\partial_t \boldsymbol{E}_h, \boldsymbol{v})_{\mathcal{T}_h} - (\boldsymbol{H}_h, \mathbf{curl}\,\boldsymbol{v})_{\mathcal{T}_h} + \langle \boldsymbol{\Lambda}_h, \boldsymbol{n}\times\boldsymbol{v}\rangle_{\partial\mathcal{T}_h} = 0,\ \forall \boldsymbol{v}\in\boldsymbol{V}_h^3, \\ (\mu\partial_t \boldsymbol{H}_h, \boldsymbol{v})_{\mathcal{T}_h} + (\mathbf{curl}\,\boldsymbol{E}_h, \boldsymbol{v})_{\mathcal{T}_h} + \langle \tau\boldsymbol{n}\times(\boldsymbol{H}_h - \boldsymbol{\Lambda}_h), \boldsymbol{n}\times\boldsymbol{v}\rangle_{\partial\mathcal{T}_h} = 0,\ \forall \boldsymbol{v}\in\boldsymbol{V}_h^3, \\ \langle \boldsymbol{n}\times\boldsymbol{E}_h, \boldsymbol{\eta}\rangle_{\partial\mathcal{T}_h} + \langle \tau(\boldsymbol{H}_h^t - \boldsymbol{\Lambda}_h), \boldsymbol{\eta}\rangle_{\partial\mathcal{T}_h} - \langle \boldsymbol{\Lambda}_h, \boldsymbol{\eta}\rangle_{\Gamma_a} = \langle \boldsymbol{g}^{\text{inc}}, \boldsymbol{\eta}\rangle_{\Gamma_a},\ \forall \boldsymbol{\eta}\in\boldsymbol{M}_h^{t,3}. \end{cases} \tag{2.44}$$

2.5.4 Semi-discrete stability when $\Gamma_a = \emptyset$

We introduce the energy function defined on $[0,T]$ by

The electromagnetic energy

$$\mathcal{E}_h(t) = \frac{1}{2}\left(\varepsilon||\boldsymbol{E}_h(t)||^2 + \mu||\boldsymbol{H}_h(t)||^2\right).$$

Theorem 1. *For all $\tau > 0$ the energy function $\mathcal{E}_h(t)$ decreases in time and $\mathcal{E}_h(t) \leq \mathcal{E}_h(0)$ for all $t > 0$.*

Proof. Taking $\boldsymbol{v} = \boldsymbol{E}_h(t)$ in the first equation, $\boldsymbol{v} = \boldsymbol{H}_h(t)$ in the second equation and $\boldsymbol{\eta} = \boldsymbol{\Lambda}_h$ in the third equation of (2.44) we obtain

$$\begin{cases} (\varepsilon\partial_t\boldsymbol{E}_h, \boldsymbol{E}_h)_{\mathcal{T}_h} - (\boldsymbol{H}_h, \mathbf{curl}\,\boldsymbol{E}_h)_{\mathcal{T}_h} + \langle\boldsymbol{\Lambda}_h, \boldsymbol{n}\times\boldsymbol{E}_h\rangle_{\partial\mathcal{T}_h} = 0, \\ (\mu\partial_t\boldsymbol{H}_h, \boldsymbol{H}_h)_{\mathcal{T}_h} + (\mathbf{curl}\,\boldsymbol{E}_h, \boldsymbol{H}_h)_{\mathcal{T}_h} + \langle\tau\boldsymbol{n}\times(\boldsymbol{H}_h - \boldsymbol{\Lambda}_h), \boldsymbol{n}\times\boldsymbol{H}_h\rangle_{\partial\mathcal{T}_h} = 0, \\ \langle\boldsymbol{n}\times\boldsymbol{E}_h, \boldsymbol{\Lambda}_h\rangle_{\partial\mathcal{T}_h} + \left\langle\tau\left(\boldsymbol{H}_h^t - \boldsymbol{\Lambda}_h\right), \boldsymbol{\Lambda}_h\right\rangle_{\partial\mathcal{T}_h} = 0. \end{cases}$$

By the formula $\partial_t||\boldsymbol{v}||^2 = 2\left(\partial_t\boldsymbol{v}, \boldsymbol{v}\right)$ and after summing the first two equations of the above system we obtain

$$\frac{1}{2}\frac{d}{dt}\left(\varepsilon||\boldsymbol{E}_h(t)||^2 + \mu||\boldsymbol{H}_h(t)||^2\right) = -\langle\boldsymbol{\Lambda}_h, \boldsymbol{n}\times\boldsymbol{E}_h\rangle_{\partial\mathcal{T}_h} - \langle\tau\boldsymbol{n}\times(\boldsymbol{H}_h - \boldsymbol{\Lambda}_h), \boldsymbol{n}\times\boldsymbol{H}_h\rangle_{\partial\mathcal{T}_h}.$$

The third equation gives us that

$$-\langle\boldsymbol{\Lambda}_h, \boldsymbol{n}\times\boldsymbol{E}_h\rangle_{\partial\mathcal{T}_h} = \left\langle\tau\left(\boldsymbol{H}_h^t - \boldsymbol{\Lambda}_h\right), \boldsymbol{\Lambda}_h\right\rangle_{\partial\mathcal{T}_h} = \langle\tau\boldsymbol{n}\times(\boldsymbol{H}_h - \boldsymbol{\Lambda}_h), \boldsymbol{n}\times\boldsymbol{\Lambda}_h\rangle_{\partial\mathcal{T}_h},$$

implies that

$$\frac{1}{2}\frac{d}{dt}\left(\varepsilon||\boldsymbol{E}_h(t)||^2 + \mu||\boldsymbol{H}_h(t)||^2\right) = -\langle\tau\boldsymbol{n}\times(\boldsymbol{H}_h - \boldsymbol{\Lambda}_h), \boldsymbol{n}\times(\boldsymbol{H}_h - \boldsymbol{\Lambda}_h)\rangle_{\partial\mathcal{T}_h} \leq 0,$$

since $\tau > 0$. Thus the energy function $\mathcal{E}_h(t)$ decreases in time and $\mathcal{E}_h(t) \leq \mathcal{E}_h(0)$, for all $t > 0$. This result shows the L^2-stability of the semi-discrete method. In particular, this method is dissipative for the considered numerical trace for $\hat{\boldsymbol{E}}_h^t$ in (2.42). □

2.5.5 Time integration

The system of equations (2.44) can be written in the form of a differential algebraic equation (DAE) such as

$$F(\boldsymbol{E}_h(t), \boldsymbol{H}_h(t), \boldsymbol{\Lambda}_h(t)) = 0, \tag{2.45}$$

while F is defined for all $\boldsymbol{v}$ in $\boldsymbol{V}_h^3$ and for all $\boldsymbol{\eta}$ in $\boldsymbol{M}_h^{t,3}$ by

$$\begin{bmatrix} (\varepsilon\partial_t\boldsymbol{E}_h, \boldsymbol{v})_{\mathcal{T}_h} - (\boldsymbol{H}_h, \mathbf{curl}\,\boldsymbol{v})_{\mathcal{T}_h} + \langle\boldsymbol{\Lambda}_h, \boldsymbol{n}\times\boldsymbol{v}\rangle_{\partial\mathcal{T}_h} \\ (\mu\partial_t\boldsymbol{H}_h, \boldsymbol{v})_{\mathcal{T}_h} + (\mathbf{curl}\,\boldsymbol{E}_h, \boldsymbol{v})_{\mathcal{T}_h} + \langle\tau\boldsymbol{n}\times(\boldsymbol{H}_h - \boldsymbol{\Lambda}_h), \boldsymbol{n}\times\boldsymbol{v}\rangle_{\partial\mathcal{T}_h} \\ \langle\boldsymbol{n}\times\boldsymbol{E}_h, \boldsymbol{\eta}\rangle_{\partial\mathcal{T}_h} + \left\langle\tau\left(\boldsymbol{H}_h^t - \boldsymbol{\Lambda}_h\right), \boldsymbol{\eta}\right\rangle_{\partial\mathcal{T}_h} - \langle\boldsymbol{\Lambda}_h, \boldsymbol{\eta}\rangle_{\Gamma_a} - \left\langle\boldsymbol{g}^{\mathrm{inc}}, \boldsymbol{\eta}\right\rangle_{\Gamma_a} \end{bmatrix}$$

As detailed in [44], the defined system is considered as a semi-explicit DAE, where the third equation of (2.45) is called *algebraic equation* and is considered as a constraint on the global system. The idea here is to transform the DAE into an ODE which can be straightforward solved using numerical methods. As a first step, the perturbation problem is considered as for all $t \in [0, T]$

Perturbation problem

$$\begin{cases} (\varepsilon\partial_t \boldsymbol{E}_h, \boldsymbol{v})_{\mathcal{T}_h} - (\boldsymbol{H}_h, \mathbf{curl}\,\boldsymbol{v})_{\mathcal{T}_h} + \langle \boldsymbol{\Lambda}_h, \boldsymbol{n}\times\boldsymbol{v}\rangle_{\partial\mathcal{T}_h} = 0,\ \forall \boldsymbol{v}\in \boldsymbol{V}_h^3, \\ (\mu\partial_t \boldsymbol{H}_h, \boldsymbol{v})_{\mathcal{T}_h} + (\mathbf{curl}\,\boldsymbol{E}_h, \boldsymbol{v})_{\mathcal{T}_h} + \langle \tau\boldsymbol{n}\times(\boldsymbol{H}_h - \boldsymbol{\Lambda}_h), \boldsymbol{n}\times\boldsymbol{v}\rangle_{\partial\mathcal{T}_h} = 0,\ \forall \boldsymbol{v}\in \boldsymbol{V}_h^3, \\ \gamma\partial_t\boldsymbol{\Lambda}_h + \langle \boldsymbol{n}\times\boldsymbol{E}_h, \boldsymbol{\eta}\rangle_{\partial\mathcal{T}_h} + \left\langle \tau\left(\boldsymbol{H}_h^t - \boldsymbol{\Lambda}_h\right), \boldsymbol{\eta}\right\rangle_{\partial\mathcal{T}_h} - \langle \boldsymbol{\Lambda}_h, \boldsymbol{\eta}\rangle_{\Gamma_a} = \left\langle \boldsymbol{g}^{\text{inc}}, \boldsymbol{\eta}\right\rangle_{\Gamma_a},\ \forall \boldsymbol{\eta}\in \boldsymbol{M}_h^{t,3}. \end{cases} \tag{2.46}$$

where $0 < \gamma << 1$.

Now, the problem can be discretized in time. A sequence of time steps is considered as

$$0 = t^0 < t^1 \cdots < t^n = T.$$

For $0 \le n \le N-1$, $\left(\boldsymbol{E}_h^{n+1}, \boldsymbol{H}_h^{n+1}, \boldsymbol{\Lambda}_h^{n+1}\right)$ is denoted by the numerical approximations to $\left(\boldsymbol{E}_h\left(t^{n+1}\right), \boldsymbol{H}_h\left(t^{n+1}\right), \boldsymbol{\Lambda}_h\left(t^{n+1}\right)\right)$ at time $t^{n+1} = (n+1)\Delta t$. Using Cranck-Nicolson scheme on each equation of (2.46), the obtained system is written as,

find $(\boldsymbol{E}_h^{n+1}, \boldsymbol{H}_h^{n+1}, \boldsymbol{\Lambda}_h^{n+1}) \in \boldsymbol{V}_h^3 \times \boldsymbol{V}_h^3 \times \boldsymbol{M}_h^{t,3}$ such as

$$\begin{cases} \left(\bar{\varepsilon}\boldsymbol{E}_h^{n+1}, \boldsymbol{v}\right)_{\mathcal{T}_h} - \left(\boldsymbol{H}_h^{n+1}, \mathbf{curl}\,\boldsymbol{v}\right)_{\mathcal{T}_h} + \left\langle \boldsymbol{\Lambda}_h^{n+1}, \boldsymbol{n}\times\boldsymbol{v}\right\rangle_{\partial\mathcal{T}_h} = \boldsymbol{b}_E,\ \forall \boldsymbol{v}\in \boldsymbol{V}_h, \\ \left(\bar{\mu}\boldsymbol{H}_h^{n+1}, \boldsymbol{v}\right)_{\mathcal{T}_h} + \left(\mathbf{curl}\,\boldsymbol{E}_h^{n+1}, \boldsymbol{v}\right)_{\mathcal{T}_h} + \left\langle \tau\boldsymbol{n}\times\left(\boldsymbol{H}_h^{n+1} - \boldsymbol{\Lambda}_h^{n+1}\right), \boldsymbol{n}\times\boldsymbol{v}\right\rangle_{\partial\mathcal{T}_h} = \boldsymbol{b}_H,\ \forall \boldsymbol{v}\in \boldsymbol{V}_h, \\ \frac{2\gamma}{\Delta t}\left(\boldsymbol{\Lambda}_h^{n+1} - \boldsymbol{\Lambda}_h^n\right) + \left\langle \boldsymbol{n}\times\boldsymbol{E}_h^{n+1}, \boldsymbol{\eta}\right\rangle_{\partial\mathcal{T}_h} + \left\langle \tau\left(\boldsymbol{H}_h^{t,n+1} - \boldsymbol{\Lambda}_h^{n+1}\right), \boldsymbol{\eta}\right\rangle_{\partial\mathcal{T}_h} - \left\langle \boldsymbol{\Lambda}_h^{n+1}, \boldsymbol{\eta}\right\rangle_{\Gamma_a} = \boldsymbol{b}_\Lambda,\ \forall \boldsymbol{\eta}\in \boldsymbol{M}_h^{t,3}. \end{cases} \tag{2.47}$$

Where

- $\bar{\varepsilon} = \frac{2\varepsilon}{\Delta t}$, $\bar{\mu} = \frac{2\mu}{\Delta t}$
- $\boldsymbol{b}_E = (\bar{\varepsilon}\boldsymbol{E}_h^n, \boldsymbol{v})_{\mathcal{T}_h} + (\boldsymbol{H}_h^n, \mathbf{curl}\,\boldsymbol{v})_{\mathcal{T}_h} - \langle \boldsymbol{\Lambda}_h^n, \boldsymbol{n}\times\boldsymbol{v}\rangle_{\partial\mathcal{T}_h}$
- $\boldsymbol{b}_H = (\bar{\mu}\boldsymbol{H}_h^n, \boldsymbol{v})_{\mathcal{T}_h} - (\mathbf{curl}\,\boldsymbol{E}_h^n, \boldsymbol{v})_{\mathcal{T}_h} - \langle \tau\boldsymbol{n}\times(\boldsymbol{H}_h^n - \boldsymbol{\Lambda}_h^n), \boldsymbol{n}\times\boldsymbol{v}\rangle_{\partial\mathcal{T}_h}$
- $\boldsymbol{b}_\Lambda = -\langle \boldsymbol{n}\times\boldsymbol{E}_h^n, \boldsymbol{\eta}\rangle_{\partial\mathcal{T}_h} - \left\langle \tau\left(\boldsymbol{H}_h^{t,n} - \boldsymbol{\Lambda}_h^n\right), \boldsymbol{\eta}\right\rangle_{\partial\mathcal{T}_h} + \left\langle \boldsymbol{\Lambda}_h^n + \boldsymbol{g}^{inc,n} + \boldsymbol{g}^{inc,n+1}, \boldsymbol{\eta}\right\rangle_{\Gamma_a}$

By the DAE theory

$$\lim_{\gamma\to 0}\frac{2\gamma}{\Delta t}\left(\boldsymbol{\Lambda}_h^{n+1} - \boldsymbol{\Lambda}_h^n\right) = 0.$$

Then, the system is finally given by

HDG Cranck-Nicolson scheme

$$\begin{cases} \left(\bar{\varepsilon}\boldsymbol{E}_h^{n+1}, \boldsymbol{v}\right)_{\mathcal{T}_h} - \left(\boldsymbol{H}_h^{n+1}, \mathbf{curl}\,\boldsymbol{v}\right)_{\mathcal{T}_h} + \left\langle \boldsymbol{\Lambda}_h^{n+1}, \boldsymbol{n}\times\boldsymbol{v}\right\rangle_{\partial\mathcal{T}_h} = \boldsymbol{b}_E,\ \forall \boldsymbol{v}\in \boldsymbol{V}_h^3, \\ \left(\bar{\mu}\boldsymbol{H}_h^{n+1}, \boldsymbol{v}\right)_{\mathcal{T}_h} + \left(\mathbf{curl}\,\boldsymbol{E}_h^{n+1}, \boldsymbol{v}\right)_{\mathcal{T}_h} + \left\langle \tau\boldsymbol{n}\times\left(\boldsymbol{H}_h^{n+1} - \boldsymbol{\Lambda}_h^{n+1}\right), \boldsymbol{n}\times\boldsymbol{v}\right\rangle_{\partial\mathcal{T}_h} = \boldsymbol{b}_H,\ \forall \boldsymbol{v}\in \boldsymbol{V}_h^3, \\ \left\langle \boldsymbol{n}\times\boldsymbol{E}_h^{n+1}, \boldsymbol{\eta}\right\rangle_{\partial\mathcal{T}_h} + \left\langle \tau\left(\boldsymbol{H}_h^{t,n+1} - \boldsymbol{\Lambda}_h^{n+1}\right), \boldsymbol{\eta}\right\rangle_{\partial\mathcal{T}_h} - \left\langle \boldsymbol{\Lambda}_h^{n+1}, \boldsymbol{\eta}\right\rangle_{\Gamma_a} = \boldsymbol{b}_\Lambda,\ \forall \boldsymbol{\eta}\in \boldsymbol{M}_h^{t,3}. \end{cases} \tag{2.48}$$

2.5.6 Well-posedness of the local solver

Definition 1. *For $\boldsymbol{\alpha} \in \boldsymbol{M}_h^{t,3}$, $(\boldsymbol{E}_h^\alpha, \boldsymbol{H}_h^\alpha)$ denotes the approximate solution at time $n+1$ whose restriction to an element $K \in \mathcal{T}_h$ is the solution to the local problem*

$$\begin{aligned} (\bar{\varepsilon}\boldsymbol{E}_h^\alpha, \boldsymbol{v}_1)_K - (\boldsymbol{H}_h^\alpha, \mathbf{curl}\, \boldsymbol{v}_1)_K + \langle \boldsymbol{\alpha}, \boldsymbol{n} \times \boldsymbol{v}_1 \rangle_{\partial K} &= \boldsymbol{b}_E, \ \forall \boldsymbol{v}_1 \in \boldsymbol{V}_h^3, \\ (\bar{\mu}\boldsymbol{H}_h^\alpha, \boldsymbol{v}_2)_K + (\mathbf{curl}\, \boldsymbol{E}_h^\alpha, \boldsymbol{v}_2)_K + \langle \tau \boldsymbol{n} \times (\boldsymbol{H}_h^\alpha - \boldsymbol{\alpha}), \boldsymbol{n} \times \boldsymbol{v}_2 \rangle_{\partial K} &= \boldsymbol{b}_H, \ \forall \boldsymbol{v}_2 \in \boldsymbol{V}_h^3. \end{aligned} \tag{2.49}$$

Theorem 2. *For $\boldsymbol{\alpha} \in \boldsymbol{M}_h^{t,3}$, there exists a unique solution $(\boldsymbol{E}_h^\alpha, \boldsymbol{H}_h^\alpha) \in \boldsymbol{V}_h^3 \times \boldsymbol{V}_h^3$ for the local solver (2.49) .*

Proof. Summing the two equations of (2.49), we obtain for all $(\boldsymbol{v}_1, \boldsymbol{v}_2) \in \boldsymbol{V}_h^3 \times \boldsymbol{V}_h^3$,

$$\begin{aligned} &(\bar{\varepsilon}\boldsymbol{E}_h^\alpha, \boldsymbol{v}_1)_K - (\boldsymbol{H}_h^\alpha, \mathbf{curl}\, \boldsymbol{v}_1)_K + \langle \boldsymbol{\alpha}, \boldsymbol{n} \times \boldsymbol{v}_1 \rangle_{\partial K} \\ &+ (\bar{\mu}\boldsymbol{H}_h^\alpha, \boldsymbol{v}_2)_K + (\mathbf{curl}\, \boldsymbol{E}_h^\alpha, \boldsymbol{v}_2)_K + \langle \tau \boldsymbol{n} \times (\boldsymbol{H}_h^\alpha - \boldsymbol{\alpha}), \boldsymbol{n} \times \boldsymbol{v}_2 \rangle_{\partial K} = \boldsymbol{b}_E + \boldsymbol{b}_H \end{aligned}$$

Since α is fixed, all the terms containing α will be moved to the right hand side to obtain

$$\mathcal{A}_h(\boldsymbol{E}_h^\alpha, \boldsymbol{H}_h^\alpha; \boldsymbol{v}_1, \boldsymbol{v}_2) = \mathcal{L}(\boldsymbol{v}_1, \boldsymbol{v}_2) \quad \forall (\boldsymbol{v}_1, \boldsymbol{v}_2) \in \boldsymbol{V}_h^3 \times \boldsymbol{V}_h^3, \tag{2.50}$$

where

$$\begin{aligned} \mathcal{A}_h(\boldsymbol{E}_h^\alpha, \boldsymbol{H}_h^\alpha; \boldsymbol{v}_1, \boldsymbol{v}_2) = &(\bar{\varepsilon}\boldsymbol{E}_h^\alpha, \boldsymbol{v}_1)_K - (\boldsymbol{H}_h^\alpha, \mathbf{curl}\, \boldsymbol{v}_1)_K \\ &+ (\bar{\mu}\boldsymbol{H}_h^\alpha, \boldsymbol{v}_2)_K + (\mathbf{curl}\, \boldsymbol{E}_h^\alpha, \boldsymbol{v}_2)_K + \langle \tau \boldsymbol{n} \times \boldsymbol{H}_h^\alpha, \boldsymbol{n} \times \boldsymbol{v}_2 \rangle_{\partial K}, \end{aligned}$$

and

$$\mathcal{L}(\boldsymbol{v}_1, \boldsymbol{v}_2) = \boldsymbol{b}_E + \boldsymbol{b}_H - \langle \boldsymbol{\alpha}, \boldsymbol{n} \times \boldsymbol{v}_1 \rangle_{\partial K} + \langle \tau \boldsymbol{n} \times \alpha, \boldsymbol{n} \times \boldsymbol{v}_2 \rangle_{\partial K}.$$

Since $\boldsymbol{V}_h^3$ is a finite dimensional space, proving the existence and the uniqueness of the solution for (2.50) requires proving the injectivity of $\mathcal{A}_h$. To do so, we will set $\boldsymbol{v}_1 = \boldsymbol{E}_h^\alpha$ and $\boldsymbol{v}_2 = \boldsymbol{H}_h^\alpha$ to obtain

$$\mathcal{A}_h(\boldsymbol{E}_h^\alpha, \boldsymbol{H}_h^\alpha; \boldsymbol{E}_h^\alpha, \boldsymbol{H}_h^\alpha) = (\bar{\varepsilon}\boldsymbol{E}_h^\alpha, \boldsymbol{E}_h^\alpha)_K + (\bar{\mu}\boldsymbol{H}_h^\alpha, \boldsymbol{H}_h^\alpha)_K + \langle \tau \boldsymbol{n} \times \boldsymbol{H}_h^\alpha, \boldsymbol{n} \times \boldsymbol{H}_h^\alpha \rangle_{\partial K}.$$

Assuming that $\tau > 0$, and since $\bar{\varepsilon}$ and $\bar{\mu}$ are strictly positive real numbers, the last equation implies that $\mathcal{A}_h(\boldsymbol{E}_h^\alpha, \boldsymbol{H}_h^\alpha; \boldsymbol{E}_h^\alpha, \boldsymbol{H}_h^\alpha) = 0 \Rightarrow \boldsymbol{E}_h^\alpha = \boldsymbol{H}_h^\alpha = 0$ on K, so $\mathcal{A}_h$ is injective and we have a unique solution for the local solver (2.49). □

2.5.7 Characterization of the reduced problem

Theorem 3. *If we assume $\tau > 0$, then the implicit HDGTD method (2.48) has a unique solution $\left(\boldsymbol{E}_h^{\boldsymbol{\Lambda}_h}, \boldsymbol{H}_h^{\boldsymbol{\Lambda}_h}, \boldsymbol{\Lambda}_h\right)$ for any time iteration $n \geq 1$.*

Proof. For all $\boldsymbol{\eta} \in \boldsymbol{M}_h^{t,3}$, we set

- $\boldsymbol{v} = \boldsymbol{E}_h^{\boldsymbol{\eta}}$ in the first equation of (2.48),
- $\boldsymbol{v} = \boldsymbol{H}_h^{\boldsymbol{\eta}}$ in the second equation of (2.48),

and we obtain

$$\begin{cases} \left(\bar{\varepsilon}\boldsymbol{E}_h^{\boldsymbol{\Lambda}_h}, \boldsymbol{E}_h^{\boldsymbol{\eta}}\right)_{\mathcal{T}_h} - \left(\boldsymbol{H}_h^{\boldsymbol{\Lambda}_h}, \mathbf{curl}\, \boldsymbol{E}_h^{\boldsymbol{\eta}}\right)_{\mathcal{T}_h} + \left\langle \boldsymbol{\Lambda}_h, \boldsymbol{n} \times \boldsymbol{E}_h^{\boldsymbol{\eta}} \right\rangle_{\partial\mathcal{T}_h} = \boldsymbol{b}_E, \\ \left(\bar{\mu}\boldsymbol{H}_h^{\boldsymbol{\Lambda}_h}, \boldsymbol{H}_h^{\boldsymbol{\eta}}\right)_{\mathcal{T}_h} + \left(\mathbf{curl}\, \boldsymbol{E}_h^{\boldsymbol{\Lambda}_h}, \boldsymbol{H}_h^{\boldsymbol{\eta}}\right)_{\mathcal{T}_h} + \left\langle \tau\boldsymbol{n} \times \left(\boldsymbol{H}_h^{\boldsymbol{\Lambda}_h} - \boldsymbol{\Lambda}_h\right), \boldsymbol{n} \times \boldsymbol{H}_h^{\boldsymbol{\eta}} \right\rangle_{\partial\mathcal{T}_h} = \boldsymbol{b}_H. \\ \left\langle \boldsymbol{n} \times \boldsymbol{E}_h^{\boldsymbol{\Lambda}_h}, \boldsymbol{\eta} \right\rangle_{\partial\mathcal{T}_h} + \left\langle \tau\boldsymbol{n} \times \left(\boldsymbol{H}_h^{\boldsymbol{\Lambda}_h} - \boldsymbol{\Lambda}_h\right), \boldsymbol{n} \times \boldsymbol{\eta} \right\rangle_{\partial\mathcal{T}_h} - \left\langle \boldsymbol{\Lambda}_h, \boldsymbol{\eta} \right\rangle_{\Gamma_a} = \boldsymbol{b}_\Lambda, \end{cases}$$

Summing the first two equations and substracting the result from the third equation, we obtain

$$\mathcal{A}_h\left(\boldsymbol{\Lambda}_h, \boldsymbol{\eta}\right) = \mathcal{L}(\boldsymbol{\eta}), \quad \forall \boldsymbol{\eta} \in \boldsymbol{M}_h^{t,3}, \tag{2.51}$$

where,

$$\begin{aligned} \mathcal{A}_h\left(\boldsymbol{\Lambda}_h, \boldsymbol{\eta}\right) = & \left(\bar{\varepsilon}\boldsymbol{E}_h^{\boldsymbol{\Lambda}_h}, \boldsymbol{E}_h^{\boldsymbol{\eta}}\right)_{\mathcal{T}_h} - \left(\boldsymbol{H}_h^{\boldsymbol{\Lambda}_h}, \mathbf{curl}\, \boldsymbol{E}_h^{\boldsymbol{\eta}}\right)_{\mathcal{T}_h} + \left\langle \boldsymbol{\Lambda}_h, \boldsymbol{n} \times \boldsymbol{E}_h^{\boldsymbol{\eta}} \right\rangle_{\partial\mathcal{T}_h} \\ & + \left(\bar{\mu}\boldsymbol{H}_h^{\boldsymbol{\Lambda}_h}, \boldsymbol{H}_h^{\boldsymbol{\eta}}\right)_{\mathcal{T}_h} + \left(\mathbf{curl}\, \boldsymbol{E}_h^{\boldsymbol{\Lambda}_h}, \boldsymbol{H}_h^{\boldsymbol{\eta}}\right)_{\mathcal{T}_h} + \left\langle \tau\boldsymbol{n} \times \left(\boldsymbol{H}_h^{\boldsymbol{\Lambda}_h} - \boldsymbol{\Lambda}_h\right), \boldsymbol{n} \times \left(\boldsymbol{H}_h^{\boldsymbol{\eta}} - \boldsymbol{\eta}\right) \right\rangle_{\partial\mathcal{T}_h} \\ & - \left\langle \boldsymbol{n} \times \boldsymbol{E}_h^{\boldsymbol{\Lambda}_h}, \boldsymbol{\eta} \right\rangle_{\partial\mathcal{T}_h} + \left\langle \boldsymbol{\Lambda}_h, \boldsymbol{\eta} \right\rangle_{\Gamma_a}, \end{aligned}$$

and

$$\mathcal{L}(\boldsymbol{\eta}) = \boldsymbol{b}_E + \boldsymbol{b}_H - \boldsymbol{b}_\Lambda.$$

Since $\boldsymbol{M}_h^{t,3}$ is a finite dimensional space, proving the existence and the uniqueness of the solution requires proving the injectivity of $\mathcal{A}_h$. To do so, we must show that the kernel of $\mathcal{A}_h$ is null.

$$\mathcal{A}_h\left(\boldsymbol{\Lambda}_h, \boldsymbol{\Lambda}_h\right) = \bar{\varepsilon}\left\|\boldsymbol{E}_h^{\boldsymbol{\Lambda}_h}\right\|_{\mathcal{T}_h}^2 + \bar{\mu}\left\|\boldsymbol{H}_h^{\boldsymbol{\Lambda}_h}\right\|_{\mathcal{T}_h}^2 + \left\|\tau\boldsymbol{n} \times \left(\boldsymbol{H}_h^{\boldsymbol{\Lambda}_h} - \boldsymbol{\Lambda}_h\right)\right\|_{\partial\mathcal{T}_h}^2 + \|\boldsymbol{\Lambda}_h\|_{\Gamma_a}^2 = 0$$

implies that all the terms are zero since $\bar{\varepsilon} = \bar{\mu} = \tau > 0$.
The first two terms give us that $\boldsymbol{E}_h^{\boldsymbol{\Lambda}_h} = \boldsymbol{H}_h^{\boldsymbol{\Lambda}_h} = 0$ while the third and the fourth terms gives us that $\boldsymbol{\Lambda}_h = 0$ on $\partial\mathcal{T}_h$ and on Γ_a, so $\boldsymbol{\Lambda}_h = 0$ everywhere. □

2.5.8 Energy variation and unconditional stability when $\Gamma_a = \emptyset$

The total discrete electromagnetic energy in $\mathcal{T}_h$ at time t^n is given by

The total discrete electromagnetic energy

$$\mathcal{E}_h^n = \frac{1}{2}\left(\bar{\varepsilon}||\boldsymbol{E}_h^n||^2 + \bar{\mu}||\boldsymbol{H}_h^n||^2\right).$$

Lemma 1. *The total discrete electromagnetic energy defined above is non-increasing in time i.e $\mathcal{E}^{n+1} \leq \mathcal{E}^n$. Then, the totally discretized problem (2.48) is unconditionally stable.*

Proof. Choosing

- $\boldsymbol{v} = \dfrac{\boldsymbol{E}_h^{n+1} + \boldsymbol{E}_h^n}{2} \in \boldsymbol{V}_h^3$ in the first equation of (2.48)

- $\boldsymbol{v} = \dfrac{\boldsymbol{H}_h^{n+1} + \boldsymbol{H}_h^n}{2} \in \boldsymbol{V}_h^3$ in the second equation of (2.48)

and summing the two equations we obtain

$$\begin{aligned}
&\frac{1}{2}\left(\bar{\varepsilon}||\boldsymbol{E}_h^{n+1}||^2 + \bar{\mu}||\boldsymbol{H}_h^{n+1}||^2\right) + \left\langle \boldsymbol{\Lambda}_h^{n+1}, \boldsymbol{n} \times \left(\frac{\boldsymbol{E}_h^{n+1} + \boldsymbol{E}_h^n}{2}\right)\right\rangle_{\partial\mathcal{T}_h} \\
&+ \left\langle \tau \boldsymbol{n} \times \left(\boldsymbol{H}_h^{n+1} - \boldsymbol{\Lambda}_h^{n+1}\right), \boldsymbol{n} \times \left(\frac{\boldsymbol{H}_h^{n+1} + \boldsymbol{H}_h^n}{2}\right)\right\rangle \\
&= \frac{1}{2}\left(\bar{\varepsilon}||\boldsymbol{E}_h^{n}||^2 + \bar{\mu}||\boldsymbol{H}_h^{n}||^2\right) - \left\langle \boldsymbol{\Lambda}_h^{n}, \boldsymbol{n} \times \left(\frac{\boldsymbol{E}_h^{n+1} + \boldsymbol{E}_h^n}{2}\right)\right\rangle_{\partial\mathcal{T}_h} \\
&- \left\langle \tau \boldsymbol{n} \times \left(\boldsymbol{H}_h^{n} - \boldsymbol{\Lambda}_h^{n}\right), \boldsymbol{n} \times \left(\frac{\boldsymbol{H}_h^{n+1} + \boldsymbol{H}_h^n}{2}\right)\right\rangle.
\end{aligned}$$

From the last equation, we can see that the energy variation is given by

$$\begin{aligned}
\mathcal{E}_h^{n+1} - \mathcal{E}_h^n = &- \left\langle \left(\boldsymbol{\Lambda}_h^{n+1} + \boldsymbol{\Lambda}_h^n\right), \boldsymbol{n} \times \left(\frac{\boldsymbol{E}_h^{n+1} + \boldsymbol{E}_h^n}{2}\right)\right\rangle_{\partial\mathcal{T}_h} \\
&- \left\langle \tau \boldsymbol{n} \times \left(\boldsymbol{H}_h^{n+1} + \boldsymbol{H}_h^n\right), \boldsymbol{n} \times \left(\frac{\boldsymbol{H}_h^{n+1} + \boldsymbol{H}_h^n}{2}\right)\right\rangle_{\partial\mathcal{T}_h} \\
&+ \left\langle \tau \boldsymbol{n} \times \left(\boldsymbol{\Lambda}_h^{n+1} + \boldsymbol{\Lambda}_h^n\right), \boldsymbol{n} \times \left(\frac{\boldsymbol{H}_h^{n+1} + \boldsymbol{H}_h^n}{2}\right)\right\rangle_{\partial\mathcal{T}_h}.
\end{aligned}$$

Taking now $\eta = \left(\boldsymbol{\Lambda}_h^{n+1} + \boldsymbol{\Lambda}_h^n\right) \in \boldsymbol{M}_h^{t,3}$ in the third equation of (2.48), we obtain

$$\begin{aligned}
\left\langle \boldsymbol{n} \times \left(\frac{\boldsymbol{E}_h^{n+1} + \boldsymbol{E}_h^n}{2}\right), \boldsymbol{\Lambda}_h^{n+1} + \boldsymbol{\Lambda}_h^n\right\rangle_{\partial\mathcal{T}_h} = &- \left\langle \tau \boldsymbol{n} \times \left(\boldsymbol{\Lambda}_h^{n+1} + \boldsymbol{\Lambda}_h^n\right), \boldsymbol{n} \times \left(\frac{\boldsymbol{H}_h^{n+1} + \boldsymbol{H}_h^n}{2}\right)\right\rangle_{\partial\mathcal{T}_h} \\
&+ \tau \left\|\boldsymbol{n} \times \left(\boldsymbol{\Lambda}_h^{n+1} + \boldsymbol{\Lambda}_h^n\right)\right\|^2
\end{aligned}$$

We can deduce that

$$\begin{aligned}
\mathcal{E}_h^{n+1} - \mathcal{E}_h^n = &\left\langle \tau \boldsymbol{n} \times \left(\boldsymbol{\Lambda}_h^{n+1} + \boldsymbol{\Lambda}_h^n\right), \boldsymbol{n} \times \left(\boldsymbol{H}_h^{n+1} + \boldsymbol{H}_h^n\right)\right\rangle_{\partial\mathcal{T}_h} \\
&- \frac{\tau}{2}\left\|\boldsymbol{n} \times \left(\boldsymbol{H}_h^{n+1} + \boldsymbol{H}_h^n\right)\right\|^2 - \tau\left\|\boldsymbol{n} \times \left(\boldsymbol{\Lambda}_h^{n+1} + \boldsymbol{\Lambda}_h^n\right)\right\|^2.
\end{aligned}$$

Since

$$\left\langle \tau \boldsymbol{n} \times \left(\boldsymbol{\Lambda}_h^{n+1} + \boldsymbol{\Lambda}_h^n\right), \boldsymbol{n} \times \left(\boldsymbol{H}_h^{n+1} + \boldsymbol{H}_h^n\right)\right\rangle_{\partial\mathcal{T}_h} \leq \frac{\tau}{2}\left\|\boldsymbol{n} \times \left(\boldsymbol{H}_h^{n+1} + \boldsymbol{H}_h^n\right)\right\|^2 + \frac{\tau}{2}\left\|\boldsymbol{n} \times \left(\boldsymbol{\Lambda}_h^{n+1} + \boldsymbol{\Lambda}_h^n\right)\right\|^2,$$

finally we obtain

$$\mathcal{E}_h^{n+1} - \mathcal{E}_h^n \leq -\frac{\tau}{2}\left\|\boldsymbol{n} \times \left(\boldsymbol{\Lambda}_h^{n+1} + \boldsymbol{\Lambda}_h^n\right)\right\|^2 \leq 0.$$

□

2.5.9 Implementation

Following the same notations of section 2.4.4, we develop the HDG formulation presented in (2.48) for the Maxwell's equations with a Cranck-Nicholson time discretization.

Discretization of the local equations

For the right hand side we have

- $$b_{E,1} = \bar{\varepsilon}\mathbb{M}^e \underline{E}_x^{n,e} + \mathbb{D}_z^e \underline{H}_y^{n,e} - \mathbb{D}_y^e \underline{H}_z^{n,e} - \sum_{l=1}^{|\nu_e|} \Big[\Big(n_z^{(e,l)} u_y^{\sigma(e,l)} - n_y^{(e,l)} u_z^{\sigma(e,l)} \Big) \mathbb{F}^{(e,l)} \underline{\Lambda}_{\boldsymbol{u}}^{n,\sigma(e,l)} + \Big(n_z^{(e,l)} w_y^{\sigma(e,l)} - n_y^{(e,l)} w_z^{\sigma(e,l)} \Big) \mathbb{F}^{(e,l)} \underline{\Lambda}_{\boldsymbol{w}}^{n,\sigma(e,l)} \Big]$$

- $$b_{E,2} = \bar{\varepsilon}\mathbb{M}^e \underline{E}_y^{n,e} - \mathbb{D}_z^e \underline{H}_x^{n,e} + \mathbb{D}_x^e \underline{H}_z^{n,e} - \sum_{l=1}^{|\nu_e|} \Big[\Big(n_x^{(e,l)} u_z^{\sigma(e,l)} - n_z^{(e,l)} u_x^{\sigma(e,l)} \Big) \mathbb{F}^{(e,l)} \underline{\Lambda}_{\boldsymbol{u}}^{n,\sigma(e,l)} + \Big(n_x^{(e,l)} w_z^{\sigma(e,l)} - n_z^{(e,l)} w_x^{\sigma(e,l)} \Big) \mathbb{F}^{(e,l)} \underline{\Lambda}_{\boldsymbol{w}}^{n,\sigma(e,l)} \Big]$$

- $$b_{E,3} = \bar{\varepsilon}\mathbb{M}^e \underline{E}_z^{n,e} + \mathbb{D}_y^e \underline{H}_x^{n,e} - \mathbb{D}_x^e \underline{H}_y^{n,e} - \sum_{l=1}^{|\nu_e|} \Big[\Big(n_y^{(e,l)} u_x^{\sigma(e,l)} - n_x^{(e,l)} u_y^{\sigma(e,l)} \Big) \mathbb{F}^{(e,l)} \underline{\Lambda}_{\boldsymbol{u}}^{n,\sigma(e,l)} + \Big(n_y^{(e,l)} w_x^{\sigma(e,l)} - n_x^{(e,l)} w_y^{\sigma(e,l)} \Big) \mathbb{F}^{(e,l)} \underline{\Lambda}_{\boldsymbol{w}}^{n,\sigma(e,l)} \Big]$$

- $$b_{H,1} = \bar{\mu}\mathbb{M}^e \underline{H}_x^{n,e} + (\mathbb{D}_z^e)^T \underline{E}_y^{n,e} - (\mathbb{D}_y^e)^T \underline{E}_z^{n,e} + \sum_{l=1}^{|\nu_e|} \tau^{(e,l)} \Big(u_x^{\sigma(e,l)} \mathbb{F}^{(e,l)} \underline{\Lambda}_{\boldsymbol{u}}^{n,\sigma(e,l)} + w_x^{\sigma(e,l)} \mathbb{F}^{(e,l)} \underline{\Lambda}_{\boldsymbol{w}}^{n,\sigma(e,l)} \Big) - \sum_{l=1}^{|\nu_e|} \tau^{(e,l)} \Big[\Big(1 - (n_x^{(e,l)})^2 \Big) \mathbb{E}^{(e,l)} \underline{H}_x^{n,e} - n_x^{(e,l)} n_y^{(e,l)} \mathbb{E}^{(e,l)} \underline{H}_y^{n,e} - n_x^{(e,l)} n_z^{(e,l)} \mathbb{E}^{(e,l)} \underline{H}_z^{n,e} \Big]$$

- $$b_{H,2} = \bar{\mu}\mathbb{M}^e \underline{H}_y^{n,e} - (\mathbb{D}_z^e)^T \underline{E}_x^{n,e} + (\mathbb{D}_x^e)^T \underline{E}_z^{n,e} + \sum_{l=1}^{|\nu_e|} \tau^{(e,l)} \Big(u_y^{\sigma(e,l)} \mathbb{F}^{(e,l)} \underline{\Lambda}_{\boldsymbol{u}}^{n,\sigma(e,l)} + w_y^{\sigma(e,l)} \mathbb{F}^{(e,l)} \underline{\Lambda}_{\boldsymbol{w}}^{n,\sigma(e,l)} \Big) - \sum_{l=1}^{|\nu_e|} \tau^{(e,l)} \Big[\Big(1 - (n_y^{(e,l)})^2 \Big) \mathbb{E}^{(e,l)} \underline{H}_y^{n,e} - n_x^{(e,l)} n_y^{(e,l)} \mathbb{E}^{(e,l)} \underline{H}_x^{n,e} - n_y^{(e,l)} n_z^{(e,l)} \mathbb{E}^{(e,l)} \underline{H}_z^{n,e} \Big]$$

- $$b_{H,3} = \bar{\mu}\mathbb{M}^e \underline{H}_z^{n,e} + (\mathbb{D}_y^e)^T \underline{E}_x^{n,e} - (\mathbb{D}_x^e)^T \underline{E}_y^{n,e} + \sum_{l=1}^{|\nu_e|} \tau^{(e,l)} \Big(u_z^{\sigma(e,l)} \mathbb{F}^{(e,l)} \underline{\Lambda}_{\boldsymbol{u}}^{n,\sigma(e,l)} + w_z^{\sigma(e,l)} \mathbb{F}^{(e,l)} \underline{\Lambda}_{\boldsymbol{w}}^{n,\sigma(e,l)} \Big) - \sum_{l=1}^{|\nu_e|} \tau^{(e,l)} \Big[\Big(1 - (n_z^{(e,l)})^2 \Big) \mathbb{E}^{(e,l)} \underline{H}_z^{n,e} - n_x^{(e,l)} n_z^{(e,l)} \mathbb{E}^{(e,l)} \underline{H}_x^{n,e} - n_y^{(e,l)} n_z^{(e,l)} \mathbb{E}^{(e,l)} \underline{H}_y^{n,e} \Big].$$

For the left hand side we have

$$
\begin{cases}
\bar{\varepsilon}\mathbb{M}^e \underline{E}_x^{n+1,e} - \mathbb{D}_z^e \underline{H}_y^{n+1,e} + \mathbb{D}_y^e \underline{H}_z^{n+1,e} \\
+ \sum_{l=1}^{|\nu_e|} \Big[\Big(n_z^{(e,l)} u_y^{\sigma(e,l)} - n_y^{(e,l)} u_z^{\sigma(e,l)} \Big) \mathbb{F}^{(e,l)} \underline{\Lambda}_{\boldsymbol{u}}^{n+1,\sigma(e,l)} \\
+ \Big(n_z^{(e,l)} w_y^{\sigma(e,l)} - n_y^{(e,l)} w_z^{\sigma(e,l)} \Big) \mathbb{F}^{(e,l)} \underline{\Lambda}_{\boldsymbol{w}}^{n+1,\sigma(e,l)} \Big] = b_{E,1}, \\
\\
\bar{\varepsilon}\mathbb{M}^e \underline{E}_y^{n+1,e} + \mathbb{D}_z^e \underline{H}_x^{n+1,e} - \mathbb{D}_x^e \underline{H}_z^{n+1,e} \\
+ \sum_{l=1}^{|\nu_e|} \Big[\Big(n_x^{(e,l)} u_z^{\sigma(e,l)} - n_z^{(e,l)} u_x^{\sigma(e,l)} \Big) \mathbb{F}^{(e,l)} \underline{\Lambda}_{\boldsymbol{u}}^{n+1,\sigma(e,l)} \\
+ \Big(n_x^{(e,l)} w_z^{\sigma(e,l)} - n_z^{(e,l)} w_x^{\sigma(e,l)} \Big) \mathbb{F}^{(e,l)} \underline{\Lambda}_{\boldsymbol{w}}^{n+1,\sigma(e,l)} \Big] = b_{E,2} \\
\\
\bar{\varepsilon}\mathbb{M}^e \underline{E}_z^{n+1,e} - \mathbb{D}_y^e \underline{H}_x^{n+1,e} + \mathbb{D}_x^e \underline{H}_y^{n+1,e} \\
+ \sum_{l=1}^{|\nu_e|} \Big[\Big(n_y^{(e,l)} u_x^{\sigma(e,l)} - n_x^{(e,l)} u_y^{\sigma(e,l)} \Big) \mathbb{F}^{(e,l)} \underline{\Lambda}_{\boldsymbol{u}}^{n+1,\sigma(e,l)} \\
+ \Big(n_y^{(e,l)} w_x^{\sigma(e,l)} - n_x^{(e,l)} w_y^{\sigma(e,l)} \Big) \mathbb{F}^{(e,l)} \underline{\Lambda}_{\boldsymbol{w}}^{n+1,\sigma(e,l)} \Big] = b_{E,3}, \\
\\
\bar{\mu}\mathbb{M}^e \underline{H}_x^{n+1,e} - (\mathbb{D}_z^e)^T \underline{E}_y^{n+1,e} + (\mathbb{D}_y^e)^T \underline{E}_z^{n+1,e} \\
- \sum_{l=1}^{|\nu_e|} \tau^{(e,l)} \Big(u_x^{\sigma(e,l)} \mathbb{F}^{(e,l)} \underline{\Lambda}_{\boldsymbol{u}}^{n+1,\sigma(e,l)} + w_x^{\sigma(e,l)} \mathbb{F}^{(e,l)} \underline{\Lambda}_{\boldsymbol{w}}^{n+1,\sigma(e,l)} \Big) \\
+ \sum_{l=1}^{|\nu_e|} \tau^{(e,l)} \Bigg[\Big(1 - (n_x^{(e,l)})^2 \Big) \mathbb{E}^{(e,l)} \underline{H}_x^{n+1,e} \\
- n_x^{(e,l)} n_y^{(e,l)} \mathbb{E}^{(e,l)} \underline{H}_y^{n+1,e} - n_x^{(e,l)} n_z^{(e,l)} \mathbb{E}^{(e,l)} \underline{H}_z^{n+1,e} \Bigg] = b_{H,1}, \\
\\
\bar{\mu}\mathbb{M}^e \underline{H}_y^{n+1,e} + (\mathbb{D}_z^e)^T \underline{E}_x^{n+1,e} - (\mathbb{D}_x^e)^T \underline{E}_z^{n+1,e} \\
- \sum_{l=1}^{|\nu_e|} \tau^{(e,l)} \Big(u_y^{\sigma(e,l)} \mathbb{F}^{(e,l)} \underline{\Lambda}_{\boldsymbol{u}}^{n+1,\sigma(e,l)} + w_y^{\sigma(e,l)} \mathbb{F}^{(e,l)} \underline{\Lambda}_{\boldsymbol{w}}^{n+1,\sigma(e,l)} \Big) \\
+ \sum_{l=1}^{|\nu_e|} \tau^{(e,l)} \Bigg[\Big(1 - (n_y^{(e,l)})^2 \Big) \mathbb{E}^{(e,l)} \underline{H}_y^{n+1,e} \\
- n_x^{(e,l)} n_y^{(e,l)} \mathbb{E}^{(e,l)} \underline{H}_x^{n+1,e} - n_y^{(e,l)} n_z^{(e,l)} \mathbb{E}^{(e,l)} \underline{H}_z^{n+1,e} \Bigg] = b_{H,2}, \\
\\
\bar{\mu}\mathbb{M}^e \underline{H}_z^{n+1,e} - (\mathbb{D}_y^e)^T \underline{E}_x^{n+1,e} + (\mathbb{D}_x^e)^T \underline{E}_y^{n+1,e} \\
- \sum_{l=1}^{|\nu_e|} \tau^{(e,l)} \Big(u_z^{\sigma(e,l)} \mathbb{F}^{(e,l)} \underline{\Lambda}_{\boldsymbol{u}}^{n+1,\sigma(e,l)} + w_z^{\sigma(e,l)} \mathbb{F}^{(e,l)} \underline{\Lambda}_{\boldsymbol{w}}^{n+1,\sigma(e,l)} \Big) \\
+ \sum_{l=1}^{|\nu_e|} \tau^{(e,l)} \Bigg[\Big(1 - (n_z^{(e,l)})^2 \Big) \mathbb{E}^{(e,l)} \underline{H}_z^{n+1,e} \\
- n_x^{(e,l)} n_z^{(e,l)} \mathbb{E}^{(e,l)} \underline{H}_x^{n+1,e} - n_y^{(e,l)} n_z^{(e,l)} \mathbb{E}^{(e,l)} \underline{H}_y^{n+1,e} \Bigg] = b_{H,3},
\end{cases}
\tag{2.52}
$$

Where

$$\begin{cases} \underline{E}_{\xi}^{n+1,e} = \left[\underline{E}_{\xi}^{n+1,e}[1], \cdots, \underline{E}_{\xi}^{n+1,e}[N_K^e] \right]^T, \quad \xi \in \{x,y,z\}, \\ \underline{H}_{\xi}^{n+1,e} = \left[\underline{H}_{\xi}^{n+1,e}[1], \cdots, \underline{H}_{\xi}^{n+1,e}[N_K^e] \right]^T, \quad \xi \in \{x,y,z\}, \\ \underline{\Lambda}_{\boldsymbol{\nu}}^{n+1,\sigma(e,l)} = \left[\underline{\Lambda}_{\boldsymbol{\nu}}^{n+1,\sigma(e,l)}[1], \cdots, \underline{\Lambda}_{\boldsymbol{\nu}}^{n+1,\sigma(e,l)}[N_F^{\sigma(e,l)}] \right]^T, \quad \boldsymbol{\nu} \in \{\boldsymbol{u}, \boldsymbol{w}\}, \\ \mathbb{M}^e[i,j] = \displaystyle\int_{K_e} \varphi_i^e \varphi_j^e \, \mathrm{d}\boldsymbol{x}, \quad 1 \le i,j \le N_K^e, \\ \mathbb{D}_{\xi}^e[i,j] = \displaystyle\int_{K_e} (\partial_{\xi}\varphi_i^e)\varphi_j^e \, \mathrm{d}\boldsymbol{x}, \quad 1 \le i,j \le N_K^e \text{ et } \xi \in \{x,y,z\}, \\ \mathbb{E}^{(e,l)}[i,j] = \displaystyle\int_{\partial K_e^l} \varphi_i^e \varphi_j^e \, \mathrm{d}\boldsymbol{s}, \quad 1 \le i,j \le N_K^e, \\ \mathbb{F}^{(e,l)}[i,j] = \displaystyle\int_{\partial K_e^l} \varphi_i^e \psi_j^{\sigma(e,l)} \, \mathrm{d}\boldsymbol{s}, \quad 1 \le i \le N_e^K \text{ et } 1 \le j \le N_F^{\sigma(e,l)}. \end{cases}$$

Now we can write the local linear system associated to the element K_e as

$$\mathbb{A}^e \begin{bmatrix} \underline{E}_x^{n+1,e} \\ \underline{E}_y^{n+1,e} \\ \underline{E}_z^{n+1,e} \\ \underline{H}_x^{n+1,e} \\ \underline{H}_y^{n+1,e} \\ \underline{H}_z^{n+1,e} \end{bmatrix} + \sum_{l=1}^{|\nu_e|} \mathbb{C}^{(e,l)} \begin{bmatrix} \underline{\Lambda}_{\boldsymbol{u}}^{n+1,\sigma(e,l)} \\ \underline{\Lambda}_{\boldsymbol{w}}^{n+1,\sigma(e,l)} \end{bmatrix} = \mathbb{P}^{n,e}, \tag{2.53}$$

where

- $\mathbb{A}^e$ matrix of size $6N_K^e \times 6N_K^e$, defined by

$$\mathbb{A}^e = \begin{bmatrix} \bar{\varepsilon}\mathbb{M}^e & 0 & 0 & 0 & -\mathbb{D}_z^e & \mathbb{D}_y^e \\ 0 & \bar{\varepsilon}\mathbb{M}^e & 0 & \mathbb{D}_z^e & 0 & -\mathbb{D}_x^e \\ 0 & 0 & \bar{\varepsilon}\mathbb{M}^e & -\mathbb{D}_y^e & \mathbb{D}_x^e & 0 \\ 0 & -\left[\mathbb{D}_z^e\right]^T & \left[\mathbb{D}_y^e\right]^T & \bar{\mu}\mathbb{M}^e + \mathbb{E}_x^e & -\mathbb{E}_{xy}^e & -\mathbb{E}_{xz}^e \\ \left[\mathbb{D}_z^e\right]^T & 0 & -\left[\mathbb{D}_x^e\right]^T & -\mathbb{E}_{xy}^e & \bar{\mu}\mathbb{M}^e + \mathbb{E}_y^e & -\mathbb{E}_{yz}^e \\ -\left[\mathbb{D}_y^e\right]^T & \left[\mathbb{D}_x^e\right]^T & 0 & -\mathbb{E}_{xz}^e & -\mathbb{E}_{yz}^e & \bar{\mu}\mathbb{M}^e + \mathbb{E}_z^e \end{bmatrix},$$

- $\mathbb{C}^{(e,l)}$ matrix of size $6N_K^e \times 2N_F^{\sigma(e,l)}$, defined by

$$\mathbb{C}^{(e,l)} = \begin{bmatrix} (n_z^{(e,l)} u_y^{\sigma(e,l)} - n_y^{(e,l)} u_z^{\sigma(e,l)})\mathbb{F}^{(e,l)} & (n_z^{(e,l)} w_y^{\sigma(e,l)} - n_y^{(e,l)} w_z^{\sigma(e,l)})\mathbb{F}^{(e,l)} \\ (n_x^{(e,l)} u_z^{\sigma(e,l)} - n_z^{(e,l)} u_x^{\sigma(e,l)})\mathbb{F}^{(e,l)} & (n_x^{(e,l)} w_z^{\sigma(e,l)} - n_z^{(e,l)} w_x^{\sigma(e,l)})\mathbb{F}^{(e,l)} \\ (n_y^{(e,l)} u_x^{\sigma(e,l)} - n_x^{(e,l)} u_y^{\sigma(e,l)})\mathbb{F}^{(e,l)} & (n_y^{(e,l)} w_x^{\sigma(e,l)} - n_x^{(e,l)} w_y^{\sigma(e,l)})\mathbb{F}^{(e,l)} \\ -\tau^{(e,l)} u_x^{\sigma(e,l)} \mathbb{F}^{(e,l)} & -\tau^{(e,l)} w_x^{\sigma(e,l)} \mathbb{F}^{(e,l)} \\ -\tau^{(e,l)} u_y^{\sigma(e,l)} \mathbb{F}^{(e,l)} & -\tau^{(e,l)} w_y^{\sigma(e,l)} \mathbb{F}^{(e,l)} \\ -\tau^{(e,l)} u_z^{\sigma(e,l)} \mathbb{F}^{(e,l)} & -\tau^{(e,l)} w_z^{\sigma(e,l)} \mathbb{F}^{(e,l)} \end{bmatrix}.$$

- $\mathbb{P}^e = [b_{E,1}, b_{E,2}, b_{E,3}, b_{H,1}, b_{H,2}, b_{H,3}]^T$

Discretisation of the global problem for Λ

Let $F_f \in \mathcal{F}_h^I$, the conservativity condition for F_f and for all $\boldsymbol{\eta} \in \boldsymbol{M}_h^{t,3}$

$$\begin{aligned}
&\left\langle \boldsymbol{n} \times \boldsymbol{E}_h^{n+1}, \boldsymbol{\eta} \right\rangle_{\partial K_e^l} - \tau^{(e,l)} \left\langle \boldsymbol{n} \times (\boldsymbol{n} \times \boldsymbol{H}_h^{n+1}), \boldsymbol{\eta} \right\rangle_{\partial K_e^l} - \tau^{(e,l)} \left\langle \boldsymbol{\Lambda}_h^{n+1}, \boldsymbol{\eta} \right\rangle_{\partial K_e^l} \\
&+ \left\langle \boldsymbol{n} \times \boldsymbol{E}_h^{n+1}, \boldsymbol{\eta} \right\rangle_{\partial K_g^k} - \tau^{(g,k)} \left\langle \boldsymbol{n} \times (\boldsymbol{n} \times \boldsymbol{H}_h^{n+1}), \boldsymbol{\eta} \right\rangle_{\partial K_g^k} - \tau^{(g,k)} \left\langle \boldsymbol{\Lambda}_h^{n+1}, \boldsymbol{\eta} \right\rangle_{\partial K_g^k} \\
&= \\
&- \left\langle \boldsymbol{n} \times \boldsymbol{E}_h^{n}, \boldsymbol{\eta} \right\rangle_{\partial K_e^l} + \tau^{(e,l)} \left\langle \boldsymbol{n} \times (\boldsymbol{n} \times \boldsymbol{H}_h^{n}), \boldsymbol{\eta} \right\rangle_{\partial K_e^l} + \tau^{(e,l)} \left\langle \boldsymbol{\Lambda}_h^{n}, \boldsymbol{\eta} \right\rangle_{\partial K_e^l} \\
&- \left\langle \boldsymbol{n} \times \boldsymbol{E}_h^{n}, \boldsymbol{\eta} \right\rangle_{\partial K_g^k} + \tau^{(g,k)} \left\langle \boldsymbol{n} \times (\boldsymbol{n} \times \boldsymbol{H}_h^{n}), \boldsymbol{\eta} \right\rangle_{\partial K_g^k} + \tau^{(g,k)} \left\langle \boldsymbol{\Lambda}_h^{n}, \boldsymbol{\eta} \right\rangle_{\partial K_g^k} .
\end{aligned} \tag{2.54}$$

For a boundary face $F_f \in \Gamma_a$, the conservativity condition for all $\boldsymbol{\eta} \in \boldsymbol{M}_h^{t,3}$

$$\begin{aligned}
&\left\langle \boldsymbol{n} \times \boldsymbol{E}_h^{n+1}, \boldsymbol{\eta} \right\rangle_{\partial K_e^l} - \tau^{(e,l)} \left\langle \boldsymbol{n} \times (\boldsymbol{n} \times \boldsymbol{H}_h^{n+1}), \boldsymbol{\eta} \right\rangle_{\partial K_e^l} \\
&\qquad - (1 + \tau^{(e,l)}) \left\langle \boldsymbol{\Lambda}_h^{n+1}, \boldsymbol{\eta} \right\rangle_{\partial K_e^l} = \left\langle \boldsymbol{\Lambda}_h^{n} + \boldsymbol{g}^{inc,n} + \boldsymbol{g}^{inc,n+1}, \boldsymbol{\eta} \right\rangle_{\partial K_e^l} .
\end{aligned} \tag{2.55}$$

For (2.54) we have

$$\begin{cases}
\left(n_z^{(e,l)} u_y^{\sigma(e,l)} - n_y^{(e,l)} u_z^{\sigma(e,l)}\right) \left[\mathbb{F}^{(e,l)}\right]^T \underline{E}_x^{n+1,e} + \left(n_x^{(e,l)} u_z^{\sigma(e,l)} - n_z^{(e,l)} u_x^{\sigma(e,l)}\right) \left[\mathbb{F}^{(e,l)}\right]^T \underline{E}_y^{n+1,e} \\
+ \left(n_z^{(e,l)} u_y^{\sigma(e,l)} - n_y^{(e,l)} u_z^{\sigma(e,l)}\right) \left[\mathbb{F}^{(e,l)}\right]^T \underline{E}_z^{n+1,e} + \tau_x^{(e,l)} \left[\mathbb{F}^{(e,l)}\right]^T \underline{H}_x^{n,e} + \tau^{(e,l)} u_y^{\sigma(e,l)} \left[\mathbb{F}^{(e,l)}\right]^T \underline{H}_y^{n+1,e} \\
+ \tau^{(e,l)} u_z^{\sigma(e,l)} \left[\mathbb{F}^{(e,l)}\right]^T \underline{H}_z^{n+1,e} - \tau^{(e,l)} \mathbb{G}^{(e,l)} \underline{\Lambda}_{\boldsymbol{u}}^{n+1,\sigma(e,l)} - \tau^{(e,l)} \left(\boldsymbol{u}^{\sigma(e,l)} \cdot \boldsymbol{w}^{\sigma(e,l)}\right) \mathbb{G}^{(e,l)} \underline{\Lambda}_{\boldsymbol{w}}^{n+1,\sigma(e,l)} + R_{\boldsymbol{u}}^{n+1,(g,k)} \\
= -R_{\boldsymbol{u}}^{n,(e,l)} - R_{\boldsymbol{u}}^{n,(g,k)}, \\
\\
\left(n_z^{(e,l)} w_y^{\sigma(e,l)} - n_y^{(e,l)} w_z^{\sigma(e,l)}\right) \left[\mathbb{F}^{(e,l)}\right]^T \underline{E}_x^{n+1,e} + \left(n_x^{(e,l)} w_z^{\sigma(e,l)} - n_z^{(e,l)} w_x^{\sigma(e,l)}\right) \left[\mathbb{F}^{(e,l)}\right]^T \underline{E}_y^{n+1,e} \\
+ \left(n_z^{(e,l)} w_y^{\sigma(e,l)} - n_y^{(e,l)} w_z^{\sigma(e,l)}\right) \left[\mathbb{F}^{(e,l)}\right]^T \underline{E}_z^{n+1,e} + \tau^{(e,l)} w_x^{\sigma(e,l)} \left[\mathbb{F}^{(e,l)}\right]^T \underline{H}_x^{n+1,e} + \tau^{(e,l)} w_y^{\sigma(e,l)} \left[\mathbb{F}^{(e,l)}\right]^T \underline{H}_y^{n+1,e} \\
+ \tau^{(e,l)} w_z^{\sigma(e,l)} \left[\mathbb{F}^{(e,l)}\right]^T \underline{H}_z^{n+1,e} - \tau^{(e,l)} \left(\boldsymbol{u}^{\sigma(e,l)} \cdot \boldsymbol{w}^{\sigma(e,l)}\right) \mathbb{G}^{(e,l)} \underline{\Lambda}_{\boldsymbol{u}}^{n+1,\sigma(e,l)} - \tau^{(e,l)} \mathbb{G}^{(e,l)} \underline{\Lambda}_{\boldsymbol{w}}^{n+1,\sigma(e,l)} + R_{\boldsymbol{w}}^{n+1,(g,k)} \\
= -R_{\boldsymbol{w}}^{n,(e,l)} - R_{\boldsymbol{w}}^{n,(g,k)},
\end{cases} \tag{2.56}$$

where

$$\mathbb{G}^{(e,l)}[i,j] = \int_{\partial K_e^l} \psi_i^{\sigma(e,l)} \psi_j^{\sigma(e,l)} \, \mathrm{d}s, \quad 1 \le i,j \le N_F^{\sigma(e,l)}.$$

For (2.55) we have

$$
\begin{cases}
\left(n_z^{(e,l)} u_y^{\sigma(e,l)} - n_y^{(e,l)} u_z^{\sigma(e,l)}\right) \left[\mathbb{F}^{(e,l)}\right]^T \underline{E}_x^{n+1,e} + \left(n_x^{(e,l)} u_z^{\sigma(e,l)} - n_z^{(e,l)} u_x^{\sigma(e,l)}\right) \left[\mathbb{F}^{(e,l)}\right]^T \underline{E}_y^{n+1,e} \\
+ \left(n_z^{(e,l)} u_y^{\sigma(e,l)} - n_y^{(e,l)} u_z^{\sigma(e,l)}\right) \left[\mathbb{F}^{(e,l)}\right]^T \underline{E}_z^{n+1,e} + \tau_x^{(e,l)} \left[\mathbb{F}^{(e,l)}\right]^T \underline{H}_x^{n+1,e} + \tau^{(e,l)} u_y^{\sigma(e,l)} \left[\mathbb{F}^{(e,l)}\right]^T \underline{H}_y^{n+1,e} \\
+ \tau^{(e,l)} u_z^{\sigma(e,l)} \left[\mathbb{F}^{(e,l)}\right]^T \underline{H}_z^{n+1,e} - \left(1 + \tau^{(e,l)}\right) \mathbb{G}^{(e,l)} \underline{\Lambda}_{\boldsymbol{u}}^{n+1,\sigma(e,l)} - \left(1 + \tau^{(e,l)}\right) \left(\boldsymbol{u}^{\sigma(e,l)} \cdot \boldsymbol{w}^{\sigma(e,l)}\right) \mathbb{G}^{(e,l)} \underline{\Lambda}_{\boldsymbol{w}}^{n+1,\sigma(e,l)} \\
= -R_{\boldsymbol{u}}^{n,(e,l)} + \mathbb{G}^{(e,l)} \underline{\boldsymbol{g}}_{\boldsymbol{u}}^{\sigma(e,l)}, \\
\\
\left(n_z^{(e,l)} w_y^{\sigma(e,l)} - n_y^{(e,l)} w_z^{\sigma(e,l)}\right) \left[\mathbb{F}^{(e,l)}\right]^T \underline{E}_x^{n+1,e} + \left(n_x^{(e,l)} w_z^{\sigma(e,l)} - n_z^{(e,l)} w_x^{\sigma(e,l)}\right) \left[\mathbb{F}^{(e,l)}\right]^T \underline{E}_y^{n+1,e} \\
+ \left(n_z^{(e,l)} w_y^{\sigma(e,l)} - n_y^{(e,l)} w_z^{\sigma(e,l)}\right) \left[\mathbb{F}^{(e,l)}\right]^T \underline{E}_z^{n+1,e} + \tau^{(e,l)} w_x^{\sigma(e,l)} \left[\mathbb{F}^{(e,l)}\right]^T \underline{H}_x^{n+1,e} + \tau^{(e,l)} w_y^{\sigma(e,l)} \left[\mathbb{F}^{(e,l)}\right]^T \underline{H}_y^{n+1,e} \\
+ \tau^{(e,l)} w_z^{\sigma(e,l)} \left[\mathbb{F}^{(e,l)}\right]^T \underline{H}_z^{n+1,e} - \left(1 + \tau^{(e,l)}\right) \left(\boldsymbol{u}^{\sigma(e,l)} \cdot \boldsymbol{w}^{\sigma(e,l)}\right) \mathbb{G}^{(e,l)} \underline{\Lambda}_{\boldsymbol{u}}^{n+1,\sigma(e,l)} - \left(1 + \tau^{(e,l)}\right) \mathbb{G}^{(e,l)} \underline{\Lambda}_{\boldsymbol{w}}^{n+1,\sigma(e,l)} \\
= -R_{\boldsymbol{w}}^{n,(e,l)} + \mathbb{G}^{(e,l)} \underline{\boldsymbol{g}}_{\boldsymbol{w}}^{\sigma(e,l)},
\end{cases}
\tag{2.57}
$$

with

$$
\underline{\boldsymbol{g}}_{\boldsymbol{\nu}}^{\sigma(e,l)} = \left[(\underline{\boldsymbol{g}}_{\boldsymbol{\nu}}^{n,\mathrm{inc},\sigma(e,l)} + \underline{\boldsymbol{g}}_{\boldsymbol{\nu}}^{n+1,\mathrm{inc},\sigma(e,l)})[1], \cdots, (\underline{\boldsymbol{g}}_{\boldsymbol{\nu}}^{n,\mathrm{inc},\sigma(e,l)} + \underline{\boldsymbol{g}}_{\boldsymbol{\nu}}^{n+1,\mathrm{inc},\sigma(e,l)})[N_F^{\sigma(e,l)}] \right]^T, \boldsymbol{\nu} \in \{\boldsymbol{u}, \boldsymbol{w}\}.
$$

we define a matrix $\mathcal{A}_{HDG}^e$ of size

$$
\sum_{l=1}^{|\nu_e|} 2N_F^{\sigma(e,l)} \times \sum_{f=1}^{|\mathcal{F}_h|} 2N_F^f,
$$

such that

$$
\mathcal{A}_{HDG}^e \underline{\Lambda} = \left[\underline{\Lambda}^{\sigma(e,1)}, \cdots, \underline{\Lambda}^{\sigma(e,|\nu_e|)} \right]^T.
$$

adding all equations involving interior face (2.56) and every boundary face (2.57) element-by-element we have

$$
\sum_{e=1}^{|\mathcal{T}_h|} [\mathcal{A}_{HDG}^e]^T \left(\mathbb{B}^e \underline{W}^{n+1,e} + \mathbb{G}^e \mathcal{A}_{HDG}^e \underline{\Lambda}^{n+1} \right) = \sum_{e=1}^{|\mathcal{T}_h|} [\mathcal{A}_{HDG}^e]^T \left(-\mathbb{B}^e \underline{W}^{n,e} - \mathbb{G}^e \mathcal{A}_{HDG}^e \underline{\Lambda}^n + \underline{\boldsymbol{g}}^{e,n} \right),
\tag{2.58}
$$

where

- $\underline{W}^{n+1,e}$ the column vector of size $6N_K^e$, defined by $\underline{W}^e = \left[\underline{\boldsymbol{E}}^{n+1,e}, \underline{\boldsymbol{H}}^{n+1,e}\right]^T$,
- $\mathbb{B}^e$ the matrix of size $\displaystyle\sum_{l=1}^{|\nu_e|} 2N_F^{\sigma(e,l)} \times 6N_K^e$, defined by

  $\mathbb{B}^e =$

$$
\begin{bmatrix}
\mathbb{F}_{zy,u}^{(e,1)} & \mathbb{F}_{xz,u}^{(e,1)} & \mathbb{F}_{yx,u}^{(e,1)} & \tau^{(e,1)} u_x^{\sigma(e,1)} \left[\mathbb{F}^{(e,1)}\right]^T & \tau^{(e,1)} u_y^{\sigma(e,1)} \left[\mathbb{F}^{(e,1)}\right]^T & \tau^{(e,1)} u_z^{\sigma(e,1)} \left[\mathbb{F}^{(e,1)}\right]^T \\
\mathbb{F}_{zy,w}^{(e,1)} & \mathbb{F}_{xz,w}^{(e,1)} & \mathbb{F}_{yx,w}^{(e,1)} & \tau^{(e,1)} w_x^{\sigma(e,1)} \left[\mathbb{F}^{(e,1)}\right]^T & \tau^{(e,1)} w_y^{\sigma(e,1)} \left[\mathbb{F}^{(e,1)}\right]^T & \tau^{(e,1)} w_z^{\sigma(e,1)} \left[\mathbb{F}^{(e,1)}\right]^T \\
\mathbb{F}_{zy,u}^{(e,2)} & \mathbb{F}_{xz,u}^{(e,2)} & \mathbb{F}_{yx,u}^{(e,2)} & \tau^{(e,2)} u_x^{\sigma(e,2)} \left[\mathbb{F}^{(e,2)}\right]^T & \tau^{(e,2)} u_y^{\sigma(e,2)} \left[\mathbb{F}^{(e,2)}\right]^T & \tau^{(e,2)} u_z^{\sigma(e,2)} \left[\mathbb{F}^{(e,2)}\right]^T \\
\cdots & \cdots & \cdots & \cdots & \cdots & \cdots \\
\mathbb{F}_{zy,w}^{(e,|\nu_e|)} & \mathbb{F}_{xz,w}^{(e,|\nu_e|)} & \mathbb{F}_{yx,w}^{(e,|\nu_e|)} & \tau^{(e,|\nu_e|)} w_x^{\sigma(e,|\nu_e|)} \left[\mathbb{F}^{(e,|\nu_e|)}\right]^T & \tau^{(e,|\nu_e|)} w_y^{\sigma(e,|\nu_e|)} \left[\mathbb{F}^{(e,|\nu_e|)}\right]^T & \tau^{(e,|\nu_e|)} w_z^{\sigma(e,|\nu_e|)} \left[\mathbb{F}^{(e,|\nu_e|)}\right]^T
\end{bmatrix},
$$

with

$$\mathbb{F}^{(e,l)}_{\xi\zeta,\nu} = \left(n^{(e,l)}_{\xi}\nu^{\sigma(e,l)}_{\zeta} - n^{(e,l)}_{\zeta}\nu^{\sigma(e,l)}_{\xi}\right)\left[\mathbb{F}^{(e,l)}\right]^T,\ l = 1,\cdots,|\nu_e|,\ \xi,\zeta \in \{x,y,z\},\ \nu \in \{u,w\},$$

- $\mathbb{G}^e$ the matrix of size $\sum_{l=1}^{|\nu_e|} 2N_F^{\sigma(e,l)} \times \sum_{l=1}^{|\nu_e|} 2N_F^{\sigma(e,l)}$, defined by

$$\mathbb{G}^e = \begin{bmatrix} -\kappa^{(e,1)}\mathbb{G}^{(e,1)} & -\kappa^{(e,1)}(\boldsymbol{u}^{\sigma(e,1)}\cdot\boldsymbol{w}^{\sigma(e,1)})\mathbb{G}^{(e,1)} & \cdots & 0 \\ -\kappa^{(e,1)}(\boldsymbol{u}^{\sigma(e,1)}\cdot\boldsymbol{w}^{\sigma(e,1)})\mathbb{G}^{(e,1)} & -\kappa^{(e,1)}\mathbb{G}^{(e,1)} & \cdots & 0 \\ \cdots & \cdots & \cdots & \cdots \\ 0 & 0 & \cdots & -\kappa^{(e,|\nu_e|)}(\boldsymbol{u}^{\sigma(e,|\nu_e|)}\cdot\boldsymbol{w}^{\sigma(e,|\nu_e|)})\mathbb{G}^{(e,|\nu_e|)} \\ 0 & 0 & \cdots & -\kappa^{(e,|\nu_e|)}\mathbb{G}^{(e,|\nu_e|)} \end{bmatrix},$$

with

$$\kappa^{(e,l)} = \begin{cases} \tau^{(e,l)}, \text{ if the face } F_{\sigma(e,l)} \in \mathcal{F}_h \setminus \Gamma_a, \\ 1+\tau^{(e,l)}, \text{ if the face } F_{\sigma(e,l)} \in \mathcal{F}_h^B \cap \Gamma_a, \end{cases} \quad l = 1,\cdots,|\nu_e|,$$

- $\underline{\boldsymbol{g}}^e$ the column vector of size $\sum_{l=1}^{|\nu_e|} 2N_F^{\sigma(e,l)}$, defined by

$$\underline{\boldsymbol{g}}^e = \left[\underline{\boldsymbol{g}}^{\sigma(e,1)},\cdots,\underline{\boldsymbol{g}}^{\sigma(e,|\nu_e|)}\right]^T,$$

where

$$\underline{\boldsymbol{g}}^{\sigma(e,l)} = \begin{cases} \mathbb{G}^{(e,l)}\,\underline{\boldsymbol{g}\boldsymbol{g}}_{\boldsymbol{u}}^{\sigma(e,l)} \\ \mathbb{G}^{(e,l)}\,\underline{\boldsymbol{g}\boldsymbol{g}}_{\boldsymbol{w}}^{\sigma(e,l)} \end{cases} \text{ and } \underline{\boldsymbol{g}\boldsymbol{g}}_{\boldsymbol{\nu}}^{\sigma(e,l)} = \begin{cases} 0 & \text{if } F_{\sigma(e,l)} \in \mathcal{F}_h \setminus \Gamma_a \\ \underline{\boldsymbol{g}}_{\boldsymbol{\nu}}^{n,\text{inc},\sigma(e,l)} + \underline{\boldsymbol{g}}_{\boldsymbol{\nu}}^{n+1,\text{inc},\sigma(e,l)} & \text{if } F_{\sigma(e,l)} \in \mathcal{F}_h^B \cap \Gamma_a \end{cases} \quad \boldsymbol{\nu} \in \{\boldsymbol{u},\boldsymbol{w}\}.$$

Now we can rewrite the equation for the local solver (2.53) as

$$\mathbb{A}^e\underline{W}^{n+1,e} + \mathbb{C}^e\mathcal{A}^e_{HDG}\underline{\Lambda}^{n+1} = \mathbb{P}^{n,e}, \tag{2.59}$$

where $\mathbb{C}^e$ is the matrix of size $6N_K^e \times \sum_{l=1}^{|\nu_e|} N_F^{\sigma(e,l)}$, defined by $\mathbb{C}^e = \left[\mathbb{C}^{(e,1)} \quad \cdots \quad \mathbb{C}^{(e,|\nu_e|)}\right]$.

Finally we substitute $\underline{W}^{n+1,e}$ by the solution of the local system (2.59) in (2.58) to obtain

$$\sum_{e=1}^{|\mathcal{T}_h|}[\mathcal{A}^e_{HDG}]^T\left(\mathbb{B}^e\left[\mathbb{A}^e\right]^{-1}\left[\mathbb{P}^{n,e} - \mathbb{C}^e\mathcal{A}^e_{HDG}\underline{\Lambda}^{n+1}\right] + \mathbb{G}^e\mathcal{A}^e_{HDG}\underline{\Lambda}^{n+1}\right) = \sum_{e=1}^{|\mathcal{T}_h|}[\mathcal{A}^e_{HDG}]^T\left(-\mathbb{B}^e\underline{W}^{n,e} - \mathbb{G}^e\mathcal{A}^e_{HDG}\underline{\Lambda}^n + \underline{\boldsymbol{g}}^{e,n}\right).$$

$$\Rightarrow \left[\sum_{e=1}^{|\mathcal{T}_h|}[\mathcal{A}^e_{HDG}]^T\left(-\mathbb{B}^e\left[\mathbb{A}^e\right]^{-1}\mathbb{C}^e + \mathbb{G}^e\right)\mathcal{A}^e_{HDG}\right]\underline{\Lambda}^{n+1} = \sum_{e=1}^{|\mathcal{T}_h|}[\mathcal{A}^e_{HDG}]^T\left(-\mathbb{B}^e\underline{W}^{n,e} - \mathbb{G}^e\mathcal{A}^e_{HDG}\underline{\Lambda}^n - \mathbb{B}^e\left[\mathbb{A}^e\right]^{-1}\mathbb{P}^{n,e} + \underline{\boldsymbol{g}}^{e,n}\right).$$

Thus we write the following linear system for the global trace $\underline{\Lambda}^{n+1}$

$$\mathbb{K}\underline{\Lambda}^{n+1} = \underline{\boldsymbol{g}}^n, \tag{2.60}$$

where

- $\mathbb{K}$ the matrix of size $\sum_{f=1}^{|\mathcal{F}_h|} 2N_F^f \times \sum_{f=1}^{|\mathcal{F}_h|} 2N_F^f$, defined by

$$\mathbb{K} = \sum_{e=1}^{|\mathcal{T}_h|} [\mathcal{A}_{HDG}^e]^T \, \mathbb{K}^e \mathcal{A}_{HDG}^e = \sum_{e=1}^{|\mathcal{T}_h|} [\mathcal{A}_{HDG}^e]^T \left(\mathbb{G}^e - \mathbb{B}^e \, [\mathbb{A}^e]^{-1} \, \mathbb{C}^e \right) \mathcal{A}_{HDG}^e,$$

- $\underline{\boldsymbol{g}}^n$ the column vector $\sum_{f=1}^{|\mathcal{F}_h|} 2N_F^f$, defined by

$$\underline{\boldsymbol{g}}^n = \sum_{e=1}^{|\mathcal{T}_h|} [\mathcal{A}_{HDG}^e]^T \left(-\mathbb{B}^e \underline{W}^{n,e} - \mathbb{G}^e \mathcal{A}_{HDG}^e \underline{\Lambda}^n - \mathbb{B}^e \, [\mathbb{A}^e]^{-1} \, \mathbb{P}^{n,e} + \underline{\boldsymbol{g}}^{e,n} \right).$$

Remark 3. If we consider a uniform degree of interpolation for elements and faces, then the total numbers of globally coupled DoFs are

- DG method: $(p+1)(p+2)(p+3)|\mathcal{T}_h|$
- HDG method: $(p+1)(p+2)|\mathcal{F}_h|$

For $|\mathcal{F}_h| \approx 2|\mathcal{T}_h|$, $\dfrac{2}{p+3}$ is the ratio of the number of globally coupled DoFs of HDG method to DG method.

Remark 4. For the numerical results we can see in [43] that, as expected, we have a $k+1$ convergence order in space while we have a convergence of second order in time. And we can obviously see that the HDG method outperforms the DG method both on the memory requirement and CPU time metrics, especially at higher interpolation orders.

2.5.10 Numerical results

In this section, we will present the numerical results for the fully implicit HDGTD method described above for the propagation of a standing wave in a cubic PEC cavity [43].

Propagation of a standing wave in a cubic PEC cavity

In order to validate and study the numerical convergence of the proposed HDG method, we consider the propagation of an eigenmode in a source-free *i.e* $\boldsymbol{J} = 0$ closed cavity (the unit cube $\Omega := (0, L)^3$, $L := 1m$) with perfectly metallic walls. The frequency of the wave is $\omega = \sqrt{3}\pi c_0/L$ where c_0 is the speed of light in vacuum. The electric permittivity and the magnetic permeability are set to the constant vacuum values. The exact time-domain solution is given by

$$\begin{cases} E_x(x,y,z,t) &= -\cos(\pi x)\sin(\pi y)\sin(\pi z)\cos(\omega t), \\ E_y(x,y,z,t) &= 0, \\ E_z(x,y,z,t) &= \sin(\pi x)\sin(\pi y)\cos(\pi z)\cos(\omega t), \\ H_x(x,y,z,t) &= -\dfrac{\pi}{\omega}\sin(\pi x)\cos(\pi y)\cos(\pi z)\sin(\omega t), \\ H_y(x,y,z,t) &= \dfrac{2\pi}{\omega}\cos(\pi x)\sin(\pi y)\cos(\pi z)\sin(\omega t), \\ H_z(x,y,z,t) &= -\dfrac{\pi}{\omega}\cos(\pi x)\cos(\pi y)\sin(\pi z)\sin(\omega t), \end{cases} \tag{2.61}$$

The electromagnetic field is initialized at $t = 0$ as $E_y = H_x = H_y = H_z = 0$ and

$$\begin{cases} E_x(x, y, z, t = 0) &= -\cos(\pi x)\sin(\pi y)\sin(\pi z), \\ E_z(x, y, z, t = 0) &= \sin(\pi x)\sin(\pi y)\cos(\pi z). \end{cases} \tag{2.62}$$

The parameter τ in the HDG traces is taken equal to 1. The time step is chosen as $\Delta t = c_{\text{CFL}}\Delta t_{min}$ where Δt_{min} is the global minimal time step over the whole mesh. The value of the time step is chosen such that the accuracy does not affect the accuracy in space. The maximal L^2-norm of the error is measure for a sequence of successively refined tetrahedral meshes starting from a uniform coarse mesh. The latter is obtained by subdividing a finite difference grid of the unit cube. An optimal convergence order is observed for the electromagnetic field, namely $k+1$. A comparison is made between the proposed time-implicit HDG and a classical centered flux time-implicit DGTD method [31] in terms of memory occupation and CPU time for the same problem. The coefficient c_{CFL} is set to 1. Simulations are performed on a workstation equipped with an Intel Xeon E5-2630@2.60 GHz processor. The obtained results are summarized in Table (2.1) for two interpolation orders. We clearly see that the HDG method outperforms the DG method both on the memory requirement and CPU time metrics, especially at higher interpolation orders.

	$\mathbb{P}_1$		$\mathbb{P}_3$	
	DG	HDG	DG	HDG
Number of non-zero entries	2 988 320	1 562 112	64 448 080	17 356 800
Factorization time (s)	46	3	8308	143
L^2 error	4.68e-02	4.22e-02	3.61e-02	3.60e-02

Table 2.1 | Standing wave in a PEC cavity: comparaison between the time-implicit DGTD method and the time-implicit HDGTD method.

3

An explicit HDGTD method for Maxwell equations

3.1 Introduction

As mentioned previously, HDG methods were essentially created for stationary problems and unsteady problems treated with time implicit schemes. Our ultimate goal is to devise a high order hybrid explicit-implicit HDG method. A preliminary step considered in this chapter is therefore to elaborate on the principles of a fully explicit HDG formulation. It happens that fully explicit HDG methods have been studied recently for the acoustic wave equation by Kronbichler al. [45] and Stanglmeier al. [38]. The work reported in [45] is in fact a comparison of implicit and explicit HDG formulations. In the explicit HDG scheme, the trace of the acoustic pressure on a face is computed from the solution of the two elements adjacent to the face at the previous time step. The adopted time integration schemes are diagonally implicit and explicit Runge-Kutta schemes. The conclusion of this study is that for the considered acoustic wave propagation problems, the computing time per time step is much lower for the explicit scheme, despite the stability restriction on the time step of the explicit scheme. In [38] the authors present a fully explicit, high order accurate in both space and time HDG method. The method coincides with the classical upwind flux-based DG method for a particular choice of the stabilization parameter in the HDG numerical traces. Time integration is obtained by a strong stability preserving Runge-Kutta scheme. This HDG method provides an optimal convergence rate for the solution and its gradient and is amenable to local post-processing to obtain a superconvergence property with a rate $k+2$ if k, $k \geq 1$, is the interpolation order in the L^2-norm, depending on the form of the numerical fluxes.

In this chapter we propose a fully explicit high order accurate HDG method for the solution of the system of time-domain Maxwell equations. We adopt a low storage Runge-Kutta scheme [46] for

the time integration of the semi-discrete HDG equations. It also provides an optimal convergence rate for the solution and is amenable to local post-processing to obtain a superconvergence property with a rate $k+1$ if $k \geq 1$ is the interpolation order in the H^{curl}-norm instead of k. As in [38], we show that for a particular choice of the stabilization parameter in the definition of the HDG numerical traces, we recover the classical upwind flux-based DG method [8]. This work is a first step towards the construction of a hybrid explicit-implicit HDG method for time-domain electromagnetics.

3.2 Global formulation

Our starting point for this chapter is the HDG formulation proposed in chapter 2 for the Maxwell equations in time-domain (2.43).

HDG formulation

$$\begin{aligned}
(\varepsilon\partial_t \boldsymbol{E}_h, \boldsymbol{v})_{\mathcal{T}_h} - (\boldsymbol{H}_h, \mathbf{curl}\, \boldsymbol{v})_{\mathcal{T}_h} + \langle \boldsymbol{\Lambda}_h, \boldsymbol{n}\times\boldsymbol{v}\rangle_{\partial\mathcal{T}_h} &= 0,\ \forall \boldsymbol{v}\in \boldsymbol{V}_h^3,\\
(\mu\partial_t \boldsymbol{H}_h, \boldsymbol{v})_{\mathcal{T}_h} + (\boldsymbol{E}_h, \mathbf{curl}\, \boldsymbol{v})_{\mathcal{T}_h} - \left\langle \hat{\boldsymbol{E}}_h^t, \boldsymbol{n}\times\boldsymbol{v}\right\rangle_{\partial\mathcal{T}_h} &= 0,\ \forall \boldsymbol{v}\in \boldsymbol{V}_h^3,\\
\left\langle [\![\hat{\boldsymbol{E}}_h]\!], \boldsymbol{\eta}\right\rangle_{\mathcal{F}_h} - \langle \boldsymbol{\Lambda}_h, \boldsymbol{\eta}\rangle_{\Gamma_a} - \langle \boldsymbol{g}^{\text{inc}}, \boldsymbol{\eta}\rangle_{\Gamma_a} &= 0,\ \forall \boldsymbol{\eta}\in \boldsymbol{M}_h^{t,3},
\end{aligned}$$

The idea here is to use the third equation of the HDG formulation above, to calculate for every F, $\boldsymbol{\Lambda}_{h|_F}$ and $\hat{\boldsymbol{E}}^t_{h|_F}$ in terms of $\boldsymbol{H}^{t,+}_{h|K^+}$, $\boldsymbol{H}^{t,-}_{h|K^-}$, $\boldsymbol{E}^{t,+}_{h|K^+}$ and $\boldsymbol{E}^{t,-}_{h|K^-}$. Next step is to inject the new expressions of $\boldsymbol{\Lambda}_h$ and $\hat{\boldsymbol{E}}^t_h$ in the first two equations. This HDGTD method can be seen as a generalization of the classical DGTD scheme based on upwind fluxes. In particular, it coincides with the latter scheme for a particular choice of the stabilization parameter introduced in the definition of numerical traces in the HDG framework.

3.2.1 Reformulation with numerical fluxes

From the third equation of (2.43) we have

$$\left\langle [\![\hat{\boldsymbol{E}}^t_h]\!], \boldsymbol{\eta}\right\rangle_{\mathcal{F}_h^I} = 0 \quad \forall \boldsymbol{\eta}\in \boldsymbol{M}_h \cap \{\boldsymbol{\eta} = 0 \quad \text{on}\,(\mathcal{F}_h\cap\Gamma_m)\cup(\mathcal{F}_h\cap\Gamma_a)\}.$$

Now, let us prove that the function

$$\boldsymbol{\eta}_1 = \begin{cases} [\![\hat{\boldsymbol{E}}^t_h]\!] & \text{on} \quad \mathcal{F}_h^I \\ 0 & \text{on} \quad (\mathcal{F}_h\cap\Gamma_m)\cup(\mathcal{F}_h\cap\Gamma_a)\,, \end{cases}$$

belongs to the space $\boldsymbol{M}_h \cap \{\boldsymbol{\eta} = 0\,\text{on}\,(\mathcal{F}_h\cap\Gamma_m)\cup(\mathcal{F}_h\cap\Gamma_a)\}$. First it is clear that $\boldsymbol{n}\cdot\boldsymbol{\eta}_1|_F = 0$ for all F in $\mathcal{F}_h^I$ and we have

$$\begin{aligned}
[\![\hat{\boldsymbol{E}}^t_h]\!] &= \boldsymbol{n}^+\times\hat{\boldsymbol{E}}^{t,+}_h + \boldsymbol{n}^-\times\hat{\boldsymbol{E}}^{t,-}_h\\
&= \boldsymbol{n}^+\times\boldsymbol{E}^+_{h|K^+} + \tau_{K^+}\boldsymbol{n}^+\times\boldsymbol{n}^+\times(\boldsymbol{\Lambda}_h - \boldsymbol{H}^+_{h|K^+})\\
&\quad + \boldsymbol{n}^-\times\boldsymbol{E}^-_{h|K^-} + \tau_{K^-}\boldsymbol{n}^-\times\boldsymbol{n}^-\times(\boldsymbol{\Lambda}_h - \boldsymbol{H}^-_{h|K^-}).
\end{aligned}$$

Since K is a bounded domain and $\boldsymbol{n}$ is constant on every face we have that $\left(\boldsymbol{n}\times\boldsymbol{E}_{h|K}\right)_{|F}$ and $\left(\boldsymbol{n}\times\boldsymbol{H}_{h|K}\right)_{|F}$ are bounded polynoms in $\left[\mathbb{P}_{p_F}(F)\right]^3$ for all F in ∂K, which implies that $\boldsymbol{\eta}_1 \in \left[L^2\left(\mathcal{F}_h\right)\right]^3$ and $\boldsymbol{\eta}_1|_F \in \left[\mathbb{P}_{p_F}(F)\right]^3$ for all F in ∂K. We obtain $\left\langle [\![\hat{\boldsymbol{E}}_h^t]\!], \boldsymbol{\eta}_1\right\rangle_{\mathcal{F}_h^I} = ||[\![\hat{\boldsymbol{E}}_h^t]\!]||^2 = 0$, which is equivalent to $[\![\hat{\boldsymbol{E}}_h^t]\!]_{\mathcal{F}_h^I} = 0$. From (2.42), we have

$$[\![\boldsymbol{E}_h^t + \tau\boldsymbol{n}\times(\boldsymbol{\Lambda}_h - \boldsymbol{H}_h^t)]\!]_{\mathcal{F}_h^I} = 0,$$

by expanding we obtain

$$[\![\boldsymbol{E}_h^t]\!]_F - \left(\tau_{K^+} + \tau_{K^-}\right)\boldsymbol{\Lambda}_h + \tau_{K^+}\boldsymbol{H}_h^{t,+} + \tau_{K^-}\boldsymbol{H}_h^{t,-} = 0 \quad \forall F \in \mathcal{F}_h^I,$$

yielding

$$\boldsymbol{\Lambda}_h = \frac{1}{\tau_{K^+} + \tau_{K^-}}\left([\![\boldsymbol{E}_h^t]\!]_F + \tau_{K^+}\boldsymbol{H}_h^{t,+} + \tau_{K^-}\boldsymbol{H}_h^{t,-}\right) \quad \forall F \in \mathcal{F}_h^I. \tag{3.1}$$

Proceeding similarly for an absorbing boundary face and for a metalic boundary face, the conservativity condition writes $\left\langle \boldsymbol{n}\times\hat{\boldsymbol{E}}_h^t - \boldsymbol{\Lambda}_h - \boldsymbol{g}^{\text{inc}}, \boldsymbol{\eta}\right\rangle_{\Gamma_a} = 0$ and $\left\langle \boldsymbol{n}\times\hat{\boldsymbol{E}}_h^t, \boldsymbol{\eta}\right\rangle_{\Gamma_m} = 0$. In particular, for an absorbing boundary face

$$\boldsymbol{n}\times\hat{\boldsymbol{E}}_h^t - \boldsymbol{\Lambda}_h - \boldsymbol{g}^{\text{inc}} = 0 \quad \text{on } \Gamma_a,$$

and by (2.42) we have

$$\boldsymbol{n}\times\boldsymbol{E}_h^t - (\tau_K + 1)\boldsymbol{\Lambda}_h + \tau_K\boldsymbol{H}_h^t - \boldsymbol{g}^{\text{inc}} = 0 \quad \text{on } \Gamma_a.$$

Proceeding similarly for the metalic boundary and summarizing, we obtain

$$\boldsymbol{\Lambda}_h = \begin{cases} \dfrac{1}{\tau_{K^+} + \tau_{K^-}}\left(2\left\{\tau_K\boldsymbol{H}_h^t\right\}_F + [\![\boldsymbol{E}_h^t]\!]_F\right), & \text{if } F \in \mathcal{F}_h^I, \\ \dfrac{1}{\tau_K}\boldsymbol{n}\times\boldsymbol{E}_h^t + \boldsymbol{H}_h^t, & \text{if } F \in \mathcal{F}_h \cap \Gamma_m, \\ \dfrac{1}{\tau_K + 1}\left(\tau_K\boldsymbol{H}_h^t + \boldsymbol{n}\times\boldsymbol{E}_h^t - \boldsymbol{g}^{\text{inc}}\right). & \text{if } F \in \mathcal{F}_h \cap \Gamma_a. \end{cases} \tag{3.2}$$

By replacing (3.2) in (2.42) we obtain $\hat{\boldsymbol{E}}_h^t = \hat{\boldsymbol{E}}_h^{t,+} = \hat{\boldsymbol{E}}_h^{t,-}$ with

$$\hat{\boldsymbol{E}}_h^t = \begin{cases} \dfrac{\tau_{K^+}\tau_{K^-}}{\tau_{K^+} + \tau_{K^-}}\left(2\left\{\dfrac{1}{\tau_K}\boldsymbol{E}_h^t\right\}_F - [\![\boldsymbol{H}_h^t]\!]_F\right), & \text{if } F \in \mathcal{F}_h^I, \\ 0, & \text{if } F \in \mathcal{F}_h \cap \Gamma_m, \\ \dfrac{1}{\tau_K + 1}\left(\boldsymbol{E}_h^t - \tau_K\boldsymbol{n}\times\boldsymbol{H}_h^t - \tau_K\boldsymbol{n}\times\boldsymbol{g}^{\text{inc}}\right). & \text{if } F \in \mathcal{F}_h \cap \Gamma_a. \end{cases} \tag{3.3}$$

Thus, the numerical traces (2.41) and (2.42) have been reformulated from the conservativity condition. This means that the conservativity condition is now included in the new formulation of the numerical fluxes and can be omitted in the global system of equations. Hence, the local system (2.39) takes the form of a classical DG formulation, for all $\boldsymbol{v} \in \boldsymbol{V}_h$

$$\begin{cases} (\varepsilon\partial_t\boldsymbol{E}_h, \boldsymbol{v})_K - (\boldsymbol{H}_h, \mathbf{curl}\,\boldsymbol{v})_K + \left\langle \hat{\boldsymbol{H}}_h^t, \boldsymbol{n}\times\boldsymbol{v}\right\rangle_{\partial K} = 0, \\ (\mu\partial_t\boldsymbol{H}_h, \boldsymbol{v})_K + (\boldsymbol{E}_h, \mathbf{curl}\,\boldsymbol{v})_K - \left\langle \hat{\boldsymbol{E}}_h^t, \boldsymbol{n}\times\boldsymbol{v}\right\rangle_{\partial K} = 0, \end{cases} \tag{3.4}$$

where the numerical fluxes are defined by (3.2) and (3.3).

Remark 5. Let $Y_K = \sqrt{\varepsilon_K}/\sqrt{\mu_K}$ be the local admittance associated to cell K and $Z_K = 1/Y_K$ the corresponding local impedance. If we set $\tau_K = Z_K$ in (3.2) and $1/\tau_K = Y_K$ in (3.3), the obtained numerical traces coincide with those adopted in the classical upwind flux DGTD method [8].

3.3 Stability and conservation properties

3.3.1 Formulation

Let us introduce

$$\boldsymbol{v}_h = \begin{pmatrix} \boldsymbol{H}_h \\ \boldsymbol{E}_h \end{pmatrix},$$

$\lambda = \mathrm{diag}(\mu, \varepsilon)$ and for all K in $\mathcal{T}_h$, all $\boldsymbol{v}$ in $\mathbb{V}_h$

$$\zeta_K(\boldsymbol{v}) = \begin{pmatrix} \mathbf{curl}\left(\boldsymbol{v}_{2|K}\right) \\ -\mathbf{curl}\left(\boldsymbol{v}_{1|K}\right) \end{pmatrix}.$$

After summing the two equations of the local formulation (3.4) we obtain $\forall \boldsymbol{v}'_h \in \mathbb{V}_h = \boldsymbol{V}_h \times \boldsymbol{V}_h$

$$\left(\lambda \partial_t \boldsymbol{v}_h, \boldsymbol{v}'_h\right)_K = \left(\boldsymbol{v}_h, \zeta_K(\boldsymbol{v}'_h)\right)_K - \left\langle \boldsymbol{F}^{\tau}_{K,h}(\boldsymbol{v}_h), \boldsymbol{v}'_h \right\rangle_{\partial K}. \tag{3.5}$$

Assuming τ is constant in $\mathcal{T}_h$ and $\boldsymbol{g}^{inc} = 0$, the numerical flux $\boldsymbol{F}^{\tau}_{K,h}$ is defined on ∂K by

$$\boldsymbol{F}^{\tau}_{K,h}(\boldsymbol{v})_{|\partial K \cap \mathcal{F}^I_h} = \begin{pmatrix} \dfrac{\tau}{2}\left(\dfrac{2}{\tau}\boldsymbol{n} \times \{\boldsymbol{v}_2\} - \boldsymbol{n} \times [\![\boldsymbol{v}_1]\!]\right) \\ -\dfrac{1}{2\tau}\left(2\tau \boldsymbol{n} \times \{\boldsymbol{v}_1\} + \boldsymbol{n} \times [\![\boldsymbol{v}_2]\!]\right) \end{pmatrix},$$

and

$$\boldsymbol{F}^{\tau}_{K,h}(\boldsymbol{v})_{|\partial K \cap \Gamma_m} = \begin{pmatrix} 0 \\ \dfrac{1}{\tau}\left(\boldsymbol{n} \times \boldsymbol{n} \times \boldsymbol{v}_2\right) + \boldsymbol{n} \times \boldsymbol{v}_1 \end{pmatrix},$$

$$\boldsymbol{F}^{\tau}_{K,h}(\boldsymbol{v})_{|\partial K \cap \Gamma_a} = \begin{pmatrix} -\dfrac{1}{\tau+1}\left(\boldsymbol{n} \times \boldsymbol{v}_2\right) + \dfrac{\tau}{\tau+1}\left(\boldsymbol{n} \times \boldsymbol{n} \times \boldsymbol{v}_1\right) \\ \dfrac{\tau}{\tau+1}\left(\boldsymbol{n} \times \boldsymbol{v}_1\right) + \dfrac{1}{\tau+1}\left(\boldsymbol{n} \times \boldsymbol{n} \times \boldsymbol{v}_2\right) \end{pmatrix}.$$

For the global weak formulation we define for all $\boldsymbol{v}$ in $\mathbb{V}_h$

$$\zeta_h(\boldsymbol{v}) = \begin{pmatrix} \mathbf{curl}_h\left(\boldsymbol{v}_2\right) \\ -\mathbf{curl}_h\left(\boldsymbol{v}_1\right) \end{pmatrix},$$

with $\mathbf{curl}_h$ is the piecewise curl operator defined on each K and for all $\mathbf{b}_h$ as $\left(\mathbf{curl}_h\left(\mathbf{b}_h\right)\right)_{|K} = \mathbf{curl}\left(\mathbf{b}_{h|K}\right)$. Intrducing the bilinear forms m, a, b_τ defined on $\mathbb{V}_h \times \mathbb{V}_h$ such that,

for all $(\boldsymbol{v}, \boldsymbol{v}') \in \mathbb{V}_h \times \mathbb{V}_h$

$$\begin{cases} m(\boldsymbol{v}, \boldsymbol{v}') = (\boldsymbol{v}, \boldsymbol{v}')_\lambda = (\lambda \boldsymbol{v}, \boldsymbol{v}')_{\mathcal{T}_h} \\ a(\boldsymbol{v}, \boldsymbol{v}') = (\boldsymbol{v}, \zeta_h(\boldsymbol{v}'))_{\mathcal{T}_h} \\ b_\tau(\boldsymbol{v}, \boldsymbol{v}') = \left\langle \{\boldsymbol{v}_2\}, [\![\boldsymbol{v}_1']\!] \right\rangle_{\mathcal{F}_h^I} - \dfrac{\tau}{2} \left\langle [\![\boldsymbol{v}_1]\!], [\![\boldsymbol{v}_1']\!] \right\rangle_{\mathcal{F}_h^I} - \left\langle \{\boldsymbol{v}_1\}, [\![\boldsymbol{v}_2']\!] \right\rangle_{\mathcal{F}_h^I} \\ - \dfrac{1}{2\tau} \left\langle [\![\boldsymbol{v}_2]\!], [\![\boldsymbol{v}_2']\!] \right\rangle_{\mathcal{F}_h^I} - \dfrac{1}{\tau} \displaystyle\int_{\Gamma_m} (\boldsymbol{n} \times \boldsymbol{v}_2) \cdot (\boldsymbol{n} \times \boldsymbol{v}_2') \\ + \displaystyle\int_{\Gamma_m} (\boldsymbol{n} \times \boldsymbol{v}_1) \cdot \boldsymbol{v}_2' - \dfrac{1}{\tau+1} \displaystyle\int_{\Gamma_a} (\boldsymbol{n} \times \boldsymbol{v}_2) \cdot \boldsymbol{v}_1' \\ - \dfrac{\tau}{\tau+1} \displaystyle\int_{\Gamma_a} (\boldsymbol{n} \times \boldsymbol{v}_1) \cdot (\boldsymbol{n} \times \boldsymbol{v}_1') + \dfrac{\tau}{\tau+1} \displaystyle\int_{\Gamma_a} (\boldsymbol{n} \times \boldsymbol{v}_1) \cdot \boldsymbol{v}_2' \\ - \dfrac{1}{\tau+1} \displaystyle\int_{\Gamma_a} (\boldsymbol{n} \times \boldsymbol{v}_2) \cdot (\boldsymbol{n} \times \boldsymbol{v}_2'). \end{cases} \tag{3.6}$$

Then, the global formulation of the semi-discrete HDG scheme writes as

$$m(\partial_t \boldsymbol{v}_h, \boldsymbol{v}_h') = a(\boldsymbol{v}_h, \boldsymbol{v}_h') + b_\tau(\boldsymbol{v}_h, \boldsymbol{v}_h'). \tag{3.7}$$

3.3.2 Semi-discrete stability

We introduce the energy function defined on $[0, T]$ by

The total discrete electromagnetic energy

$$\mathcal{E}_h(t) = \frac{1}{2} \left(\varepsilon ||\boldsymbol{E}_h(t)||^2 + \mu ||\boldsymbol{H}_h(t)||^2 \right) = \frac{1}{2} m(\boldsymbol{v}_h, \boldsymbol{v}_h) = \frac{1}{2} ||\boldsymbol{v}_h||_\lambda^2.$$

Theorem 4. *For all $\tau > 0$ the energy function $\mathcal{E}_h(t)$ decreases in time and $\mathcal{E}_h(t) \leq \mathcal{E}_h(0)$ for all $t > 0$.*

Proof. By the formula $\partial_t ||\boldsymbol{v}||^2 = 2\,(\partial_t \boldsymbol{v}, \boldsymbol{v})$ we have $\partial_t \mathcal{E}_h(t) = m(\partial_t \boldsymbol{v}_h, \boldsymbol{v}_h)$ and, using the formula $\displaystyle\int_K \mathbf{curl}\, \mathbf{u} \cdot \mathbf{v} = \int_K \mathbf{curl}\, \mathbf{v} \cdot \mathbf{u} + \int_{\partial K} (\boldsymbol{n} \times \mathbf{u}) \cdot \mathbf{v}$, we deduce from (3.7) that

$$\partial_t \mathcal{E}_h(t) = a(\boldsymbol{v}_h, \boldsymbol{v}_h) + b_\tau(\boldsymbol{v}_h, \boldsymbol{v}_h).$$

We have

$$a(\boldsymbol{v}_h, \boldsymbol{v}_h) = (\boldsymbol{v}_1, \mathbf{curl}\, \boldsymbol{v}_2)_{\mathcal{T}_h} - (\boldsymbol{v}_1, \mathbf{curl}\, \boldsymbol{v}_2)_{\mathcal{T}_h} = 0,$$

and for all $\tau > 0$,

$$
\begin{aligned}
b_\tau(\boldsymbol{v}_h, \boldsymbol{v}_h) = & - \left\langle \boldsymbol{n} \times \boldsymbol{v}_1^+, \boldsymbol{v}_2^+ \right\rangle_{\mathcal{F}_h^I} + \left\langle \boldsymbol{n} \times \boldsymbol{v}_1^-, \boldsymbol{v}_2^- \right\rangle_{\mathcal{F}_h^I} - \int_{\partial\Omega} (\boldsymbol{n} \times \boldsymbol{v}_1) \cdot \boldsymbol{v}_2 \\
& + \frac{1}{2} \left\langle \boldsymbol{v}_2^+, \boldsymbol{n} \times \boldsymbol{v}_1^+ \right\rangle_{\mathcal{F}_h^I} - \frac{1}{2} \left\langle \boldsymbol{v}_2^+, \boldsymbol{n} \times \boldsymbol{v}_1^- \right\rangle_{\mathcal{F}_h^I} + \frac{1}{2} \left\langle \boldsymbol{v}_2^-, \boldsymbol{n} \times \boldsymbol{v}_1^+ \right\rangle_{\mathcal{F}_h^I} \\
& - \frac{1}{2} \left\langle \boldsymbol{v}_2^-, \boldsymbol{n} \times \boldsymbol{v}_1^- \right\rangle_{\mathcal{F}_h^I} - \frac{1}{2} \left\langle \boldsymbol{v}_1^+, \boldsymbol{n} \times \boldsymbol{v}_2^+ \right\rangle_{\mathcal{F}_h^I} - \frac{1}{2} \left\langle \boldsymbol{v}_1^+, \boldsymbol{n} \times \boldsymbol{v}_2^- \right\rangle_{\mathcal{F}_h^I} \\
& - \frac{1}{2} \left\langle \boldsymbol{v}_1^-, \boldsymbol{n} \times \boldsymbol{v}_2^+ \right\rangle_{\mathcal{F}_h^I} + \frac{1}{2} \left\langle \boldsymbol{v}_1^-, \boldsymbol{n} \times \boldsymbol{v}_2^- \right\rangle_{\mathcal{F}_h^I} \\
& - \frac{\tau}{2} ||[\![\boldsymbol{v}_1]\!]||^2_{\mathcal{F}_h^I} - \frac{1}{2\tau} ||[\![\boldsymbol{v}_2]\!]||^2_{\mathcal{F}_h^I} + \frac{1}{\tau+1} \int_{\Gamma_a} (\boldsymbol{n} \times \boldsymbol{v}_1) \cdot \boldsymbol{v}_2 \\
& + \int_{\Gamma_m} (\boldsymbol{n} \times \boldsymbol{v}_1) \cdot \boldsymbol{v}_2 + \frac{\tau}{\tau+1} \int_{\Gamma_a} (\boldsymbol{n} \times \boldsymbol{v}_1) \cdot \boldsymbol{v}_2 \\
& - \frac{\tau}{\tau+1} ||\boldsymbol{n} \times \boldsymbol{v}_1||^2_{\Gamma_a} - \frac{1}{\tau} ||\boldsymbol{n} \times \boldsymbol{v}_2||^2_{\Gamma_m} - \frac{1}{\tau+1} ||\boldsymbol{n} \times \boldsymbol{v}_2||^2_{\Gamma_a} \\
= & - \frac{\tau}{2} ||[\![\boldsymbol{v}_1]\!]||^2_{\mathcal{F}_h^I} - \frac{1}{2\tau} ||[\![\boldsymbol{v}_2]\!]||^2_{\mathcal{F}_h^I} - \frac{\tau}{\tau+1} ||\boldsymbol{n} \times \boldsymbol{v}_1||^2_{\Gamma_a} \\
& - \frac{1}{\tau} ||\boldsymbol{n} \times \boldsymbol{v}_2||^2_{\Gamma_m} - \frac{1}{\tau+1} ||\boldsymbol{n} \times \boldsymbol{v}_2||^2_{\Gamma_a} \\
\leq & 0.
\end{aligned}
$$

□

This result shows the L^2-stability of the semi-discrete HDG method. In particular, this method is dissipative for the considered numerical trace for $\hat{\boldsymbol{E}}_h^t$ in (2.42).

3.3.3 Fully discrete stability

For the sake of simplicity, we will consider $\Gamma_a = \emptyset$ in this section. We introduce the linear operator $\mathbf{L}_h : \mathbb{V}_h \to \mathbb{V}_h$ defined for all $(\boldsymbol{\iota}, \boldsymbol{\nu})$ in $\mathbb{V}_h \times \mathbb{V}_h$ by

$$
(\mathbf{L}_h \boldsymbol{\iota}, \boldsymbol{\nu}) = a(\boldsymbol{\iota}, \boldsymbol{\nu}) + b_\tau(\boldsymbol{\iota}, \boldsymbol{\nu}).
$$

We infer from (3.7) that

$$
\lambda \frac{d}{dt} \upsilon_h = \mathbf{L}_h(\upsilon_h).
$$

We also recall the following inverse estimates from [47] : For all i in $\{1, \cdots, |\mathcal{T}_h|\}$, there exist $c_{1,i} > 0$ and $c_{2,i} > 0$ such that

$$
\begin{aligned}
|| \operatorname{curl}(\boldsymbol{u})||_{L^2(K)} &\leq c_{1,i}\, h_K^{-1} ||\boldsymbol{u}||_{L^2(K)}, \\
||\boldsymbol{u}||_{L^2(\partial K_i)} &\leq c_{2,i}\, h^{-\frac{1}{2}} ||\boldsymbol{u}||_{L^2(K_i)}.
\end{aligned}
\tag{3.8}
$$

With these inverse estimates we can prove the following lemma.

Lemma 2. *For all $\boldsymbol{\iota}$ in $\mathbb{V}_h$, there exists $c(\tau) > 0$ such that*

$$
\sup_{\boldsymbol{\nu} \in \mathbb{V}_h} \frac{|\,(\boldsymbol{L}_h \boldsymbol{\iota}, \boldsymbol{\nu})\,|}{||\boldsymbol{\nu}||_{\mathcal{T}_h}} \leq c(\tau) h^{-1} ||\boldsymbol{\iota}||_{\mathcal{T}_h}. \tag{3.9}
$$

Proof. The proof is classical. Inverse estimations are used to upper bound the operator $\mathbf{L}_h$. First an upper bound for the bilinear form a is found, and then we show how to upper bound the first term of b_τ. The other terms of b_τ can be treated in the same way. For all $\boldsymbol{\iota}$ in $\mathbb{V}_h$ we have

$$\sup_{\boldsymbol{\nu}\in\mathbb{V}_h} \frac{|\left(\mathbf{L}_h\boldsymbol{\iota},\boldsymbol{\nu}\right)|}{||\boldsymbol{\nu}||_{\mathcal{T}_h}} = \sup_{\boldsymbol{\nu}\in\mathbb{V}_h} \frac{|a(\boldsymbol{\iota},\boldsymbol{\nu})+b_\tau(\boldsymbol{\iota},\boldsymbol{\nu})|}{||\boldsymbol{\nu}||_{\mathcal{T}_h}} \leq \sup_{\boldsymbol{\nu}\in\mathbb{V}_h} \frac{|a(\boldsymbol{\iota},\boldsymbol{\nu})|}{||\boldsymbol{\nu}||_{\mathcal{T}_h}} + \sup_{\boldsymbol{\nu}\in\mathbb{V}_h} \frac{|b_\tau(\boldsymbol{\iota},\boldsymbol{\nu})|}{||\boldsymbol{\nu}||_{\mathcal{T}_h}}.$$

On one hand we have for all $\boldsymbol{\iota}$ in $\mathbb{V}_h$,

$$\begin{aligned}
|a(\boldsymbol{\iota},\boldsymbol{\nu})| &= \left|\sum_{i=1}^{|\mathcal{T}_h|} \left(\boldsymbol{\iota},\zeta_{K_i}(\boldsymbol{\nu})\right)_{K_i}\right| \\
&\leq \sum_{i=1}^{|\mathcal{T}_h|} \left|\left(\boldsymbol{\iota},\zeta_{K_i}(\boldsymbol{\nu})\right)_{K_i}\right| \\
&\leq \sum_{i=1}^{|\mathcal{T}_h|} ||\boldsymbol{\iota}||_{K_i}\ ||\zeta_K(\boldsymbol{\nu})||_{K_i} \\
&\leq \sum_{i=1}^{|\mathcal{T}_h|} ||\boldsymbol{\iota}||_{K_i} \left(||\mathbf{curl}(\boldsymbol{\nu}_{2/K_i})||^2_{K_i} + ||\mathbf{curl}(\boldsymbol{\nu}_{1/K_i})||^2_{K_i}\right)^{\frac{1}{2}} \\
&\leq \sum_{i=1}^{|\mathcal{T}_h|} ||\boldsymbol{\iota}||_{K_i} \left(\left[c_{1,i}h^{-1}||\boldsymbol{\nu}_{2/K_i}||_{K_i}\right]^2 + \left[c_{1,i}h^{-1}||\boldsymbol{\nu}_{1/K_i}||_{K_i}\right]^2\right)^{\frac{1}{2}}.
\end{aligned}$$

Introducing $c_1 = \max_{i\in\{1,\cdots,|\mathcal{T}_h|\}} c_{1,i}$, we obtain

$$\begin{aligned}
|a(\boldsymbol{\iota},\boldsymbol{\nu})| &\leq c_1 h^{-1} \sum_{i=1}^{|\mathcal{T}_h|} ||\boldsymbol{\iota}||_{K_i}\ ||\boldsymbol{\nu}||_{K_i} \\
&\leq c_1 h^{-1} \left(\sum_{i=1}^{|\mathcal{T}_h|} ||\boldsymbol{\iota}||^2_{K_i}\right)^{\frac{1}{2}} \left(\sum_{i=1}^{|\mathcal{T}_h|} ||\boldsymbol{\nu}||^2_{K_i}\right)^{\frac{1}{2}}, \\
&\leq c_1 h^{-1} ||\boldsymbol{\iota}||_{\mathcal{T}_h} ||\boldsymbol{\nu}||_{\mathcal{T}_h},
\end{aligned}$$

therefore

$$\sup_{\boldsymbol{\nu}\in\mathbb{V}_h} \frac{|a(\boldsymbol{\iota},\boldsymbol{\nu})|}{||\boldsymbol{\nu}||_{\mathcal{T}_h}} \leq c_1 h^{-1} ||\boldsymbol{\iota}||_{\mathcal{T}_h}. \tag{3.10}$$

On the other hand we have for all $\boldsymbol{\iota}$ in $\mathbb{V}_h$,

$$\begin{aligned}
|b_\tau(\boldsymbol{\iota},\boldsymbol{\nu})| =& |\left\langle\{\boldsymbol{\iota}_2\}, [\![\boldsymbol{\nu}_1]\!]\right\rangle_{\mathcal{F}_h^I} - \frac{\tau}{2}\left\langle[\![\boldsymbol{\iota}_1]\!], [\![\boldsymbol{\nu}_1]\!]\right\rangle_{\mathcal{F}_h^I} - \left\langle\{\boldsymbol{\iota}_1\}, [\![\boldsymbol{\nu}_2]\!]\right\rangle_{\mathcal{F}_h^I} \\
&- \frac{1}{2\tau}\left\langle[\![\boldsymbol{\iota}_2]\!], [\![\boldsymbol{\nu}_2]\!]\right\rangle_{\mathcal{F}_h^I} - \frac{1}{\tau}\int_{\Gamma_m} (\boldsymbol{n}\times\boldsymbol{\iota}_2)\cdot(\boldsymbol{n}\times\boldsymbol{\nu}_2) \\
&+ \int_{\Gamma_m} (\boldsymbol{n}\times\boldsymbol{\iota}_1)\cdot\boldsymbol{\nu}_2| \\
\leq& \left|\left\langle\{\boldsymbol{\iota}_2\}, [\![\boldsymbol{\nu}_1]\!]\right\rangle_{\mathcal{F}_h^I}\right| + \frac{\tau}{2}\left|\left\langle[\![\boldsymbol{\iota}_1]\!], [\![\boldsymbol{\nu}_1]\!]\right\rangle_{\mathcal{F}_h^I}\right| + \left|\left\langle\{\boldsymbol{\iota}_1\}, [\![\boldsymbol{\nu}_2]\!]\right\rangle_{\mathcal{F}_h^I}\right| \\
&+ \frac{1}{2\tau}\left|\left\langle[\![\boldsymbol{\iota}_2]\!], [\![\boldsymbol{\nu}_2]\!]\right\rangle_{\mathcal{F}_h^I}\right| + \frac{1}{\tau}\int_{\Gamma_m} |(\boldsymbol{n}\times\boldsymbol{\iota}_2)\cdot(\boldsymbol{n}\times\boldsymbol{\nu}_2)| \\
&+ \int_{\Gamma_m} |(\boldsymbol{n}\times\boldsymbol{\iota}_1)\cdot\boldsymbol{\nu}_2|.
\end{aligned}$$

We want to expand the first term and all others terms are treated similarly:

$$\begin{aligned}
\left|\langle\{\boldsymbol{\iota}_2\}, [\![\boldsymbol{\nu}_1]\!]\rangle_{\mathcal{F}_h^I}\right| &= \left|\sum_{F\in\mathcal{F}_h^I} \frac{1}{2}\left\langle \boldsymbol{\iota}_2^+ + \boldsymbol{\iota}_2^-, \boldsymbol{n}\times(\boldsymbol{\nu}_1^+ - \boldsymbol{\nu}_1^-)\right\rangle_F\right| \\
&\leq \sum_{F\in\mathcal{F}_h^I} \frac{1}{2}(||\boldsymbol{\iota}_2^+||_F + ||\boldsymbol{\iota}_2^-||_F)(||\boldsymbol{\nu}_1^+||_F + ||\boldsymbol{\nu}_1^-||_F) \\
&\leq \sum_{i=1}^{|\mathcal{T}_h|}\sum_{F\in\partial K_i} \frac{1}{2}(||\boldsymbol{\iota}_2^+||_F + ||\boldsymbol{\iota}_2^-||_F)(||\boldsymbol{\nu}_1^+||_F + ||\boldsymbol{\nu}_1^-||_F),
\end{aligned}$$

then

$$\begin{aligned}
\left|\langle\{\boldsymbol{\iota}_2\}, [\![\boldsymbol{\nu}_1]\!]\rangle_{\mathcal{F}_h^I}\right| &\leq \frac{1}{2}\sum_{i=1}^{|\mathcal{T}_h|}\sum_{F\in\partial K_i}\Big[||\boldsymbol{\iota}_2^+||_F\,||\boldsymbol{\nu}_1^+||_F + ||\boldsymbol{\iota}_2^+||_F\,||\boldsymbol{\nu}_1^-||_F + \\
&\qquad\qquad ||\boldsymbol{\iota}_2^-||_F||\boldsymbol{\nu}_1^+||_F + ||\boldsymbol{\iota}_2^-||_F||\boldsymbol{\nu}_1^-||_F\Big] \\
&\leq \frac{1}{2}\sum_{i=1}^{|\mathcal{T}_h|}\Big[4||\boldsymbol{\iota}_2||_{\partial K_i}\,||\boldsymbol{\nu}_1||_{\partial K_i} + \sum_{j\in\nu_i}\big(||\boldsymbol{\iota}_2||_{\partial K_j}\,||\boldsymbol{\nu}_1||_{\partial K_j} + \\
&\qquad\qquad ||\boldsymbol{\iota}_2||_{\partial K_j}\,||\boldsymbol{\nu}_1||_{\partial K_i} + ||\boldsymbol{\iota}_2||_{\partial K_i}||\boldsymbol{\nu}_1||_{\partial K_j}\big)\Big] \\
&\leq \frac{1}{2}\sum_{i=1}^{|\mathcal{T}_h|}\Big[4||\boldsymbol{\iota}_2||_{\partial K_i}\,||\boldsymbol{\nu}_1||_{\partial K_i} + \sum_{j\in\nu_i}||\boldsymbol{\iota}_2||_{\partial K_j}\,||\boldsymbol{\nu}_1||_{\partial K_j} + \\
&\qquad\qquad ||\boldsymbol{\nu}_1||_{\partial K_i}\sum_{j\in\nu_i}||\boldsymbol{\iota}_2||_{\partial K_j} + ||\boldsymbol{\iota}_2||_{\partial K_i}\sum_{j\in\nu_i}||\boldsymbol{\nu}_1||_{\partial K_j}\Big] \\
&\leq 2\sum_{i=1}^{|\mathcal{T}_h|}||\boldsymbol{\iota}_2||_{\partial K_i}\,||\boldsymbol{\nu}_1||_{\partial K_i} + \frac{1}{2}\sum_{i=1}^{|\mathcal{T}_h|}\sum_{j\in\nu_i}||\boldsymbol{\iota}_2||_{\partial K_j}\,||\boldsymbol{\nu}_1||_{\partial K_j} \\
&\quad + \frac{1}{2}\sum_{i=1}^{|\mathcal{T}_h|}\left(||\boldsymbol{\nu}_1||_{\partial K_i}\sum_{j\in\nu_i}||\boldsymbol{\iota}_2||_{\partial K_j}\right) \\
&\quad + \frac{1}{2}\sum_{i=1}^{|\mathcal{T}_h|}\left(||\boldsymbol{\iota}_2||_{\partial K_i}\sum_{j\in\nu_i}||\boldsymbol{\nu}_1||_{\partial K_j}\right).
\end{aligned}$$

Since we are in $\mathbb{R}^3$ every K_i has 4 neighbours except the cells on the boundary ($i.e$ $|\nu_i| \leq 4$)

$$\frac{1}{2}\sum_{i=1}^{|\mathcal{T}_h|}\sum_{j\in\nu_i}||\boldsymbol{\iota}_2||_{\partial K_j}\,||\boldsymbol{\nu}_1||_{\partial K_j} \leq 2\sum_{i=1}^{|\mathcal{T}_h|}||\boldsymbol{\iota}_2||_{\partial K_i}\,||\boldsymbol{\nu}_1||_{\partial K_i},$$

and we also have

$$\begin{aligned}
\frac{1}{2}\sum_{i=1}^{|\mathcal{T}_h|}\left(||\boldsymbol{\nu}_1||_{\partial K_i}\sum_{j\in\nu_i}||\boldsymbol{\iota}_2||_{\partial K_j}\right) &\leq \frac{1}{2}\left(\sum_{i=1}^{|\mathcal{T}_h|}||\boldsymbol{\nu}_1||^2_{\partial K_i}\right)^{\frac{1}{2}} \\
&\quad\times\left(\sum_{i=1}^{|\mathcal{T}_h|}\left(\sum_{j\in\nu_i}||\boldsymbol{\iota}_2||_{\partial K_j}\right)^2\right)^{\frac{1}{2}}.
\end{aligned}$$

By using the well known formula $(a_1+a_2)^2 \leq 2(a_1^2+a_2^2)$ so by induction we have

$$\left(\sum_{i=1}^{4} a_i\right)^2 \leq 8a_1^2+8a_2^2+4a_3^2+2a_4^2 \leq 8\sum_{i=1}^{4} a_i^2,$$

then

$$\left(\sum_{i=1}^{|\mathcal{T}_h|}\left(\sum_{j\in\nu_i}||\boldsymbol{\iota}_2||_{\partial K_j}\right)^2\right)^{\frac{1}{2}} \leq 4\sqrt{2}\left(\sum_{i=1}^{|\mathcal{T}_h|}||\boldsymbol{\iota}_2||^2_{\partial K_i}\right)^{\frac{1}{2}},$$

which implies

$$\frac{1}{2}\sum_{i=1}^{|\mathcal{T}_h|}\left(||\boldsymbol{\nu}_1||_{\partial K_i}\sum_{j\in\nu_i}||\boldsymbol{\iota}_2||_{\partial K_j}\right) \leq 2\sqrt{2}\left(\sum_{i=1}^{|\mathcal{T}_h|}||\boldsymbol{\nu}_1||^2_{\partial K_i}\right)^{\frac{1}{2}}\left(\sum_{i=1}^{|\mathcal{T}_h|}||\boldsymbol{\iota}_2||^2_{\partial K_i}\right)^{\frac{1}{2}}.$$

So for now we have

$$\begin{aligned}\left|\langle\{\boldsymbol{\iota}_2\},[\![\boldsymbol{\nu}_1]\!]\rangle_{\mathcal{F}_h^I}\right| &\leq 4\sum_{i=1}^{|\mathcal{T}_h|}||\boldsymbol{\iota}_2||_{\partial K_i}||\boldsymbol{\nu}_1||_{\partial K_i}\\ &\quad+4\sqrt{2}\left(\sum_{i=1}^{|\mathcal{T}_h|}||\boldsymbol{\nu}_1||^2_{\partial K_i}\right)^{\frac{1}{2}}\left(\sum_{i=1}^{|\mathcal{T}_h|}||\boldsymbol{\iota}_2||^2_{\partial K_i}\right)^{\frac{1}{2}}\\ &\leq 4(1+\sqrt{2})\left(\sum_{i=1}^{|\mathcal{T}_h|}||\boldsymbol{\nu}_1||^2_{\partial K_i}\right)^{\frac{1}{2}}\left(\sum_{i=1}^{|\mathcal{T}_h|}||\boldsymbol{\iota}_2||^2_{\partial K_i}\right)^{\frac{1}{2}}.\end{aligned}$$

From the inverse estimates (3.8) we deduce

$$\begin{aligned}&\leq 4c_2^2(1+\sqrt{2})h^{-1}\left(\sum_{i=1}^{|\mathcal{T}_h|}||\boldsymbol{\nu}_1||^2_{K_i}\right)^{\frac{1}{2}}\left(\sum_{i=1}^{|\mathcal{T}_h|}||\boldsymbol{\iota}_2||^2_{K_i}\right)^{\frac{1}{2}}\\ &\leq c_3h^{-1}||\boldsymbol{\iota_2}||_{\mathcal{T}_h}||\boldsymbol{\nu_1}||_{\mathcal{T}_h}.\end{aligned}$$

Since $||\boldsymbol{\iota}||_{\mathcal{T}_h} = \left(||\boldsymbol{\iota_1}||^2_{\mathcal{T}_h}+||\boldsymbol{\iota_2}||^2_{\mathcal{T}_h}\right)^{\frac{1}{2}}$ and the same for $||\nu||_{\mathcal{T}_h}$ finally we have

$$\left|\langle\{\boldsymbol{\iota}_2\},[\![\boldsymbol{\nu}_1]\!]\rangle_{\mathcal{F}_h^I}\right| \leq c_3h^{-1}||\boldsymbol{\iota}||_{\mathcal{T}_h}||\boldsymbol{\nu}||_{\mathcal{T}_h}.$$

Back to b_τ we deduce that

$$|b_\tau(\boldsymbol{\iota},\boldsymbol{\nu})| \leq c_3\max\left(1,\frac{1}{\tau},\frac{\tau}{2}\right)h^{-1}||\boldsymbol{\iota}||_{\mathcal{T}_h}||\boldsymbol{\nu}||_{\mathcal{T}_h},$$

then

$$\sup_{\boldsymbol{\nu}\in\mathbb{V}_h}\frac{|b_\tau(\boldsymbol{\iota},\boldsymbol{\nu})|}{||\boldsymbol{\nu}||_{\mathcal{T}_h}} \leq c_3\max\left(1,\frac{1}{\tau},\frac{\tau}{2}\right)h^{-1}||\boldsymbol{\iota}||_{\mathcal{T}_h}. \tag{3.11}$$

Finally with (3.10) and (3.11)

$$\sup_{\boldsymbol{\nu}\in\mathbb{V}_h} \frac{|\,(\mathbf{L}_h\boldsymbol{\iota},\boldsymbol{\nu})\,|}{||\boldsymbol{\nu}||_{\mathcal{T}_h}} \leq \left[c_1 + c_3 \max\left(1, \frac{\tau}{2}, \frac{1}{\tau}\right)\right] h^{-1}||\boldsymbol{\iota}||_{\mathcal{T}_h}.$$

This concludes the proof of lemma 2. □

Remark 6. The proof is valid in the case of a uniform mesh. For the case of a quasi uniform mesh, i.e. there exists $\eta > 0$, independent of h, such that for all K_i in $\mathcal{T}_h$ and for all j in ν_i, $h_i/h_j \leq \eta$, the constant $c(\tau)$ of the lemma 2 will be replaced by $c(\tau)\eta$.

In the next proposition we prove the stability of the fully explicit scheme obtained by using a Runge-Kutta RK2 scheme. The RK2 scheme can be expressed in its two steps version as follows for all n in $\mathbb{N}$ [48]

Two steps version of the RK2 scheme

$$\boldsymbol{\omega}^n = \boldsymbol{\upsilon}_h^n + \Delta t\lambda^{-1}\mathbf{L}_h(\boldsymbol{\upsilon}_h^n) \tag{3.12}$$

and

$$\boldsymbol{\upsilon}_h^{n+1} = \frac{1}{2}(\boldsymbol{\upsilon}_h^n + \boldsymbol{\omega}^n) + \frac{1}{2}\Delta t\lambda^{-1}\mathbf{L}_h(\boldsymbol{\omega}^n). \tag{3.13}$$

Proposition 1. *Let $\tau \geq 0$, under a $\frac{4}{3} - CFL$ condition, i.e $\Delta t \leq c(\tau)h^{\frac{4}{3}}$, the explicit HDGTD scheme with a RK2 discretization in time is stable in finite time.*

Proof. Let us study the variation of the energy defined by $\mathcal{E}_h^n = \frac{1}{2}||\boldsymbol{\upsilon}_h^n||_\lambda^2$. We have

$$\lambda\frac{d}{dt}\upsilon_h = \mathbf{L}_h(\boldsymbol{\upsilon}_h).$$

We start by proving the following formula

$$||\boldsymbol{\upsilon}_h^{n+1}||_\lambda^2 - ||\boldsymbol{\upsilon}_h^n||_\lambda^2 = ||\boldsymbol{\upsilon}_h^{n+1} - \boldsymbol{\omega}^n||_\lambda^2 + \Delta t((\mathbf{L}_h(\boldsymbol{\upsilon}_h^n), \boldsymbol{\upsilon}_h^n)_{\mathcal{T}_h} + (\mathbf{L}_h(\boldsymbol{\omega}^n), \boldsymbol{\omega}^n)_{\mathcal{T}_h}). \tag{3.14}$$

We have

$$\begin{aligned}
||\boldsymbol{\upsilon}_h^{n+1} - \boldsymbol{\omega}^n||_\lambda^2 &= (\boldsymbol{\upsilon}_h^{n+1} - \boldsymbol{\omega}^n, \boldsymbol{\upsilon}_h^{n+1} - \boldsymbol{\omega}^n)_\lambda \\
&= ||\boldsymbol{\upsilon}_h^{n+1}||_\lambda^2 - 2(\boldsymbol{\upsilon}_h^{n+1}, \boldsymbol{\omega}^n)_\lambda + (\boldsymbol{\omega}^n, \boldsymbol{\omega}^n)_\lambda \\
&= ||\boldsymbol{\upsilon}_h^{n+1}||_\lambda^2 \\
&\quad - (\boldsymbol{\upsilon}_h^n + \boldsymbol{\omega}^n + \Delta t\lambda^{-1}\mathbf{L}_h(\boldsymbol{\omega}^n), \boldsymbol{\upsilon}_h^n + \Delta t\lambda^{-1}\mathbf{L}_h(\boldsymbol{\upsilon}_h^n))_\lambda \\
&\quad + (\boldsymbol{\omega}^n, \boldsymbol{\omega}^n)_\lambda \\
&= ||\boldsymbol{\upsilon}_h^{n+1}||_\lambda^2 - ||\boldsymbol{\upsilon}_h^n||_\lambda^2 - (\boldsymbol{\upsilon}_h^n, \Delta t\lambda^{-1}\mathbf{L}_h(\boldsymbol{\upsilon}_h^n))_\lambda - (\boldsymbol{\omega}^n, \boldsymbol{\upsilon}_h^n)_\lambda \\
&\quad - (\boldsymbol{\omega}^n, \Delta t\lambda^{-1}\mathbf{L}_h(\boldsymbol{\upsilon}_h^n))_\lambda - (\boldsymbol{\upsilon}_h^n, \Delta t\lambda^{-1}\mathbf{L}_h(\boldsymbol{\omega}^n))_\lambda \\
&\quad - (\Delta t\lambda^{-1}\mathbf{L}_h(\boldsymbol{\omega}^n), \Delta t\lambda^{-1}\mathbf{L}_h(\boldsymbol{\upsilon}_h^n))_\lambda + (\boldsymbol{\omega}^n, \boldsymbol{\omega}^n)_\lambda.
\end{aligned}$$

We notice that

$$(\boldsymbol{\upsilon}_h^n, \Delta t\lambda^{-1}\mathbf{L}_h(\boldsymbol{\upsilon}_h^n))_\lambda = \Delta t(\mathbf{L}_h(\boldsymbol{\upsilon}_h^n), \boldsymbol{\upsilon}_h^n)_{\mathcal{T}_h},$$

furthermore $(\Delta t\lambda^{-1}\mathbf{L}_h(\boldsymbol{\omega}^n), \boldsymbol{v}_h^n + \Delta t\lambda^{-1}\mathbf{L}_h(\boldsymbol{v}_h^n))_\lambda = \Delta t(\mathbf{L}_h(\boldsymbol{\omega}^n), \boldsymbol{\omega}^n)_{\mathcal{T}_h}$ then

$$(\boldsymbol{v}_h^n, \lambda^{-1}\mathbf{L}_h(\boldsymbol{\omega}^n))_\lambda + (\Delta t\lambda^{-1}\mathbf{L}_h(\boldsymbol{\omega}^n), \lambda^{-1}\mathbf{L}_h(\boldsymbol{v}_h^n))_\lambda = (\mathbf{L}_h(\boldsymbol{\omega}^n), \boldsymbol{\omega}^n)_{\mathcal{T}_h}.$$

Finally

$$\begin{aligned}-(\boldsymbol{\omega}^n, \boldsymbol{v}_h^n)_\lambda - (\boldsymbol{\omega}^n, \Delta t\lambda^{-1}\mathbf{L}_h(\boldsymbol{v}_h^n))_\lambda + (\boldsymbol{\omega}^n, \boldsymbol{\omega}^n)_\lambda &= (\boldsymbol{\omega}^n, -\boldsymbol{\omega}^n + \boldsymbol{\omega}^n)_\lambda \\ &= 0.\end{aligned}$$

We then obtain

$$\begin{aligned}||\boldsymbol{v}_h^{n+1}||_\lambda^2 - ||\boldsymbol{v}_h^n||_\lambda^2 &= ||\boldsymbol{v}_h^{n+1} - \boldsymbol{\omega}^n||_\lambda^2 \\ &\quad + \Delta t((\mathbf{L}_h(\boldsymbol{v}_h^n), \boldsymbol{v}_h^n)_{\mathcal{T}_h} + (\mathbf{L}_h(\boldsymbol{\omega}^n), \boldsymbol{\omega}^n)_{\mathcal{T}_h}) \\ &\leq ||\boldsymbol{v}_h^{n+1} - \boldsymbol{\omega}^n||_\lambda^2.\end{aligned}$$

Furthermore from (3.13) we obtain

$$\begin{aligned}\boldsymbol{v}_h^{n+1} - \boldsymbol{\omega}^n &= \frac{1}{2}\boldsymbol{v}_h^n - \frac{1}{2}\boldsymbol{\omega}^n + \frac{1}{2}\Delta t\lambda^{-1}\mathbf{L}_h(\boldsymbol{\omega}^n) \\ &= -\frac{1}{2}\Delta t\lambda^{-1}\mathbf{L}_h(\boldsymbol{v}_h^n) + \frac{1}{2}\Delta t\lambda^{-1}\mathbf{L}_h(\boldsymbol{\omega}^n) \\ &= -\frac{1}{2}\Delta t\lambda^{-1}\mathbf{L}_h(\boldsymbol{v}_h^n - \boldsymbol{\omega}^n).\end{aligned}$$

So we can deduce that

$$\begin{aligned}||\boldsymbol{v}_h^{n+1} - \boldsymbol{\omega}^n||_\lambda^2 &= \left\|\frac{1}{2}\Delta t\lambda^{-1}\mathbf{L}_h(\boldsymbol{v}_h^n - \boldsymbol{\omega}^n)\right\|_\lambda^2 \\ &= \frac{1}{4}\Delta t^2(\lambda^{-1}\mathbf{L}_h(\boldsymbol{v}_h^n - \boldsymbol{\omega}^n), \lambda^{-1}\mathbf{L}_h(\boldsymbol{v}_h^n - \boldsymbol{\omega}^n))_\lambda \\ &= \frac{1}{4}\Delta t^2||\mathbf{L}_h(\boldsymbol{v}_h^n - \boldsymbol{\omega}^n)||_{\lambda^{-1}}^2 \\ &\leq \frac{1}{4}\Delta t^2||\mathbf{L}_h(\boldsymbol{v}_h^n - \boldsymbol{\omega}^n)||_\lambda^2.\end{aligned}$$

We infer from Lemma 2 that

$$||\boldsymbol{v}_h^{n+1} - \boldsymbol{\omega}^n||_\lambda^2 \leq \frac{1}{4}(\Delta t c_1 h^{-1}\eta)^2||\boldsymbol{v}_h^n - \boldsymbol{\omega}^n||_\lambda^2$$

and with the help of (3.12)

$$\begin{aligned}||\boldsymbol{v}_h^{n+1} - \boldsymbol{\omega}^n||_\lambda^2 &\leq \frac{1}{4}(\Delta t^2 c_1 h^{-1}\eta)^2(\lambda^{-1}\mathbf{L}_h(\boldsymbol{v}_h^n), \lambda^{-1}\mathbf{L}_h(\boldsymbol{v}_h^n))_\lambda \\ &\leq \frac{1}{4}(\Delta t^2 c_1 h^{-1}\eta)^2||\mathbf{L}_h(\boldsymbol{v}_h^n)||_{\lambda^{-1}}^2 \\ &\leq \frac{1}{4}(\Delta t^2 c_1 h^{-1}\eta)^2||\mathbf{L}_h(\boldsymbol{v}_h^n)||_\lambda^2 \\ &\leq \frac{1}{4}(\Delta t^2 c_1 h^{-1}\eta)^2(c_2 h^{-1}\eta)^2||\boldsymbol{v}_h^n||_\lambda^2 \\ &\leq \frac{1}{4}\Delta t^4 c_3 h^{-4}||\boldsymbol{v}_h^n||_\lambda^2.\end{aligned}$$

We now deduce from (3.14) that

$$\frac{1}{2}||\boldsymbol{v}_h^{n+1}||_\lambda^2 - \frac{1}{2}||\boldsymbol{v}_h^n||_\lambda^2 \leq \frac{1}{8}\Delta t^4 c_3 h^{-4}||\boldsymbol{v}_h^n||_\lambda^2,$$

then

$$\mathcal{E}_h^{n+1} - \mathcal{E}_h^n \leq \frac{1}{4}\Delta t^4 c_3 h^{-4}\mathcal{E}_h^n,$$

so for $\Delta t \leq c_4 h^{\frac{4}{3}}$ we obtain by Gronwall's lemma the existence of a constant $c_5 \geq 0$ such that for all $n \geq 0$

$$\mathcal{E}_h^{n+1} - \mathcal{E}_h^n \leq c_5 \Delta t \mathcal{E}_h^n,$$

and then

$$\mathcal{E}_h^n \leq e^{c_5 T}\mathcal{E}_h^0.$$

This concludes the proof of Proposition 1. □

3.4 Implementation aspects

In this section we will present all the details elaborating the explicit HDGTD method.

3.4.1 Local HDG weak form

We assume that for an internal interface $F = \overline{K}^+ \cap \overline{K}^-$, the normal vector $\boldsymbol{n} = \boldsymbol{n}^+ = -\boldsymbol{n}^-$ is directed from K^+ to K^-. For a boundary interface, we implicitly have that $\boldsymbol{n} = \boldsymbol{n}^+$ and we simply denote by K in place of K^+ the element attached to the interface. Replacing the numerical traces (3.2) and (3.3) in (3.4) we obtain

$$\begin{cases} (\varepsilon\partial_t \boldsymbol{E}_h, \boldsymbol{v})_K - (\boldsymbol{H}_h, \mathbf{curl}\,\boldsymbol{v})_K \\ + \displaystyle\sum_{F\in\partial K\cap\mathcal{F}_h^I} \left\langle \frac{1}{\tau_{K^+}+\tau_{K^-}}\left(\tau_{K^+}\boldsymbol{H}_h^{t,+} + \tau_{K^-}\boldsymbol{H}_h^{t,-}\right)\boldsymbol{n}\times\boldsymbol{v}\right\rangle_F \\ + \displaystyle\sum_{F\in\partial K\cap\mathcal{F}_h^I} \left\langle \frac{1}{\tau_{K^+}+\tau_{K^-}}\left(\boldsymbol{n}^+\times\boldsymbol{E}_h^{t,+} + \boldsymbol{n}^-\times\boldsymbol{E}_h^{t,-}\right), \boldsymbol{n}\times\boldsymbol{v}\right\rangle_F \\ + \displaystyle\sum_{F\in\partial K\cap\Gamma_m} \left\langle \frac{1}{\tau_K}\boldsymbol{n}\times\boldsymbol{E}_h^t + \boldsymbol{H}_h^t, \boldsymbol{n}\times\boldsymbol{v}\right\rangle_F \\ + \displaystyle\sum_{F\in\partial K\cap\Gamma_a} \left\langle \frac{1}{\tau_K+1}\left(\tau_K\boldsymbol{H}_h^t + \boldsymbol{n}\times\boldsymbol{E}_h^t - \boldsymbol{g}^{inc}\right), \boldsymbol{n}\times\boldsymbol{v}\right\rangle_F = 0, \\ \\ (\mu\partial_t \boldsymbol{H}_h, \boldsymbol{v})_K + (\boldsymbol{E}_h, \mathbf{curl}\,\boldsymbol{v})_K - \\ \displaystyle\sum_{F\in\partial K\cap\mathcal{F}_h^I} \left\langle \frac{\tau_{K^+}\tau_{K^-}}{\tau_{K^+}+\tau_{K^-}}\left(\frac{\boldsymbol{E}_h^{t,+}}{\tau_{K^+}} + \frac{\boldsymbol{E}_h^{t,-}}{\tau_{K^-}} - \boldsymbol{n}^+\times\boldsymbol{H}_h^{t,+} - \boldsymbol{n}^-\times\boldsymbol{H}_h^{t,-}\right), \boldsymbol{n}\times\boldsymbol{v}\right\rangle_F \\ - \displaystyle\sum_{F\in\partial K\cap\Gamma_a} \left\langle \frac{1}{\tau_K+1}\left(\boldsymbol{E}_h^t - \tau_K\boldsymbol{n}\times\boldsymbol{H}_h^t - \tau_K\boldsymbol{n}\times\boldsymbol{g}^{inc}\right), \boldsymbol{n}\times\boldsymbol{v}\right\rangle_F = 0, \end{cases} \tag{3.15}$$

where $\boldsymbol{H}_h^{t,+}$ and $\boldsymbol{E}_h^{t,+}$ $\left(\text{respectively } \boldsymbol{H}_h^{t,-} \text{ and } \boldsymbol{E}_h^{t,-}\right)$ are the tagential traces of $\boldsymbol{H}_h$ and $\boldsymbol{E}_h$ from element K^+ (respectively K^-).

3.4.2 Local HDG matrices

Let $\mathcal{T}_h$ be the set of all K_i with $i \in \{1, \cdots, |\mathcal{T}_h|\}$, and let d_i be the number of degrees of freedom in element K_i. From now on, for a given element $K_i \in \mathcal{T}_h$, we consider that $K^+ \equiv K_i$ and $K^- \equiv K_j$. We define the restricted fields $\boldsymbol{E}_i = \boldsymbol{E}_{h_{|K_i}} = \begin{pmatrix} E_i^x \\ E_i^y \\ E_i^z \end{pmatrix}$ and $\boldsymbol{H}_i = \boldsymbol{H}_{h_{|K_i}} = \begin{pmatrix} H_i^x \\ H_i^y \\ H_i^z \end{pmatrix}$. We will now develop the equation for E_i^x in (3.15) in order to exhibit the local matrices characterizing the semi-discrete HDG scheme. Let $(\Phi_{ik})_{1 \le k \le d_i}$ be the set of scalar basis functions defined in K_i. By setting $\boldsymbol{v} = \boldsymbol{\Phi}_{ik}^x = \begin{pmatrix} \Phi_{ik} \\ 0 \\ 0 \end{pmatrix}$ for $1 \le k \le d_i$ the equation for E_i^x in (3.15) becomes

$$
\begin{aligned}
&\int_{K_i} \varepsilon \partial_t E_i^x \Phi_{ik} - \int_{K_i} \left(H_i^y \partial_z \Phi_{ik} - H_i^z \partial_y \Phi_{ik} \right) + \\
&\sum_{F \in \partial K_i \cap \mathcal{F}_h^I} \int_F \frac{1}{\tau_{K_i} + \tau_{K_j}} \Big[\tau_{K_i} H_i^{t,y} + \tau_{K_j} H_j^{t,y} + \\
&\qquad \left(\boldsymbol{n}^+ \times \boldsymbol{E}_i^t \right)^y + \left(\boldsymbol{n}^- \times \boldsymbol{E}_j^t \right)^y \Big] n_z \Phi_{ik} - \\
&\qquad \frac{1}{\tau_{K_i} + \tau_{K_j}} \Big[\tau_{K_i} H_i^{t,z} + \tau_{K_j} H_j^{t,z} + \\
&\qquad \left(\boldsymbol{n}^+ \times \boldsymbol{E}_i^t \right)^z + \left(\boldsymbol{n}^- \times \boldsymbol{E}_j^t \right)^z \Big] n_y \Phi_{ik} + \\
&\sum_{F \in \partial K_i \cap \Gamma_m} \int_F \left(\frac{1}{\tau} \left(\boldsymbol{n} \times \boldsymbol{E}_i^t \right)^y + H_i^{t,y} \right) n_z \Phi_{ik} - \\
&\qquad \left(\frac{1}{\tau} \left(\boldsymbol{n} \times \boldsymbol{E}_i^t \right)^z + H_i^{t,z} \right) n_y \Phi_{ik} + \\
&\sum_{F \in \partial K_i \cap \Gamma_a} \int_F \frac{1}{\tau_{K_i} + 1} \left(\tau_{K_i} H_i^{t,y} + \left(\boldsymbol{n} \times \boldsymbol{E}_i^t \right)^y - g^{inc,y} \right) n_z \Phi_{ik} - \\
&\qquad \frac{1}{\tau_{K_i} + 1} \left(\tau_{K_i} H_i^{t,z} + \left(\boldsymbol{n} \times \boldsymbol{E}_i^t \right)^z - g^{inc,z} \right) n_y \Phi_{ik} = 0.
\end{aligned}
\tag{3.16}
$$

Note that we obtain d_i equations of the form (3.16), one for each value of k. The different terms appearing in (3.16) can be developed as follows:

- **Mass matrix.** Assuming that ε is constant on every K_i, we obtain

$$
\begin{aligned}
\int_{K_i} \varepsilon_i \partial_t E_i^x \Phi_{ik} &= \varepsilon_i \int_{K_i} \sum_{l=1}^{d_i} \partial_t E_{il}^x \Phi_{il} \Phi_{ik} \\
&= \varepsilon_i \sum_{l=1}^{d_i} \partial_t E_{il}^x \int_{K_i} \Phi_{il} \Phi_{ik} \\
&= \varepsilon_i \left(\mathbb{M}_i \partial_t \overline{\boldsymbol{E}}_i^x \right)_k, \ 1 \le k \le d_i,
\end{aligned}
\tag{3.17}
$$

where $\mathbb{M}_i$ is the mass matrix, of dimension $d_i \times d_i$

$$\mathbb{M}_i = \left(\int_{K_i} \Phi_{il} \Phi_{ik} \right)_{1 \le l,k \le d_i},$$

and assuming that the vector of all the degrees of freedom of $\boldsymbol{E}$ in K_i has been ordered as

$$\overline{\boldsymbol{E}}_i = \begin{pmatrix} \overline{\boldsymbol{E}}_i^x \\ \overline{\boldsymbol{E}}_i^y \\ \overline{\boldsymbol{E}}_i^z \end{pmatrix} = \begin{pmatrix} (E_{il}^x)_{1 \le l \le d_i} \\ (E_{il}^y)_{1 \le l \le d_i} \\ (E_{il}^z)_{1 \le l \le d_i} \end{pmatrix}.$$

- **Stiffness matrix**

$$\begin{aligned} \int_{K_i} H_i^y \partial_z \Phi_{ik} - H_i^z \partial_y \Phi_{ik} &= \int_{K_i} \sum_{l=1}^{d_i} \left(H_{il}^y \Phi_{il} \ \partial_z \Phi_{ik} - H_{il}^z \Phi_{il} \ \partial_y \Phi_{ik} \right) \\ &= \sum_{l=1}^{d_i} H_{il}^y \int_{K_i} \Phi_{il} \ \partial_z \Phi_{ik} - \sum_{l=1}^{d_i} H_{il}^z \int_{K_i} \Phi_{il} \ \partial_y \Phi_{ik} \\ &= \left(\mathbb{K}_i^z \overline{\boldsymbol{H}}_i^y - \mathbb{K}_i^y \overline{\boldsymbol{H}}_i^z \right)_k \\ &= - \left(\overline{\mathbb{K}}_i \times \overline{\boldsymbol{H}}_i \right)_k^x, \ 1 \le k \le d_i. \end{aligned} \tag{3.18}$$

Here, the three stiffness matrices were introduced

$$(\mathbb{K}_i^\nu) = \left(\int_{K_i} \Phi_{il} \ \partial_\nu \ \Phi_{ik} \right)_{1 \le l,k \le d_i} \qquad \text{for } \nu \in \{x, y, z\},$$

and where we have introduced the $3d_i \times d_i$ stiffness matrix that will be used in the final system

$$\overline{\mathbb{K}}_i = \begin{bmatrix} \mathbb{K}_i^x \\ \mathbb{K}_i^y \\ \mathbb{K}_i^z \end{bmatrix},$$

and

$$\overline{\boldsymbol{H}}_i = \begin{pmatrix} \overline{\boldsymbol{H}}_i^x \\ \overline{\boldsymbol{H}}_i^y \\ \overline{\boldsymbol{H}}_i^z \end{pmatrix} = \begin{pmatrix} (H_{il}^x)_{1 \le l \le d_i} \\ (H_{il}^y)_{1 \le l \le d_i} \\ (H_{il}^z)_{1 \le l \le d_i} \end{pmatrix}.$$

- **Flux matrix.** For simplicity of the presentation, we assume that the mesh is a conforming mesh (i.e. without hanging nodes). We know that $\boldsymbol{n} = \boldsymbol{n}^+ = -\boldsymbol{n}^-$, therefore, for an interior face we have

$$
\begin{aligned}
F_{ik}^{E_x,1} \equiv & \int_F \frac{1}{\tau_{K_i}+\tau_{K_j}} \Big[\tau_{K_i} H_i^{t,y} + \tau_{K_j} H_j^{t,y} + \\
& \qquad \left(\boldsymbol{n}^+ \times \boldsymbol{E}_i^t\right)^y + \left(\boldsymbol{n}^- \times \boldsymbol{E}_j^t\right)^y \Big] n_z \Phi_{ik} - \\
& \frac{1}{\tau_{K_i}+\tau_{K_j}} \Big[\tau_{K_i} H_i^{t,z} + \tau_{K_j} H_j^{t,z} + \\
& \qquad \left(\boldsymbol{n}^+ \times \boldsymbol{E}_i^t\right)^z + \left(\boldsymbol{n}^- \times \boldsymbol{E}_j^t\right)^z \Big] n_y \Phi_{ik} \\
= & \int_F \frac{1}{\tau_{K_i}+\tau_{K_j}} \Bigg[\left(\sum_{l=1}^{d_i} \tau_{K_i} H_{il}^{t,y} \Phi_{il} + \sum_{m=1}^{d_j} \tau_{K_j} H_{jm}^{t,y} \Phi_{jm} \right) + \\
& \qquad \left(n_z^+ \sum_{l=1}^{d_i} E_{il}^{t,x} \Phi_{il} - n_x^+ \sum_{l=1}^{d_i} E_{il}^{t,z} \Phi_{il} \right) + \\
& \qquad \left(n_z^- \sum_{m=1}^{d_j} E_{jm}^{t,x} \Phi_{jm} - n_x^- \sum_{m=1}^{d_j} E_{jm}^{t,z} \Phi_{jm} \right) \Bigg] n_z \Phi_{ik} - \\
& \frac{1}{\tau_{K_i}+\tau_{K_j}} \Bigg[\left(\sum_{l=1}^{d_i} \tau_{K_i} H_{il}^{t,z} \Phi_{il} + \sum_{m=1}^{d_j} \tau_{K_j} H_{jm}^{t,z} \Phi_{jm} \right) + \\
& \qquad \left(n_x^+ \sum_{l=1}^{d_i} E_{il}^{t,y} \Phi_{il} - n_y^+ \sum_{l=1}^{d_i} E_{il}^{t,x} \Phi_{il} \right) + \\
& \qquad \left(n_x^- \sum_{m=1}^{d_j} E_{jm}^{t,y} \Phi_{jm} - n_y^- \sum_{m=1}^{d_j} E_{jm}^{t,x} \Phi_{jm} \right) \Bigg] n_y \Phi_{ik} \\
= & \frac{1}{\tau_{K_i}+\tau_{K_j}} \Bigg[n_z \sum_{l=1}^{d_i} \left(\tau_{K_i} H_{il}^{t,y} + n_z^+ E_{il}^{t,x} - n_x^+ E_{il}^{t,z} \right) \int_F \Phi_{il} \Phi_{ik} + \\
& \qquad n_z \sum_{m=1}^{d_j} \left(\tau_{K_j} H_{jm}^{t,y} + n_z^- E_{jm}^{t,x} - n_x^- E_{jm}^{t,z} \right) \int_F \Phi_{jm} \Phi_{ik} + \\
& \qquad n_y \sum_{l=1}^{d_i} \left(-\tau_{K_i} H_{il}^{t,z} - n_x^+ E_{il}^{t,y} + n_y^+ E_{il}^{t,x} \right) \int_F \Phi_{il} \Phi_{ik} + \\
& \qquad n_y \sum_{m=1}^{d_j} \left(-\tau_{K_j} H_{jm}^{t,z} - n_x^- E_{jm}^{t,y} + n_y^- E_{jm}^{t,x} \right) \int_F \Phi_{jm} \Phi_{ik} \Bigg],
\end{aligned}
$$

$$
\begin{aligned}
F_{ik}^{E_x,1} \quad = \quad \frac{1}{\tau_{K_i}+\tau_{K_j}} \Bigg[& \sum_{l=1}^{d_i} \tau_{K_i} \left(n_z H_{il}^{t,y} - n_y H_{il}^{t,z} \right) \int_F \Phi_{il}\Phi_{ik} + \\
& \sum_{m=1}^{d_j} \tau_{K_j} \left(n_z H_{jm}^{t,y} - n_y H_{jm}^{t,z} \right) \int_F \Phi_{jm}\Phi_{ik} + \\
& \underbrace{\left(n_z^{+2} + n_y^{+2} \right)}_{\left(1-n_x^{+2}\right)} \left(\sum_{l=1}^{d_i} E_{il}^{t,x} \int_F \Phi_{il}\Phi_{ik} - \sum_{m=1}^{d_j} E_{jm}^{t,x} \int_F \Phi_{jm}\Phi_{ik} \right) + \\
& n_x^+ n_z^+ \left(\sum_{m=1}^{d_j} E_{jm}^{t,z} \int_F \Phi_{jm}\Phi_{ik} - \sum_{l=1}^{d_i} E_{il}^{t,z} \int_F \Phi_{il}\Phi_{ik} \right) + \\
& n_x^+ n_y^+ \left(\sum_{m=1}^{d_j} E_{jm}^{t,y} \int_F \Phi_{jm}\Phi_{ik} - \sum_{l=1}^{d_i} E_{il}^{t,y} \int_F \Phi_{il}\Phi_{ik} \right) \Bigg],
\end{aligned}
$$

that is

$$
\begin{aligned}
F_{ik}^{E_x,1} \quad = \quad \frac{1}{\tau_{K_i}+\tau_{K_j}} \Bigg[& \sum_{l=1}^{d_i} \tau_{K_i} \left(\boldsymbol{H}_{il}^t \times \boldsymbol{n} \right)^x \int_F \Phi_{il}\Phi_{ik} + \\
& \sum_{m=1}^{d_j} \tau_{K_j} \left(\boldsymbol{H}_{jm}^t \times \boldsymbol{n} \right)^x \int_F \Phi_{jm}\Phi_{ik} + \\
& \sum_{m=1}^{d_j} \boldsymbol{V}_F^x \cdot \boldsymbol{E}_{jm}^t \int_F \Phi_{jm}\Phi_{ik} - \sum_{l=1}^{d_i} \boldsymbol{V}_F^x \cdot \boldsymbol{E}_{il}^t \int_F \Phi_{il}\Phi_{ik} \Bigg],
\end{aligned}
$$

if we further assume that the interpolation degree is the same for each element K_i, i.e. $d_i = d_j = d$, then $\int_F \Phi_{il}\Phi_{ik} = \int_F \Phi_{jm}\Phi_{ik}$ and we get

$$
F_{ik}^{E_x,1} = \frac{1}{\tau_{K_i}+\tau_{K_j}} \left(\mathbb{S}_{F,i} \boldsymbol{V}^{1,i,x} \right)_k, \ 1 \le k \le d,
$$

where

$$
\boldsymbol{V}_F^x = \begin{pmatrix} n_x^2 - 1 \\ n_x n_y \\ n_x n_z \end{pmatrix}, \ \mathbb{S}_{F,i} = \left(\int_F \Phi_{il}\Phi_{ik} \right)_{1 \le l,k \le d},
$$

and

$$
\boldsymbol{V}^{1,i,x} = \left(\tau_{K_i} \left(\boldsymbol{H}_{il}^t \times \boldsymbol{n} \right)^x + \tau_{K_j} \left(\boldsymbol{H}_{jl}^t \times \boldsymbol{n} \right)^x + \boldsymbol{V}_F^x \cdot \left(\boldsymbol{E}_{jl}^t - \boldsymbol{E}_{il}^t \right) \right)_{1 \le l \le d},
$$

where we have introduced the vectors

$$
\boldsymbol{E}_{il} = \begin{pmatrix} E_{il}^x \\ E_{il}^y \\ E_{il}^z \end{pmatrix} \text{ and } \boldsymbol{H}_{il} = \begin{pmatrix} H_{il}^x \\ H_{il}^y \\ H_{il}^z \end{pmatrix}.
$$

Proceeding similarly for the last two terms of (3.16), we obatin

$$F_{ik}^{E_x,2} = \frac{1}{\tau_{K_i}} \left(\mathbb{S}_{F,i} \boldsymbol{V}^{2,i,x}\right)_k, F_{ik}^{E_x,3} = \frac{1}{\tau_{K_i}+1} \mathbb{S}_{F,i} \left(\boldsymbol{V}^{2,i,x} + \left(\boldsymbol{n} \times \boldsymbol{g}_i^{inc}\right)^x\right)_k, \ 1 \le k \le d,$$

where

$$\boldsymbol{V}^{2,i,x} = \left(\tau_{K_i} \left(\boldsymbol{H}_{il}^t \times \boldsymbol{n}\right)^x - \boldsymbol{V}_F^x \cdot \boldsymbol{E}_{il}^t\right)_{1 \le l \le d},$$

and

$$\left(\boldsymbol{n} \times \boldsymbol{g}_i^{inc}\right)^x = \left(\left(\boldsymbol{n} \times \boldsymbol{g}_{il}^{inc}\right)^x\right)_{1 \le l \le d}.$$

Now, by setting $\boldsymbol{v} = \boldsymbol{\Phi}_{ik}^x = \begin{pmatrix} \Phi_{ik} \\ 0 \\ 0 \end{pmatrix}$ for $1 \le k \le d$ the equation for H_i^x in (3.15) becomes

$$\begin{aligned}
&\int_{K_i} \mu_i \partial_t H_i^x \Phi_{ik} + \int_{K_i} \left(E_i^y \partial_z \Phi_{ik} - E_i^z \partial_y \Phi_{ik}\right) - \\
&\sum_{F \in \partial K_i \cap \mathcal{F}_h^I} \int_F \frac{\tau_{K_i}\tau_{K_j}}{\tau_{K_i}+\tau_{K_j}} \left[\frac{E_i^{t,y}}{\tau_{K_i}} + \frac{E_j^{t,y}}{\tau_{K_j}} - \right. \\
&\qquad \left. \left(\boldsymbol{n}^+ \times \boldsymbol{H}_i^t\right)^y - \left(\boldsymbol{n}^- \times \boldsymbol{H}_j^t\right)^y\right] n_z \Phi_{ik} - \\
&\qquad \frac{\tau_{K_i}\tau_{K_j}}{\tau_{K_i}+\tau_{K_j}} \left[\frac{E_i^{t,z}}{\tau_{K_i}} + \frac{E_j^{t,z}}{\tau_{K_j}} - \right. \\
&\qquad \left. \left(\boldsymbol{n}^+ \times \boldsymbol{H}_i^t\right)^z + \left(\boldsymbol{n}^- \times \boldsymbol{H}_j^t\right)^z\right] n_y \Phi_{ik} - \\
&\sum_{F \in \partial K_i \cap \Gamma_a} \int_F \frac{1}{\tau_{K_i}+1} \left[\left(E_i^{t,y} - \tau_{K_i} \left(\boldsymbol{n} \times \boldsymbol{H}_i^t\right)^y - \tau_{K_i} \left(\boldsymbol{n} \times \boldsymbol{g}^{inc}\right)^y\right) n_z \Phi_{ik} - \right. \\
&\qquad \left. \frac{1}{\tau_{K_i}+1} \left(E_i^{t,z} - \tau_{K_i} \left(\boldsymbol{n} \times \boldsymbol{H}_i^t\right)^z - \tau_{K_i} \left(\boldsymbol{n} \times \boldsymbol{g}^{inc}\right)^z\right) n_y \Phi_{ik}\right] = 0.
\end{aligned} \tag{3.19}$$

Developing the different terms in (3.19) with obtain similar expressions. In particular for the boundary terms, we have

$$F_{ik}^{H_x,1} = \frac{\tau_{K_i}\tau_{K_j}}{\tau_{K_i}+\tau_{K_j}} \left(\mathbb{S}_{F,i} \boldsymbol{V}^{3,i,x}\right)_k, \ 1 \le k \le n_d,$$

where

$$\boldsymbol{V}^{3,i,x} = \left(\frac{1}{\tau_{K_i}} \left(\boldsymbol{E}_{il}^t \times \boldsymbol{n}\right)^x + \frac{1}{\tau_{K_j}} \left(\boldsymbol{E}_{jl}^t \times \boldsymbol{n}\right)^x + \boldsymbol{V}_F^x \cdot \left(\boldsymbol{H}_{il}^t - \boldsymbol{H}_{jl}^t\right)\right)_{1 \le l \le d},$$

and

$$F_{ik}^{H_x,2} = \frac{\tau_{K_i}}{\tau_{K_i}+1} \mathbb{S}_{F,i} \left(\boldsymbol{V}^{4,i,x} + \boldsymbol{V}_F^x \cdot \boldsymbol{g}_i^{inc}\right)_k, \ 1 \le k \le d,$$

where

$$\boldsymbol{V}^{4,i,x} = \left(\frac{1}{\tau_{K_i}} \left(\boldsymbol{E}_{il}^t \times \boldsymbol{n}\right)^x + \boldsymbol{V}_F^x \cdot \boldsymbol{H}_{il}^t\right)_{1 \le l \le d}.$$

and

$$\boldsymbol{V}_F^x \cdot \boldsymbol{g}_i^{inc} = \left(\boldsymbol{V}_F^x \cdot \boldsymbol{g}_{il}^{inc}\right)_{1\le l\le d}.$$

We can easily see that if $\boldsymbol{E}_{il}^t = \boldsymbol{H}_{il}^t = 0$, $\boldsymbol{E}_{jl} = \boldsymbol{E}_{jl}^{inc}$ and $\boldsymbol{H}_{jl} = \boldsymbol{H}_{jl}^{inc}$ we have

$$\left(\boldsymbol{n}\times \boldsymbol{g}_i^{inc}\right)^x = \boldsymbol{V}^{1,i,x} \quad \text{and} \quad \boldsymbol{V}_F^x \cdot \boldsymbol{g}_i^{inc} = \boldsymbol{V}^{2,i,x},$$

so for a given K_i and for $\boldsymbol{v} = \boldsymbol{\Phi}_{ik}^x$, $1 \le k \le d$ we have

$$\left\{\begin{array}{lll}
\varepsilon_i\left(\mathbb{M}_i\partial_t\overline{\boldsymbol{E}}_i^x\right) & + & \left(\overline{\mathbb{K}}_i\times\overline{\boldsymbol{H}}_i\right)^x + \displaystyle\sum_{F\in\partial K_i\cap\mathcal{F}_h^I}\frac{1}{\tau_{K_i}+\tau_{K_j}}\mathbb{S}_{F,i}\boldsymbol{V}^{1,i,x} \\
 & + & \displaystyle\sum_{F\in\partial K_i\cap\Gamma_m}\frac{1}{\tau_{K_i}}\left(\mathbb{S}_{F,i}\boldsymbol{V}^{2,i,x}\right) \\
 & + & \displaystyle\sum_{F\in\partial K_i\cap\Gamma_a}\frac{1}{\tau_{K_i}+1}\mathbb{S}_{F,i}\left(\boldsymbol{V}^{2,i,x}+\left(\boldsymbol{n}\times\boldsymbol{g}_i^{inc}\right)^x\right) = 0, \\
\mu_i\left(\mathbb{M}_i\partial_t\overline{\boldsymbol{H}}_i^x\right) & - & \left(\overline{\mathbb{K}}_i\times\overline{\boldsymbol{E}}_i\right)^x - \displaystyle\sum_{F\in\partial K_i\cap\mathcal{F}_h^I}\frac{\tau_{K_i}\tau_{K_j}}{\tau_{K_i}+\tau_{K_j}}\mathbb{S}_{F,i}\boldsymbol{V}^{3,i,x} \\
 & - & \displaystyle\sum_{F\in\partial K_i\cap\Gamma_a}\frac{\tau_{K_i}}{\tau_{K_i}+1}\mathbb{S}_{F,i}\left(\boldsymbol{V}^{4,i,x}+\boldsymbol{V}_F^x\cdot\boldsymbol{g}_i^{inc}\right) = 0.
\end{array}\right. \tag{3.20}$$

By doing the same calculations with $\boldsymbol{v} = \boldsymbol{\Phi}_{ik}^y = \begin{pmatrix} 0 \\ \Phi_{ik} \\ 0 \end{pmatrix}$

and $\boldsymbol{v} = \boldsymbol{\Phi}_{ik}^z = \begin{pmatrix} 0 \\ 0 \\ \Phi_{ik} \end{pmatrix}$ for a fixed K_i we obtain for the first system of equations of (3.20)

$$\begin{array}{rl}
 & \varepsilon_i\begin{pmatrix}\mathbb{M}_i & 0_{d\times d} & 0_{d\times d}\\ 0_{d\times d} & \mathbb{M}_i & 0_{d\times d}\\ 0_{d\times d} & 0_{d\times d} & \mathbb{M}_i\end{pmatrix}\begin{pmatrix}\partial_t\overline{\boldsymbol{E}}_i^x\\ \partial_t\overline{\boldsymbol{E}}_i^y\\ \partial_t\overline{\boldsymbol{E}}_i^z\end{pmatrix} + \begin{pmatrix}\left(\overline{\mathbb{K}}_i\times\overline{\boldsymbol{H}}_i\right)^x\\ \left(\overline{\mathbb{K}}_i\times\overline{\boldsymbol{H}}_i\right)^y\\ \left(\overline{\mathbb{K}}_i\times\overline{\boldsymbol{H}}_i\right)^z\end{pmatrix} \\
+ & \displaystyle\sum_{F\in\partial K_i\cap\mathcal{F}_h^I}\frac{1}{\tau_{K_i}+\tau_{K_j}}\begin{pmatrix}\mathbb{S}_{F,i} & 0_{d\times d} & 0_{d\times d}\\ 0_{d\times d} & \mathbb{S}_{F,i} & 0_{d\times d}\\ 0_{d\times d} & 0_{d\times d} & \mathbb{S}_{F,i}\end{pmatrix}\begin{pmatrix}\boldsymbol{V}^{1,i,x}\\ \boldsymbol{V}^{1,i,y}\\ \boldsymbol{V}^{1,i,z}\end{pmatrix} \\
+ & \displaystyle\sum_{F\in\partial K_i\cap\Gamma_m}\frac{1}{\tau_{K_i}}\begin{pmatrix}\mathbb{S}_{F,i} & 0_{d\times d} & 0_{d\times d}\\ 0_{d\times d} & \mathbb{S}_{F,i} & 0_{d\times d}\\ 0_{d\times d} & 0_{d\times d} & \mathbb{S}_{F,i}\end{pmatrix}\begin{pmatrix}\boldsymbol{V}^{2,i,x}\\ \boldsymbol{V}^{2,i,y}\\ \boldsymbol{V}^{2,i,z}\end{pmatrix} \\
+ & \displaystyle\sum_{F\in\partial K_i\cap\Gamma_a}\frac{1}{\tau_{K_i}+1}\begin{pmatrix}\mathbb{S}_{F,i} & 0_{d\times d} & 0_{d\times d}\\ 0_{d\times d} & \mathbb{S}_{F,i} & 0_{d\times d}\\ 0_{d\times d} & 0_{d\times d} & \mathbb{S}_{F,i}\end{pmatrix}\begin{pmatrix}\boldsymbol{V}^{2,i,x}\\ \boldsymbol{V}^{2,i,y}\\ \boldsymbol{V}^{2,i,z}\end{pmatrix} \\
+ & \displaystyle\frac{1}{\tau_{K_i}+1}\begin{pmatrix}\mathbb{S}_{F,i} & 0_{d\times d} & 0_{d\times d}\\ 0_{d\times d} & \mathbb{S}_{F,i} & 0_{d\times d}\\ 0_{d\times d} & 0_{d\times d} & \mathbb{S}_{F,i}\end{pmatrix}\begin{pmatrix}\left(\boldsymbol{n}\times\boldsymbol{g}_i^{inc}\right)^x\\ \left(\boldsymbol{n}\times\boldsymbol{g}_i^{inc}\right)^y\\ \left(\boldsymbol{n}\times\boldsymbol{g}_i^{inc}\right)^z\end{pmatrix} = 0,
\end{array} \tag{3.21}$$

and

$$
\begin{aligned}
&\mu_i \begin{pmatrix} \mathbb{M}_i & 0_{d\times d} & 0_{d\times d} \\ 0_{d\times d} & \mathbb{M}_i & 0_{d\times d} \\ 0_{d\times d} & 0_{d\times d} & \mathbb{M}_i \end{pmatrix} \begin{pmatrix} \partial_t \overline{\boldsymbol{H}}_i^x \\ \partial_t \overline{\boldsymbol{H}}_i^y \\ \partial_t \overline{\boldsymbol{H}}_i^z \end{pmatrix} - \begin{pmatrix} \left(\overline{\mathbb{K}}_i \times \overline{\boldsymbol{E}}_i\right)^x \\ \left(\overline{\mathbb{K}}_i \times \overline{\boldsymbol{E}}_i\right)^y \\ \left(\overline{\mathbb{K}}_i \times \overline{\boldsymbol{E}}_i\right)^z \end{pmatrix} \\
- &\sum_{F\in\partial K_i\cap\mathcal{F}_h^I} \frac{\tau_{K_i}\tau_{K_j}}{\tau_{K_i}+\tau_{K_j}} \begin{pmatrix} \mathbb{S}_{F,i} & 0_{d\times d} & 0_{d\times d} \\ 0_{d\times d} & \mathbb{S}_{F,i} & 0_{d\times d} \\ 0_{d\times d} & 0_{d\times d} & \mathbb{S}_{F,i} \end{pmatrix} \begin{pmatrix} \boldsymbol{V}^{3,i,x} \\ \boldsymbol{V}^{3,i,y} \\ \boldsymbol{V}^{3,i,z} \end{pmatrix} \\
- &\sum_{F\in\partial K_i\cap\Gamma_a} \frac{1}{\tau_{K_i}+1} \begin{pmatrix} \mathbb{S}_{F,i} & 0_{d\times d} & 0_{d\times d} \\ 0_{d\times d} & \mathbb{S}_{F,i} & 0_{d\times d} \\ 0_{d\times d} & 0_{d\times d} & \mathbb{S}_{F,i} \end{pmatrix} \begin{pmatrix} \boldsymbol{V}^{4,i,x} \\ \boldsymbol{V}^{4,i,y} \\ \boldsymbol{V}^{4,i,z} \end{pmatrix} \\
+ &\frac{\tau_{K_i}}{\tau_{K_i}+1} \begin{pmatrix} \mathbb{S}_{F,i} & 0_{d\times d} & 0_{d\times d} \\ 0_{d\times d} & \mathbb{S}_{F,i} & 0_{d\times d} \\ 0_{d\times d} & 0_{d\times d} & \mathbb{S}_{F,i} \end{pmatrix} \begin{pmatrix} \boldsymbol{V}_F^x \cdot \boldsymbol{g}_i^{inc} \\ \boldsymbol{V}_F^y \cdot \boldsymbol{g}_i^{inc} \\ \boldsymbol{V}_F^z \cdot \boldsymbol{g}_i^{inc} \end{pmatrix} = 0
\end{aligned}
\tag{3.22}
$$

where

$$
\boldsymbol{V}_F^y = \begin{pmatrix} n_y n_x \\ n_y^2 - 1 \\ n_y n_z \end{pmatrix}, \boldsymbol{V}_F^z = \begin{pmatrix} n_z n_x \\ n_z n_y \\ n_z^2 - 1 \end{pmatrix} ,
$$

so for every K_i we have

$$
\begin{cases}
\varepsilon_i \left(\overline{\mathbb{M}}_i \partial_t \overline{\boldsymbol{E}}_i\right) + \left(\overline{\mathbb{K}}_i \times \overline{\boldsymbol{H}}_i\right) + \displaystyle\sum_{F\in\partial K_i\cap\mathcal{F}_h^I} \frac{1}{\tau_{K_i}+\tau_{K_j}} \overline{\mathbb{S}}_{F,i} \boldsymbol{V}^{1,i} + \\
\displaystyle\sum_{F\in\partial K_i\cap\Gamma_m} \frac{1}{\tau_{K_i}} \left(\overline{\mathbb{S}}_{F,i} \boldsymbol{V}^{2,i}\right) + \\
\displaystyle\sum_{F\in\partial K_i\cap\Gamma_a} \frac{1}{\tau_{K_i}+1} \overline{\mathbb{S}}_{F,i} \left(\boldsymbol{V}^{2,i} + \boldsymbol{n} \times \mathbf{g}^{\mathbf{inc}}\right) = 0, \\
\mu_i \left(\overline{\mathbb{M}}_i \partial_t \overline{\boldsymbol{H}}_i\right) - \left(\overline{\mathbb{K}}_i \times \overline{\boldsymbol{E}}_i\right) - \displaystyle\sum_{F\in\partial K_i\cap\mathcal{F}_h^I} \frac{\tau_{K_i}\tau_{K_j}}{\tau_{K_i}+\tau_{K_j}} \overline{\mathbb{S}}_{F,i} \boldsymbol{V}^{3,i} - \\
\displaystyle\sum_{F\in\partial K_i\cap\Gamma_a} \frac{1}{\tau_{K_i}+1} \overline{\mathbb{S}}_{F,i} \left(\boldsymbol{V}^{4,i} + \tau_{K_i} \boldsymbol{V}_F^{inc}\right) = 0,
\end{cases}
\tag{3.23}
$$

where

$$
\boldsymbol{V}_F^{inc} = \begin{pmatrix} \boldsymbol{V}_F^x \cdot \boldsymbol{g}^{inc} \\ \boldsymbol{V}_F^y \cdot \boldsymbol{g}^{inc} \\ \boldsymbol{V}_F^z \cdot \boldsymbol{g}^{inc} \end{pmatrix} .
$$

3.4.3 Time integration: Low-Storage Runge-Kutta (LSRK) method

In this section, we are using a time scheme which is more efficient than the RK2 scheme studied in section 3.3.3, even we are not going to prove its stability. We can rewrite problem (3.23) obtained after space discretization as

$$
M\dot{U}_h(t) + KU_h(t) = B(t), \quad U_h(0) = U_{h,0} \tag{3.24}
$$

where for each $t \in [0, T]$, the vector $U_h(t)$ contains the coefficients defining $\boldsymbol{E}_h(t)$ and $\boldsymbol{H}_h(t)$ in the nodal basis of $\boldsymbol{V}_h$, M and K are the usual mass and stiffness matrices associated with (3.23), and $U_{h,0}$ is the interpolation of the initial conditions in the discretization space.

Classically, the key asset of DG schemes is that the mass matrix is block-diagonal, and hence, easy to invert. Thus, we may safely rewrite (3.24) as

$$\dot{U}_h(t) = -GU_h(t) + F(t), \quad U_h(0) = U_{h,0}, \tag{3.25}$$

where $G := M^{-1}K$ and $F(t) := M^{-1}B(t)$. At this point, we recognize in (3.25) a system of ordinary differential equation, that can be discretized with a time marching scheme. For equation (3.24), the standard s-stage Runge-Kutta scheme writes

Runge-Kutta scheme

$$\begin{cases} K_1 = -GU_h^n + F(t_n), \\ K_i = -G\left(U_h^n + \Delta t \sum_{j=1}^{i-1} a_{i,j} K_j\right) + F(t_n + c_i \Delta t), \text{ for } \; i = 2, \cdots, s, \\ U_h^{n+1} = U_h^n + \Delta t \sum_{j=1}^{s} b_j K_j. \end{cases}$$

We can easily see that this scheme is a sN-storage scheme where N is the number of equations. In this situation the memory consumption can quickly become a constraining factor for large problems. A possible solution is given by Williamson [49], who shows that the RK scheme can be cast in $2N$-storage format that we will refer to a LSRK(s,p) scheme. After fixing a time-step Δt, we iteratively construct approximations U_h^n of $U_h(t_n)$, $t_n := n\Delta t$. Specifically, we let $U_h^0 := U_{h,0}$, and for $n \geq 0$, U_h^{n+1} is deduced from U_h^n through the following algorithm

Low Storage Runge-Kutta scheme

$$\begin{cases} V_h^1 = U_h^n \\ \left.\begin{array}{rcl} V_h^2 & = & a_k V_h^2 + \Delta t \left(GV_h^1 + F(t_n + c_k \Delta T)\right) \\ V_h^1 & = & V_h^1 + b_k V_h^2 \end{array}\right\} \text{ for } \; k = 1, \cdots, s \\ U_h^{n+1} = V_h^1, \end{cases}$$

Since Williamson [49] has demonstrated that the four-stage fourth-order (4,4) RK scheme could not, in general, be implemented in the $2N$-storage format, we will use in this chapter the LSRK($s = 5$, $p = 4$) proposed by Carpenter and Kennedy [46]. The coefficients a_k, b_k and c_k are described in Table 3.1.

Table 3.1 | The values of the coefficients of the LSRK(5,4) scheme.

Coeff	Value	Coeff	Value	Coeff	Value
A_1	0	B_1	$\frac{1432997174477}{9575080441755}$	c_1	0
A_2	$-\frac{567301805773}{1357537059087}$	B_2	$\frac{5161836677717}{1361206829357}$	c_2	$\frac{1432997174477}{9575080441755}$
A_3	$-\frac{2404267990393}{2016746695238}$	B_3	$\frac{1720146321549}{2090206949498}$	c_3	$\frac{2526269341429}{6820363962896}$
A_4	$-\frac{3550918686646}{2091501179385}$	B_4	$\frac{3134564353537}{4481467310338}$	c_4	$\frac{2006345519317}{3224310063776}$
A_5	$-\frac{1275806237668}{842570457699}$	B_5	$\frac{2277821191437}{14882151754819}$	c_5	$\frac{2802321613138}{2924317926251}$

Classically, as this time integration scheme is explicit, it is stable under a CFL condition linking together the mesh size h and the selected time step Δt. Specifically, given a mesh $\mathcal{T}_h$, we fix the time step by

$$\Delta t := \alpha_k \min_{K \in \mathcal{T}_h} \frac{1}{c_K} \frac{V_K}{A_K}, \tag{3.26}$$

where, $c_K := 1/\sqrt{\varepsilon_K \mu_K}$ is the wave speed in the element K, and V_K and A_K are respectively the volume and the area of K. The constant α_k is selected according to the polynomial degree k. Here, we use the values listed in Table 3.2, that we obtained after testing the scheme on simple test-cases.

k	1	2	3	4
α_k	0.70	0.46	0.30	0.21

Table 3.2 | Values of α_k in CFL condition (3.26).

3.5 Numerical results

The time explicit HDG method presented in the previous section has been implemented in the 3D case considering conforming tetrahedral meshes with DIOGENeS software suite described below in section 3.5.1.

3.5.1 DIOGENeS (DIscOntinuous GalErkin Nanoscale Solvers)

Diogenes is a software suite dedicated to computational nanophotonics/nanoplasmonics, which is developed by Inria. This software suite integrates several variants of the Discontinuous Galerkin (DG) method, which is particularly well adapted to accurately and efficiently deal with the multiscale characteristics of nanoscale light/matter interaction problems. DIOGENeS relies on an object-oriented architecture implemented in Fortran 2008. There are two main components in this software suite.

On the one hand, a library of structures and module, referred as the core library named DIOGENeS-common, giving access to all the functionalities needed to devise DG type methods formulated on unstructured or hybrid structured/unstructured meshes. On the other hand, a set

of dedicated simulators (i.e. solvers), which are designed on top of the core library, for dealing with applications relevant to nanophotonics/nanoplasmonics. Numerical kernels of the core library and dedicated solvers are adapted to high-performance computing thanks to a classical SPMD strategy combining a partitioning of the underlying mesh with a message-passing programming paradigm implemented with the MPI standard. The purpose of using Diogenes to code the fully explicit HDG method is that this method is similar to the classical DG method, but with generalized fluxes. So we updated all the routines treating the numerical fluxes on the interior faces, also on the perfectly metallic boundary and the absorbing boundary faces.

3.5.2 Propagation of a standing wave in a cubic PEC cavity

In order to validate and study the numerical convergence of the proposed HDG method, we consider the propagation of an eigenmode in a source-free *i.e* $\boldsymbol{J} = 0$ closed cavity (the unit cube $\Omega := (0, L)^3$, $L := 1m$) with perfectly metallic walls. The frequency of the wave is $\omega = \sqrt{3}\pi c_0/L$ where c_0 is the speed of light in vacuum. The electric permittivity and the magnetic permeability are set to the constant vacuum values. The exact time-domain solution is given by (2.61) and the electromagnetic field is initialized at $t = 0$ as in (2.62).

Uniform $\tau = 1$

In order to ensure the stability of the method, numerical CFL conditions are determined for each value of the interpolation order p_K. For the present test case, the relative ε_K and μ_k are constant and equal to 1 for all K in $\mathcal{T}_h$, so we have verified that, as we said in Remark 3, for $\tau = 1$, the values of the CFL number correspond to those obained for the classical upwind flux-based DG method. In Table 3.3 we summarize the maximum value of Δt to ensure the stability of the HDG scheme

Interpolation order	$\mathbb{P}_1$	$\mathbb{P}_2$
Δt max (s.)	0.32×10^{-9}	0.19×10^{-9}
Interpolation order	$\mathbb{P}_3$	$\mathbb{P}_4$
Δt max (s.)	0.13×10^{-9}	0.94×10^{-10}

Table 3.3 | Numerically obtained values of maximum Δt.

Given these values of Δt, the L^2-norm of the error is calculated for a uniform tetrahedral mesh with 3072 elements which is constructed from a finite difference grid with $n_x = n_y = n_z = 9$ points, each cell of this grid yielding 6 tetrahedra. The wave is propagated in the cavity during a physical time $t_{\max}$ corresponding to 8 periods. Figure 3.1 shows the time evolution of the exact and the numerical solution of E_x at a fixed point in the mesh. Figures 3.2 and 3.3 depicts a comparison of the time evolution of the L^2-norm of the error between the solution obtained with an HDG method and a classical upwind flux-based DG method for different values of the interpolation order. An optimal convergence with order $p_K + 1$ is obtained as shown in Figure 3.4.

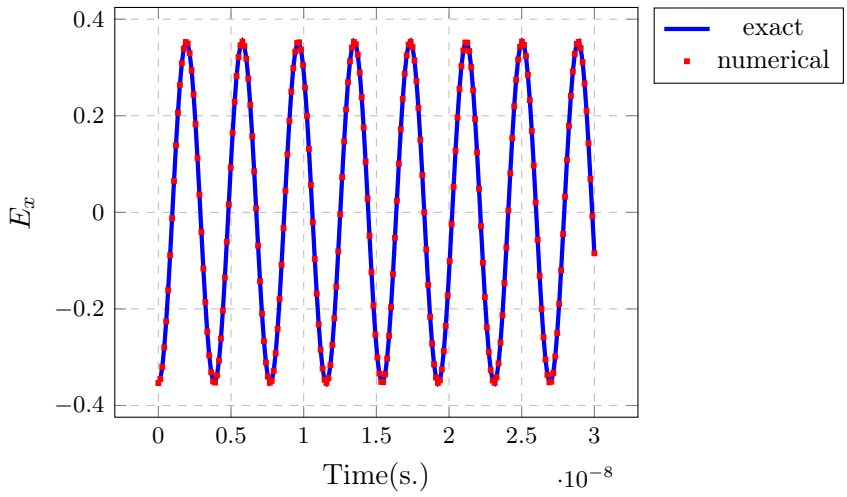

Figure 3.1 | Time evolution of the exact and the numerical solution of E_x at point $A(0.25, 0.25, 0.25)$ with a $\mathbb{P}_3$ interpolation.

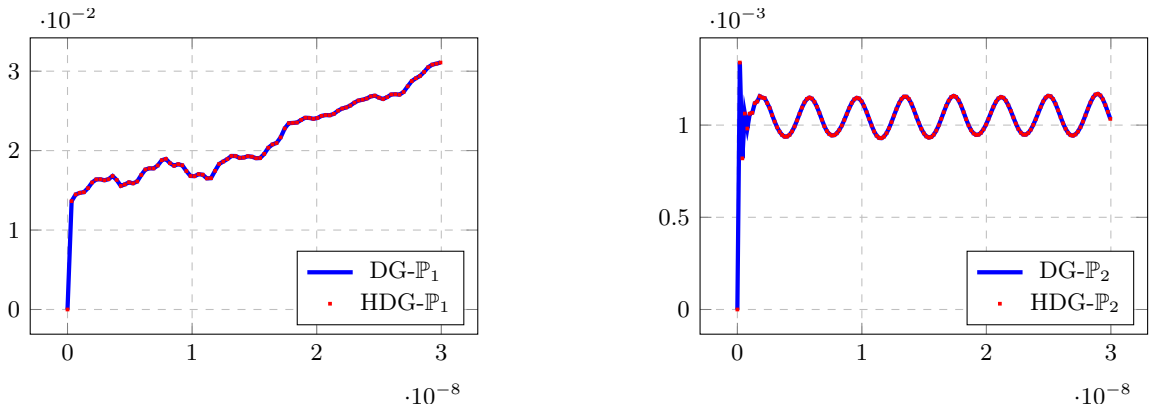

Figure 3.2 | Time evolution of the L^2-norm of the error for $\mathbb{P}_1$ and $\mathbb{P}_2$.

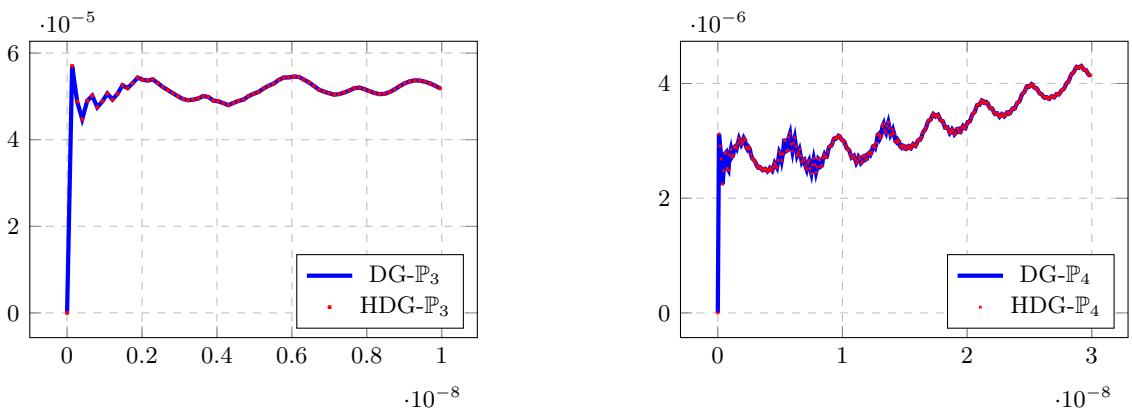

Figure 3.3 | Time evolution of the L^2-norm of the error for $\mathbb{P}_3$ and $\mathbb{P}_4$.

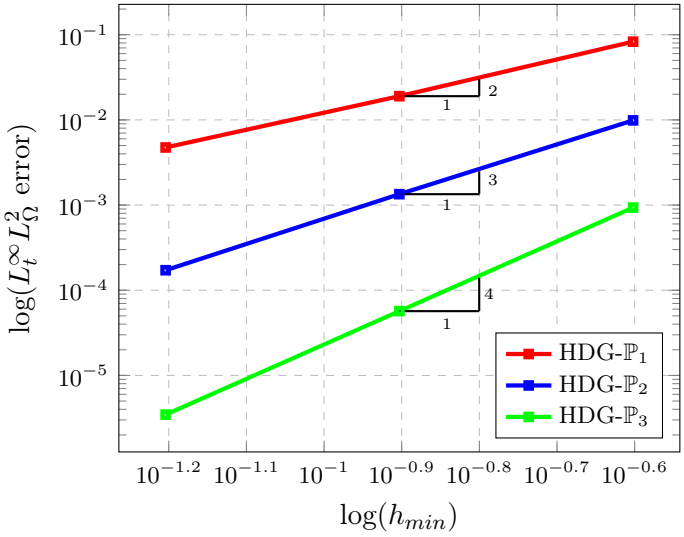

Figure 3.4 | Numerical convergence order of the time explicit HDG method for $\tau = 1$.

Influence of τ

We keep the same case than previously and we assess the behavior of the HDG method for various values of the penalization parameter τ. We have seen in the fully discrete stability analysis that the CFL number depends on τ. Numerically when we fixed Δt to the value shown in Table 3.3 (corresponding to $\tau = 1$) and change the value of τ we observed that the time evolution of the electromagnetic energy increases in time for any interpolation order. In fact, it is necessary to reevaluate the Δt max for each value of τ (see Figure 3.5). In Figure 3.6, we show the time evolution of the L^2-error for several values of τ with respect to the maximal Δt for the considered parameters. In addition, Table 3.5 summarizes the numerical results in terms of maximum L^2-errors and convergence rates. It appears that the order of convergence is not affected when we change the value of the stabilization parameter (with their associated CFL conditions).

Tau	0.1	1.0	2.0
Δt max (sec)	0.31×10^{-10}	0.32×10^{-9}	0.17×10^{-9}

Tau	5.0	10.0
Δt max (sec)	0.66×10^{-10}	0.32×10^{-10}

Table 3.4 | Numerically obtained values of the CFL number as a function of the stabilization parameter τ for a $\mathbb{P}1$ interpolation.

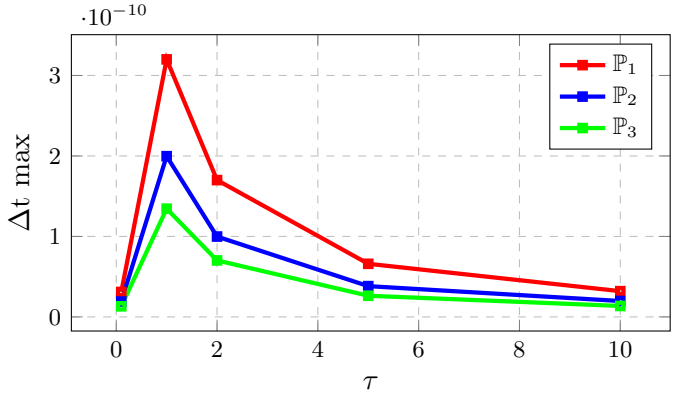

Figure 3.5 | Variation of the Δt max as a function of τ.

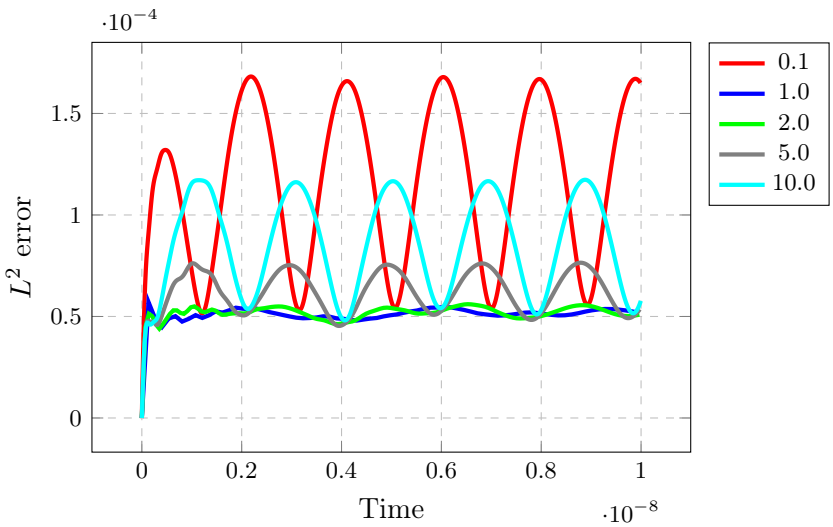

Figure 3.6 | Time evolution of the L^2-error as a function of τ with a $\mathbb{P}_3$ interpolation.

$1/h$	$\tau = 1.0$ $\mathbb{P}_1$, $\Delta t = 0.16 \times 10^{-09}$		$\mathbb{P}_2$, $\Delta t = 0.99 \times 10^{-10}$		$\mathbb{P}_3$, $\Delta t = 0.66 \times 10^{-10}$	
1/4	8.29e-02	-	9.87e-03	-	9.34e-04	-
1/8	1.90e-02	**2.13**	1.34e-03	**2.88**	5.68e-05	**4.04**
1/16	4.74e-03	**2.00**	1.72e-04	**2.97**	3.46e-06	**4.04**

$1/h$	$\tau = 0.1$ $\mathbb{P}_1$, $\Delta t = 0.16 \times 10^{-10}$		$\mathbb{P}_2$, $\Delta t = 0.96 \times 10^{-11}$		$\mathbb{P}_3$, $\Delta t = 0.66 \times 10^{-11}$	
1/4	2.14e-01	-	1.78e-02	-	2.19e-03	-
1/8	5.46e-02	**1.97**	2.85e-03	**2.65**	1.68e-04	**3.70**
1/16	1.18e-02	**2.21**	4.06e-04	**2.81**	1.14e-05	**3.88**

$1/h$	$\tau = 10.0$ $\mathbb{P}_1$, $\Delta t = 0.16 \times 10^{-10}$		$\mathbb{P}_2$, $\Delta t = 0.96 \times 10^{-11}$		$\mathbb{P}_3$, $\Delta t = 0.68 \times 10^{-11}$	
1/6	1.74e-01	-	1.53e-02	-	1.68e-03	-
1/12	4.24e-02	**2.04**	2.23e-03	**2.76**	1.17e-04	**3.84**
1/24	9.4e-03	**2.16**	3.10e-04	**2.87**	7.81e-06	**3.91**

Table 3.5 | Maximum L^2-errors and convergence orders.

3.5.3 Propagation of a plane wave in a homogeneous domain

We now consider the propagation of a plane wave in a homogeneous domain. Specifically, we consider Maxwell's equations (2.37) with $\Omega := (0, L)^3$, $L := 1m$, $\Gamma_a = \partial\Omega$. The right-hand side $\boldsymbol{J} = 0$, and g^{inc} is defined by (2.15) with

$$\boldsymbol{E}^{\text{inc}}(t, \boldsymbol{x}) := \boldsymbol{E}_p \cos\left(\omega\left(t - \sqrt{\mu_r \varepsilon_r}\frac{\boldsymbol{k}\cdot\boldsymbol{x}}{|\boldsymbol{k}|}\right)\right), \quad \boldsymbol{H}^{\text{inc}}(t, \boldsymbol{x}) := \sqrt{\frac{\varepsilon_r}{\mu_r}}\frac{\boldsymbol{k}}{|\boldsymbol{k}|} \times \boldsymbol{E}(t, \boldsymbol{x}),$$

where $\boldsymbol{E}_p := (1, 0, 0)^T$ is the polarization and $\boldsymbol{k} := (0, 0, 1)^T$ is the direction of propagation and $\omega = c_0/L$ is the angular frequency. The relative electric permittivity and the relative magnetic permeability are set to the constant vacuum value 1.0. We impose the initial conditions with $\boldsymbol{E}_0 := \boldsymbol{E}^{\text{inc}}|_{t=0}$ and $\boldsymbol{H}_0 := \boldsymbol{H}^{\text{inc}}|_{t=0}$. Then, since the medium under consideration is homogeneous, no reflection and/or diffraction occur, and the analytical solution is simply $\boldsymbol{E} = \boldsymbol{E}^{\text{inc}}$ and $\boldsymbol{H} = \boldsymbol{H}^{\text{inc}}$. As for the cubic cavity test, we consider structured meshes $\mathcal{T}_h$, that we obtain by first splitting Ω into $n \times n \times n$ cubes ($n := L/h$ and $h := 1/12$), and then splitting each cube into 6 tetrahedra. The time step is selected using (3.26). Figure 3.7 shows the time evolution of the exact and the numerical solution of E_x at a fixed point in the domain. An optimal convergence with order $p_K + 1$ is obtained as shown in Figure 3.8. Figure 3.9 shows the time evolution of the L^2-norm of the error with different polynomial orders.

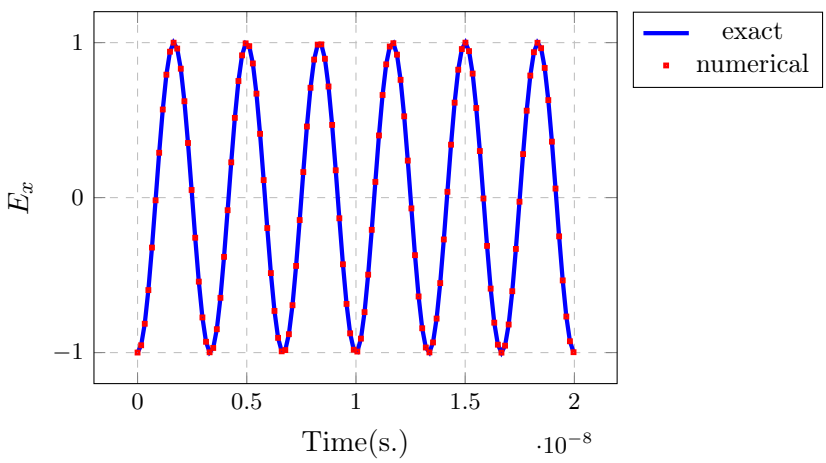

Figure 3.7 | Time evolution of the exact and the numerical solution of E_x at point $A(0.25, 0.25, 0.25)$ with a $\mathbb{P}_3$ interpolation.

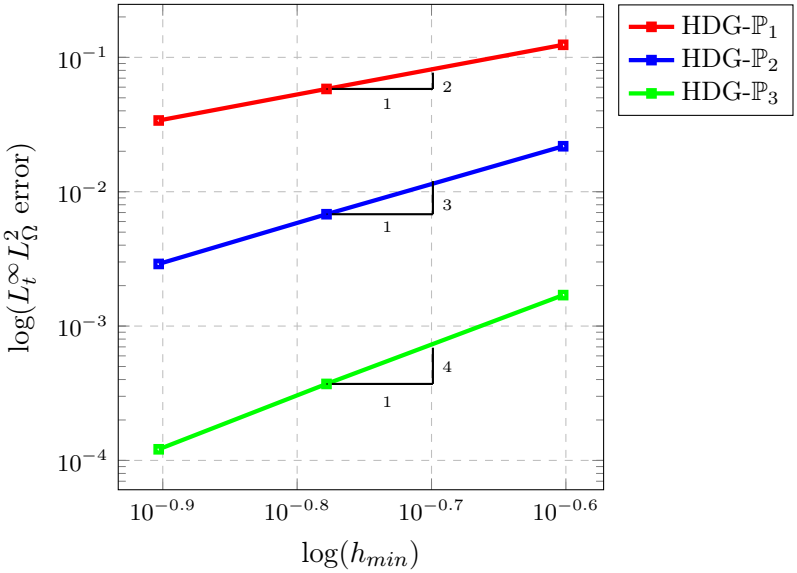

Figure 3.8 | Numerical convergence order of the time explicit HDG method for $\tau = 1$.

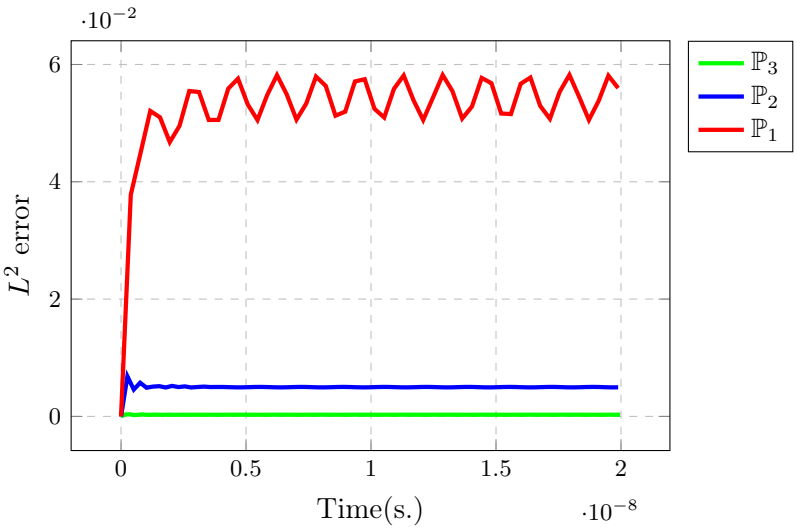

Figure 3.9 | Time evolution of the L^2-norm of the error for $\mathbb{P}_1$, $\mathbb{P}_2$ and $\mathbb{P}_3$.

3.5.4 Scattering of a plane wave by a dielectric sphere

We now consider a problem involving a dielectric sphere of radius 0.15 meter, with $\varepsilon_r = 2$ and $\mu_r = 1$. The computational domain is bounded by a cube of side 1 meter on which the Silver-Muller absorbing condition is applied and the simulation time is $T = 3$ ns. A plane wave traveling in the z direction is considered, impinging in normal incidence from the bottom. The numerical simulation is computed for polynomial order $\mathbb{P}_1$ on a coarse mesh and $\mathbb{P}_4$ on a fine mesh (Figure 3.10) with the particular stabilization parameter $\tau_K = \sqrt{\mu_K}/\sqrt{\varepsilon_K}$. The right-hand sides $\boldsymbol{J}$ and $\boldsymbol{g}^{inc}$ are the same as in section 3.5.3. The numerical simulation is computed firstly on an unstructured tetrahedral mesh consisting of 9227 elements with 96 elements in the sphere with $\mathbb{P}_1$ elements (Figure 3.10

left) and secondly on another unstructured tetrahedral mesh consisting of 32602 elements with 565 elements in the sphere with $\mathbb{P}_4$ elements (Figure 3.10 right). The simulation is computed on 22 cores, it takes 1 minute and 42 seconds for 136 time steps in the case of $\mathbb{P}_1$ interpolation with the first mesh, and takes 3 hours and 23 minutes for 699 time steps in the case of $\mathbb{P}_4$ interpolation with the second mesh. The purpose of this section is to validate the fully explicit HDGTD formulation in a heterogeneous domain, in other words the aim of this section is to validate the formulation with a non uniform τ on the mesh. We can see in Figure 3.10 that the incident plane wave, when meeting the dielectric sphere, is well scattered by it, and the value of the norm of the electric field is clearly increased in that sphere.

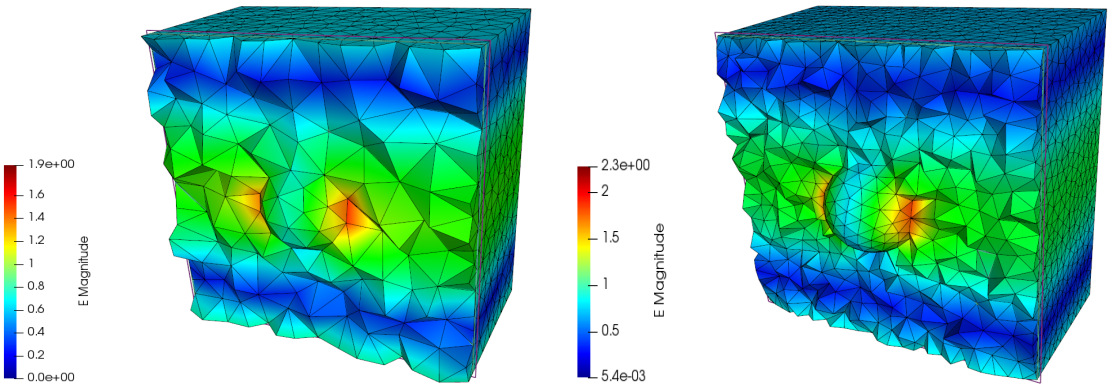

Figure 3.10 | Snapshot of the 3D simulation of the norm of the the electric field at a fixed time on a coarse mesh with $\mathbb{P}_1$ elements (left) and on a fine mesh with $\mathbb{P}_4$ elements (right).

3.6 Conclusion

We have formulated a fully explicit HDG method for the 3D time-domain Maxwell equations and proved the semi and fully-discrete stability of the scheme. The method can be seen as a generalization of the classical DGTD scheme based on upwind fluxes. It coincides with the latter scheme for a particular choice of the stabilization parameter τ introduced in the definition of numerical traces in the HDG framework . We have assessed numerically the influence of this parameter on the scheme and we presented the numerical solution of Maxwell equations in the case of propagation of a standing wave in a cubic PEC cavity, propagation of a plane wave in a homogeneous domain and scattering of a plane wave by a dielectric sphere.

4

A postprocessing for the fully explicit HDG discretization of time-dependent Maxwell equations

4.1 Introduction

In this chapter, we present a novel postprocessing technique for a hybrid discontinuous Galerkin discretization of time-dependent Maxwell's equations that we couple with an explicit Runge-Kutta time-marching scheme. The postprocessed electromagnetic field converges one order faster than the unprocessed solution in the $H(\text{curl})$-norm. The proposed approach is local, in the sense that the enhanced solution is computed independently in each cell of the computational mesh, and at each time step of interest. As a result, it is inexpensive to compute, especially if the region of interest is localized, either in time or space. The key ideas behind this postprocessing stem for hybridizable Galerkin methods, which are equivalent to the analyzed scheme for specific choices of penalization parameters. We present several numerical experiments that highlight the super-convergence properties of the postprocessed electromagnetic fields. The numerical results presented in this chapter are obtained with the DIOGENeS software suite described in section 3.5.1, that was extended to include different routines for the purpose of calculating the $H(\text{curl})$-norm of the solution first, and then finding the postprocessed solution defined later in this chapter. Our postprocessing technique is inspired by two recent works, namely, a postprocessing for an explicit HDG discretization of the

2D acoustic wave equation [38], and a postprocessing for a HDG discretization of the 3D time-harmonic Maxwell's equations [39]. Note that, before describing our novel local postprocessing done for the Maxwell equations in time domain for the first time, we will represent first the work done for the local postprocessing of the 3D time-harmonic Maxwell's equations. We rewrite the results for a test-case showing that the convergence of the electromagnetic field is one order faster than the unprocessed solution in the $H(\text{curl})$-norm, while this order remains the same in the case of the L^2-norm.

4.2 Local postprocessing for a HDG discretization of the 3D time-harmonic Maxwell's equations

A new local postprocessing method is proposed in [39] to obtain new approximations of the electric and magnetic fields, with an additional order in the $H^{curl}(\mathcal{T}_h)$. In other words, we expect that the post processed solution $\boldsymbol{E}_h^\star$ and $\boldsymbol{H}_h^\star$ converge with order $k+1$ in the $H^{curl}(\mathcal{T}_h)$-norm, whereas $\boldsymbol{E}_h$ and $\boldsymbol{H}_h$ described in section 2.4 converge with order k in the $H^{curl}(\mathcal{T}_h)$-norm.

Definition 2. *The $L^2(\mathcal{T}_h)$ and $H^{curl}(\mathcal{T}_h)$ norms of a vector field are defined by*

$$||\cdot||_{L^2(\mathcal{T}_h)} = \sum_{K\in\mathcal{T}_h} ||\cdot||_{L^2(K)},$$
$$||\cdot||_{H^{curl}(\mathcal{T}_h)} = \sum_{K\in\mathcal{T}_h} ||\cdot||_{L^2(K)} + ||\nabla\times\cdot||_{L^2(K)}.$$

Formulation

The new approximate electric field $\boldsymbol{E}_h^*$ introduced in [39] as the element of $[\mathbb{P}_{k+1}(K)]^3$ such that for all $K\in\mathcal{T}_h$,

Local postprocessing of $\boldsymbol{E}_h$

$$\begin{cases} (\nabla\times\boldsymbol{E}_h^\star, \nabla\times\boldsymbol{W})_K = -(i\omega\mu_r\boldsymbol{H}_h, \nabla\times\boldsymbol{W})_K, & \forall\boldsymbol{W}\in[\mathbb{P}_{k+1}(K)]^3,\\ (\boldsymbol{E}_h^\star, \nabla Y)_K = (\boldsymbol{E}_h, \nabla Y)_K & \forall Y\in\mathbb{P}_{k+2}(K).\end{cases}$$

Similarly, the new approximate magnetic field $\boldsymbol{H}_h^*$ introduced in [39] is found as the element of $[\mathbb{P}_{k+1}(K)]^3$ such that for all $K\in\mathcal{T}_h$,

Local postprocessing of $\boldsymbol{H}_h$

$$\begin{cases} (\nabla\times\boldsymbol{H}_h^\star, \nabla\times\boldsymbol{W})_K = (i\omega\varepsilon_r\boldsymbol{E}_h + \boldsymbol{J}, \nabla\times\boldsymbol{W})_K, & \forall\boldsymbol{W}\in[\mathbb{P}_{k+1}(K)]^3,\\ (\boldsymbol{H}_h^\star, \nabla Y)_K = (\boldsymbol{H}_h, \nabla Y)_K & \forall Y\in\mathbb{P}_{k+2}(K).\end{cases}$$

It is obvious that $\boldsymbol{\nabla}\times\boldsymbol{E}_h^\star$ and $\boldsymbol{\nabla}\times\boldsymbol{H}_h^\star$ are nothing but the projection of $i\omega\mu_r\boldsymbol{H}_h$ and $i\omega\varepsilon_r\boldsymbol{E}_h+\boldsymbol{J}$ onto the space of divergence-free functions in $[\mathbb{P}_{k+1}(K)]^3$. To show the efficiency of the method,

numerical results are presented in [39] that we resume them here. The time-harmonic Maxwell's equations (2.14) are considered on a unit cube $\Omega = (0,1)^3$ with $\mu = 1, \varepsilon = 2$ and $\omega = 1$. For $\boldsymbol{J} = 0$ the problem has the exact solution

$$\begin{aligned} Ex(x,y,z) &= sin(\omega y)sin(\omega z), & Hx(x,y,z) &= isin(\omega x)\left(cos(\omega y) - cos(\omega z)\right), \\ Ey(x,y,z) &= sin(\omega x)sin(\omega z), & Hy(x,y,z) &= isin(\omega y)\left(cos(\omega z) - cos(\omega x)\right), \\ Ez(x,y,z) &= sin(\omega y)sin(\omega x), & Hz(x,y,z) &= isin(\omega z)\left(cos(\omega x) - cos(\omega y)\right). \end{aligned} \tag{4.1}$$

The boundary data $\boldsymbol{g}^{inc}$ in 2.15 is determined from the exact solution. The tetrahedral meshes are constructed upon regular $n \times n \times n$ cartesian grids ($h = 1/n$) by splitting each cube into six tetrahedral.
The L^2-errors and orders of convergence of the numerical approximations and the postprocessed quantities for the electric field are presented in Table 4.1. We observe that the approximate electric field converge with order $k+1$ in the L^2-norm, but only with order k in the H^{curl}-norm, while we observe that the postprocessed electric field converge with order $k+1$ in the H^{curl}-norm which are one order higher than the original approximations.

		$\tau = 1.0$							
		$\|\|E - E_h\|\|_{L^2}$		$\|\|E - E_h^*\|\|_{L^2}$		$\|\|E - E_h\|\|_{H^{curl}}$		$\|\|E - E_h^*\|\|_{H^{curl}}$	
P_k	$1/h$	Error	order	Error	order	Error	order	Error	order
P_1	1/4	7.77e-03	-	8.42e-03	-	4.46e-02	-	9.05e-03	-
	1/6	1.94e-03	**2.00**	2.10e-03	**2.00**	2.14e-02	**1.06**	2.27e-03	**1.99**
	1/8	4.81e-04	**2.01**	5.23e-04	**2.01**	1.05e-02	**1.02**	5.68e-04	**2.00**
P_2	1/4	1.33e-04	-	1.34e-04	-	3.37e-03	-	2.07e-04	-
	1/6	1.90e-05	**2.81**	1.91e-05	**2.81**	3.37e-03	**1.99**	2.76e-05	**2.91**
	1/8	2.87e-06	**2.73**	2.88e-06	**2.73**	8.47e-04	**2.00**	3.81e-06	**2.86**
P_3	1/4	5.59e-06	-	5.43e-06	-	1.73e-04	-	6.71e-06	-
	1/6	3.53e-07	**3.99**	3.44e-07	**3.98**	2.15e-05	**3.01**	4.26e-07	**3.98**
	1/8	2.22e-08	**3.99**	2.17e-08	**3.99**	2.67e-06	**3.00**	2.69e-08	**3.99**

Table 4.1 | Maximum L^2 & H^{curl}-errors and convergence orders.

4.3 A novel postprocessing for a HDG discretization of the 3D time-domain Maxwell's equations with an explicit time scheme

The purpose of this section is to introduce postprocessed solutions $\boldsymbol{E}_h^{n\star}$ and $\boldsymbol{H}_h^{n\star}$ that are more accurate representations of $\boldsymbol{E}(t_n)$ and $\boldsymbol{H}(t_n)$ than $\boldsymbol{E}_h^n$ and $\boldsymbol{H}_h^n$ described in chapter 3. This postprocessing is purely local in time, in the sense that the computation of $\boldsymbol{E}_h^{n\star}$ and $\boldsymbol{H}_h^{n\star}$ only involves $\boldsymbol{E}_h^n$ and $\boldsymbol{H}_h^n$. It is also local in space as the computation are local to each element $K \in \mathcal{T}_h$. Actually, $\boldsymbol{E}_h^{n\star}|_K$ (resp. $\boldsymbol{H}_h^{n\star}|_K$) only depends on $\boldsymbol{E}_h^n|_{\widetilde{K}}$ (resp. $\boldsymbol{H}_h^n|_{\widetilde{K}}$), where $\widetilde{K}$ is the union of all elements $K' \in \mathcal{T}_h$ sharing (at least) one face with K.

Our approach closely follows previous works. Specifically, similar postprocessing strategies have been derived for the time-harmonic Maxwell's equations [39], as well as time-dependent acoustic wave equation [38]. These works develop in the context of hybridizable discontinuous Galerkin (HDG) methods, but can be easily applied to the DG scheme under consideration, as we depict hereafter.

4.3.1 Definition of the postprocessed solution

Our postprocessing hinges on element-wise finite-element saddle-point problems. For each element $K \in \mathcal{T}_h$, there exists a unique pair $(\boldsymbol{E}_h^{n\star}, p) \in [\mathbb{P}_{k+1}(K)]^3 \times \mathbb{P}_{k+2}(K)/\mathbb{R}$ such that

Postprocessed electric field

$$\left\{\begin{array}{rcl} (\boldsymbol{\nabla} \times \boldsymbol{E}_h^{n\star}, \boldsymbol{\nabla} \times \boldsymbol{w})_K + (\boldsymbol{\nabla} p, \boldsymbol{w})_K & = & (\boldsymbol{\nabla} \times \boldsymbol{E}_h^{n}, \boldsymbol{\nabla} \times \boldsymbol{w})_K \\ & + & \langle \boldsymbol{E}_h^{n,\mathrm{t}} - \widehat{\boldsymbol{E}}_h^{n,\mathrm{t}}, \boldsymbol{n} \times \boldsymbol{\nabla} \times \boldsymbol{w} \rangle_{\partial K}, \\ (\boldsymbol{E}_h^{n\star}, \boldsymbol{\nabla} v)_K & = & (\boldsymbol{E}_h^{n}, \boldsymbol{\nabla} v)_K, \end{array}\right. \tag{4.2}$$

for all $\boldsymbol{w} \in [\mathbb{P}_{k+1}(K)]^3$ and $v \in \mathbb{P}_{k+2}(K)/\mathbb{R}$. Similarly, for the magnetic field, there exists a unique pair $(\boldsymbol{H}_h^{n\star}, q) \in [\mathbb{P}_{k+1}(K)]^3 \times \mathbb{P}_{k+2}(K)/\mathbb{R}$ such that

Postprocessed magnetic field

$$\left\{\begin{array}{rcl} (\boldsymbol{\nabla} \times \boldsymbol{H}_h^{n\star}, \boldsymbol{\nabla} \times \boldsymbol{w})_K + (\boldsymbol{\nabla} q, \boldsymbol{w})_K & = & (\boldsymbol{\nabla} \times \boldsymbol{H}_h^{n}, \boldsymbol{\nabla} \times \boldsymbol{w})_K \\ & + & \langle \boldsymbol{H}_h^{n,\mathrm{t}} - \widehat{\boldsymbol{H}}_h^{n,\mathrm{t}}, \boldsymbol{n} \times \boldsymbol{\nabla} \times \boldsymbol{w} \rangle_{\partial K}, \\ (\boldsymbol{H}_h^{n\star}, \boldsymbol{\nabla} v)_K & = & (\boldsymbol{H}_h^{n}, \boldsymbol{\nabla} v)_K, \end{array}\right. \tag{4.3}$$

for all $\boldsymbol{w} \in [\mathbb{P}_{k+1}(K)]^3$ and $q \in \mathbb{P}_{k+2}(K)/\mathbb{R}$. $\widehat{\boldsymbol{E}}_h^{n,\mathrm{t}}$ and $\widehat{\boldsymbol{H}}_h^{n,\mathrm{t}}$ are the numerical fluxes considered in (3.2) and (3.3). $\boldsymbol{E}_h^{n\star}$ and $\boldsymbol{H}_h^{n\star}$ are then our postprocessed approximations to $\boldsymbol{E}(t_n)$ and $\boldsymbol{H}(t_n)$.

The left-hand sides of the above definition lead to solve symmetric linear systems of small size. In addition, observing that the left-hand side is actually the same for the two postprocessing schemes, we deduce that only one matrix factorization is required per element.

The right-hand sides further show that for each $K \in \mathcal{T}_h$, the postprocessed field $\boldsymbol{E}_h^{n\star}|_K$ only depends on $\boldsymbol{E}_h^{n}|_K$ and the value at the flux $\widehat{\boldsymbol{E}}_h^{n,\mathrm{t}}|_F$ on each face $F \in \mathcal{F}_K$. In turn, since the flux is defined using the two elements sharing the face F, we see that $\boldsymbol{E}_h^{n}|_K$ depends on the values taken by $\boldsymbol{E}_h^{n}$ on all the elements K' sharing at least one face with K. A similar comment holds true for $\boldsymbol{H}_h^{n\star}$.

4.3.2 Existence and uniqueness of the solution

Theorem 5. *There exists a unique solution $(\boldsymbol{E}_h^{n\star}, p)$ and $(\boldsymbol{H}_h^{n\star}, q)$ for the problems (4.2) and (4.3).*

Proof. We will prove the existence and uniqueness for the solution of the problem (4.2), and the proof will be the same for (4.3). The spaces $[\mathbb{P}_{k+1}(K)]^3$ and $\mathbb{P}_{k+2}(K)/\mathbb{R}$ are of finite dimension, so the problem (4.2) can be written as the linear system below

$$\mathcal{K} \underbrace{\left[E_h^{x,n\star}, E_h^{y,n\star}, E_h^{z,n\star}, p\right]^T}_{\mathcal{X}} = \mathcal{L} \tag{4.4}$$

while $dim(\mathcal{K}) = (3dim(\mathbb{P}_{k+1}) + dim(\mathbb{P}_{k+2}) - 1) \times (3dim(\mathbb{P}_{k+1}) + dim(\mathbb{P}_{k+2}) - 1)$. $\mathcal{X}$ and $\mathcal{L}$ are two vectors of dimension $3dim(\mathbb{P}_{k+1}) + dim(\mathbb{P}_{k+2}) - 1$. Proving the existence and the uniqueness

of the solution for (4.4) will be nothing than proving the injectivity of the matrix $\mathcal{K}$.
The proof is divided into two parts, the first part is to prove that p is always null and the second one is to deduce that $\boldsymbol{E}_h^{n\star}$ is equal to zero when $\mathcal{K}\mathcal{X} = 0$.
Back to (4.2) we have that p belongs to the space $\mathbb{P}_{k+2}(K)/\mathbb{R}$, so $\boldsymbol{\nabla} p$ belongs to the space $[\mathbb{P}_{k+1}(K)]^3$. The first equation of (4.2) holds for every $\boldsymbol{w} \in [\mathbb{P}_{k+1}(K)]^3$. Thus, we can consider a particular $\boldsymbol{w} = \boldsymbol{\nabla} p$ and replace it in the equation to obtain

$$(\boldsymbol{\nabla} \times \boldsymbol{E}_h^{n\star}, \boldsymbol{\nabla} \times \boldsymbol{\nabla} p)_K + (\boldsymbol{\nabla} p, \boldsymbol{\nabla} p)_K = (\boldsymbol{\nabla} \times \boldsymbol{E}_h^{n}, \boldsymbol{\nabla} \times \boldsymbol{\nabla} p)_K, + \langle \boldsymbol{E}_h^{n,\mathrm{t}} - \widehat{\boldsymbol{E}}_h^{n,\mathrm{t}}, \boldsymbol{n} \times \boldsymbol{\nabla} \times \boldsymbol{\nabla} p \rangle_{\partial K}.$$

The curl of a gradient is always zero, so we can deduce that $\|\boldsymbol{\nabla} p\|_K^2$ is zero and thus $\boldsymbol{\nabla} p$ is null. Finally, p belongs to $\mathbb{P}_{k+2}(K)/\mathbb{R}$ and its gradient is null, we can deduce that $p = 0$.
For the second part of the proof, we have that $\boldsymbol{E}_h^{n\star}$ belongs to the space $[\mathbb{P}_{k+1}(K)]^3$, thus we will set $\boldsymbol{w} = \boldsymbol{E}_h^{n\star}$ to obtain $\|\boldsymbol{\nabla} \times \boldsymbol{E}_h^{n\star}\|_K^2 = 0$, then $\boldsymbol{\nabla} \times \boldsymbol{E}_h^{n\star} = 0$, so there exists ϕ in $\mathbb{P}_{k+2}(K)/\mathbb{R}$ such that $\boldsymbol{E}_h^{n\star} = \boldsymbol{\nabla}\phi$. Now we will set $v = \phi$ to obtain

$$(\boldsymbol{E}_h^{n\star}, \boldsymbol{\nabla}\phi)_K = (\boldsymbol{E}_h^{n\star}, \boldsymbol{E}_h^{n\star})_K = \|\boldsymbol{E}_h^{n\star}\|_K^2 = 0.$$

Finally, we have $\boldsymbol{E}_h^{n\star} = 0$, so the matrix $\mathcal{K}$ is injective and we have a unique solution for the problem (4.2). □

4.3.3 Compact formulation

In this section, we will introduce new variables and write the compact formulations of (4.2) and (4.3) in terms of these variables. Let $\boldsymbol{l}_h^n$ and $\boldsymbol{o}_h^n$ in $\boldsymbol{V}(K)$ such that,

$$(\boldsymbol{l}_h^n, \boldsymbol{v})_K = (\boldsymbol{E}_h^n, \boldsymbol{\nabla} \times \boldsymbol{v})_K - \langle \hat{\boldsymbol{E}}_h^{t,n}, \boldsymbol{n} \times \boldsymbol{v} \rangle_{\partial K} \quad \forall \boldsymbol{v} \in \boldsymbol{V}(K),$$

and

$$(\boldsymbol{o}_h^n, \boldsymbol{v})_K = (\boldsymbol{H}_h^n, \boldsymbol{\nabla} \times \boldsymbol{v})_K - \langle \hat{\boldsymbol{H}}_h^{t,n}, \boldsymbol{n} \times \boldsymbol{v} \rangle_{\partial K} \quad \forall \boldsymbol{v} \in \boldsymbol{V}(K).$$

In other terms, we can consider $\boldsymbol{l}_h^n$ and $\boldsymbol{o}_h^n$ in $\boldsymbol{V}(K)$ such that,

$$(\boldsymbol{l}_h^n, \boldsymbol{\nabla} \times \boldsymbol{w})_K = (\boldsymbol{E}_h^n, \boldsymbol{\nabla} \times \boldsymbol{\nabla} \times \boldsymbol{w})_K - \langle \hat{\boldsymbol{E}}_h^{t,n}, \boldsymbol{n} \times \boldsymbol{\nabla} \times \boldsymbol{w} \rangle_{\partial K} \quad \forall \boldsymbol{w} \in [\mathbb{P}_{k+1}(K)]^3,$$

and

$$(\boldsymbol{o}_h^n, \boldsymbol{\nabla} \times \boldsymbol{w})_K = (\boldsymbol{H}_h^n, \boldsymbol{\nabla} \times \boldsymbol{\nabla} \times \boldsymbol{w})_K - \langle \hat{\boldsymbol{H}}_h^{t,n}, \boldsymbol{n} \times \boldsymbol{\nabla} \times \boldsymbol{w} \rangle_{\partial K} \quad \forall \boldsymbol{w} \in [\mathbb{P}_{k+1}(K)]^3.$$

After integrating by parts $(\boldsymbol{E}_h^n, \boldsymbol{\nabla} \times \boldsymbol{\nabla} \times \boldsymbol{w})_K$ and $(\boldsymbol{H}_h^n, \boldsymbol{\nabla} \times \boldsymbol{\nabla} \times \boldsymbol{w})_K$ we obtain that for all $\boldsymbol{w}$ in $[\mathbb{P}_{k+1}(K)]^3$

$$(\boldsymbol{l}_h^n, \boldsymbol{\nabla} \times \boldsymbol{w})_K = (\boldsymbol{\nabla} \times \boldsymbol{E}_h^n, \boldsymbol{\nabla} \times \boldsymbol{w})_K, + \langle \boldsymbol{E}_h^{n,\mathrm{t}} - \widehat{\boldsymbol{E}}_h^{n,\mathrm{t}}, \boldsymbol{n} \times \boldsymbol{\nabla} \times \boldsymbol{w} \rangle_{\partial K},$$

and

$$(\boldsymbol{o}_h^n, \boldsymbol{\nabla} \times \boldsymbol{w})_K = (\boldsymbol{\nabla} \times \boldsymbol{H}_h^n, \boldsymbol{\nabla} \times \boldsymbol{w})_K, + \langle \boldsymbol{H}_h^{n,\mathrm{t}} - \widehat{\boldsymbol{H}}_h^{n,\mathrm{t}}, \boldsymbol{n} \times \boldsymbol{\nabla} \times \boldsymbol{w} \rangle_{\partial K}.$$

And finally

$$\begin{cases} (\boldsymbol{\nabla} \times \boldsymbol{E}_h^{n\star}, \boldsymbol{\nabla} \times \boldsymbol{w})_K = (\boldsymbol{l}_h^n, \boldsymbol{\nabla} \times \boldsymbol{w})_K, & \forall \boldsymbol{w} \in [\mathbb{P}_{k+1}(K)]^3, \\ (\boldsymbol{E}_h^{n\star}, \boldsymbol{\nabla} v)_K = (\boldsymbol{E}_h^n, \boldsymbol{\nabla} v)_K & \forall v \in \mathbb{P}_{k+2}(K)/\mathbb{R}, \end{cases} \tag{4.5}$$

and

$$\begin{cases} (\boldsymbol{\nabla} \times \boldsymbol{H}_h^{n\star}, \boldsymbol{\nabla} \times \boldsymbol{w})_K = (\boldsymbol{o}_h^n, \boldsymbol{\nabla} \times \boldsymbol{w})_K, & \forall \boldsymbol{w} \in [\mathbb{P}_{k+1}(K)]^3, \\ (\boldsymbol{H}_h^{n\star}, \boldsymbol{\nabla} v)_K = (\boldsymbol{H}_h^n, \boldsymbol{\nabla} v)_K & \forall v \in \mathbb{P}_{k+2}(K)/\mathbb{R}. \end{cases} \tag{4.6}$$

4.3.4 Implementation

Firstly, we compute $\boldsymbol{l}_h^n$ and $\boldsymbol{o}_h^n$ by locally solving the following system

$$\begin{cases} (\boldsymbol{l}_h^n, \boldsymbol{v})_K = (\boldsymbol{E}_h^n, \boldsymbol{\nabla} \times \boldsymbol{v})_K - \langle \hat{\boldsymbol{E}}_h^{t,n}, \boldsymbol{n} \times \boldsymbol{v} \rangle_{\partial K} \quad \forall \boldsymbol{v} \in \boldsymbol{V}(K), \\ (\boldsymbol{o}_h^n, \boldsymbol{v})_K = (\boldsymbol{H}_h^n, \boldsymbol{\nabla} \times \boldsymbol{v})_K - \langle \hat{\boldsymbol{H}}_h^{t,n}, \boldsymbol{n} \times \boldsymbol{v} \rangle_{\partial K} \quad \forall \boldsymbol{v} \in \boldsymbol{V}(K), \end{cases}$$

and then find $(\boldsymbol{E}_h^{n\star}, \boldsymbol{H}_h^{n\star}) \in [\mathbb{P}_{k+1}(K)]^3 \times [\mathbb{P}_{k+1}(K)]^3$ such that

$$\begin{cases} (\boldsymbol{\nabla} \times \boldsymbol{E}_h^{n\star}, \boldsymbol{\nabla} \times \boldsymbol{w})_K = (\boldsymbol{l}_h^n, \boldsymbol{\nabla} \times \boldsymbol{w})_K & \forall \boldsymbol{w} \in [\mathbb{P}_{k+1}(K)]^3, \\ (\boldsymbol{E}_h^{n\star}, \boldsymbol{\nabla} v)_K = (\boldsymbol{E}_h^n, \boldsymbol{\nabla} v)_K & \forall v \in \mathbb{P}_{k+2}(K)/\mathbb{R}, \end{cases}$$

and

$$\begin{cases} (\boldsymbol{\nabla} \times \boldsymbol{H}_h^{n\star}, \boldsymbol{\nabla} \times \boldsymbol{w})_K = (\boldsymbol{o}_h^n, \boldsymbol{\nabla} \times \boldsymbol{w})_K & \forall \boldsymbol{w} \in [\mathbb{P}_{k+1}(K)]^3, \\ (\boldsymbol{H}_h^{n\star}, \boldsymbol{\nabla} v)_K = (\boldsymbol{H}_h^n, \boldsymbol{\nabla} v)_K & \forall v \in \mathbb{P}_{k+2}(K)/\mathbb{R}. \end{cases}$$

We now detail the discretization of $\boldsymbol{E}^\star$.
Let $(\theta_l)_{1 \le l \le d_k}$, $(\Phi_j)_{1 \le j \le d_{k+1}}$ and $(\psi_a)_{1 \le a \le d_{k+2}}$ be the polynomial basis of $\mathbb{P}_k$, $\mathbb{P}_{k+1}$ and $\mathbb{P}_{k+2}$ respectively.

Let us consider $m \in [1, d_{k+1}]$. Then for $\boldsymbol{w} = \Phi_m^1 = \begin{pmatrix} \Phi_m \\ 0 \\ 0 \end{pmatrix}$,we have $\boldsymbol{\nabla} \times \boldsymbol{w} = \begin{pmatrix} 0 \\ \partial_z \Phi_m \\ -\partial_y \Phi_m \end{pmatrix}$.

$$\boldsymbol{\nabla} \times \boldsymbol{E}_h^{n\star} = \begin{pmatrix} \sum_{j=1}^{d_{k+1}} \left(E_{hj}^{z,n\star}\right) \partial_y \Phi_j - \sum_{j=1}^{d_{k+1}} \left(E_{hj}^{y,n\star}\right) \partial_z \Phi_j \\ \sum_{j=1}^{d_{k+1}} \left(E_{hj}^{x,n\star}\right) \partial_z \Phi_j - \sum_{j=1}^{d_{k+1}} \left(E_{hj}^{z,n\star}\right) \partial_x \Phi_j \\ \sum_{j=1}^{d_{k+1}} \left(E_{hj}^{y,n\star}\right) \partial_x \Phi_j - \sum_{j=1}^{d_{k+1}} \left(E_{hj}^{x,n\star}\right) \partial_y \Phi_j \end{pmatrix}$$

We deduce now that for all $m \in [1, d_{k+1}]$

$$\begin{aligned} & (\boldsymbol{\nabla} \times \boldsymbol{E}_h^{n\star}, \boldsymbol{\nabla} \times \Phi_m^1)_K \\ &= \int_K \left[\sum_{j=1}^{d_{k+1}} E_{hj}^{x,n\star} \partial_z \Phi_j - \sum_{j=1}^{d_{k+1}} E_{hj}^{z,n\star} \partial_x \Phi_j \right] \partial_z \Phi_m - \left[\sum_{j=1}^{d_{k+1}} E_{hj}^{y,n\star} \partial_x \Phi_j - \sum_{j=1}^{d_{k+1}} E_{hj}^{x,n\star} \partial_y \Phi_j \right] \partial_y \Phi_m \\ &= \sum_{j=1}^{d_{k+1}} E_{hj}^{x,n\star} \int_K \partial_z \Phi_m \partial_z \Phi_j - \sum_{j=1}^{d_{k+1}} E_{hj}^{z,n\star} \int_K \partial_z \Phi_m \partial_x \Phi_j - \sum_{j=1}^{d_{k+1}} E_{hj}^{y,n\star} \int_K \partial_y \Phi_m \partial_x \Phi_j \\ &+ \sum_{j=1}^{d_{k+1}} E_{hj}^{x,n\star} \int_K \partial_y \Phi_m \partial_y \Phi_j \end{aligned}$$

By considering all the values $m \in [1, d_{k+1}]$ we can form the following system

$$
\begin{aligned}
\begin{pmatrix} (\boldsymbol{\nabla} \times \boldsymbol{E}_h^{n\star}, \boldsymbol{\nabla} \times \Phi_1^1)_K \\ \vdots \\ (\boldsymbol{\nabla} \times \boldsymbol{E}_h^{n\star}, \boldsymbol{\nabla} \times \Phi_{d_{k+1}}^1)_K \end{pmatrix} &= \begin{pmatrix} \int_K \partial_z \Phi_1 \partial_z \Phi_1 & \cdots & \int_K \partial_z \Phi_1 \partial_z \Phi_{d_{k+1}} \\ & \ddots & \\ \int_K \partial_z \Phi_{d_{k+1}} \partial_z \Phi_1 & \cdots & \int_K \partial_z \Phi_{d_{k+1}} \partial_z \Phi_{d_{k+1}} \end{pmatrix} \begin{pmatrix} E_{h1}^{x,n\star} \\ \vdots \\ E_{hd_{k+1}}^{x,n\star} \end{pmatrix} \\
&- \begin{pmatrix} \int_K \partial_z \Phi_1 \partial_x \Phi_1 & \cdots & \int_K \partial_z \Phi_1 \partial_x \Phi_{d_{k+1}} \\ & \ddots & \\ \int_K \partial_z \Phi_{d_{k+1}} \partial_x \Phi_1 & \cdots & \int_K \partial_z \Phi_{d_{k+1}} \partial_x \Phi_{d_{k+1}} \end{pmatrix} \begin{pmatrix} E_{h1}^{z,n\star} \\ \vdots \\ E_{hd_{k+1}}^{z,n\star} \end{pmatrix} \\
&- \begin{pmatrix} \int_K \partial_y \Phi_1 \partial_x \Phi_1 & \cdots & \int_K \partial_y \Phi_1 \partial_x \Phi_{d_{k+1}} \\ & \ddots & \\ \int_K \partial_y \Phi_{d_{k+1}} \partial_x \Phi_1 & \cdots & \int_K \partial_y \Phi_{d_{k+1}} \partial_x \Phi_{d_{k+1}} \end{pmatrix} \begin{pmatrix} E_{h1}^{y,n\star} \\ \vdots \\ E_{hd_{k+1}}^{y,n\star} \end{pmatrix} \\
&+ \begin{pmatrix} \int_K \partial_y \Phi_1 \partial_y \Phi_1 & \cdots & \int_K \partial_y \Phi_1 \partial_y \Phi_{d_{k+1}} \\ & \ddots & \\ \int_K \partial_y \Phi_{d_{k+1}} \partial_y \Phi_1 & \cdots & \int_K \partial_y \Phi_{d_{k+1}} \partial_y \Phi_{d_{k+1}} \end{pmatrix} \begin{pmatrix} E_{h1}^{x,n\star} \\ \vdots \\ E_{hd_{k+1}}^{x,n\star} \end{pmatrix}.
\end{aligned}
$$

For the RHS we have

$$
\begin{aligned}
(\boldsymbol{l}_h^n, \boldsymbol{\nabla} \times \Phi_m^1)_K &= \int_K \left[\sum_{j=1}^{d_k} l_{h,j}^{y,n} \theta_j \right] \partial_z \Phi_m - \left[\sum_{j=1}^{d_k} l_{h,j}^{z,n} \theta_j \right] \partial_y \Phi_m \\
&= \sum_{j=1}^{d_k} l_{h,j}^{y,n} \int_K \partial_z \Phi_m \theta_j - \sum_{j=1}^{d_k} l_{h,j}^{z,n} \int_K \partial_y \Phi_m \theta_j
\end{aligned}
$$

$$
\begin{aligned}
\begin{pmatrix} (\boldsymbol{l}_h^n, \boldsymbol{\nabla} \times \Phi_1^1)_K \\ \vdots \\ (\boldsymbol{l}_h^n, \boldsymbol{\nabla} \times \Phi_{d_{k+1}}^1)_K \end{pmatrix} &= \begin{pmatrix} \int_K \partial_z \Phi_1 \theta_1 & \cdots & \int_K \partial_z \Phi_1 \theta_{d_k} \\ & \ddots & \\ \int_K \partial_z \Phi_{d_{k+1}} \theta_1 & \cdots & \int_K \partial_z \Phi_{d_{k+1}} \theta_{d_k} \end{pmatrix} \begin{pmatrix} l_{h,1}^{y,n} \\ \vdots \\ l_{h,d_k}^{y,n} \end{pmatrix} \\
&- \begin{pmatrix} \int_K \partial_y \Phi_1 \theta_1 & \cdots & \int_K \partial_y \Phi_1 \theta_{d_k} \\ & \ddots & \\ \int_K \partial_y \Phi_{d_{k+1}} \theta_1 & \cdots & \int_K \partial_y \Phi_{d_{k+1}} \theta_{d_k} \end{pmatrix} \begin{pmatrix} l_{h,1}^{z,n} \\ \vdots \\ l_{h,d_k}^{z,n} \end{pmatrix}.
\end{aligned}
$$

By following the same ideas above, and by setting firstly $\boldsymbol{w} = \Phi_m^2 = \begin{pmatrix} 0 \\ \Phi_m \\ 0 \end{pmatrix}$ and secondly $\boldsymbol{w} = \Phi_m^3 = \begin{pmatrix} 0 \\ 0 \\ \Phi_m \end{pmatrix}$, we obtain

$$
\begin{aligned}
\begin{pmatrix} (\boldsymbol{\nabla} \times \boldsymbol{E}_h^{n\star}, \boldsymbol{\nabla} \times \Phi_1^2)_K \\ \vdots \\ (\boldsymbol{\nabla} \times \boldsymbol{E}_h^{n\star}, \boldsymbol{\nabla} \times \Phi_{d_{k+1}}^2)_K \end{pmatrix} &= \begin{pmatrix} \int_K \partial_x \Phi_1 \partial_x \Phi_1 & \cdots & \int_K \partial_x \Phi_1 \partial_x \Phi_{d_{k+1}} \\ & \ddots & \\ \int_K \partial_x \Phi_{d_{k+1}} \partial_x \Phi_1 & \cdots & \int_K \partial_x \Phi_{d_{k+1}} \partial_x \Phi_{d_{k+1}} \end{pmatrix} \begin{pmatrix} E_{h1}^{y,n\star} \\ \vdots \\ E_{hd_{k+1}}^{y,n\star} \end{pmatrix} \\
&- \begin{pmatrix} \int_K \partial_x \Phi_1 \partial_y \Phi_1 & \cdots & \int_K \partial_x \Phi_1 \partial_y \Phi_{d_{k+1}} \\ & \ddots & \\ \int_K \partial_x \Phi_{d_{k+1}} \partial_y \Phi_1 & \cdots & \int_K \partial_x \Phi_{d_{k+1}} \partial_y \Phi_{d_{k+1}} \end{pmatrix} \begin{pmatrix} E_{h1}^{x,n\star} \\ \vdots \\ E_{hd_{k+1}}^{x,n\star} \end{pmatrix} \\
&- \begin{pmatrix} \int_K \partial_z \Phi_1 \partial_y \Phi_1 & \cdots & \int_K \partial_z \Phi_1 \partial_y \Phi_{d_{k+1}} \\ & \ddots & \\ \int_K \partial_z \Phi_{d_{k+1}} \partial_y \Phi_1 & \cdots & \int_K \partial_z \Phi_{d_{k+1}} \partial_y \Phi_{d_{k+1}} \end{pmatrix} \begin{pmatrix} E_{h1}^{z,n\star} \\ \vdots \\ E_{hd_{k+1}}^{z,n\star} \end{pmatrix} \\
&+ \begin{pmatrix} \int_K \partial_z \Phi_1 \partial_z \Phi_1 & \cdots & \int_K \partial_z \Phi_1 \partial_z \Phi_{d_{k+1}} \\ & \ddots & \\ \int_K \partial_z \Phi_{d_{k+1}} \partial_z \Phi_1 & \cdots & \int_K \partial_z \Phi_{d_{k+1}} \partial_z \Phi_{d_{k+1}} \end{pmatrix} \begin{pmatrix} E_{h1}^{y,n\star} \\ \vdots \\ E_{hd_{k+1}}^{y,n\star} \end{pmatrix},
\end{aligned}
$$

and also

$$
\begin{aligned}
\begin{pmatrix} (\boldsymbol{\nabla} \times \boldsymbol{E}_h^{n\star}, \boldsymbol{\nabla} \times \Phi_1^3)_K \\ \vdots \\ (\boldsymbol{\nabla} \times \boldsymbol{E}_h^{n\star}, \boldsymbol{\nabla} \times \Phi_{d_{k+1}}^3)_K \end{pmatrix} &= \begin{pmatrix} \int_K \partial_y \Phi_1 \partial_y \Phi_1 & \cdots & \int_K \partial_y \Phi_1 \partial_y \Phi_{d_{k+1}} \\ & \ddots & \\ \int_K \partial_y \Phi_{d_{k+1}} \partial_y \Phi_1 & \cdots & \int_K \partial_y \Phi_{d_{k+1}} \partial_y \Phi_{d_{k+1}} \end{pmatrix} \begin{pmatrix} E_{h1}^{z,n\star} \\ \vdots \\ E_{hd_{k+1}}^{z,n\star} \end{pmatrix} \\
&- \begin{pmatrix} \int_K \partial_y \Phi_1 \partial_z \Phi_1 & \cdots & \int_K \partial_y \Phi_1 \partial_z \Phi_{d_{k+1}} \\ & \ddots & \\ \int_K \partial_y \Phi_{d_{k+1}} \partial_z \Phi_1 & \cdots & \int_K \partial_y \Phi_{d_{k+1}} \partial_z \Phi_{d_{k+1}} \end{pmatrix} \begin{pmatrix} E_{h1}^{y,n\star} \\ \vdots \\ E_{hd_{k+1}}^{y,n\star} \end{pmatrix}
\end{aligned}
$$

$$
-\begin{pmatrix} \int_K \partial_x\Phi_1\partial_z\Phi_1 & \cdots & \int_K \partial_x\Phi_1\partial_z\Phi_{d_{k+1}} \\ & \ddots & \\ \int_K \partial_x\Phi_{d_{k+1}}\partial_z\Phi_1 & \cdots & \int_K \partial_x\Phi_{d_{k+1}}\partial_z\Phi_{d_{k+1}} \end{pmatrix} \begin{pmatrix} E_{h1}^{x,n\star} \\ \vdots \\ E_{hd_{k+1}}^{x,n\star} \end{pmatrix}
$$

$$
+\begin{pmatrix} \int_K \partial_x\Phi_1\partial_x\Phi_1 & \cdots & \int_K \partial_x\Phi_1\partial_x\Phi_{d_{k+1}} \\ & \ddots & \\ \int_K \partial_x\Phi_{d_{k+1}}\partial_x\Phi_1 & \cdots & \int_K \partial_x\Phi_{d_{k+1}}\partial_x\Phi_{d_{k+1}} \end{pmatrix} \begin{pmatrix} E_{h1}^{z,n\star} \\ \vdots \\ E_{hd_{k+1}}^{z,n\star} \end{pmatrix}
$$

For the right hand sides, we can write

$$
\begin{pmatrix} (\boldsymbol{l}_h^n, \boldsymbol{\nabla}\times\Phi_1^2)_K \\ \vdots \\ (\boldsymbol{l}_h^n, \boldsymbol{\nabla}\times\Phi_{d_{k+1}}^2)_K \end{pmatrix} = \begin{pmatrix} \int_K \partial_x\Phi_1\theta_1 & \cdots & \int_K \partial_x\Phi_1\theta_{d_k} \\ & \ddots & \\ \int_K \partial_x\Phi_{d_{k+1}}\theta_1 & \cdots & \int_K \partial_x\Phi_{d_{k+1}}\theta_{d_k} \end{pmatrix} \begin{pmatrix} l_{h,1}^{z,n} \\ \vdots \\ l_{h,d_k}^{z,n} \end{pmatrix}
$$

$$
-\begin{pmatrix} \int_K \partial_z\Phi_1\theta_1 & \cdots & \int_K \partial_z\Phi_1\theta_{d_k} \\ & \ddots & \\ \int_K \partial_z\Phi_{d_{k+1}}\theta_1 & \cdots & \int_K \partial_z\Phi_{d_{k+1}}\theta_{d_k} \end{pmatrix} \begin{pmatrix} l_{h,1}^{x,n} \\ \vdots \\ l_{h,d_k}^{x,n} \end{pmatrix},
$$

and

$$
\begin{pmatrix} (\boldsymbol{l}_h^n, \boldsymbol{\nabla}\times\Phi_1^3)_K \\ \vdots \\ (\boldsymbol{l}_h^n, \boldsymbol{\nabla}\times\Phi_{d_{k+1}}^3)_K \end{pmatrix} = \begin{pmatrix} \int_K \partial_y\Phi_1\theta_1 & \cdots & \int_K \partial_y\Phi_1\theta_{d_k} \\ & \ddots & \\ \int_K \partial_y\Phi_{d_{k+1}}\theta_1 & \cdots & \int_K \partial_y\Phi_{d_{k+1}}\theta_{d_k} \end{pmatrix} \begin{pmatrix} l_{h,1}^{x,n} \\ \vdots \\ l_{h,d_k}^{x,n} \end{pmatrix}
$$

$$
-\begin{pmatrix} \int_K \partial_x\Phi_1\theta_1 & \cdots & \int_K \partial_x\Phi_1\theta_{d_k} \\ & \ddots & \\ \int_K \partial_x\Phi_{d_{k+1}}\theta_1 & \cdots & \int_K \partial_x\Phi_{d_{k+1}}\theta_{d_k} \end{pmatrix} \begin{pmatrix} l_{h,1}^{y,n} \\ \vdots \\ l_{h,d_k}^{y,n} \end{pmatrix}
$$

For all $a \in [1, d_{k+2}]$, and for $v = \psi_a$, we have $\boldsymbol{\nabla} v = \begin{pmatrix} \partial_x\psi_a \\ \partial_y\psi_a \\ \partial_z\psi_a \end{pmatrix}$.

We deduce now that for all a $\in [1, d_{k+2}]$

$$
\begin{aligned}
&(\boldsymbol{E}_h^{n\star}, \boldsymbol{\nabla}\psi_a)_K \\
&= \int_K \left[\sum_{j=1}^{d_{k+1}} E_{hj}^{x,n\star}\Phi_j\right]\partial_x\psi_a + \left[\sum_{j=1}^{d_{k+1}} E_{hj}^{y,n\star}\Phi_j\right]\partial_y\psi_a + \left[\sum_{j=1}^{d_{k+1}} E_{hj}^{z,n\star}\Phi_j\right]\partial_z\psi_a \\
&= \sum_{j=1}^{d_{k+1}} E_{hj}^{x,n\star}\int_K \partial_x\psi_a\Phi_j + \sum_{j=1}^{d_{k+1}} E_{hj}^{y,n\star}\int_K \partial_y\psi_a\Phi_j + \sum_{j=1}^{d_{k+1}} E_{hj}^{z,n\star}\int_K \partial_z\psi_a\Phi_j
\end{aligned}
$$

By considering all the values $a \in [1, d_{k+2}]$ we can form the following system

$$
\begin{aligned}
\begin{pmatrix} (\boldsymbol{E}_h^{n\star}, \boldsymbol{\nabla}\psi_1)_K \\ \vdots \\ (\boldsymbol{E}_h^{n\star}, \boldsymbol{\nabla}\psi_{d_{k+2}})_K \end{pmatrix} &= \begin{pmatrix} \int_K \partial_x\psi_1\Phi_1 & \cdots & \int_K \partial_x\psi_1\Phi_{d_{k+1}} \\ & \ddots & \\ \int_K \partial_x\psi_{d_{k+2}}\Phi_1 & \cdots & \int_K \partial_x\psi_{d_{k+2}}\Phi_{d_{k+1}} \end{pmatrix} \begin{pmatrix} E_{h1}^{x,n\star} \\ \vdots \\ E_{hd_{k+1}}^{x,n\star} \end{pmatrix} \\
&+ \begin{pmatrix} \int_K \partial_y\psi_1\Phi_1 & \cdots & \int_K \partial_y\psi_1\Phi_{d_{k+1}} \\ & \ddots & \\ \int_K \partial_y\psi_{d_{k+2}}\Phi_1 & \cdots & \int_K \partial_y\psi_{d_{k+2}}\Phi_{d_{k+1}} \end{pmatrix} \begin{pmatrix} E_{h1}^{y,n\star} \\ \vdots \\ E_{hd_{k+1}}^{y,n\star} \end{pmatrix} \\
&+ \begin{pmatrix} \int_K \partial_z\psi_1\Phi_1 & \cdots & \int_K \partial_z\psi_1\Phi_{d_{k+1}} \\ & \ddots & \\ \int_K \partial_z\psi_{d_{k+2}}\Phi_1 & \cdots & \int_K \partial_z\psi_{d_{k+2}}\Phi_{d_{k+1}} \end{pmatrix} \begin{pmatrix} E_{h1}^{z,n\star} \\ \vdots \\ E_{hd_{k+1}}^{z,n\star} \end{pmatrix}.
\end{aligned}
$$

For the RHS we have

$$
\begin{aligned}
&(\boldsymbol{E}_h^n, \boldsymbol{\nabla}\psi_a)_K \\
&= \int_K \left[\sum_{j=1}^{d_k} E_{hj}^{x,n}\theta_j\right] \partial_x\psi_a + \left[\sum_{j=1}^{d_k} E_{hj}^{y,n}\theta_j\right] \partial_y\psi_a + \left[\sum_{j=1}^{d_k} E_{hj}^{z,n}\theta_j\right] \partial_z\psi_a \\
&= \sum_{j=1}^{d_k} E_{hj}^{x,n} \int_K \partial_x\psi_a\theta_j + \sum_{j=1}^{d_k} E_{hj}^{y,n} \int_K \partial_y\psi_a\theta_j + \sum_{j=1}^{d_k} E_{hj}^{z,n} \int_K \partial_z\psi_a\theta_j
\end{aligned}
$$

While varying $a \in [1, d_{k+2}]$ we obtain the following system

$$
\begin{aligned}
\begin{pmatrix} (\boldsymbol{E}_h^{n}, \boldsymbol{\nabla}\psi_1)_K \\ \vdots \\ (\boldsymbol{E}_h^{n}, \boldsymbol{\nabla}\psi_{d_{k+2}})_K \end{pmatrix} &= \begin{pmatrix} \int_K \partial_x\psi_1\theta_1 & \cdots & \int_K \partial_x\psi_1\theta_{d_k} \\ & \ddots & \\ \int_K \partial_x\psi_{d_{k+2}}\theta_1 & \cdots & \int_K \partial_x\psi_{d_{k+2}}\theta_{d_k} \end{pmatrix} \begin{pmatrix} E_{h1}^{x,n} \\ \vdots \\ E_{hd_k}^{x,n} \end{pmatrix} \\
&+ \begin{pmatrix} \int_K \partial_y\psi_1\theta_1 & \cdots & \int_K \partial_y\psi_1\theta_{d_k} \\ & \ddots & \\ \int_K \partial_y\psi_{d_{k+2}}\theta_1 & \cdots & \int_K \partial_y\psi_{d_{k+2}}\theta_{d_k} \end{pmatrix} \begin{pmatrix} E_{h1}^{y,n} \\ \vdots \\ E_{hd_k}^{y,n} \end{pmatrix} \\
&+ \begin{pmatrix} \int_K \partial_z\psi_1\theta_1 & \cdots & \int_K \partial_z\psi_1\theta_{d_k} \\ & \ddots & \\ \int_K \partial_z\psi_{d_{k+2}}\theta_1 & \cdots & \int_K \partial_z\psi_{d_{k+2}}\theta_{d_k} \end{pmatrix} \begin{pmatrix} E_{h1}^{z,n} \\ \vdots \\ E_{hd_k}^{z,n} \end{pmatrix}
\end{aligned}
$$

Now we are ready to write the system leading us to find numerically $\boldsymbol{E}^\star$

$$\begin{cases} \left(C_{zz}^{\Phi,\Phi}+C_{yy}^{\Phi,\Phi}\right)E^{x,n\star}-C_{yx}^{\Phi,\Phi}E^{y,n\star}-C_{zx}^{\Phi,\Phi}E^{z,n\star}=K_z^{\Phi,\theta}l^{y,n}-K_y^{\Phi,\theta}l^{z,n} \\ -C_{xy}^{\Phi,\Phi}E^{x,n\star}+\left(C_{xx}^{\Phi,\Phi}+C_{zz}^{\Phi,\Phi}\right)E^{y,n\star}-C_{zy}^{\Phi,\Phi}E^{z,n\star}=K_x^{\Phi,\theta}l^{z,n}-K_z^{\Phi,\theta}l^{x,n} \\ -C_{xz}^{\Phi,\Phi}E^{x,n\star}-C_{yz}^{\Phi,\Phi}E^{y,n\star}+\left(C_{xx}^{\Phi,\Phi}+C_{yy}^{\Phi,\Phi}\right)E^{z,n\star}=K_y^{\Phi,\theta}l^{x,n}-K_x^{\Phi,\theta}l^{y,n} \\ K_x^{\psi,\Phi}E^{x,n\star}+K_y^{\psi,\Phi}E^{y,n\star}+K_z^{\psi,\Phi}E^{z,n\star}=K_x^{\psi,\theta}E^{x,n}+K_y^{\psi,\theta}E^{y,n}+K_z^{\psi,\theta}E^{z,n} \end{cases}$$

With,

$$C_{\nu_1\nu_2}^{\Phi,\Phi}=\left(\int_K \partial_{\nu_1}\Phi_j\partial_{\nu_2}\Phi_k\right)_{jk};\ \nu_1\,\&\,\nu_2\in\{x,y,z\},$$

$$K_\nu^{\Phi,\theta}=\left(\int_K \partial_\nu\Phi_j\theta_k\right)_{jk};\ \nu\in\{x,y,z\},$$

$$K_\nu^{\psi,\Phi}=\left(\int_K \partial_\nu\psi_j\Phi_k\right)_{jk};\ \nu\in\{x,y,z\},$$

$$K_\nu^{\psi,\theta}=\left(\int_K \partial_\nu\psi_j\theta_k\right)_{jk};\ \nu\in\{x,y,z\}.$$

In matrix form

$$\underbrace{\begin{pmatrix} \left(C_{zz}^{\Phi,\Phi}+C_{yy}^{\Phi,\Phi}\right) & -C_{yx}^{\Phi,\Phi} & -C_{zx}^{\Phi,\Phi} \\ -C_{xy}^{\Phi,\Phi} & \left(C_{xx}^{\Phi,\Phi}+C_{zz}^{\Phi,\Phi}\right) & -C_{zy}^{\Phi,\Phi} \\ -C_{xz}^{\Phi,\Phi} & -C_{yz}^{\Phi,\Phi} & \left(C_{xx}^{\Phi,\Phi}+C_{yy}^{\Phi,\Phi}\right) \\ K_x^{\psi,\Phi} & K_y^{\psi,\Phi} & K_z^{\psi,\Phi} \end{pmatrix}}_{\mathcal{A}} \begin{pmatrix} E^{x,n\star} \\ E^{y,n\star} \\ E^{z,n\star} \end{pmatrix}$$

$$=\underbrace{\begin{pmatrix} 0 & K_z^{\Phi,\theta} & -K_y^{\Phi,\theta} & 0 & 0 & 0 \\ -K_z^{\Phi,\theta} & 0 & K_x^{\Phi,\theta} & 0 & 0 & 0 \\ K_y^{\Phi,\theta} & -K_x^{\Phi,\theta} & 0 & 0 & 0 & 0 \\ 0 & 0 & 0 & K_x^{\psi,\theta} & K_y^{\psi,\theta} & K_z^{\psi,\theta} \end{pmatrix}}_{\mathcal{B}} \begin{pmatrix} l^{x,n} \\ l^{y,n} \\ l^{z,n} \\ E^{x,n} \\ E^{y,n} \\ E^{z,n} \end{pmatrix}$$

We have that

$$dim(\mathcal{A})=(3\,dim(\mathcal{P}_{k+1})+dim(\mathcal{P}_{k+2}))\times 3\,dim(\mathcal{P}_{k+1}).$$

The matrix $\mathcal{A}$ is rectangular, and we know already the existence and the uniqueness of the solution $\boldsymbol{E}_h^\star$ from Theorem 5. Note that the Moore-Penrose inverse or also called the pseudoinverse matrix exists for any matrix $\mathcal{A}$, but, when the latter has full rank (that is, the rank of $\mathcal{A}$ is $\min(m,n)$), then $\mathcal{A}^+$ can be expressed as a simple algebraic formula. We verified numerically that $rank(\mathcal{A})=3\,dim(\mathcal{P}_{k+1})$ (number of columns) so the Moore-Penrose inverse (pseudoinverse) $\mathcal{A}^+$ of $\mathcal{A}$ is equal to

$$\mathcal{A}^+=(\mathcal{A}^T\mathcal{A})^{-1}\mathcal{A}^T.$$

So finally we can deduce that

$$\begin{pmatrix} E^{x,n\star} \\ E^{y,n\star} \\ E^{z,n\star} \end{pmatrix} = \mathcal{A}^{+}\mathcal{B}.$$

4.4 Numerical experiments

In this section, we are going to study the same numerical cases considered in chapter 3 section 3.5 and show that the postprocessed electromagnetic field converges one order faster than the unprocessed solution in the $H(\text{curl})$-norm.

4.4.1 Propagation of a standing wave in a cubic PEC cavity

We consider structured meshes $\mathcal{T}_h$, that we obtain by first splitting Ω into $n \times n \times n$ cubes ($n = L/h$), and then splitting each cube into 6 tetrahedra. The time step Δt is selected following CFL condition (3.26).

Figures 4.1 and 4.2 show the behavior of the error for the original and postprocessed discrete solutions with respect to time on fixed mesh built from a $8 \times 8 \times 8$ Cartesian partition. Both the original and the postprocessed error exhibits an oscillatory behavior, which is typical of this particular test case. The postprocessed solution is about 10 times more accurate than the original one.

Table 4.2 presents in more detail our results on a series of meshes and for different polynomial degrees. We see that in each case, the curl of the postprocessed solution converges with the expected order, namely $k + 1$.

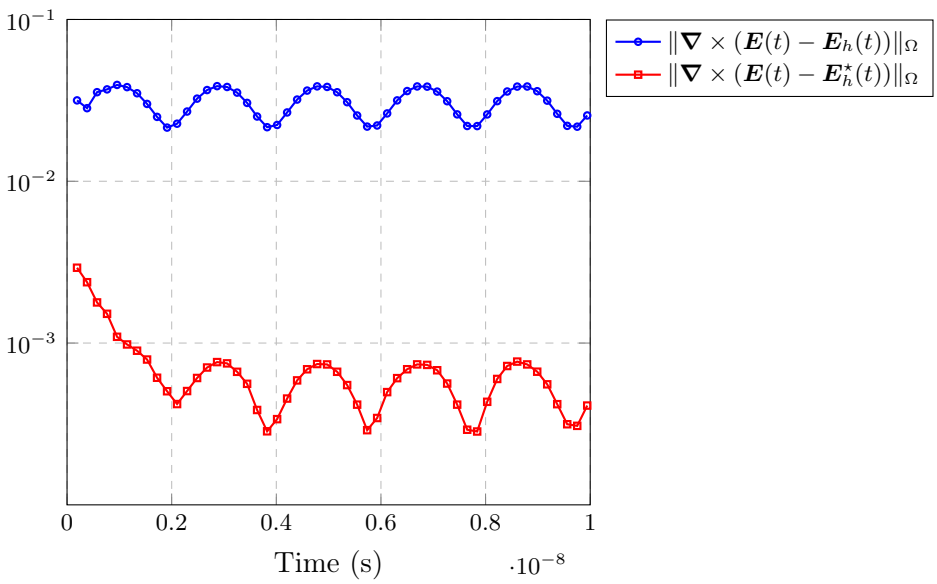

Figure 4.1 | Time evolution of the electric field error for the cavity example.

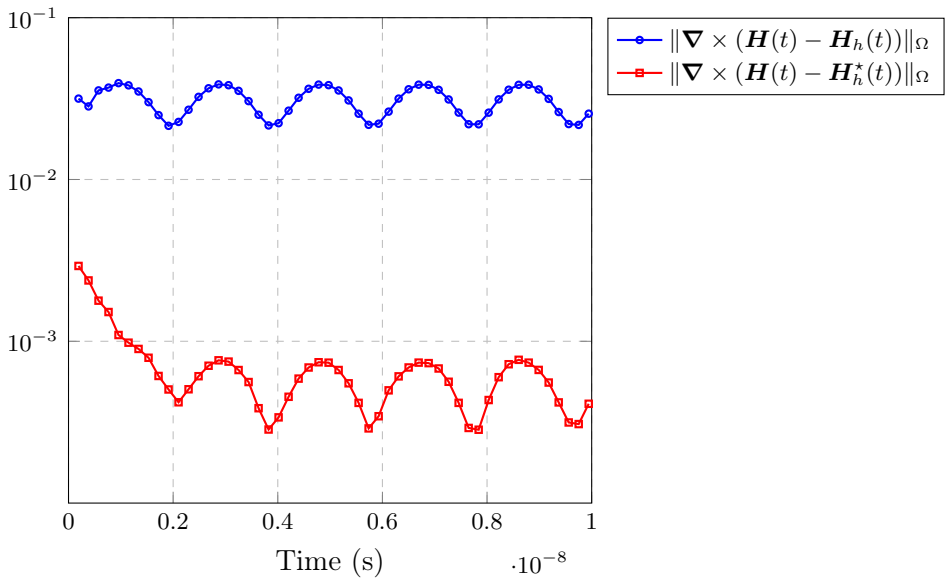

Figure 4.2 | Time evolution of the magnetic field error for the cavity example.

	h	$\left\|\nabla \times \left(\boldsymbol{E}(t_N) - \boldsymbol{E}_h^N\right)\right\|_\Omega$		$\left\|\nabla \times \left(\boldsymbol{E}(t_N) - \boldsymbol{E}_h^{N,\star}\right)\right\|_\Omega$	
P_1	1/4	9.30e-01		6.83e-01	
	1/6	5.84e-01	(**eoc 1.14**)	3.10e-01	(**eoc 1.95**)
	1/8	4.34e-01	(**eoc 1.03**)	1.67e-01	(**eoc 2.15**)
P_2	1/4	1.67e-01		4.28e-02	
	1/6	7.46e-02	(**eoc 1.98**)	1.19e-02	(**eoc 3.16**)
	1/8	4.29e-02	(**eoc 1.92**)	4.90e-03	(**eoc 3.06**)
P_3	1/4	2.30e-02		5.00e-03	
	1/6	7.10e-03	(**eoc 2.90**)	1.10e-03	(**eoc 3.79**)
	1/8	3.00e-03	(**eoc 2.99**)	3.58e-04	(**eoc 3.84**)
	h	$\left\|\nabla \times \left(\boldsymbol{H}(t_N) - \boldsymbol{H}_h^N\right)\right\|_\Omega$		$\left\|\nabla \times \left(\boldsymbol{H}(t_N) - \boldsymbol{H}_h^{N,\star}\right)\right\|_\Omega$	
P_1	1/4	8.86e-01		7.17e-01	
	1/6	5.53e-01	(**eoc 1.16**)	3.03e-01	(**eoc 2.12**)
	1/8	4.03e-01	(**eoc 1.10**)	1.60e-01	(**eoc 2.22**)
P_2	1/4	1.55e-01		3.62e-02	
	1/6	6.97e-02	(**eoc 1.96**)	9.80e-03	(**eoc 3.23**)
	1/8	3.94e-02	(**eoc 1.98**)	4.00e-03	(**eoc 3.12**)
P_3	1/4	2.14e-02		4.50e-03	
	1/6	6.50e-03	(**eoc 2.95**)	9.64e-04	(**eoc 3.77**)
	1/8	2.70e-03	(**eoc 3.00**)	3.30e-04	(**eoc 3.73**)

Table 4.2 | Convergence histories for the cavity examples.

4.4.2 Propagation of a plane wave in a homogeneous domain

As for the cubic cavity test, we consider structured meshes $\mathcal{T}_h$, that we obtain by first splitting Ω into $n \times n \times n$ cubes ($n = L/h$), and then splitting each cube into 6 tetrahedra. We select the simulation time $T = 10$ ns, and as explained above, the time step is selected using (3.26). Figures 4.3 and 4.4 show the behavior of the error for the original and postprocessed discrete solutions with respect to time on a fixed mesh based on a $12 \times 12 \times 12$ Cartesian partition. The postprocessed solution is about 5 times more accurate than the oringial. Table 4.3 presents in more detail our results on a series of meshes and for different polynomial degrees. We see that in each cases the curl of the postprocessed solution converges with the expected order, namely $k + 1$.

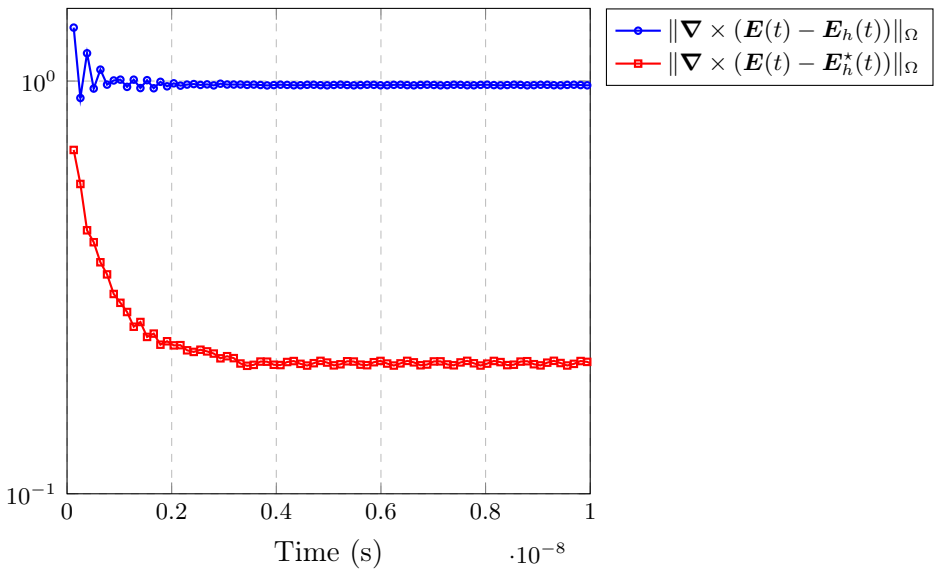

Figure 4.3 | Time evolution of the electric field error for the plane wave in free space example.

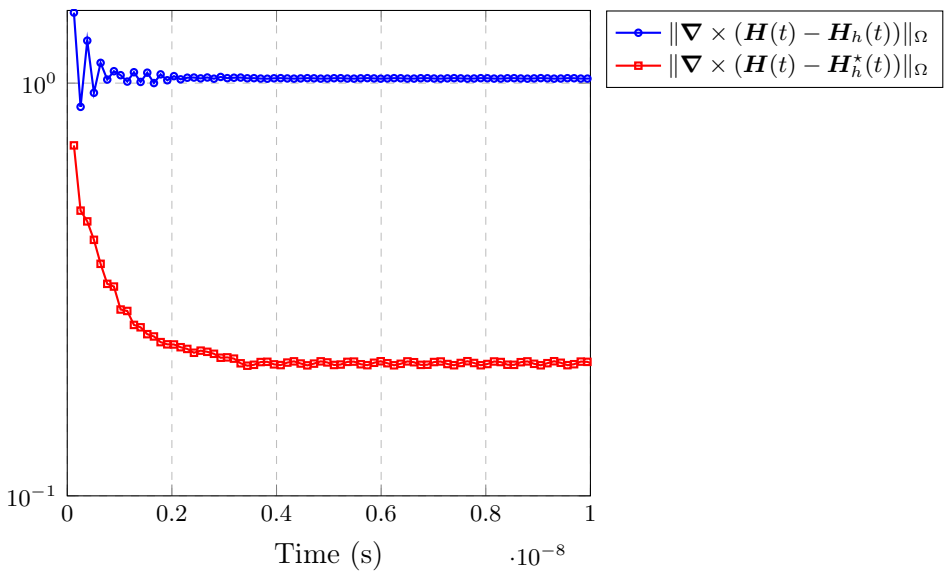

Figure 4.4 | Time evolution of the magnetic field error for the plane wave in free space example.

	h	$\left\|\boldsymbol{\nabla}\times\left(\boldsymbol{E}(t_N)-\boldsymbol{E}_h^N\right)\right\|_\Omega$		$\left\|\boldsymbol{\nabla}\times\left(\boldsymbol{E}(t_N)-\boldsymbol{E}_h^{N,\star}\right)\right\|_\Omega$	
P_1	1/8	5.37e-00		6.02e-00	
	1/10	4.38e-00	(**eoc 0.92**)	3.99e-00	(**eoc 1.84**)
	1/12	3.75e-00	(**eoc 0.86**)	2.73e-00	(**eoc 2.08**)
P_2	1/8	1.98e-00		7.92e-01	
	1/10	1.36e-00	(**eoc 1.70**)	3.72e-01	(**eoc 3.38**)
	1/12	9.77e-01	(**eoc 1.81**)	2.08e-01	(**eoc 3.18**)
P_3	1/8	4.63e-01		1.01e-01	
	1/10	2.44e-01	(**eoc 2.88**)	4.25e-02	(**eoc 3.87**)
	1/12	1.43e-01	(**eoc 2.93**)	2.22e-02	(**eoc 3.56**)
	h	$\left\|\boldsymbol{\nabla}\times\left(\boldsymbol{H}(t_N)-\boldsymbol{H}_h^N\right)\right\|_\Omega$		$\left\|\boldsymbol{\nabla}\times\left(\boldsymbol{H}(t_N)-\boldsymbol{H}_h^{N,\star}\right)\right\|_\Omega$	
P_1	1/8	5.89e-00		6.01e-00	
	1/10	4.68e-00	(**eoc 1.03**)	3.97e-00	(**eoc 1.85**)
	1/12	4.00e-00	(**eoc 0.86**)	2.75e-00	(**eoc 2.03**)
P_2	1/8	2.16e-00		7.60e-01	
	1/10	1.45e-00	(**eoc 1.79**)	3.71e-01	(**eoc 3.21**)
	1/12	1.03e-00	(**eoc 1.89**)	2.11e-01	(**eoc 3.10**)
P_3	1/8	4.87e-01		1.01e-01	
	1/10	2.54e-01	(**eoc 2.93**)	4.32e-02	(**eoc 3.79**)
	1/12	1.48e-01	(**eoc 2.96**)	2.29e-02	(**eoc 3.48**)

Table 4.3 | Convergence histories for the plane wave in free space examples.

4.4.3 Scattering of a plane wave by a dielectric sphere

We now consider the same problem of scattering of a plane wave by a dielectric sphere described in 3.5.4. The simulation time is $T = 3$ ns. We select $\mathbb{P}_2$ elements while Δt is chosen via (3.26), and denote by $(\boldsymbol{E}_h, \boldsymbol{H}_h)$ and $(\boldsymbol{E}_h^\star, \boldsymbol{H}_h^\star)$ the original and postprocessed solutions. As the analytical solution to the problem is unavailable, we compute a reference solution $(\boldsymbol{E}_\mathrm{r}, \boldsymbol{H}_\mathrm{r})$ with $\mathbb{P}_4$ elements on the fine mesh presented in 3.5.4 and the time step is $\Delta t_\mathrm{r} := \Delta t/3$. Δt_r is chosen as an integral division of Δt to facilitate comparisons. We chose to divide Δt by 3 since, following Table 3.2, it is the smallest integer for which CFL condition (3.26) holds true. To assess the impact of the postprocessing, we consider a set of evaluation points $\boldsymbol{A}$, and we compute relative errors

$$\mathrm{err}(\boldsymbol{V})^2 = \frac{\sum_{n=1}^N ||\boldsymbol{\nabla}\times(\boldsymbol{V}_\mathrm{r}(t_n,\boldsymbol{A}) - \boldsymbol{V}_h^n(\boldsymbol{A}))||^2}{\sum_{n=1}^N ||\boldsymbol{\nabla}\times(\boldsymbol{V}_\mathrm{r})(t_n,\boldsymbol{A})||^2}$$

and

$$\mathrm{err}^\star(\boldsymbol{V})^2 = \frac{\sum_{n=1}^N ||\boldsymbol{\nabla}\times(\boldsymbol{V}_\mathrm{r}(t_n,\boldsymbol{A}) - \boldsymbol{V}_h^{n,\star}(\boldsymbol{A}))||^2}{\sum_{n=1}^N ||\boldsymbol{\nabla}\times(\boldsymbol{V}_\mathrm{r})(t_n,\boldsymbol{A})||^2}$$

with $\boldsymbol{V} := \boldsymbol{E}$ or $\boldsymbol{H}$ and $N := T/\Delta t$. Table 4.4 shows that $\mathrm{err}^\star$ is less than err for the 9 evaluation points that we have selected.

Point	Field	err	err*
	$\boldsymbol{E}$	**0.083**	**0.033**
$A_1(0, 0, 0.45)$	$\boldsymbol{H}$	**0.103**	**0.048**
	$\boldsymbol{E}$	**0.008**	**0.005**
$A_2(0.2, -0.3, 0.8)$	$\boldsymbol{H}$	**0.008**	**0.006**
	$\boldsymbol{E}$	**0.019**	**0.005**
$A_3(0.2, -0.3, 0.2)$	$\boldsymbol{H}$	**0.020**	**0.006**
	$\boldsymbol{E}$	**0.015**	**0.004**
$A_4(0.2, 0.3, 0.2)$	$\boldsymbol{H}$	**0.017**	**0.005**
	$\boldsymbol{E}$	**0.019**	**0.007**
$A_5(0.2, 0.3, 0.8)$	$\boldsymbol{H}$	**0.027**	**0.007**
	$\boldsymbol{E}$	**0.015**	**0.008**
$A_6(-0.2, -0.3, 0.8)$	$\boldsymbol{H}$	**0.014**	**0.008**
	$\boldsymbol{E}$	**0.027**	**0.008**
$A_7(-0.2, -0.3, 0.2)$	$\boldsymbol{H}$	**0.028**	**0.008**
	$\boldsymbol{E}$	**0.021**	**0.007**
$A_8(-0.2, 0.3, 0.2)$	$\boldsymbol{H}$	**0.024**	**0.007**
	$\boldsymbol{E}$	**0.010**	**0.005**
$A_9(-0.2, 0.3, 0.8)$	$\boldsymbol{H}$	**0.011**	**0.005**

Table 4.4 | Scattering of a plane wave by a dielectric sphere: L^2 error between the reference solution and the solution with a $\mathbb{P}_2$ interpolation with and without applying the postprocessing.

4.5 Conclusion

In this chapter we have presented a postprocessing approach for the fully explicit hybridizable discretization of the time-dependent Maxwell's equations in 3D. This postprocessing technique is inexpensive, and can be computed independently in each mesh element of the mesh, and at every time step of interest. It is thus well adapted to parallel computer architectures. Moreover, it is particularly suited to applications requiring a higher accuracy in localized regions, either in time or space. We have presented numerical examples, both with analytical solution and in complicated geometries, that indicate that our postprocessing approach improves the convergence rate of the discrete solution in the $H(curl)$-norm by one order. Overall, this contribution is to be employed as an efficient way of reducing the $H(curl)$-norm error of discontinuous Galerkin discretizations.

5

Hybrid implicit/explicit (IMEX) HDG methods for Maxwell equations

5.1 Introduction

5.1.1 Motivations and objectives of the study

This chapter deals with the time-domain formulation of Maxwell equations. We consider hybridized discontinuous Galerkin time-domain (HDGTD) methods and propose efficient time integration methods when using non-uniform (locally refined) meshes. Two attractive features of hybrid discontinuous Galerkin (HDG) spatial discretizations are, on one hand, their ability to handle locally refined space grids to take into account geometrical details and, on the other hand, they reduced requirement in term of the number of coupled degrees of freedom in the global problem as compared to classical DG formulations. However, locally refined meshes lead to severe stability constraints when considering fully explicit time integration methods in combination with high order HDG spatial discretization. If relatively few refined elements are present in the grid, this time step restriction can be removed by blending an implicit and an explicit (IMEX) time-integration schemes where only the degrees of freedom associated with small elements are treated implicitly. This approach requires the solve of a linear system at each time step, but the size of this system is limited, since it only corresponds to the finest regions of the space grids where the implicit scheme is applied. Note that, Diogenes software only works with explicit time schemes. For the implicit and hybrid implicit explicit time schemes we made a 2D code with MATLAB to obtain all the numerical results needed for the validation of our formulation.

5.1.2 Review of related works

HDGTD method is nowadays a very popular numerical method in the computational electromagnetics community. Explicit time schemes [37]-[45] are very popular for providing integration process cheap in memory since they let us to locally solve the problem. However, for stability purposes the time step is restricted by the CFL (Courant-Friedrichs-Lewy) condition which depends on the order of the space discretization method and the size of the smallest elements of the mesh. As a consequence, even few small elements can make the value of the global time step so small that the computational cost becomes prohibitive. Implicit time schemes [45]-[43] are known to have better stability properties. In particular, most of the implicit schemes are unconditionally stable. This means that there is no stability constraint for those schemes and the only constraint on the time step depends on the accuracy level. However, for 3D realistic problems, using only implicit methods is not always feasible, since they are extremely memory consuming and we have to inverse a huge global matrix at each time-step. Combined with DGTD spatial discretization, an approach has been considered in [30]-[31] is to use a hybrid explicit-implicit (or locally implicit) time integration strategy. Such a strategy relies on a component splitting deduced from a partitioning of the mesh cells in two sets respectively gathering coarse and fine elements. In these works, a second order explicit leap-frog scheme is combined with a second order implicit Crank-Nicolson scheme in the framework of a non-dissipative (centered flux based) DG discretization in space. At each time step, a large linear system must be solved whose structure is partly diagonal (for those rows of the system associated to the explicit unknowns) and partly sparse (for those rows of the system associated to the implicit unknowns). In [50] a locally implicit time integration is proposed in the frame work of an upwind flux DG discretization in space. The computational efficiency of this locally implicit DGTD method depends on the size of the set of fine elements that directly influences the size of the sparse part of the matrix system. Therefore, an approach for reducing the size of the subsystem of globally coupled (i.e. implicit) unknowns is worth considering if one wants to solve very large-scale problems. A particularly appealing solution in this context is given by the concept of combining hybridizable discontinuous Galerkin (HDG) method with IMEX time schemes which is proposed and detailed in this chapter. An alternative solution has been proposed in [51], where IMEX HDG-DG schemes is proposed for planar and spherical shallow water systems. They split the governing system into a stiff part describing the gravity wave and a non-stiff part associated with nonlinear advection. The former is discretized implicitly with the HDG method while an explicit Runge-Kutta DG discretization is employed for the latter. In [52], several IMEX time schemes with different orders were proposed for the purpose of solving an ODE, which its right hand side can be written as the sum of two terms, a stiff one and a non stiff one. And finally, in [53] and following the ideas of [26], locally implicit schemes with an arbitrary order of accuracy for linear ODEs are constructed. The general rules for their development share same ideas as in [26] (locally explicit time stepping methods in which we can choose different time steps while solving the problem) except that they used implicit schemes in the region covered with a refined mesh. In their work they proposed IMEX time schemes with a HDG discretization in space and show numerical results for the acoustic wave equation. In this chapter we will present a different IMEX HDGTD scheme. We will start by dividing the semi discrete scheme into sum over the coarse and fine elements, and then we will apply different IMEX time schemes mentioned in [52] while considering $\boldsymbol{\Lambda}$ as an intermediate variable computed globally on the skeleton of the mesh leading us to find $\boldsymbol{E}$ and $\boldsymbol{H}$ locally in the mesh.

5.2 Semi-discrete HDG method

Our starting point for this chapter is the HDG formulation (2.44) proposed in chapter 2 for the Maxwell's equations in time-domain. After explicitly referencing the coarse and fine regions defined in 2.2, we obtain the following system

Semi-discrete HDG method

$$\left\{\begin{array}{lcl}
(\varepsilon\partial_t \boldsymbol{E}_h, \boldsymbol{v})_{\mathcal{T}_h} & = & (\boldsymbol{H}_h, \mathbf{curl}\,\boldsymbol{v})_{\mathcal{T}_h^{FI}} - \langle \boldsymbol{\Lambda}_h, \boldsymbol{n}\times\boldsymbol{v}\rangle_{\partial\mathcal{T}_h^{FI}} \\
 & + & (\boldsymbol{H}_h, \mathbf{curl}\,\boldsymbol{v})_{\mathcal{T}_h^{CO}} - \langle \boldsymbol{\Lambda}_h, \boldsymbol{n}\times\boldsymbol{v}\rangle_{\partial\mathcal{T}_h^{CO}}\,,\ \forall \boldsymbol{v}\in\boldsymbol{V}_h, \\
(\mu\partial_t \boldsymbol{H}_h, \boldsymbol{v})_{\mathcal{T}_h} & = & -\left(\mathbf{curl}\,\boldsymbol{E}_h, \boldsymbol{v}\right)_{\mathcal{T}_h^{FI}} \\
 & - & \langle \tau\boldsymbol{n}\times(\boldsymbol{H}_h - \boldsymbol{\Lambda}_h), \boldsymbol{n}\times\boldsymbol{v}\rangle_{\partial\mathcal{T}_h^{FI}} \\
 & - & \left(\mathbf{curl}\,\boldsymbol{E}_h, \boldsymbol{v}\right)_{\mathcal{T}_h^{CO}} \\
 & - & \langle \tau\boldsymbol{n}\times(\boldsymbol{H}_h - \boldsymbol{\Lambda}_h), \boldsymbol{n}\times\boldsymbol{v}\rangle_{\partial\mathcal{T}_h^{CO}}\,,\ \forall \boldsymbol{v}\in\boldsymbol{V}_h, \\
\langle \boldsymbol{n}\times\boldsymbol{E}_h, \boldsymbol{\eta}\rangle_{\partial\mathcal{T}_h^{FI}} & = & -\left\langle \tau\left(\boldsymbol{H}_h^t - \boldsymbol{\Lambda}_h\right), \boldsymbol{\eta}\right\rangle_{\partial\mathcal{T}_h^{FI}} - \langle \boldsymbol{n}\times\boldsymbol{E}_h, \boldsymbol{\eta}\rangle_{\partial\mathcal{T}_h^{CO}} \\
 & - & \left\langle \tau\left(\boldsymbol{H}_h^t - \boldsymbol{\Lambda}_h\right), \boldsymbol{\eta}\right\rangle_{\partial\mathcal{T}_h^{CO}}\,,\ \forall \boldsymbol{\eta}\in\boldsymbol{M}_h.
\end{array}\right. \tag{5.1}$$

5.2.1 Compact formulation

We now introduce some notations to obtain a compact expression of semi-discrete HDG global weak formulation (5.1). After summing the first two equations of (5.1) we obtain, $\forall(\boldsymbol{v}_h', \boldsymbol{\eta}_h) \in \mathbb{V}_h \times \boldsymbol{M}_h$

$$\left\{\begin{array}{lcl}
m\left(\partial_t \boldsymbol{v}_h, \boldsymbol{v}_h'\right) & = & a^{\mathcal{FI}}\left(\boldsymbol{v}_h, \boldsymbol{v}_h'\right) + b_\tau^{\mathcal{FI}}\left(\boldsymbol{v}_h, \boldsymbol{\Lambda}_h, \boldsymbol{v}_h'\right) \\
 & + & a^{\mathcal{CO}}\left(\boldsymbol{v}_h, \boldsymbol{v}_h'\right) + b_\tau^{\mathcal{CO}}\left(\boldsymbol{v}_h, \boldsymbol{\Lambda}_h, \boldsymbol{v}_h'\right), \\
c^{\mathcal{FI}}\left(\boldsymbol{v}_h, \boldsymbol{\Lambda}_h, \boldsymbol{\eta}_h\right) & = & -c^{\mathcal{CO}}\left(\boldsymbol{v}_h, \boldsymbol{\Lambda}_h, \boldsymbol{\eta}_h\right),
\end{array}\right. \tag{5.2}$$

where $\boldsymbol{v}_h = \begin{pmatrix}\boldsymbol{H}_h \\ \boldsymbol{E}_h\end{pmatrix}$, $\lambda = \mathrm{diag}(\mu, \varepsilon)$ and $\mathbb{V}_h = \boldsymbol{V}_h \times \boldsymbol{V}_h$. We define $\forall \boldsymbol{v}, \boldsymbol{v}' \in \mathbb{V}_h$,

$$\zeta_{1,h}\left(\boldsymbol{v}\right) = \begin{pmatrix} -\,\mathbf{curl}\left(\boldsymbol{v}_2\right) \\ \boldsymbol{v}_1 \end{pmatrix}, \quad \zeta_{2,h}\left(\boldsymbol{v}'\right) = \begin{pmatrix} \boldsymbol{v}_1' \\ \mathbf{curl}\left(\boldsymbol{v}_2'\right) \end{pmatrix}.$$

The bilinear forms m, $a^{\mathcal{FI}}, a^{\mathcal{CO}}$ are defined on $\mathbb{V}_h \times \mathbb{V}_h$ such that, $\forall(\boldsymbol{v}, \boldsymbol{v}') \in \mathbb{V}_h \times \mathbb{V}_h$

$$\left\{\begin{array}{lcl}
m(\boldsymbol{v}, \boldsymbol{v}') & = & (\boldsymbol{v}, \boldsymbol{v}')_\lambda = (\lambda\boldsymbol{v}, \boldsymbol{v}')_{\mathcal{T}_h}, \\
a^{\mathcal{FI}}(\boldsymbol{v}, \boldsymbol{v}') & = & (\zeta_1(\boldsymbol{v}), \zeta_2(\boldsymbol{v}'))_{\mathcal{T}_h^{FI}}\,, \\
a^{\mathcal{CO}}(\boldsymbol{v}, \boldsymbol{v}') & = & (\zeta_1(\boldsymbol{v}), \zeta_2(\boldsymbol{v}'))_{\mathcal{T}_h^{CO}}\,,
\end{array}\right. \tag{5.3}$$

and $b_\tau^{\mathcal{FI}}$ and $b_\tau^{\mathcal{CO}}$ are defined on $\mathbb{V}_h \times \boldsymbol{M}_h \times \mathbb{V}_h$ such that, $\forall\left(\boldsymbol{v}, \boldsymbol{\eta}, \boldsymbol{v}'\right) \in \mathbb{V}_h \times \boldsymbol{M}_h \times \mathbb{V}_h$

$$\begin{array}{lcl}
b_\tau^{\mathcal{FI}}\left(\boldsymbol{v}, \boldsymbol{\eta}, \boldsymbol{v}'\right) & = & -\langle \boldsymbol{\eta}, \boldsymbol{n}\times\boldsymbol{v}_2'\rangle_{\partial\mathcal{T}_h^{FI}} - \langle \tau\boldsymbol{n}\times\left(\boldsymbol{v}_1 - \boldsymbol{\eta}\right), \boldsymbol{n}\times\boldsymbol{v}_1'\rangle_{\partial\mathcal{T}_h^{FI}}\,, \\
b_\tau^{\mathcal{CO}}\left(\boldsymbol{v}, \boldsymbol{\eta}, \boldsymbol{v}'\right) & = & -\langle \boldsymbol{\eta}, \boldsymbol{n}\times\boldsymbol{v}_2'\rangle_{\partial\mathcal{T}_h^{CO}} - \langle \tau\boldsymbol{n}\times\left(\boldsymbol{v}_1 - \boldsymbol{\eta}\right), n\times\boldsymbol{v}_1'\rangle_{\partial\mathcal{T}_h^{CO}}\,.
\end{array}$$

Finally, $c^{\mathcal{FI}}$ and $c^{\mathcal{CO}}$ are defined on $\mathbb{V}_h \times \boldsymbol{M}_h \times \boldsymbol{M}_h$ such that, $\forall\,(\boldsymbol{v},\boldsymbol{\eta},\boldsymbol{\mu}) \in \mathbb{V}_h \times \boldsymbol{M}_h \times \boldsymbol{M}_h$

$$\begin{aligned} c^{\mathcal{FI}}(\boldsymbol{v},\boldsymbol{\eta},\boldsymbol{\mu}) &= \langle \boldsymbol{n}\times\boldsymbol{v}_2,\boldsymbol{\mu}\rangle_{\partial\mathcal{T}_h^{FI}} + \langle \tau\boldsymbol{n}\times(\boldsymbol{v}_1-\boldsymbol{\eta}),\boldsymbol{n}\times\boldsymbol{\mu}\rangle_{\partial\mathcal{T}_h^{FI}}\,, \\ c^{\mathcal{CO}}(\boldsymbol{v},\boldsymbol{\eta},\boldsymbol{\mu}) &= \langle \boldsymbol{n}\times\boldsymbol{v}_2,\boldsymbol{\mu}\rangle_{\partial\mathcal{T}_h^{CO}} + \langle \tau\boldsymbol{n}\times(\boldsymbol{v}_1-\boldsymbol{\eta}),\boldsymbol{n}\times\boldsymbol{\mu}\rangle_{\partial\mathcal{T}_h^{CO}}\,. \end{aligned}$$

Let us now define the three operators

$$\mathbf{L}_h^{\mathcal{FI}}\ ,\ \mathbf{L}_h^{\mathcal{CO}} \text{ and } \mathbf{L}_h : \mathbb{V}_h \times \boldsymbol{M}_h \to \mathbb{V}_h,$$

such that $\forall(\boldsymbol{v},\boldsymbol{\eta},\boldsymbol{v}') \in \mathbb{V}_h \times \boldsymbol{M}_h \times \mathbb{V}_h$

$$\begin{aligned} (\mathbf{L}_h^{\mathcal{FI}}(\boldsymbol{v},\boldsymbol{\eta}),\boldsymbol{v}') &= a^{\mathcal{FI}}(\boldsymbol{v},\boldsymbol{v}') + b_\tau^{\mathcal{FI}}(\boldsymbol{v},\boldsymbol{\eta},\boldsymbol{v}'), \\ (\mathbf{L}_h^{\mathcal{CO}}(\boldsymbol{v},\boldsymbol{\eta}),\boldsymbol{v}') &= a^{\mathcal{CO}}(\boldsymbol{v},\boldsymbol{v}') + b_\tau^{\mathcal{CO}}(\boldsymbol{v},\boldsymbol{\eta},\boldsymbol{v}'), \\ (\mathbf{L}_h(\boldsymbol{v},\boldsymbol{\eta}),\boldsymbol{v}') &= (\mathbf{L}_h^{\mathcal{FI}}(\boldsymbol{v},\boldsymbol{\eta}),\boldsymbol{v}') + (\mathbf{L}_h^{\mathcal{CO}}(\boldsymbol{v},\boldsymbol{\eta}),\boldsymbol{v}'). \end{aligned}$$

Then, the semi-discrete HDG scheme for Maxwell equations in compact form writes as

Semi-discrete HDG scheme in compact form

$$\left\{\begin{aligned} m\left(\partial_t\boldsymbol{v}_h,\boldsymbol{v}_h'\right) &= \left(\mathbf{L}_h^{\mathcal{FI}}\left(\boldsymbol{v}_h,\boldsymbol{\Lambda}_h\right),\boldsymbol{v}_h'\right) + \left(\mathbf{L}_h^{\mathcal{CO}}(\boldsymbol{v}_h,\boldsymbol{\Lambda}_h),\boldsymbol{v}_h'\right), \\ c^{\mathcal{FI}}\left(\boldsymbol{v}_h,\boldsymbol{\Lambda}_h,\boldsymbol{\eta}_h\right) &= -c^{\mathcal{CO}}\left(\boldsymbol{v}_h,\boldsymbol{\Lambda}_h,\boldsymbol{\eta}_h\right), \end{aligned}\right. \tag{5.4}$$

for all test functions $(\boldsymbol{v}_h',\boldsymbol{\eta}_h)$ that belong to the space $\mathbb{V}_h \times \boldsymbol{M}_h$.

5.2.2 Preliminary results

We first note that $\forall\,\mathbf{Set} \in \{\mathcal{FI},\mathcal{CO}\}$, we have that $\forall\boldsymbol{v} \in \mathbb{V}_h$,

$$a^{\mathbf{Set}}(\boldsymbol{v},\boldsymbol{v}) = 0.$$

Lemma 3. *$\forall\,\mathbf{Set} \in \{\mathcal{FI},\mathcal{CO}\}$, we have that $\forall\,(\boldsymbol{v},\boldsymbol{\eta}) \in \mathbb{V}_h \times \boldsymbol{M}_h$,*

$$b_\tau^{\mathbf{Set}}(\boldsymbol{v},\boldsymbol{\eta},\boldsymbol{v}) + c^{\mathbf{Set}}(\boldsymbol{v},\boldsymbol{\eta},\boldsymbol{\eta}) \le 0.$$

Proof.

$$\begin{aligned} b_\tau^{\mathbf{Set}}(\boldsymbol{v},\boldsymbol{\eta},\boldsymbol{v}) + c^{\mathbf{Set}}(\boldsymbol{v},\boldsymbol{\eta},\boldsymbol{\eta}) &= \cancel{-\langle\boldsymbol{\eta},\boldsymbol{n}\times\boldsymbol{v}_2\rangle_{\partial\mathbf{Set}}} \\ &- \langle\tau\boldsymbol{n}\times(\boldsymbol{v}_1-\boldsymbol{\eta}),\boldsymbol{n}\times\boldsymbol{v}_1\rangle_{\partial\mathbf{Set}} \\ &+ \langle\boldsymbol{n}\times\boldsymbol{v}_2,\boldsymbol{\eta}\rangle_{\partial\mathbf{Set}} \\ &+ \langle\tau\boldsymbol{n}\times(\boldsymbol{v}_1-\boldsymbol{\eta}),\boldsymbol{n}\times\boldsymbol{\eta}\rangle_{\partial\mathbf{Set}} \\ &= -\tau||\boldsymbol{n}\times(\boldsymbol{v}_1-\boldsymbol{\eta})||^2_{\partial\mathbf{Set}} \\ &\le 0. \end{aligned}$$

□

Inverse estimations

Since we have a shaped-regular mesh we can deduce from [47] that $\forall K \in \mathcal{T}_h$, $\exists c_{1,K}, c_{2,K} > 0$; $\forall\boldsymbol{u} \in \boldsymbol{V}_h$,

$$||\,\mathbf{curl}(\boldsymbol{u})||_{L^2(K)} \le c_{1,K}\,h_K^{-1}||\boldsymbol{u}||_{L^2(K)},$$

$$||\boldsymbol{u}||_{L^2(\partial K)} \le c_{2,K}\,h_K^{-\frac{1}{2}}||\boldsymbol{u}||_{L^2(K)}.$$

Lemma 4. *There exists two positive constants c_1 and c_2, such that $\forall(\boldsymbol{v},\boldsymbol{v}') \in \mathbb{V}_h \times \mathbb{V}_h$ and $\forall(\boldsymbol{\eta},\boldsymbol{\mu}) \in \boldsymbol{M}_h \times \boldsymbol{M}_h$*

$$
\begin{aligned}
|\left(\boldsymbol{L}_h^{\mathcal{CO}}(\boldsymbol{v},\boldsymbol{\eta}),\boldsymbol{v}'\right)| \quad &\leq \quad c_1 h_{\mathcal{T}_h^{CO}}^{-1}||\boldsymbol{v}||_{\mathcal{T}_h^{CO}}||\boldsymbol{v}'||_{\mathcal{T}_h^{CO}} + \\
&\qquad c_2 h_{\mathcal{T}_h^{CO}}^{-\frac{1}{2}}\left(||\boldsymbol{\eta}||_{\partial\mathcal{T}_h^{CO}} + \tau||\boldsymbol{v}_1-\boldsymbol{\eta}||_{\partial\mathcal{T}_h^{CO}}\right)||\boldsymbol{v}'||_{\mathcal{T}_h^{CO}}, \\
&\qquad \text{and} \\
|c^{\mathcal{CO}}(\boldsymbol{v},\boldsymbol{\eta},\boldsymbol{\mu})| \quad &\leq \quad \left(||\boldsymbol{v}_2||_{\partial\mathcal{T}_h^{CO}} + \tau||\boldsymbol{v}_1-\boldsymbol{\eta}||_{\partial\mathcal{T}_h^{CO}}\right)||\boldsymbol{\mu}||_{\partial\mathcal{T}_h^{CO}}.
\end{aligned}
$$

Proof. First, we have $\forall(\boldsymbol{v},\boldsymbol{v}') \in \mathbb{V}_h \times \mathbb{V}_h$,

$$
\begin{aligned}
|a^{\mathcal{CO}}(\boldsymbol{v},\boldsymbol{v}')| &= \left|\left(-\,\mathbf{curl}\,(\boldsymbol{v}_2)\,,\boldsymbol{v}_1'\right)_{\mathcal{T}_h^{CO}} + \left(\mathbf{curl}\,(\boldsymbol{v}_2')\,,\boldsymbol{v}_1\right)_{\mathcal{T}_h^{CO}}\right| \\
&\leq \left|\left(\mathbf{curl}\,(\boldsymbol{v}_2)\,,\boldsymbol{v}_1'\right)_{\mathcal{T}_h^{CO}}\right| + \left|\left(\mathbf{curl}\,(\boldsymbol{v}_2')\,,\boldsymbol{v}_1\right)_{\mathcal{T}_h^{CO}}\right| \\
&\leq ||\,\mathbf{curl}(\boldsymbol{v}_2)||_{\mathcal{T}_h^{CO}}||\boldsymbol{v}_1'||_{\mathcal{T}_h^{CO}} + ||\,\mathbf{curl}(\boldsymbol{v}_2')||_{\mathcal{T}_h^{CO}}||\boldsymbol{v}_1||_{\mathcal{T}_h^{CO}} \\
&\leq c_1 h_{\mathcal{T}_h^{CO}}^{-1}\left(||\boldsymbol{v}_2||_{\mathcal{T}_h^{CO}}||\boldsymbol{v}_1'||_{\mathcal{T}_h^{CO}} + ||\boldsymbol{v}_2'||_{\mathcal{T}_h^{CO}}||\boldsymbol{v}_1||_{\mathcal{T}_h^{CO}}\right) \\
&\leq c_1 h_{\mathcal{T}_h^{CO}}^{-1}||\boldsymbol{v}||_{\mathcal{T}_h^{CO}}||\boldsymbol{v}'||_{\mathcal{T}_h^{CO}}.
\end{aligned}
$$

Then, we have $\forall(\boldsymbol{v},\boldsymbol{\eta},\boldsymbol{v}') \in \mathbb{V}_h \times \boldsymbol{M}_h \times \mathbb{V}_h$,

$$
\begin{aligned}
|b_\tau^{\mathcal{CO}}\left(\boldsymbol{v},\boldsymbol{\eta},\boldsymbol{v}'\right)| &= \left|-\left\langle\boldsymbol{\eta},\boldsymbol{n}\times\boldsymbol{v}_2'\right\rangle_{\partial\mathcal{T}_h^{CO}} - \left\langle\tau\boldsymbol{n}\times(\boldsymbol{v}_1-\boldsymbol{\eta})\,,\boldsymbol{n}\times\boldsymbol{v}_1'\right\rangle_{\partial\mathcal{T}_h^{CO}}\right| \\
&\leq \left|\left\langle\boldsymbol{\eta},\boldsymbol{n}\times\boldsymbol{v}_2'\right\rangle_{\partial\mathcal{T}_h^{CO}}\right| + \left|\left\langle\tau\boldsymbol{n}\times(\boldsymbol{v}_1-\boldsymbol{\eta})\,,\boldsymbol{n}\times\boldsymbol{v}_1'\right\rangle_{\partial\mathcal{T}_h^{CO}}\right| \\
&\leq ||\boldsymbol{\eta}||_{\partial\mathcal{T}_h^{CO}}||\boldsymbol{v}_2'||_{\partial\mathcal{T}_h^{CO}} + \tau||\boldsymbol{v}_1-\boldsymbol{\eta}||_{\partial\mathcal{T}_h^{CO}}||\boldsymbol{v}_1'||_{\partial\mathcal{T}_h^{CO}} \\
&\leq \left(||\boldsymbol{\eta}||_{\partial\mathcal{T}_h^{CO}} + \tau||\boldsymbol{v}_1-\boldsymbol{\eta}||_{\partial\mathcal{T}_h^{CO}}\right)||\boldsymbol{v}'||_{\partial\mathcal{T}_h^{CO}} \\
&\leq c_2 h_{\mathcal{T}_h^{CO}}^{-\frac{1}{2}}\left(||\boldsymbol{\eta}||_{\partial\mathcal{T}_h^{CO}} + \tau||\boldsymbol{v}_1-\boldsymbol{\eta}||_{\partial\mathcal{T}_h^{CO}}\right)||\boldsymbol{v}'||_{\mathcal{T}_h^{CO}}.
\end{aligned}
$$

Finally, $\forall(\boldsymbol{v},\boldsymbol{\eta},\boldsymbol{\mu}) \in \mathbb{V}_h \times \boldsymbol{M}_h \times \boldsymbol{M}_h$,

$$
\begin{aligned}
|c^{\mathcal{CO}}(\boldsymbol{v},\boldsymbol{\eta},\boldsymbol{\mu})| &= \left|\langle\boldsymbol{n}\times\boldsymbol{v}_2,\boldsymbol{\mu}\rangle_{\partial\mathcal{T}_h^{CO}} + \langle\tau\boldsymbol{n}\times(\boldsymbol{v}_1-\boldsymbol{\eta})\,,\boldsymbol{n}\times\boldsymbol{\mu}\rangle_{\partial\mathcal{T}_h^{CO}}\right| \\
&\leq \left|\langle\boldsymbol{n}\times\boldsymbol{v}_2,\boldsymbol{\mu}\rangle_{\partial\mathcal{T}_h^{CO}}\right| + \left|\langle\tau\boldsymbol{n}\times(\boldsymbol{v}_1-\boldsymbol{\eta})\,,\boldsymbol{n}\times\boldsymbol{\mu}\rangle_{\partial\mathcal{T}_h^{CO}}\right| \\
&\leq ||\boldsymbol{v}_2||_{\partial\mathcal{T}_h^{CO}}||\boldsymbol{\mu}||_{\partial\mathcal{T}_h^{CO}} + \tau||\boldsymbol{v}_1-\boldsymbol{\eta}||_{\partial\mathcal{T}_h^{CO}}||\boldsymbol{\mu}||_{\partial\mathcal{T}_h^{CO}} \\
&\leq \left(||\boldsymbol{v}_2||_{\partial\mathcal{T}_h^{CO}} + \tau||\boldsymbol{v}_1-\boldsymbol{\eta}||_{\partial\mathcal{T}_h^{CO}}\right)||\boldsymbol{\mu}||_{\partial\mathcal{T}_h^{CO}}.
\end{aligned}
$$

□

Corollary 4.1. *For any time t_m and $t_{m'}$ we have*

$$
\left|\left(\boldsymbol{L}_h^{\mathcal{CO}}(\boldsymbol{v}_h^m,\boldsymbol{\Lambda}_h^m) - \boldsymbol{L}_h^{\mathcal{CO}}(\boldsymbol{v}_h^{m'},\boldsymbol{\Lambda}_h^{m'}),\boldsymbol{v}_h^{m'}\right)\right| \leq
$$

$$
ch_{\mathcal{T}_h^{CO}}^{-1}\left(||\boldsymbol{v}_h^{m'}-\boldsymbol{v}_h^m||_{\mathcal{T}_h^{CO}}||\boldsymbol{v}_h^m||_{\mathcal{T}_h^{CO}} + ||\boldsymbol{v}_h^{m'}-\boldsymbol{v}_h^m||_{\mathcal{T}_h^{CO}}^2 + ||\boldsymbol{v}_h^m||_{\mathcal{T}_h^{CO}}^2\right).
$$

Proof. Let $X = \left(\mathbf{L}_h^{\mathcal{CO}}(\boldsymbol{v}_h^m, \boldsymbol{\Lambda}_h^m), \boldsymbol{v}_h^{m'}\right) - \left(\mathbf{L}_h^{\mathcal{CO}}(\boldsymbol{v}_h^{m'}, \boldsymbol{\Lambda}_h^{m'}), \boldsymbol{v}_h^{m'}\right)$.

We have that

$$
\begin{aligned}
X &= \left(\mathbf{L}_h^{\mathcal{CO}}(\boldsymbol{v}_h^m, \boldsymbol{\Lambda}_h^m), \boldsymbol{v}_h^{m'}\right) - \cancelto{0}{a^{\mathcal{CO}}(\boldsymbol{v}_h^{m'}, \boldsymbol{v}_h^{m'})} - b_\tau^{\mathcal{CO}}(\boldsymbol{v}_h^{m'}, \boldsymbol{\Lambda}_h^{m'}, \boldsymbol{v}_h^{m'}) \\
&= \underbrace{\left(\mathbf{L}_h^{\mathcal{CO}}(\boldsymbol{v}_h^m, \boldsymbol{\Lambda}_h^m), \boldsymbol{v}_h^{m'} - \boldsymbol{v}_h^m\right)}_{X_1} + \underbrace{\left(\mathbf{L}_h^{\mathcal{CO}}(\boldsymbol{v}_h^m, \boldsymbol{\Lambda}_h^m), \boldsymbol{v}_h^m\right)}_{X_2} \\
&\quad - \underbrace{b_\tau^{\mathcal{CO}}(\boldsymbol{v}_h^{m'}, \boldsymbol{\Lambda}_h^{m'}, \boldsymbol{v}_h^{m'} - \boldsymbol{v}_h^m)}_{X_3} - \underbrace{b_\tau^{\mathcal{CO}}(\boldsymbol{v}_h^{m'}, \boldsymbol{\Lambda}_h^{m'}, \boldsymbol{v}_h^m)}_{X_4}.
\end{aligned}
$$

$$
\begin{aligned}
-X_3 &= \left\langle \boldsymbol{\Lambda}_h^{m'}, \boldsymbol{n} \times \left(\boldsymbol{v}_{2,h}^{m'} - \boldsymbol{v}_{2,h}^m\right)\right\rangle_{\partial\mathcal{T}_h^{CO}} \\
&\quad + \left\langle \tau\boldsymbol{n} \times \left(\boldsymbol{v}_{1,h}^{m'} - \boldsymbol{\Lambda}_h^{m'}\right), \boldsymbol{n} \times \left(\boldsymbol{v}_{1,h}^{m'} - \boldsymbol{v}_{1,h}^m\right)\right\rangle_{\partial\mathcal{T}_h^{CO}} \\
&= \left\langle \boldsymbol{\Lambda}_h^{m'} - \boldsymbol{\Lambda}_h^m, \boldsymbol{n} \times \left(\boldsymbol{v}_{2,h}^{m'} - \boldsymbol{v}_{2,h}^m\right)\right\rangle_{\partial\mathcal{T}_h^{CO}} \\
&\quad + \left\langle \boldsymbol{\Lambda}_h^m, \boldsymbol{n} \times \left(\boldsymbol{v}_{2,h}^{m'} - \boldsymbol{v}_{2,h}^m\right)\right\rangle_{\partial\mathcal{T}_h^{CO}} \\
&\quad + \left\langle \tau\boldsymbol{n} \times \left(\boldsymbol{v}_{1,h}^{m'} - \boldsymbol{v}_{1,h}^m\right), \boldsymbol{n} \times \left(\boldsymbol{v}_{1,h}^{m'} - \boldsymbol{v}_{1,h}^m\right)\right\rangle_{\partial\mathcal{T}_h^{CO}} \\
&\quad + \left\langle \tau\boldsymbol{n} \times \boldsymbol{v}_{1,h}^m, \boldsymbol{n} \times \left(\boldsymbol{v}_{1,h}^{m'} - \boldsymbol{v}_{1,h}^m\right)\right\rangle_{\partial\mathcal{T}_h^{CO}} \\
&\quad - \left\langle \tau\boldsymbol{n} \times \left(\boldsymbol{\Lambda}_h^{m'} - \boldsymbol{\Lambda}_h^m\right), \boldsymbol{n} \times \left(\boldsymbol{v}_{1,h}^{m'} - \boldsymbol{v}_{1,h}^m\right)\right\rangle_{\partial\mathcal{T}_h^{CO}} \\
&\quad - \left\langle \tau\boldsymbol{n} \times \boldsymbol{\Lambda}_h^m, n \times \left(\boldsymbol{v}_{1,h}^{m'} - \boldsymbol{v}_{1,h}^m\right)\right\rangle_{\partial\mathcal{T}_h^{CO}}.
\end{aligned}
$$

$$
\begin{aligned}
-X_4 &= \left\langle \boldsymbol{\Lambda}_h^{m'}, \boldsymbol{n} \times \boldsymbol{v}_{2,h}^m\right\rangle_{\partial\mathcal{T}_h^{CO}} + \left\langle \tau\boldsymbol{n} \times \left(\boldsymbol{v}_{1,h}^{m'} - \boldsymbol{\Lambda}_h^{m'}\right), \boldsymbol{n} \times \boldsymbol{v}_{1,h}^m\right\rangle_{\partial\mathcal{T}_h^{CO}} \\
&= \left\langle \boldsymbol{\Lambda}_h^{m'} - \boldsymbol{\Lambda}_h^m, \boldsymbol{n} \times \boldsymbol{v}_{2,h}^m\right\rangle_{\partial\mathcal{T}_h^{CO}} + \left\langle \boldsymbol{\Lambda}_h^m, \boldsymbol{n} \times \boldsymbol{v}_{2,h}^m\right\rangle_{\partial\mathcal{T}_h^{CO}} \\
&\quad + \left\langle \tau\boldsymbol{n} \times \left(\boldsymbol{v}_{1,h}^{m'} - \boldsymbol{v}_{1,h}^m\right), \boldsymbol{n} \times \boldsymbol{v}_{1,h}^m\right\rangle_{\partial\mathcal{T}_h^{CO}} + \left\langle \tau\boldsymbol{n} \times \boldsymbol{v}_{1,h}^m, \boldsymbol{n} \times \boldsymbol{v}_{1,h}^m\right\rangle_{\partial\mathcal{T}_h^{CO}} \\
&\quad - \left\langle \tau\boldsymbol{n} \times \left(\boldsymbol{\Lambda}_h^{m'} - \boldsymbol{\Lambda}_h^m\right), \boldsymbol{n} \times \boldsymbol{v}_{1,h}^m\right\rangle_{\partial\mathcal{T}_h^{CO}} - \left\langle \tau\boldsymbol{n} \times \boldsymbol{\Lambda}_h^m, \boldsymbol{n} \times \boldsymbol{v}_{1,h}^m\right\rangle_{\partial\mathcal{T}_h^{CO}}.
\end{aligned}
$$

We have

$$
|X| \leq |X_1| + |X_2| + |X_3| + |X_4|.
$$

From Lemma 4 we can deduce that

$$
\begin{aligned}
|X_1| &\leq c_1 h_{\mathcal{T}_h^{CO}}^{-1} ||\boldsymbol{v}_h^m||_{\mathcal{T}_h^{CO}} ||\boldsymbol{v}_h^{m'} - \boldsymbol{v}_h^m||_{\mathcal{T}_h^{CO}} \\
&\quad + c_2 h_{\mathcal{T}_h^{CO}}^{-\frac{1}{2}} \left(||\boldsymbol{\Lambda}_h^m||_{\partial \mathcal{T}_h^{CO}} + \tau ||\boldsymbol{v}_{h,1}^m - \boldsymbol{\Lambda}_h^m||_{\partial \mathcal{T}_h^{CO}} \right) ||\boldsymbol{v}_h^{m'} - \boldsymbol{v}_h^m||_{\mathcal{T}_h^{CO}} \\
&\leq c_1 h_{\mathcal{T}_h^{CO}}^{-1} ||\boldsymbol{v}_h^m||_{\mathcal{T}_h^{CO}} ||\boldsymbol{v}_h^{m'} - \boldsymbol{v}_h^m||_{\mathcal{T}_h^{CO}} \\
&\quad + c_2 h_{\mathcal{T}_h^{CO}}^{-\frac{1}{2}} \Bigg(c_3 h_{\mathcal{T}_h^{CO}}^{-\frac{1}{2}} ||\boldsymbol{v}_h^m||_{\mathcal{T}_h^{CO}} + \tau c_4 h_{\mathcal{T}_h^{CO}}^{-\frac{1}{2}} ||\boldsymbol{v}_h^m||_{\mathcal{T}_h^{CO}} + \\
&\qquad\qquad \tau c_3 h_{\mathcal{T}_h^{CO}}^{-\frac{1}{2}} ||\boldsymbol{v}_h^m||_{\mathcal{T}_h^{CO}} \Bigg) ||\boldsymbol{v}_h^{m'} - \boldsymbol{v}_h^m||_{\mathcal{T}_h^{CO}} \\
&\leq (c_1 + c_5 + \tau c_6 + \tau c_5) h_{\mathcal{T}_h^{CO}}^{-1} ||\boldsymbol{v}_h^m||_{\mathcal{T}_h^{CO}} ||\boldsymbol{v}_h^{m'} - \boldsymbol{v}_h^m||_{\mathcal{T}_h^{CO}} \\
&\leq k_1 h_{\mathcal{T}_h^{CO}}^{-1} ||\boldsymbol{v}_h^m||_{\mathcal{T}_h^{CO}} ||\boldsymbol{v}_h^{m'} - \boldsymbol{v}_h^m||_{\mathcal{T}_h^{CO}}.
\end{aligned}
$$

$$
|X_2| \leq k_2 h_{\mathcal{T}_h^{CO}}^{-1} ||\boldsymbol{v}_h^m||_{\mathcal{T}_h^{CO}}^2.
$$

In addition it is clear that

$$
|X_3| \leq k_3 h_{\mathcal{T}_h^{CO}}^{-1} ||\boldsymbol{v}_h^{m'} - \boldsymbol{v}_h^m||_{\mathcal{T}_h^{CO}}^2 + k_4 h_{\mathcal{T}_h^{CO}}^{-1} ||\boldsymbol{v}_h^m||_{\mathcal{T}_h^{CO}} ||\boldsymbol{v}_h^{m'} - \boldsymbol{v}_h^m||_{\mathcal{T}_h^{CO}}.
$$

$$
|X_4| \leq k_5 h_{\mathcal{T}_h^{CO}}^{-1} ||\boldsymbol{v}_h^m||_{\mathcal{T}_h^{CO}} ||\boldsymbol{v}_h^{m'} - \boldsymbol{v}_h^m||_{\mathcal{T}_h^{CO}} + k_6 k_3 h_{\mathcal{T}_h^{CO}}^{-1} ||\boldsymbol{v}_h^m||_{\mathcal{T}_h^{CO}}^2.
$$

Finally

$$
|X| \leq c h_{\mathcal{T}_h^{CO}}^{-1} \left(||\boldsymbol{v}_h^{m'} - \boldsymbol{v}_h^m||_{\mathcal{T}_h^{CO}} ||\boldsymbol{v}_h^m||_{\mathcal{T}_h^{CO}} + ||\boldsymbol{v}_h^{m'} - \boldsymbol{v}_h^m||_{\mathcal{T}_h^{CO}}^2 + ||\boldsymbol{v}_h^m||_{\mathcal{T}_h^{CO}}^2 \right).
$$

□

5.3 Formulation and stability analysis of IMEX HDG methods

We consider three different hybrid implicit-explicit (IMEX) HDG methods, which are based on the following time schemes: the first order the Euler implicit-explicit method, a second order implicit-explicit Runge-Kutta method, and third order implicit-explicit SSP-LDIRK3 method, which is a mix between the explicit strong stability preserving and the L-stable diagonally implicit Runge-Kutta methods.

5.3.1 A quick overview on Runge-Kutta and IMEX methods

Runge-Kutta methods

We may rewrite problem (2.43), while conisdering $\partial\Omega = \Gamma_m$ for instance, obtained after space discretization as (*see section 2.5.9 for details*)

$$
\begin{cases}
\mathbb{M}\dot{\boldsymbol{v}}_h(t) &= -\mathbb{D}\boldsymbol{v}_h(t) - \mathbb{C}\mathcal{A}_{HDG}\boldsymbol{\Lambda}_h(t), \\
\mathbb{G}\boldsymbol{\Lambda}_h(t) &= -\mathbb{B}\boldsymbol{v}_h(t), \\
\boldsymbol{v}_h(0) &= \boldsymbol{v}_{h,0},
\end{cases}
\tag{5.5}
$$

where for each $t \in [0,T]$, the vector $\boldsymbol{v}_h(t)$ contains the coefficients defining $\boldsymbol{E}_h(t)$ and $\boldsymbol{H}_h(t)$ in the nodal basis of $\mathbb{P}_k(\mathcal{T}_h)$, $\mathbb{M}$, $\mathbb{D}$, $\mathbb{C}$, $\mathbb{G}$ and $\mathbb{B}$ are the usual matrices associated with (2.43), and $\boldsymbol{v}_{h,0}$ is the interpolation of the initial conditions onto the discretization space.

Classically, the key asset of HDG schemes is that the mass matrix is block diagonal, and hence, easy to invert. Thus, we may safely rewrite (5.5) as

$$\begin{cases} \dot{\boldsymbol{v}}_h(t) & = & f\left(t, \boldsymbol{v}_h(t), \boldsymbol{\Lambda}_h(t)\right), \\ \mathbb{G}\boldsymbol{\Lambda}_h(t) & = & -\mathbb{B}\boldsymbol{v}_h(t), \\ \boldsymbol{v}_h(0) & = & \boldsymbol{v}_h^0, \end{cases} \tag{5.6}$$

where $f\left(t, \boldsymbol{v}_h(t), \boldsymbol{\Lambda}_h(t)\right) := -\mathbb{M}^{-1}\left(\mathbb{D}\boldsymbol{v}_h(t) - \mathbb{C}\mathcal{A}_{HDG}\boldsymbol{\Lambda}_h(t)\right)$. At this point, we recognize in (5.6) an ordinary differential equation with a constraint (*the second equation for* $\boldsymbol{\Lambda}$), that can be discretized with a time marching scheme. Here, $\boldsymbol{\Lambda}_h$ is an intermediate variable computed globally on the skeleton of the mesh leading us to find $\boldsymbol{E}$ and $\boldsymbol{H}$ locally in the mesh. After fixing a time-step Δt, we iteratively construct iterations $\boldsymbol{v}_h^n$ of $\boldsymbol{v}_h(t_n)$, $t_n := n\Delta t$. Specifically, for $n \geq 0$, $\boldsymbol{v}_h^{n+1}$ is deduced from $\boldsymbol{v}_h^n$ through the following method, let s be an integer greater or equal than 1 and let b and c two vectors of $\mathbb{R}^n$, $b = (b_1, \cdots, b_n)$ and $c = (c_1, \cdots, c_n)^t$, and let A be a $s \times s$ matrix, $A = (a_{ij})_{1 \leq i,j \leq n}$. A s-stage Runge-Kutta method is defined by

$$\begin{aligned} \boldsymbol{v}_h^{n,i} & = & \boldsymbol{v}_h^n + \Delta t \sum_{j=1}^{s} a_{ij} f\left(t_0 + c_j \Delta t, \boldsymbol{v}_h^{n,j}, \boldsymbol{\Lambda}_h^{n,j}\right), \quad i = 1, \ldots, s, \\ \mathbb{G}\boldsymbol{\Lambda}^{n,i} & = & -\mathbb{B}\boldsymbol{v}^{n,i}, \quad i = 1, \ldots, s, \\ \boldsymbol{v}_h^{n+1,i} & = & \boldsymbol{v}_h^{n,i} + \Delta t \sum_{j=1}^{s} b_j f\left(t_0 + c_j \Delta t, \boldsymbol{v}_h^{n,j}, \boldsymbol{\Lambda}_h^{n,j}\right). \end{aligned} \tag{5.7}$$

The data are usually arranged in a mnemonic device, known as a Butcher's array

$$\begin{array}{c|ccccc} c_1 & a_{11} & a_{12} & \cdots & a_{1s-1} & a_{1s} \\ c_2 & a_{21} & a_{22} & \cdots & a_{2s-1} & a_{2s} \\ \vdots & \vdots & & \ddots & & \vdots \\ c_n & a_{n1} & a_{n2} & \cdots & a_{ns-1} & a_{ns} \\ \hline & b_1 & b_2 & \cdots & b_{s-1} & b_s \end{array}$$

A Runge-Kutta method is of order p if the expansion in powers of Δt of the numerical solution coincides with that of the true solution up to and including a certain order p.

IMEX Runge-Kutta methods

In order to propose the IMEX Runge-Kutta schemes, we must first rewrite (5.5) as

$$\begin{cases} \mathbb{M}\dot{\boldsymbol{v}}_h(t) & = & -\mathbb{D}^{exp}\boldsymbol{v}_h(t) - \mathbb{C}^{exp}\mathcal{A}_{HDG}\boldsymbol{\Lambda}_h(t) - \mathbb{D}^{imp}\boldsymbol{v}_h(t) - \mathbb{C}^{imp}\mathcal{A}_{HDG}\boldsymbol{\Lambda}_h(t), \\ \mathbb{G}\boldsymbol{\Lambda}_h(t) & = & -\mathbb{B}^{exp}\boldsymbol{v}_h(t) - \mathbb{B}^{imp}\boldsymbol{v}_h(t), \\ \boldsymbol{v}_h(0) & = & \boldsymbol{v}_{h,0} \end{cases} \tag{5.8}$$

where,

$$\mathbb{D}^{exp} + \mathbb{D}^{imp} = \mathbb{D},$$

$$\mathbb{C}^{exp} + \mathbb{C}^{imp} = \mathbb{C},$$

$$\mathbb{B}^{exp} + \mathbb{B}^{imp} = \mathbb{B}.$$

The idea of the IMEX methods is to apply two different Runge-Kutta methods (*implicit and explicit respectively*) *i.e*

$$\begin{array}{c|c} \hat{c} & \hat{A} \\ \hline & \hat{b}^t \end{array} \qquad \begin{array}{c|c} c & A \\ \hline & b^t \end{array}$$

where we treat the *imp* part with the first method, $\hat{A}$, $\hat{b} = (\hat{b}_1, \cdots, \hat{b}_n)$, $\hat{c} = (\hat{c}_1, \cdots, \hat{c}_n)^t$ and the *exp* part with the second method, A, $b = (b_1, \cdots, b_n)$, $c = (c_1, \cdots, c_n)^t$. From now on we shall adopt IMEX Runge-Kutta schemes with $b = \hat{b}$ [52]. It is usual to consider diagonally implicit Runge-Kutta (DIRK) schemes for the implicit part which is simple to implement. On the other hand, if the implicit Runge-Kutta method and the explicit one are both of order p, it is not necessary that the IMEX Runge-Kutta method is also of order p, we must respect the "order conditions" given in [52] to obtain the order p for the IMEX scheme. In the section below we will present three IMEX methods of different orders when combined with the HDG method for Maxwell's equations.

5.3.2 Hybrid implicit-explicit HDG methods (IMEX HDG)

First order IMEX HDG method (IMEX-HDG-Eul1)

Starting from (5.4), we formulate the IMEX Euler HDG method as

IMEX-HDG-Eul1

$$\begin{cases} m\left(\dfrac{\boldsymbol{v}_h^{n+1} - \boldsymbol{v}_h^n}{\Delta t}, \boldsymbol{v}_h'\right) = \left(\mathbf{L}_h^{\mathcal{FI}}(\boldsymbol{v}_h^{n+1}, \boldsymbol{\Lambda}_h^{n+1}), \boldsymbol{v}_h'\right) + \left(\mathbf{L}_h^{\mathcal{CO}}(\boldsymbol{v}_h^n, \boldsymbol{\Lambda}_h^n), \boldsymbol{v}_h'\right), \\ c^{\mathcal{FI}}\left(\boldsymbol{v}_h^{n+1}, \boldsymbol{\Lambda}_h^{n+1}, \boldsymbol{\eta}_h\right) = -c^{\mathcal{CO}}\left(\boldsymbol{v}_h^{n+1}, \boldsymbol{\Lambda}_h^{n+1}, \boldsymbol{\eta}_h\right), \end{cases} \tag{5.9}$$

for all test functions $(\boldsymbol{v}_h', \boldsymbol{\eta}_h)$ that belong to the space $\mathbb{V}_h \times \boldsymbol{M}_h$. In order to solve this problem we need first to compute the value of $\boldsymbol{\Lambda}_h^n$. In order to do so we need the inversion of a global matrix. However, as the trace field is defined discontinuously across the faces, by construction this matrix is a block-diagonal matrix. Therefore, the inversion of this matrix is cheap. Then, from (5.9), we can create a global problem to find the value of $\boldsymbol{\Lambda}_h^{n+1}$ on the faces. The global matrix to inverse in this step consists of a block-diagonal matrix corresponding to the degrees of freedom in the coarse part, and a sparse matrix corresponding to the degrees of freedom in the fine part. We are then able to calculate locally the solution $\boldsymbol{v}_h^{n+1}$.

Second order IMEX HDG method (IMEX-HDG-RK2)

We define the second order Runge-Kutta IMEX HDG method as

IMEX-HDG-RK2

$$\begin{cases} m\left(\dfrac{\boldsymbol{v}_h^{n+\frac{1}{2}}-\boldsymbol{v}_h^{n}}{\Delta t},\boldsymbol{v}_h'\right) &= \alpha_1\left(\mathbf{L}_h^{\mathcal{FI}}\left(\boldsymbol{v}_h^{n+\frac{1}{2}},\boldsymbol{\Lambda}_h^{n+\frac{1}{2}}\right),\boldsymbol{v}_h'\right) \\ & + \alpha_2\left(\mathbf{L}_h^{\mathcal{CO}}\left(\boldsymbol{v}_h^{n},\boldsymbol{\Lambda}_h^{n}\right),\boldsymbol{v}_h'\right), \\ c^{\mathcal{FI}}\left(\boldsymbol{v}_h^{n+\frac{1}{2}},\boldsymbol{\Lambda}_h^{n+\frac{1}{2}},\boldsymbol{\eta}_h\right) &= -c^{\mathcal{CO}}\left(\boldsymbol{v}_h^{n+\frac{1}{2}},\boldsymbol{\Lambda}_h^{n+\frac{1}{2}},\boldsymbol{\eta}_h\right), \\ m\left(\dfrac{\boldsymbol{v}_h^{n+1}-\boldsymbol{v}_h^{n}}{\Delta t},\boldsymbol{v}_h'\right) &= \left(\mathbf{L}_h\left(\boldsymbol{v}_h^{n+\frac{1}{2}},\boldsymbol{\Lambda}_h^{n+\frac{1}{2}}\right),\boldsymbol{v}_h'\right), \\ c\left(\boldsymbol{v}_h^{n+1},\boldsymbol{\Lambda}_h^{n+1},\boldsymbol{\eta}_h\right) &= 0, \end{cases} \tag{5.10}$$

for all test functions $(\boldsymbol{v}_h', \boldsymbol{\eta}_h)$ that belong to the space $\mathbb{V}_h \times \boldsymbol{M}_h$, where α_1 and α_2 are the coefficients of the butcher table for the fully implicit and explicit Runge-Kutta 2 respectively (see table 5.1). In order to solve this problem we need first to create a global problem from the first two equations of (5.10) to find the value of $\boldsymbol{\Lambda}_h^{n+\frac{1}{2}}$ on the faces. The global matrix to inverse in this step is a block-diagonal matrix corresponding to the degrees of freedom in the coarse part, and a sparse matrix corresponding to the degrees of freedom in the fine part. Then we are able to calculate locally the solution $\boldsymbol{v}_h^{n+\frac{1}{2}}$. Finally, the third equation gives us the value of the solution $\boldsymbol{v}_h^{n+1}$ in each element of the mesh.

$$\begin{array}{c|cc} 0 & 0 & 0 \\ \frac{1}{2} & 0 & \frac{1}{2} \\ \hline & 0 & 1 \end{array} \qquad\qquad \begin{array}{c|cc} 0 & 0 & \\ \frac{1}{2} & \frac{1}{2} & 0 \\ \hline & 0 & 1 \end{array}$$

Table 5.1 | Butcher tables for implicit RK2 (left) and explicit RK2 (right) with $\alpha_1 = \alpha_2 = \dfrac{1}{2}$.

Third order IMEX HDG method (IMEX-HDG-RK3)

We define the third order Runge-Kutta IMEX HDG method as

IMEX-HDG-RK3

$$
\left\{
\begin{array}{lcl}
m\left(\dfrac{\boldsymbol{v}_h^{n,1}-\boldsymbol{v}_h^{n}}{\Delta t},\boldsymbol{v}_h'\right) & = & \alpha\left(\mathbf{L}_h^{\mathcal{FI}}\left(\boldsymbol{v}_h^{n,1},\boldsymbol{\Lambda}_h^{n,1}\right),\boldsymbol{v}_h'\right),\\
c^{\mathcal{FI}}\left(\boldsymbol{v}_h^{n,1},\boldsymbol{\Lambda}_h^{n,1},\boldsymbol{\eta}_h\right) & = & -c^{\mathcal{CO}}\left(\boldsymbol{v}_h^{n,1},\boldsymbol{\Lambda}_h^{n,1},\boldsymbol{\eta}_h\right),\\
m\left(\dfrac{\boldsymbol{v}_h^{n,2}-\boldsymbol{v}_h^{n}}{\Delta t},\boldsymbol{v}_h'\right) & = & -\alpha\left(\mathbf{L}_h^{\mathcal{FI}}\left(\boldsymbol{v}_h^{n,1},\boldsymbol{\Lambda}_h^{n,1}\right),\boldsymbol{v}_h'\right)\\
 & + & \alpha\left(\mathbf{L}_h^{\mathcal{FI}}\left(\boldsymbol{v}_h^{n,2},\boldsymbol{\Lambda}_h^{n,2}\right),\boldsymbol{v}_h'\right),\\
c^{\mathcal{FI}}\left(\boldsymbol{v}_h^{n,2},\boldsymbol{\Lambda}_h^{n,2},\boldsymbol{\eta}_h\right) & = & -c^{\mathcal{CO}}\left(\boldsymbol{v}_h^{n,2},\boldsymbol{\Lambda}_h^{n,2},\boldsymbol{\eta}_h\right),\\
m\left(\dfrac{\boldsymbol{v}_h^{n,3}-\boldsymbol{v}_h^{n}}{\Delta t},\boldsymbol{v}_h'\right) & = & (1-\alpha)\left(\mathbf{L}_h^{\mathcal{FI}}\left(\boldsymbol{v}_h^{n,2},\boldsymbol{\Lambda}_h^{n,2}\right),\boldsymbol{v}_h'\right)\\
 & + & \alpha\left(\mathbf{L}_h^{\mathcal{FI}}\left(\boldsymbol{v}_h^{n,3},\boldsymbol{\Lambda}_h^{n,3}\right),\boldsymbol{v}_h'\right)\\
 & + & \left(\mathbf{L}_h^{\mathcal{CO}}\left(\boldsymbol{v}_h^{n,2},\boldsymbol{\Lambda}_h^{n,2}\right),\boldsymbol{v}_h'\right),\\
c^{\mathcal{FI}}\left(\boldsymbol{v}_h^{n,3},\boldsymbol{\Lambda}_h^{n,3},\boldsymbol{\eta}_h\right) & = & -c^{\mathcal{CO}}\left(\boldsymbol{v}_h^{n,3},\boldsymbol{\Lambda}_h^{n,3},\boldsymbol{\eta}_h\right),\\
m\left(\dfrac{\boldsymbol{v}_h^{n,4}-\boldsymbol{v}_h^{n}}{\Delta t},\boldsymbol{v}_h'\right) & = & \beta\left(\mathbf{L}_h^{\mathcal{FI}}\left(\boldsymbol{v}_h^{n,1},\boldsymbol{\Lambda}_h^{n,1}\right),\boldsymbol{v}_h'\right)\\
 & + & \eta\left(\mathbf{L}_h^{\mathcal{FI}}\left(\boldsymbol{v}_h^{n,2},\boldsymbol{\Lambda}_h^{n,2}\right),\boldsymbol{v}_h'\right)\\
 & + & \left(\dfrac{1}{2}-\beta-\eta-\alpha\right)\left(\mathbf{L}_h^{\mathcal{FI}}\left(\boldsymbol{v}_h^{n,3},\boldsymbol{\Lambda}_h^{n,3}\right),\boldsymbol{v}_h'\right)\\
 & + & \alpha\left(\mathbf{L}_h^{\mathcal{FI}}\left(\boldsymbol{v}_h^{n,4},\boldsymbol{\Lambda}_h^{n,4}\right),\boldsymbol{v}_h'\right)\\
 & + & \dfrac{1}{4}\left(\mathbf{L}_h^{\mathcal{CO}}\left(\boldsymbol{v}_h^{n,2},\boldsymbol{\Lambda}_h^{n,2}\right),\boldsymbol{v}_h'\right)\\
 & + & \dfrac{1}{4}\left(\mathbf{L}_h^{\mathcal{CO}}\left(\boldsymbol{v}_h^{n,3},\boldsymbol{\Lambda}_h^{n,3}\right),\boldsymbol{v}_h'\right),\\
c^{\mathcal{FI}}\left(\boldsymbol{v}_h^{n,4},\boldsymbol{\Lambda}_h^{n,4},\boldsymbol{\eta}_h\right) & = & -c^{\mathcal{CO}}\left(\boldsymbol{v}_h^{n,4},\boldsymbol{\Lambda}_h^{n,4},\boldsymbol{\eta}_h\right),\\
m\left(\dfrac{\boldsymbol{v}_h^{n+1}-\boldsymbol{v}_h^{n}}{\Delta t},\boldsymbol{v}_h'\right) & = & \dfrac{1}{6}\left(\mathbf{L}_h\left(\boldsymbol{v}_h^{n,2},\boldsymbol{\Lambda}_h^{n,2}\right),\boldsymbol{v}_h'\right)\\
 & + & \dfrac{1}{6}\left(\mathbf{L}_h\left(\boldsymbol{v}_h^{n,3},\boldsymbol{\Lambda}_h^{n,3}\right),\boldsymbol{v}_h'\right)\\
 & + & \dfrac{2}{3}\left(\mathbf{L}_h\left(\boldsymbol{v}_h^{n,4},\boldsymbol{\Lambda}_h^{n,4}\right),\boldsymbol{v}_h'\right),\\
c\left(\boldsymbol{v}_h^{n+1},\boldsymbol{\Lambda}_h^{n+1},\boldsymbol{\eta}_h\right) & = & 0,
\end{array}
\right.
\tag{5.11}
$$

for all test functions $(\boldsymbol{v}_h', \boldsymbol{\eta}_h)$ that belong to the space $\mathbb{V}_h \times \boldsymbol{M}_h$. where α and β and η are defined in Table 5.2.

$$
\begin{array}{c|cccc}
\alpha & \alpha & 0 & 0 & 0 \\
0 & -\alpha & \alpha & 0 & 0 \\
1 & 0 & 1-\alpha & \alpha & 0 \\
\frac{1}{2} & \beta & \eta & \frac{1}{2}-\beta-\eta-\alpha & \alpha \\
\hline
 & 0 & 1/6 & 1/6 & 2/3
\end{array}
\qquad
\begin{array}{c|cccc}
0 & 0 & 0 & 0 & 0 \\
0 & 0 & 0 & 0 & 0 \\
1 & 0 & 1 & 0 & 0 \\
\frac{1}{2} & 0 & \frac{1}{4} & \frac{1}{4} & 0 \\
\hline
 & 0 & 1/6 & 1/6 & 2/3
\end{array}
$$

Table 5.2 | Butcher tables for LDIRK3 (left) and SSP3 (right) with $\alpha = 0.2416942607882$, $\beta = \frac{\alpha}{4}$ and $\eta = 0.1291528696059$.

5.3.3 Stability of the fully discrete schemes

Euler IMEX HDG method (IMEX-HDG-Eul1)

Theorem 6. *For $\Delta t \leq \eta h^2_{\mathcal{T}_h^{CO}}$, the totally discrete hybrid implicit-explicit Euler HDG scheme is stable in the sense that for all $n \in \mathbb{N}$, there exists $\beta > 0$ (independent of h and Δt) such that*

$$\mathcal{E}_h^n \leq e^{\beta T} \mathcal{E}_h^0,$$

in which the discrete electromagnetic energy is $\mathcal{E}_h(t) = \dfrac{1}{2}||\boldsymbol{v}_h(t)||^2_\lambda$.

Proof. By replacing $\boldsymbol{v}_h' = \boldsymbol{v}_h^{n+1}$ and $\boldsymbol{\eta}_h = \boldsymbol{\Lambda}_h^{n+1}$ in (5.9) we obtain that

$$
\begin{aligned}
\left(\mathbf{L}_h^{\mathcal{FI}}(\boldsymbol{v}_h^{n+1}, \boldsymbol{\Lambda}_h^{n+1}), \boldsymbol{v}_h^{n+1}\right) &= a^{\mathcal{FI}}(\boldsymbol{v}_h^{n+1}, \boldsymbol{v}_h^{n+1}) \\
&+ b_\tau^{\mathcal{FI}}(\boldsymbol{v}_h^{n+1}, \boldsymbol{\Lambda}_h^{n+1}, \boldsymbol{v}_h^{n+1}) \\
&= \cancelto{0}{a^{\mathcal{FI}}(\boldsymbol{v}_h^{n+1}, \boldsymbol{v}_h^{n+1})} \\
&+ b_\tau^{\mathcal{FI}}(\boldsymbol{v}_h^{n+1}, \boldsymbol{\Lambda}_h^{n+1}, \boldsymbol{v}_h^{n+1}) \\
&+ c^{\mathcal{FI}}(\boldsymbol{v}_h^{n+1}, \boldsymbol{\Lambda}_h^{n+1}, \boldsymbol{\Lambda}_h^{n+1}) \\
&+ c^{\mathcal{CO}}(\boldsymbol{v}_h^{n+1}, \boldsymbol{\Lambda}_h^{n+1}, \boldsymbol{\Lambda}_h^{n+1}).
\end{aligned}
$$

From Lemma 3 we deduce that

$$\left(\mathbf{L}_h^{\mathcal{FI}}(\boldsymbol{v}_h^{n+1}, \boldsymbol{\Lambda}_h^{n+1}), \boldsymbol{v}_h^{n+1}\right) \leq c^{\mathcal{CO}}(\boldsymbol{v}_h^{n+1}, \boldsymbol{\Lambda}_h^{n+1}, \boldsymbol{\Lambda}_h^{n+1}).$$

Back to the first equation of system (5.9) we can deduce that

$$
\begin{aligned}
& m\left(\boldsymbol{v}_h^{n+1} - \boldsymbol{v}_h^n, \boldsymbol{v}_h^{n+1}\right) \\
& \leq \Delta t \Big[\left(\mathbf{L}_h^{\mathcal{CO}}(\boldsymbol{v}_h^n, \boldsymbol{\Lambda}_h^n), \boldsymbol{v}_h^{n+1}\right) + c^{\mathcal{CO}}\left(\boldsymbol{v}_h^{n+1}, \boldsymbol{\Lambda}_h^{n+1}, \boldsymbol{\Lambda}_h^{n+1}\right) \Big],
\end{aligned}
$$

which yields

$$
\begin{aligned}
& \frac{1}{2}||\boldsymbol{v}_h^{n+1}||^2_\lambda - \frac{1}{2}||\boldsymbol{v}_h^n||^2_\lambda + \frac{1}{2}||\boldsymbol{v}_h^{n+1} - \boldsymbol{v}_h^n||^2_\lambda \\
& \leq \Delta t \Big[\left(\mathbf{L}_h^{\mathcal{CO}}(\boldsymbol{v}_h^n, \boldsymbol{\Lambda}_h^n), \boldsymbol{v}_h^{n+1}\right) + c^{\mathcal{CO}}\left(\boldsymbol{v}_h^{n+1}, \boldsymbol{\Lambda}_h^{n+1}, \boldsymbol{\Lambda}_h^{n+1}\right) \Big].
\end{aligned} \tag{5.12}
$$

We deduce from (5.12) that the stability will depend only on the coarse mesh. Let RHS $= \left(\mathbf{L}_h^{\mathcal{CO}}(\boldsymbol{v}_h^n, \boldsymbol{\Lambda}_h^n), \boldsymbol{v}_h^{n+1}\right) + c^{\mathcal{CO}}\left(\boldsymbol{v}_h^{n+1}, \boldsymbol{\Lambda}_h^{n+1}, \boldsymbol{\Lambda}_h^{n+1}\right)$.

We now add and substract $\left(\mathbf{L}_h^{\mathcal{CO}}(\boldsymbol{v}_h^{n+1}, \boldsymbol{\Lambda}_h^{n+1}), \boldsymbol{v}_h^{n+1}\right)$ to obtain

$$\begin{aligned}\text{RHS} &= \left(\mathbf{L}_h^{\mathcal{CO}}(\boldsymbol{v}_h^{n}, \boldsymbol{\Lambda}_h^{n}) - \mathbf{L}_h^{\mathcal{CO}}(\boldsymbol{v}_h^{n+1}, \boldsymbol{\Lambda}_h^{n+1}), \boldsymbol{v}_h^{n+1}\right) \\ &+ \left(\mathbf{L}_h^{\mathcal{CO}}(\boldsymbol{v}_h^{n+1}, \boldsymbol{\Lambda}_h^{n+1}), \boldsymbol{v}_h^{n+1}\right) + c^{\mathcal{CO}}\left(\boldsymbol{v}_h^{n+1}, \boldsymbol{\Lambda}_h^{n+1}, \boldsymbol{\Lambda}_h^{n+1}\right).\end{aligned}$$

From Lemma 3

$$\left(\mathbf{L}_h^{\mathcal{CO}}(\boldsymbol{v}_h^{n+1}, \boldsymbol{\Lambda}_h^{n+1}), \boldsymbol{v}_h^{n+1}\right) + c^{\mathcal{CO}}\left(\boldsymbol{v}_h^{n+1}, \boldsymbol{\Lambda}_h^{n+1}, \boldsymbol{\Lambda}_h^{n+1}\right) \leq 0,$$

which implies

$$\text{RHS} \leq \left(\mathbf{L}_h^{\mathcal{CO}}(\boldsymbol{v}_h^{n}, \boldsymbol{\Lambda}_h^{n}) - \mathbf{L}_h^{\mathcal{CO}}(\boldsymbol{v}_h^{n+1}, \boldsymbol{\Lambda}_h^{n+1}), \boldsymbol{v}_h^{n+1}\right).$$

Corollary 4.1 let us deduce that

$$\begin{aligned}&|\text{RHS}| \\ &\leq c h_{\mathcal{T}_h^{CO}}^{-1}\left(||\boldsymbol{v}_h^{n+1} - \boldsymbol{v}_h^{n}||_{\mathcal{T}_h^{CO}}||\boldsymbol{v}_h^{n}||_{\mathcal{T}_h^{CO}} + ||\boldsymbol{v}_h^{n+1} - \boldsymbol{v}_h^{n}||_{\mathcal{T}_h^{CO}}^2 + ||\boldsymbol{v}_h^{n}||_{\mathcal{T}_h^{CO}}^2\right).\end{aligned}$$

Back to (5.12) we obtain

$$\begin{aligned}&\frac{1}{2}||\boldsymbol{v}_h^{n+1}||_\lambda^2 - \frac{1}{2}||\boldsymbol{v}_h^{n}||_\lambda^2 + \frac{1}{2}||\boldsymbol{v}_h^{n+1} - \boldsymbol{v}_h^{n}||_\lambda^2 \\ &\leq c h_{\mathcal{T}_h^{CO}}^{-1}\left(||\boldsymbol{v}_h^{n+1} - \boldsymbol{v}_h^{n}||_{\mathcal{T}_h^{CO}}||\boldsymbol{v}_h^{n}||_{\mathcal{T}_h^{CO}} + ||\boldsymbol{v}_h^{n+1} - \boldsymbol{v}_h^{n}||_{\mathcal{T}_h^{CO}}^2 + ||\boldsymbol{v}_h^{n}||_{\mathcal{T}_h^{CO}}^2\right).\end{aligned}$$

Therefore

$$\begin{aligned}&\frac{1}{2}||\boldsymbol{v}_h^{n+1}||_\lambda^2 - \frac{1}{2}||\boldsymbol{v}_h^{n}||_\lambda^2 + \frac{1}{2}||\boldsymbol{v}_h^{n+1} - \boldsymbol{v}_h^{n}||_\lambda^2 \\ &\leq \left(\frac{1}{2}c^2 h_{\mathcal{T}_h^{CO}}^{-2}\Delta t^2 + c\Delta t h_{\mathcal{T}_h^{CO}}^{-1}\right)||\boldsymbol{v}_h^{n}||_{\mathcal{T}_h^{CO}}^2 + \frac{1}{2}c\Delta t h_{\mathcal{T}_h^{CO}}^{-1}||\boldsymbol{v}_h^{n+1} - \boldsymbol{v}_h^{n}||_{\mathcal{T}_h^{CO}}^2.\end{aligned}$$

Since

$$||\boldsymbol{v}||_{\mathcal{T}_h^{CO}}^2 \leq ||\boldsymbol{v}||_{\mathcal{T}_h}^2 \leq ||\boldsymbol{v}||_\lambda^2, \qquad \forall \boldsymbol{v} \in \mathbb{V}_h,$$

we can deduce

$$\begin{aligned}&\frac{1}{2}||\boldsymbol{v}_h^{n+1}||_\lambda^2 - \frac{1}{2}||\boldsymbol{v}_h^{n}||_\lambda^2 + \frac{1}{2}||\boldsymbol{v}_h^{n+1} - \boldsymbol{v}_h^{n}||_\lambda^2 \\ &\leq \left(\frac{1}{2}c^2 h_{\mathcal{T}_h^{CO}}^{-2}\Delta t^2 + c\Delta t h_{\mathcal{T}_h^{CO}}^{-1}\right)||\boldsymbol{v}_h^{n}||_\lambda^2 + \frac{1}{2}c\Delta t h_{\mathcal{T}_h^{CO}}^{-1}||\boldsymbol{v}_h^{n+1} - \boldsymbol{v}_h^{n}||_\lambda^2.\end{aligned}$$

So for $\Delta t \leq c^{-1} h_{\mathcal{T}_h^{CO}}^2$, and since $h < 1$, we obtain

$$\mathcal{E}_h^{n+1} - \mathcal{E}_h^{n} \leq \Delta t \mathcal{E}_h^{n}, \qquad \forall n \in \mathbb{N}.$$

Finally, by Gronwall's lemma

$$\mathcal{E}_h^{n} \leq e^T \mathcal{E}_h^{0}.$$

□

Second order IMEX HDG method (IMEX-HDG-RK2)

Theorem 7. *For $\Delta t \leq \eta h^2_{\mathcal{T}_h^{CO}}$, the totally discrete scheme is stable for implicit-explicit Runge-Kutta 2, in the sense that for all $n \in \mathbb{N}$, there exists $\beta > 0$ (independent of h and Δt) such that*

$$\mathcal{E}_h^n \leq e^{\beta T} \mathcal{E}_h^0,$$

in which the discrete electromagnetic energy is $\mathcal{E}_h(t) = \frac{1}{2}||\boldsymbol{v}_h(t)||^2_\lambda$.

Proof. By replacing $\boldsymbol{v}'_h = \boldsymbol{v}_h^{n+\frac{1}{2}}$ in the first equation of (5.10) we obtain

$$m\left(\boldsymbol{v}_h^{n+\frac{1}{2}} - \boldsymbol{v}_h^n, \boldsymbol{v}_h^{n+\frac{1}{2}}\right) = \frac{\Delta t}{2}\left(\mathbf{L}_h^{\mathcal{FI}}\left(\boldsymbol{v}_h^{n+\frac{1}{2}}, \boldsymbol{\Lambda}_h^{n+\frac{1}{2}}\right), \boldsymbol{v}_h^{n+\frac{1}{2}}\right) + \frac{\Delta t}{2}\left(\mathbf{L}_h^{\mathcal{CO}}\left(\boldsymbol{v}_h^n, \boldsymbol{\Lambda}_h^n\right), \boldsymbol{v}_h^{n+\frac{1}{2}}\right),$$

which implies that

$$\begin{aligned}\frac{1}{2}\left\|\boldsymbol{v}_h^{n+\frac{1}{2}}\right\|^2_\lambda - \frac{1}{2}\left\|\boldsymbol{v}_h^n\right\|^2_\lambda + \frac{1}{2}\left\|\boldsymbol{v}_h^{n+\frac{1}{2}} - \boldsymbol{v}_h^n\right\|^2_\lambda = \Delta t\Bigg[&\left(\mathbf{L}_h^{\mathcal{FI}}\left(\boldsymbol{v}_h^{n+\frac{1}{2}}, \boldsymbol{\Lambda}_h^{n+\frac{1}{2}}\right), \boldsymbol{v}_h^{n+\frac{1}{2}}\right) \\ &+ \left(\mathbf{L}_h^{\mathcal{CO}}\left(\boldsymbol{v}_h^n, \boldsymbol{\Lambda}_h^n\right), \boldsymbol{v}_h^{n+\frac{1}{2}}\right)\Bigg].\end{aligned} \tag{5.13}$$

Now, by replacing $\boldsymbol{v}'_h = \boldsymbol{v}_h^{n+\frac{1}{2}}$ in the third equation of (5.10) we obtain

$$m\left(\boldsymbol{v}_h^{n+1} - \boldsymbol{v}_h^n, \boldsymbol{v}_h^{n+\frac{1}{2}}\right) = \Delta t\left(\mathbf{L}_h^{\mathcal{FI}}\left(\boldsymbol{v}_h^{n+\frac{1}{2}}, \boldsymbol{\Lambda}_h^{n+\frac{1}{2}}\right), \boldsymbol{v}_h^{n+\frac{1}{2}}\right) + \Delta t\left(\mathbf{L}_h^{\mathcal{CO}}\left(\boldsymbol{v}_h^{n+\frac{1}{2}}, \boldsymbol{\Lambda}_h^{n+\frac{1}{2}}\right), \boldsymbol{v}_h^{n+\frac{1}{2}}\right),$$

which implies that

$$\begin{aligned}&\frac{1}{2}\left\|\boldsymbol{v}_h^{n+1}\right\|^2_\lambda - \frac{1}{2}\left\|\boldsymbol{v}_h^n\right\|^2_\lambda - \frac{1}{2}\left\|\boldsymbol{v}_h^{n+1} - \boldsymbol{v}_h^{n+\frac{1}{2}}\right\|^2_\lambda + \frac{1}{2}\left\|\boldsymbol{v}_h^{n+\frac{1}{2}} - \boldsymbol{v}_h^n\right\|^2_\lambda \\ &= \Delta t\left[\left(\mathbf{L}_h^{\mathcal{FI}}\left(\boldsymbol{v}_h^{n+\frac{1}{2}}, \boldsymbol{\Lambda}_h^{n+\frac{1}{2}}\right), \boldsymbol{v}_h^{n+\frac{1}{2}}\right) + \left(\mathbf{L}_h^{\mathcal{CO}}\left(\boldsymbol{v}_h^{n+\frac{1}{2}}, \boldsymbol{\Lambda}_h^{n+\frac{1}{2}}\right), \boldsymbol{v}_h^{n+\frac{1}{2}}\right)\right].\end{aligned} \tag{5.14}$$

Back to the third equation of (5.10), let us divide the left hand side into two parts

$$m\left(\boldsymbol{v}_h^{n+1} - \boldsymbol{v}_h^n, \boldsymbol{v}_h^{n+\frac{1}{2}}\right) = m\left(\boldsymbol{v}_h^{n+1} - \boldsymbol{v}_h^{n+\frac{1}{2}}, \boldsymbol{v}_h^{n+\frac{1}{2}}\right) + m\left(\boldsymbol{v}_h^{n+\frac{1}{2}} - \boldsymbol{v}_h^n, \boldsymbol{v}_h^{n+\frac{1}{2}}\right).$$

On the other hand, we have

$$\begin{aligned}&m\left(\boldsymbol{v}_h^{n+1} - \boldsymbol{v}_h^{n+\frac{1}{2}}, \boldsymbol{v}_h^{n+\frac{1}{2}}\right) + m\left(\boldsymbol{v}_h^{n+\frac{1}{2}} - \boldsymbol{v}_h^n, \boldsymbol{v}_h^{n+\frac{1}{2}}\right) \\ &= m\left(\boldsymbol{v}_h^{n+1} - \boldsymbol{v}_h^{n+\frac{1}{2}}, \boldsymbol{v}_h^{n+\frac{1}{2}}\right) + \frac{\Delta t}{2}\left(\mathbf{L}_h^{\mathcal{FI}}\left(\boldsymbol{v}_h^{n+\frac{1}{2}}, \boldsymbol{\Lambda}_h^{n+\frac{1}{2}}\right), \boldsymbol{v}_h^{n+\frac{1}{2}}\right) \\ &+ \frac{\Delta t}{2}\left(\mathbf{L}_h^{\mathcal{CO}}\left(\boldsymbol{v}_h^n, \boldsymbol{\Lambda}_h^n\right), \boldsymbol{v}_h^{n+\frac{1}{2}}\right).\end{aligned}$$

Thus,

$$m\left(\boldsymbol{v}_h^{n+1}-\boldsymbol{v}_h^{n+\frac{1}{2}},\boldsymbol{v}_h^{n+\frac{1}{2}}\right)=\frac{\Delta t}{2}\left(\mathbf{L}_h^{\mathcal{FI}}\left(\boldsymbol{v}_h^{n+\frac{1}{2}},\boldsymbol{\Lambda}_h^{n+\frac{1}{2}}\right),\boldsymbol{v}_h^{n+\frac{1}{2}}\right)-\frac{\Delta t}{2}\left(\mathbf{L}_h^{\mathcal{CO}}\left(\boldsymbol{v}_h^{n},\boldsymbol{\Lambda}_h^{n}\right),\boldsymbol{v}_h^{n+\frac{1}{2}}\right)$$
$$+\Delta t\left(\mathbf{L}_h^{\mathcal{CO}}\left(\boldsymbol{v}_h^{n+\frac{1}{2}},\boldsymbol{\Lambda}_h^{n+\frac{1}{2}}\right),\boldsymbol{v}_h^{n+\frac{1}{2}}\right).$$

Yields to

$$\begin{aligned}&-\frac{1}{2}\left\|\boldsymbol{v}_h^{n+1}\right\|_\lambda^2+\frac{1}{2}\left\|\boldsymbol{v}_h^{n}\right\|_\lambda^2-\frac{1}{2}\left\|\boldsymbol{v}_h^{n+1}-\boldsymbol{v}_h^{n+\frac{1}{2}}\right\|_\lambda^2\\&=\frac{\Delta t}{2}\left(\mathbf{L}_h^{\mathcal{FI}}\left(\boldsymbol{v}_h^{n+\frac{1}{2}},\boldsymbol{\Lambda}_h^{n+\frac{1}{2}}\right),\boldsymbol{v}_h^{n+\frac{1}{2}}\right)-\frac{\Delta t}{2}\left(\mathbf{L}_h^{\mathcal{CO}}\left(\boldsymbol{v}_h^{n},\boldsymbol{\Lambda}_h^{n}\right),\boldsymbol{v}_h^{n+\frac{1}{2}}\right)\\&+\Delta t\left(\mathbf{L}_h^{\mathcal{CO}}\left(\boldsymbol{v}_h^{n+\frac{1}{2}},\boldsymbol{\Lambda}_h^{n+\frac{1}{2}}\right),\boldsymbol{v}_h^{n+\frac{1}{2}}\right).\end{aligned}\tag{5.15}$$

Adding (5.13) to (5.14) and then substracting the result from (5.15) we obtain

$$\begin{aligned}&\left\|\boldsymbol{v}_h^{n+1}\right\|_\lambda^2-\left\|\boldsymbol{v}_h^{n}\right\|_\lambda^2+\left\|\boldsymbol{v}_h^{n+\frac{1}{2}}-\boldsymbol{v}_h^{n}\right\|_\lambda^2\\&=\Delta t\left(\mathbf{L}_h^{\mathcal{FI}}\left(\boldsymbol{v}_h^{n+\frac{1}{2}},\boldsymbol{\Lambda}_h^{n+\frac{1}{2}}\right),\boldsymbol{v}_h^{n+\frac{1}{2}}\right)+\Delta t\left(\mathbf{L}_h^{\mathcal{CO}}\left(\boldsymbol{v}_h^{n},\boldsymbol{\Lambda}_h^{n}\right),\boldsymbol{v}_h^{n+\frac{1}{2}}\right)\\&+\Delta t\,c^{\mathcal{FI}}\left(\boldsymbol{v}_h^{n+\frac{1}{2}},\boldsymbol{\Lambda}_h^{n+\frac{1}{2}},\boldsymbol{v}_h^{n+\frac{1}{2}}\right)+\Delta t\,c^{\mathcal{CO}}\left(\boldsymbol{v}_h^{n+\frac{1}{2}},\boldsymbol{\Lambda}_h^{n+\frac{1}{2}},\boldsymbol{v}_h^{n+\frac{1}{2}}\right).\end{aligned}$$

From Lemma (3)

$$\begin{aligned}&\left\|\boldsymbol{v}_h^{n+1}\right\|_\lambda^2-\left\|\boldsymbol{v}_h^{n}\right\|_\lambda^2+\left\|\boldsymbol{v}_h^{n+\frac{1}{2}}-\boldsymbol{v}_h^{n}\right\|_\lambda^2\\&\leq\Delta t\left[\left(\mathbf{L}_h^{\mathcal{CO}}\left(\boldsymbol{v}_h^{n},\boldsymbol{\Lambda}_h^{n}\right),\boldsymbol{v}_h^{n+\frac{1}{2}}\right)+c^{\mathcal{CO}}\left(\boldsymbol{v}_h^{n+\frac{1}{2}},\boldsymbol{\Lambda}_h^{n+\frac{1}{2}},\boldsymbol{v}_h^{n+\frac{1}{2}}\right)\right].\end{aligned}\tag{5.16}$$

We deduce from (5.16) that the stability will depend only on the coarse mesh. Let RHS $=\left(\mathbf{L}_h^{\mathcal{CO}}(\boldsymbol{v}_h^{n},\boldsymbol{\Lambda}_h^{n}),\boldsymbol{v}_h^{n+\frac{1}{2}}\right)+c^{\mathcal{CO}}\left(\boldsymbol{v}_h^{n+\frac{1}{2}},\boldsymbol{\Lambda}_h^{n+\frac{1}{2}},\boldsymbol{\Lambda}_h^{n+\frac{1}{2}}\right)$.

We add now and subtract $\left(\mathbf{L}_h^{\mathcal{CO}}\left(\boldsymbol{v}_h^{n+\frac{1}{2}},\boldsymbol{\Lambda}_h^{n+\frac{1}{2}}\right),\boldsymbol{v}_h^{n+\frac{1}{2}}\right)$ to obtain

$$\begin{aligned}\text{RHS}=&\left(\mathbf{L}_h^{\mathcal{CO}}(\boldsymbol{v}_h^{n},\boldsymbol{\Lambda}_h^{n})-\mathbf{L}_h^{\mathcal{CO}}\left(\boldsymbol{v}_h^{n+\frac{1}{2}},\boldsymbol{\Lambda}_h^{n+\frac{1}{2}}\right),\boldsymbol{v}_h^{n+\frac{1}{2}}\right)\\&+\left(\mathbf{L}_h^{\mathcal{CO}}\left(\boldsymbol{v}_h^{n+\frac{1}{2}},\boldsymbol{\Lambda}_h^{n+\frac{1}{2}}\right),\boldsymbol{v}_h^{n+\frac{1}{2}}\right)+c^{\mathcal{CO}}\left(\boldsymbol{v}_h^{n+\frac{1}{2}},\boldsymbol{\Lambda}_h^{n+\frac{1}{2}},\boldsymbol{\Lambda}_h^{n+\frac{1}{2}}\right).\end{aligned}$$

From lemma (3.9)

$$\left(\mathbf{L}_h^{\mathcal{CO}}\left(\boldsymbol{v}_h^{n+\frac{1}{2}},\boldsymbol{\Lambda}_h^{n+\frac{1}{2}}\right),\boldsymbol{v}_h^{n+\frac{1}{2}}\right)+c^{\mathcal{CO}}\left(\boldsymbol{v}_h^{n+\frac{1}{2}},\boldsymbol{\Lambda}_h^{n+\frac{1}{2}},\boldsymbol{\Lambda}_h^{n+\frac{1}{2}}\right)\leq 0.$$

Implies

$$\text{RHS}\leq\left(\mathbf{L}_h^{\mathcal{CO}}(\boldsymbol{v}_h^{n},\boldsymbol{\Lambda}_h^{n})-\mathbf{L}_h^{\mathcal{CO}}\left(\boldsymbol{v}_h^{n+\frac{1}{2}},\boldsymbol{\Lambda}_h^{n+\frac{1}{2}}\right),\boldsymbol{v}_h^{n+\frac{1}{2}}\right)$$

Corollary (4.1) gives us

$$|\text{RHS}| \leq c h_{\mathcal{T}_h^{CO}}^{-1} \left(\left\| \boldsymbol{v}_h^{n+\frac{1}{2}} - \boldsymbol{v}_h^n \right\|_{\mathcal{T}_h^{CO}} \|\boldsymbol{v}_h^n\|_{\mathcal{T}_h^{CO}} + \left\| \boldsymbol{v}_h^{n+\frac{1}{2}} - \boldsymbol{v}_h^n \right\|_{\mathcal{T}_h^{CO}}^2 + \|\boldsymbol{v}_h^n\|_{\mathcal{T}_h^{CO}}^2 \right).$$

Back to (5.16), and by taking $k = \dfrac{c}{2}$ we obtain

$$\begin{aligned}
&\frac{1}{2} \left\|\boldsymbol{v}_h^{n+1}\right\|_\lambda^2 - \frac{1}{2} \|\boldsymbol{v}_h^n\|_\lambda^2 + \frac{1}{2} \left\| \boldsymbol{v}_h^{n+\frac{1}{2}} - \boldsymbol{v}_h^n \right\|_\lambda^2 \\
&\leq k \Delta t h_{\mathcal{T}_h^{CO}}^{-1} \left(\left\| \boldsymbol{v}_h^{n+\frac{1}{2}} - \boldsymbol{v}_h^n \right\|_{\mathcal{T}_h^{CO}} \|\boldsymbol{v}_h^n\|_{\mathcal{T}_h^{CO}} + \left\| \boldsymbol{v}_h^{n+\frac{1}{2}} - \boldsymbol{v}_h^n \right\|_{\mathcal{T}_h^{CO}}^2 + \|\boldsymbol{v}_h^n\|_{\mathcal{T}_h^{CO}}^2 \right).
\end{aligned}$$

Therefore

$$\begin{aligned}
&\frac{1}{2} \left\|\boldsymbol{v}_h^{n+1}\right\|_\lambda^2 - \frac{1}{2} \|\boldsymbol{v}_h^n\|_\lambda^2 + \frac{1}{2} \left\| \boldsymbol{v}_h^{n+\frac{1}{2}} - \boldsymbol{v}_h^n \right\|_\lambda^2 \\
&\leq \left(\frac{1}{2} k^2 h_{\mathcal{T}_h^{CO}}^{-2} \Delta t^2 + k \Delta t h_{\mathcal{T}_h^{CO}}^{-1} \right) \|\boldsymbol{v}_h^n\|_{\mathcal{T}_h^{CO}}^2 + \frac{1}{2} k \Delta t h_{\mathcal{T}_h^{CO}}^{-1} \left\| \boldsymbol{v}_h^{n+\frac{1}{2}} - \boldsymbol{v}_h^n \right\|_{\mathcal{T}_h^{CO}}^2.
\end{aligned}$$

Since

$$\|\boldsymbol{v}\|_{\mathcal{T}_h^{CO}}^2 \leq \|\boldsymbol{v}\|_{\mathcal{T}_h}^2 \leq \|\boldsymbol{v}\|_\lambda^2, \qquad \forall \boldsymbol{v} \in \mathbb{V}_h,$$

we can deduce

$$\begin{aligned}
&\frac{1}{2} \left\|\boldsymbol{v}_h^{n+1}\right\|_\lambda^2 - \frac{1}{2} \|\boldsymbol{v}_h^n\|_\lambda^2 + \frac{1}{2} \left\| \boldsymbol{v}_h^{n+\frac{1}{2}} - \boldsymbol{v}_h^n \right\|_\lambda^2 \\
&\leq \left(\frac{1}{2} k^2 h_{\mathcal{T}_h^{CO}}^{-2} \Delta t^2 + k \Delta t h_{\mathcal{T}_h^{CO}}^{-1} \right) \|\boldsymbol{v}_h^n\|_\lambda^2 + \frac{1}{2} k \Delta t h_{\mathcal{T}_h^{CO}}^{-1} \left\| \boldsymbol{v}_h^{n+\frac{1}{2}} - \boldsymbol{v}_h^n \right\|_\lambda^2.
\end{aligned}$$

So for $\Delta t \leq k^{-1} h_{\mathcal{T}_h^{CO}}^2$, and since $h < 1$, we obtain

$$\mathcal{E}_h^{n+1} - \mathcal{E}_h^n \leq \Delta t \mathcal{E}_h^n, \qquad \forall n \in \mathbb{N}.$$

Finally, by Gronwall's lemma

$$\mathcal{E}_h^n \leq e^T \mathcal{E}_h^0.$$

□

5.4 Numerical results

The IMEX HDG methods of order ≤ 3 presented in the previous section have been implemented in the 2D case considering conforming triangular meshes.

5.4.1 Propagation of a standing wave in a PEC cavity

In order to validate and study the numerical convergence of the proposed IMEX HDG methods, we first consider the propagation of an eigenmode in a source-free *i.e.* $\boldsymbol{J} = 0$ closed cavity (Ω is the unit square) with perfectly metallic walls. The electric permittivity and the magnetic permeability are set to the constant vacuum values. Because we consider a renormalized form of Maxwell's equations in the implementation, we thus have that $\epsilon_r = \mu_r = 1$ for the relative values of these electromagnetic parameters. The exact time-domain solution is given by

Exact solution

$$\begin{cases} E_z(x,y,t) &= \sin(\pi x)\sin(\pi y)\cos(\sqrt{2}\pi t), \\ H_x(x,y,t) &= -\dfrac{\sqrt{2}}{2}\sin(\pi x)\cos(\pi y)\sin(\sqrt{2}t), \\ H_y(x,y,t) &= \dfrac{\sqrt{2}}{2}\cos(\pi x)\sin(\pi y)\sin(\sqrt{2}t), \end{cases} \tag{5.17}$$

where the electromagnetic field is initialized at $t = 0$ as $H_x = H_y = 0$ and

$$E_z(x,y,t=0) = \sin(\pi x)\sin(\pi y).$$

Increasingly, uniform fine meshes are generated (see figure 5.1), for which the minimal edge size is denoted by $h_{min,i}$, where i is the index of the mesh. The mode is evolved until a time $t_{max} = T = 3$ m (normalized unit). For each simulation, the global $L^\infty([0,T], L^2_\Omega)$ error is computed. For two successive meshes, the numerical rate of convergence is deduced as

$$r = \frac{\log\left(\dfrac{\max_{t\in[0,T]} ||\boldsymbol{E} - \boldsymbol{E}_{h,i}||_{L^2}}{\max_{t\in[0,T]} ||\boldsymbol{E} - \boldsymbol{E}_{h,i+1}||_{L^2}}\right)}{\log\left(\dfrac{h_{min,i}}{h_{min,i+1}}\right)}. \tag{5.18}$$

We will consider the set of yellow triangles as the fine part and that of blue triangles as the coarse part. For a space discretization with polynomial order p, since we proved in section 5.3.3 that to preserve the stability, the choice of timestep will depend only on the coarse mesh, the timestep is chosen as follows

$$\Delta t = c_p h_{\mathcal{T}_h^{CO}} = c_p \min_{K\in\mathcal{CO}} \frac{A_K}{P_K},$$

where A_K is the area of the element K, P_K its perimeter and c_p is a constant chosen so that the CFL condition is satisfied.

Remark 7. It is clear that in the case of uniform meshes, we have $h_{\mathcal{T}_h^{CO}} = h$. The goal of this section is just to validate the hybrid implicit/explicit HDGTD scheme without seeing the gain this method is designed for.

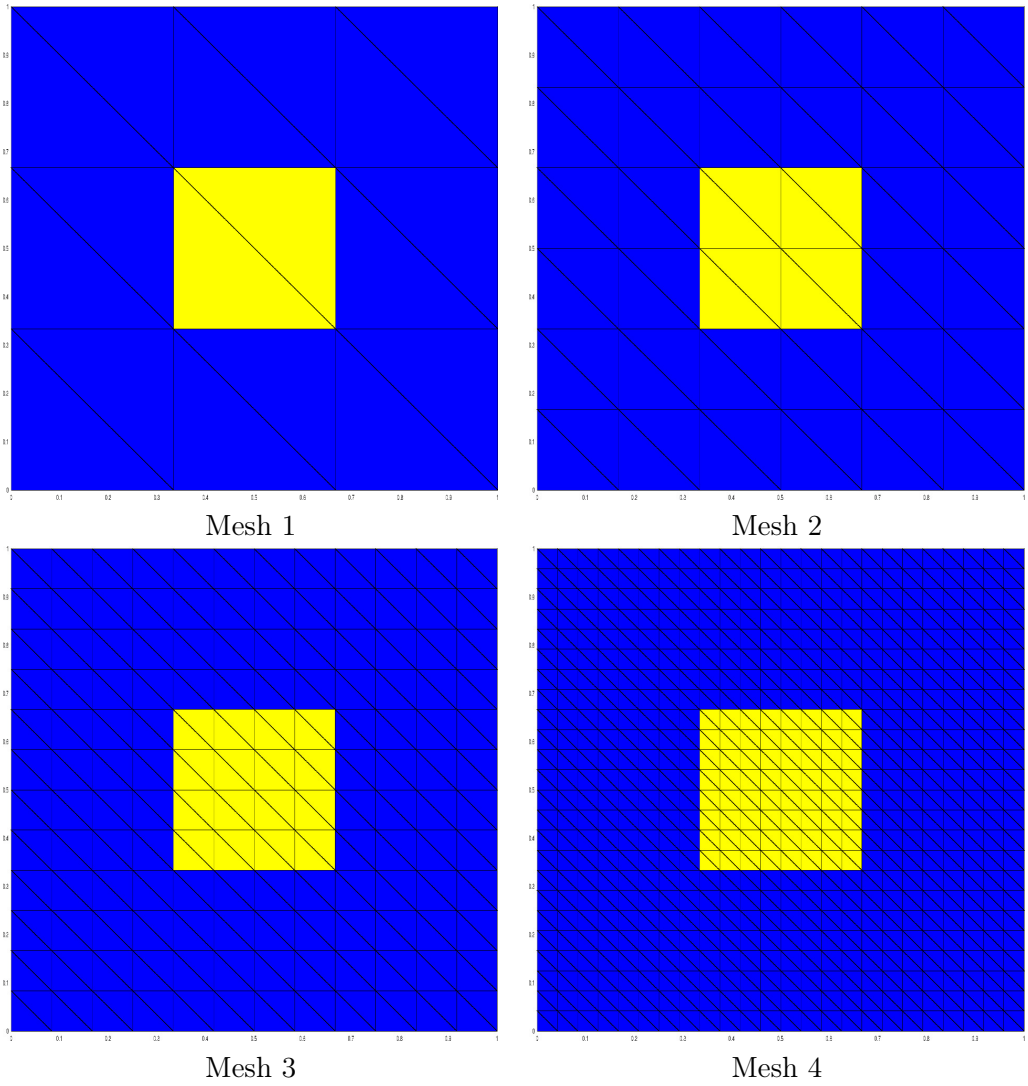

Figure 5.1 | Sequence of triangular meshes used to calculate the convergence rate of IMEX HDGTD methods.

Three IMEX HDGTD methods are studied in this case.

IMEX-HDG-Eul1

We recall the formulation IMEX-HDG-Eul1 method

$$\left\{\begin{array}{lcl} m\left(\dfrac{\boldsymbol{v}_h^{n+1}-\boldsymbol{v}_h^n}{\Delta t},\boldsymbol{v}_h'\right) & = & \left(\mathbf{L}_h^{\mathcal{FI}}\left(\boldsymbol{v}_h^{n+1},\boldsymbol{\Lambda}_h^{n+1}\right),\boldsymbol{v}_h'\right) \\ & + & \left(\mathbf{L}_h^{\mathcal{CO}}(\boldsymbol{v}_h^n,\boldsymbol{\Lambda}_h^n),\boldsymbol{v}_h'\right), \\ c\left(\boldsymbol{v}_h^{n+1},\boldsymbol{\Lambda}_h^{n+1},\boldsymbol{\eta}_h\right) & = & 0, \end{array}\right.$$

for all test functions $(\boldsymbol{v}_h',\boldsymbol{\eta}_h)$ that belong to the space $\mathbb{V}_h\times\boldsymbol{M}_h$.

A sequence of uniformly refined meshes is constructed such that, the zone treated implicitly is localized in a square of side $\frac{1}{3}$ in the middle of the domain (the yellow zone), see Fig. 5.1. The

initial EM wave from (2.61) is propagated in the cavity during a physical time $t_{\max} = 3$ m. Fig. 5.2 shows the time evolution of the exact and the numerical solution of the E_z component at a fixed point in the mesh, while Fig. 5.3 shows the time evolution of the L^2-norm of the error, which is calculated for a uniform triangular mesh with 288 elements, which is constructed from a finite difference grid with $n_x = n_y = 12$ points, each cell of this grid yielding two triangles (Mesh 3), between the numerical and exact solutions. Finally, Fig. 5.4 and Tab. 5.3 are concerned with the numerical convergence of the IMEX-HDG-Eul1 method.

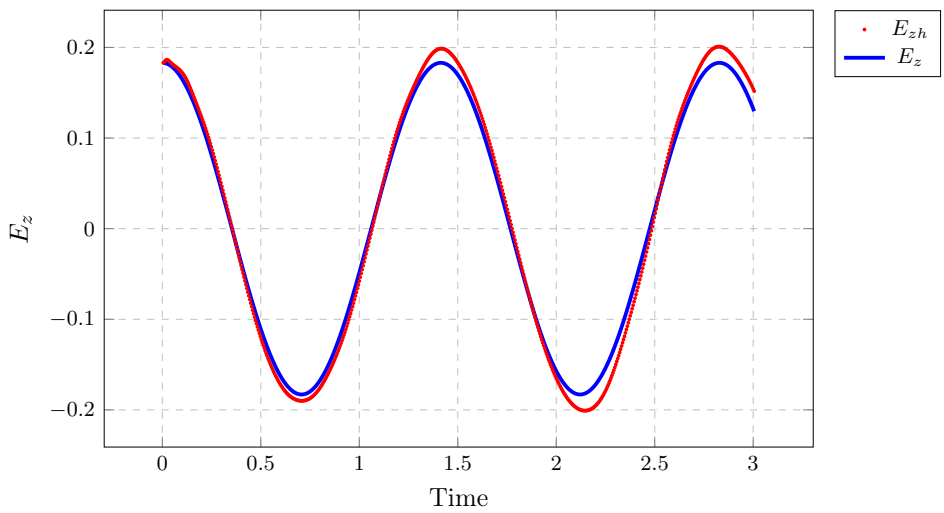

Figure 5.2 | Standing wave in a PEC cavity: IMEX-HDG-Eul1 method. Time evolution of the exact and the numerical solution of E_z at a fixed point with a $\mathbb{P}_1$ interpolation using the 3rd mesh of Fig. 5.1.

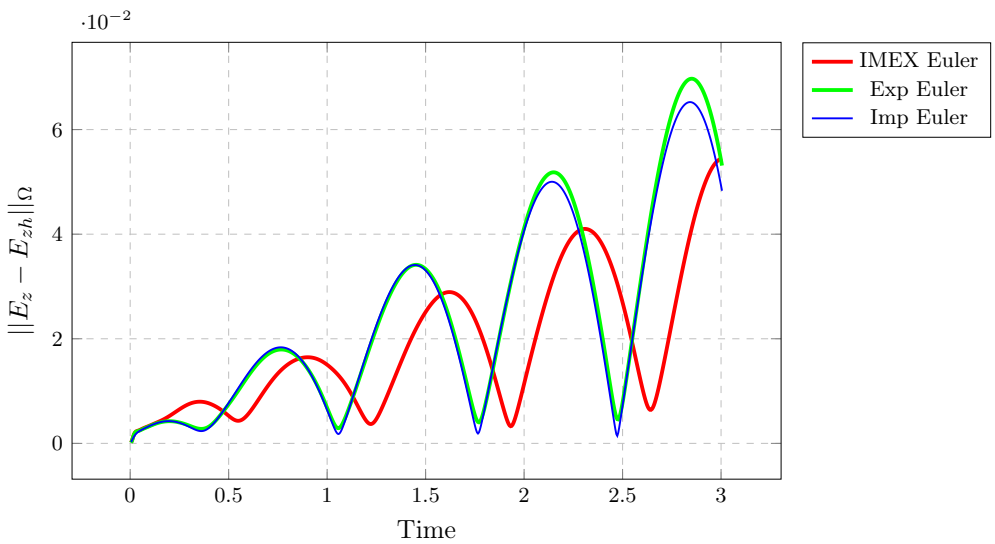

Figure 5.3 | Standing wave in a PEC cavity: IMEX-HDG-Eul1 method. Time evolution of the L^2-norm of the error on E_{zh} for a $\mathbb{P}_1$ interpolation.

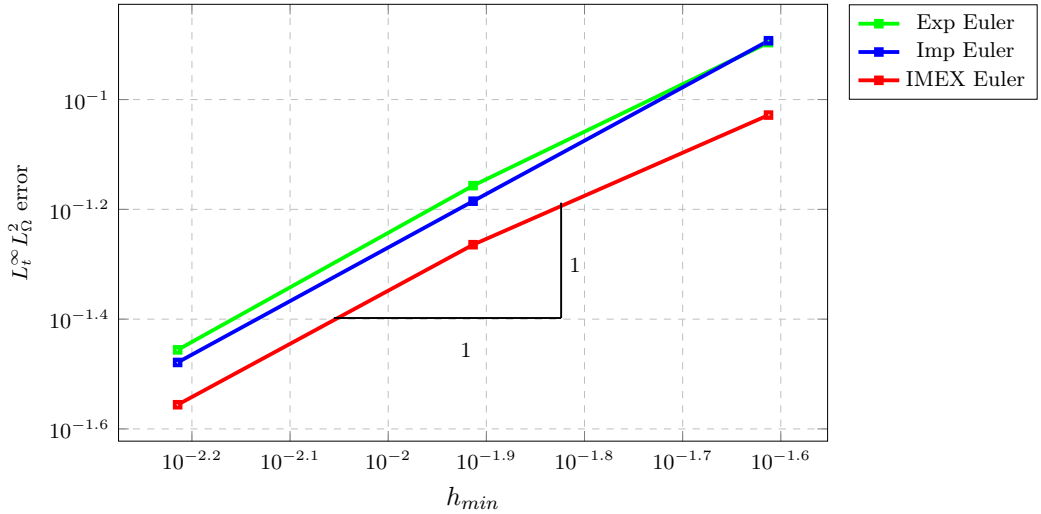

Figure 5.4 | Standing wave in a PEC cavity: IMEX-HDG-Eul1 method. Numerical convergence.

P_k	Time scheme	Mesh	h_{min}	$\|\|Ez - Ez_h\|\|_{L_t^\infty L_\Omega^2}$ Error	order
P_1	Explicit Euler	2	2.44e-02	1.27e-01	**-**
		3	1.22e-02	6.97e-02	**0.87**
		4	6.10e-03	3.50e-02	**0.99**
	Implicit Euler	2	2.44e-02	1.28e-01	**-**
		3	1.22e-02	6.53e-02	**0.97**
		4	6.10e-03	3.32e-02	**0.98**
	IMEX Euler	2	2.44e-02	9.37e-02	**-**
		3	1.22e-02	5.44e-02	**0.78**
		4	6.10e-03	2.78e-02	**0.97**

Table 5.3 | Standing wave in a PEC cavity: IMEX-HDG-Eul1 method. Maximum L^2-errors and convergence orders.

IMEX-HDG-RK2

We recall the formulation IMEX-HDG-RK2 method

$$\begin{cases} m\left(\dfrac{\boldsymbol{v}_h^{n+\frac{1}{2}} - \boldsymbol{v}_h^n}{\Delta t}, \boldsymbol{v}_h'\right) &= \alpha_1 \left(\mathbf{L}_h^{\mathcal{FI}}\left(\boldsymbol{v}_h^{n+\frac{1}{2}}, \boldsymbol{\Lambda}_h^{n+\frac{1}{2}}\right), \boldsymbol{v}_h'\right) \\ & + \alpha_2 \left(\mathbf{L}_h^{\mathcal{CO}}\left(\boldsymbol{v}_h^n, \boldsymbol{\Lambda}_h^n\right), \boldsymbol{v}_h'\right), \\ c\left(\boldsymbol{v}_h^{n+\frac{1}{2}}, \boldsymbol{\Lambda}_h^{n+\frac{1}{2}}, \boldsymbol{\eta}_h\right) &= 0, \\ m\left(\dfrac{\boldsymbol{v}_h^{n+1} - \boldsymbol{v}_h^n}{\Delta t}, \boldsymbol{v}_h'\right) &= \left(\mathbf{L}_h\left(\boldsymbol{v}_h^{n+\frac{1}{2}}, \boldsymbol{\Lambda}_h^{n+\frac{1}{2}}\right), \boldsymbol{v}_h'\right), \\ c\left(\boldsymbol{v}_h^{n+1}, \boldsymbol{\Lambda}_h^{n+1}, \boldsymbol{\eta}_h\right) &= 0, \end{cases}$$

for all test functions $(\boldsymbol{v}_h', \boldsymbol{\eta}_h)$ that belong to the space $\mathbb{V}_h \times \boldsymbol{M}_h$, where α_1 and α_2 are the coefficients of the butcher table for the fully implicit and explicit Runge-Kutta 2 respectively (see table 5.1). Then, fully discrete IMEX-HDG-RK2 scheme can be written as

$$\begin{cases} \mathbb{M}^{exp}\dfrac{\boldsymbol{v}_h^{n+\frac{1}{2}} - \boldsymbol{v}_h^n}{\Delta t} + \mathbb{M}^{imp}\dfrac{\boldsymbol{v}_h^{n+\frac{1}{2}} - \boldsymbol{v}_h^n}{\Delta t} &= -\alpha_2 \mathbb{D}^{exp}\boldsymbol{v}_h^n \\ &- \alpha_2 \mathbb{C}^{exp}\mathcal{A}_{HDG}\boldsymbol{\Lambda}_h^n \\ &- \alpha_1 \mathbb{D}^{imp}\boldsymbol{v}_h^{n+\frac{1}{2}} \\ &- \alpha_1 \mathbb{C}^{imp}\mathcal{A}_{HDG}\boldsymbol{\Lambda}_h^{n+\frac{1}{2}}, \\ \mathbb{G}\boldsymbol{\Lambda}_h^{n+\frac{1}{2}} &= -\mathbb{B}^{exp}\boldsymbol{v}_h^{n+\frac{1}{2}} - \mathbb{B}^{imp}\boldsymbol{v}_h^{n+\frac{1}{2}}, \\ \mathbb{M}\dfrac{\boldsymbol{v}_h^{n+1} - \boldsymbol{v}_h^n}{\Delta t} &= -\mathbb{D}\boldsymbol{v}_h^{n+\frac{1}{2}} - \mathbb{C}\mathcal{A}_{HDG}\boldsymbol{\Lambda}_h^{n+\frac{1}{2}}, \\ \mathbb{G}\boldsymbol{\Lambda}_h^n &= -\mathbb{B}\boldsymbol{v}_h^n. \end{cases} \tag{5.19}$$

After calculating $\boldsymbol{\Lambda}_h^n$ from the last equation of (5.19), the local problem for $\boldsymbol{v}_h^{n+\frac{1}{2}}$ is deduced from the first two equations as

- If $i \in \mathcal{CO}$

$$\begin{aligned} \mathbb{M}_{e_i}\frac{\boldsymbol{v}_{e_i}^{n+\frac{1}{2}} - \boldsymbol{v}_{e_i}^n}{\Delta t} &= -\alpha_2 \mathbb{D}_{e_i}\boldsymbol{v}_{e_i}^n - \alpha_2 \mathbb{C}_{e_i}\mathcal{A}_{HDG}^{e_i}\boldsymbol{\Lambda}^n \\ \Rightarrow \quad \boldsymbol{v}_{e_i}^{n+\frac{1}{2}} &= \boldsymbol{v}_{e_i}^n - \alpha_2 \Delta t \mathbb{M}_{e_i}^{-1}\left(\mathbb{D}_{e_i}\boldsymbol{v}_{e_i}^n + \mathbb{C}_{e_i}\mathcal{A}_{HDG}^{e_i}\boldsymbol{\Lambda}^n\right). \end{aligned} \tag{5.20}$$

- If $j \in \mathcal{FI}$

$$\begin{aligned} \mathbb{M}_{e_j}\frac{\boldsymbol{v}_{e_j}^{n+\frac{1}{2}} - \boldsymbol{v}_{e_j}^n}{\Delta t} &= -\alpha_1 \mathbb{D}_{e_j}\boldsymbol{v}_{e_j}^{n+\frac{1}{2}} - \alpha_1 \mathbb{C}_{e_j}\mathcal{A}_{HDG}^{e_j}\boldsymbol{\Lambda}^{n+\frac{1}{2}} \\ \Rightarrow \quad \left(\mathbb{M}_{e_j} + \alpha_1 \Delta t \mathbb{D}_{e_j}\right)\boldsymbol{v}_{e_j}^{n+\frac{1}{2}} &= \mathbb{M}_{e_j}\boldsymbol{v}_{e_j}^n - \alpha_1 \Delta t \mathbb{C}_{e_j}\mathcal{A}_{HDG}^{e_j}\boldsymbol{\Lambda}^{n+\frac{1}{2}} \\ \Rightarrow \quad \underbrace{\left(\frac{1}{\alpha_1 \Delta t}\mathbb{M}_{e_j} + \mathbb{D}_{e_j}\right)}_{\mathbb{A}_{e_j}}\boldsymbol{v}_{e_j}^{n+\frac{1}{2}} &= \frac{1}{\alpha_1 \Delta t}\mathbb{M}_{e_j}\boldsymbol{v}_{e_j}^n - \mathbb{C}_{e_j}\mathcal{A}_{HDG}^{e_j}\boldsymbol{\Lambda}^{n+\frac{1}{2}} \\ \Rightarrow \quad \boldsymbol{v}_{e_j}^{n+\frac{1}{2}} &= \mathbb{A}_{e_j}^{-1}\left(\frac{1}{\alpha_1 \Delta t}\mathbb{M}_{e_j}\boldsymbol{v}_{e_j}^n - \mathbb{C}_{e_j}\mathcal{A}_{HDG}^{e_j}\boldsymbol{\Lambda}^{n+\frac{1}{2}}\right). \end{aligned} \tag{5.21}$$

Then, the global problem for $\boldsymbol{\Lambda}_h^{n+\frac{1}{2}}$ is deduced from the second equation of (5.19) as

$$\begin{aligned} \sum_{l=1}^{|\mathcal{T}_h|}\left[\mathcal{A}_{HDG}^{e_l}\right]^T \mathbb{G}_{e_l}\mathcal{A}_{HDG}^{e_l}\boldsymbol{\Lambda}^{n+\frac{1}{2}} = &-\sum_{i=1}^{|\mathcal{CO}|}\left[\mathcal{A}_{HDG}^{e_i}\right]^T \mathbb{B}_{e_i}\boldsymbol{v}_{e_i}^{n+\frac{1}{2}} \\ &-\sum_{j=1}^{|\mathcal{FI}|}\left[\mathcal{A}_{HDG}^{e_j}\right]^T \mathbb{B}_{e_j}\boldsymbol{v}_{e_j}^{n+\frac{1}{2}}. \end{aligned} \tag{5.22}$$

Using (5.21) we can directly deduce that

$$\mathbb{Q}\boldsymbol{\Lambda}^{n+\frac{1}{2}} = -\sum_{i=1}^{|\mathcal{CO}|} \left[\mathcal{A}_{HDG}^{e_i}\right]^T \mathbb{B}_{e_i} \boldsymbol{v}_{e_i}^{n+\frac{1}{2}} - \frac{1}{\alpha_1 \Delta t} \sum_{j=1}^{|\mathcal{FI}|} \left[\mathcal{A}_{HDG}^{e_j}\right]^T \mathbb{B}_{e_j} \mathbb{A}_{e_j}^{-1} \mathbb{M}_{e_j} \boldsymbol{v}_{e_j}^{n}, \tag{5.23}$$

while

$$\mathbb{Q} = \mathbb{G} - \sum_{j=1}^{|\mathcal{FI}|} \left[\mathcal{A}_{HDG}^{e_j}\right]^T \mathbb{B}_{e_j} \mathbb{A}_{e_j}^{-1} \mathbb{C}_{e_j} \mathcal{A}_{HDG}^{e_j}. \tag{5.24}$$

Now, (5.22) gives globally the value of $\boldsymbol{\Lambda}_h^{n+\frac{1}{2}}$, and locally the value of $\boldsymbol{v}_h^{n+\frac{1}{2}}$ in the fine part using (5.21). Since (5.20) gives the value $\boldsymbol{v}_h^{n+\frac{1}{2}}$ on the coase part, we can calculate its value for the whole mesh. Finally we can find locally the solution $\boldsymbol{v}_h^{n+1}$ using the last equation in (5.10).

Remark 8. If we consider $\mathcal{FI} = \emptyset$ (*i.e.* $|\mathcal{FI}| = 0$), the global matrix $\mathbb{K}$ becomes equal to $\mathbb{G}$, which corresponds to the case of a fully explicit time scheme, and if $\mathcal{CO} = \emptyset$, *i.e.* , $|\mathcal{FI}| = |\mathcal{T}_h|$) we obtain

$$\mathbb{Q} = \mathbb{G} - \sum_{j=1}^{|\mathcal{T}_h|} \left[\mathcal{A}_{HDG}^{e_j}\right]^T \mathbb{B}_{e_j} \mathbb{A}_{e_j}^{-1} \mathbb{C}_{e_j} \mathcal{A}_{HDG}^{e_j},$$

which corresponds to the case of a fully implicit time scheme.

Fig. (5.5) shows the difference in sparsity for the global matrix $\mathbb{Q}$ between the explicit HDG, implicit HDG and IMEX-HDG-RK2 methods. We can see that, due to the IMEX scheme, we have a block-diagonal matrix corresponding to the degrees of freedom in the coarse part and a sparse matrix in the fine part while it is not the case for the fully implicit scheme. In particular, in comparison with the fully implicit scheme, we have a much cheaper global matrix to inverse at each time step with the IMEX-HDG-RK2 method.

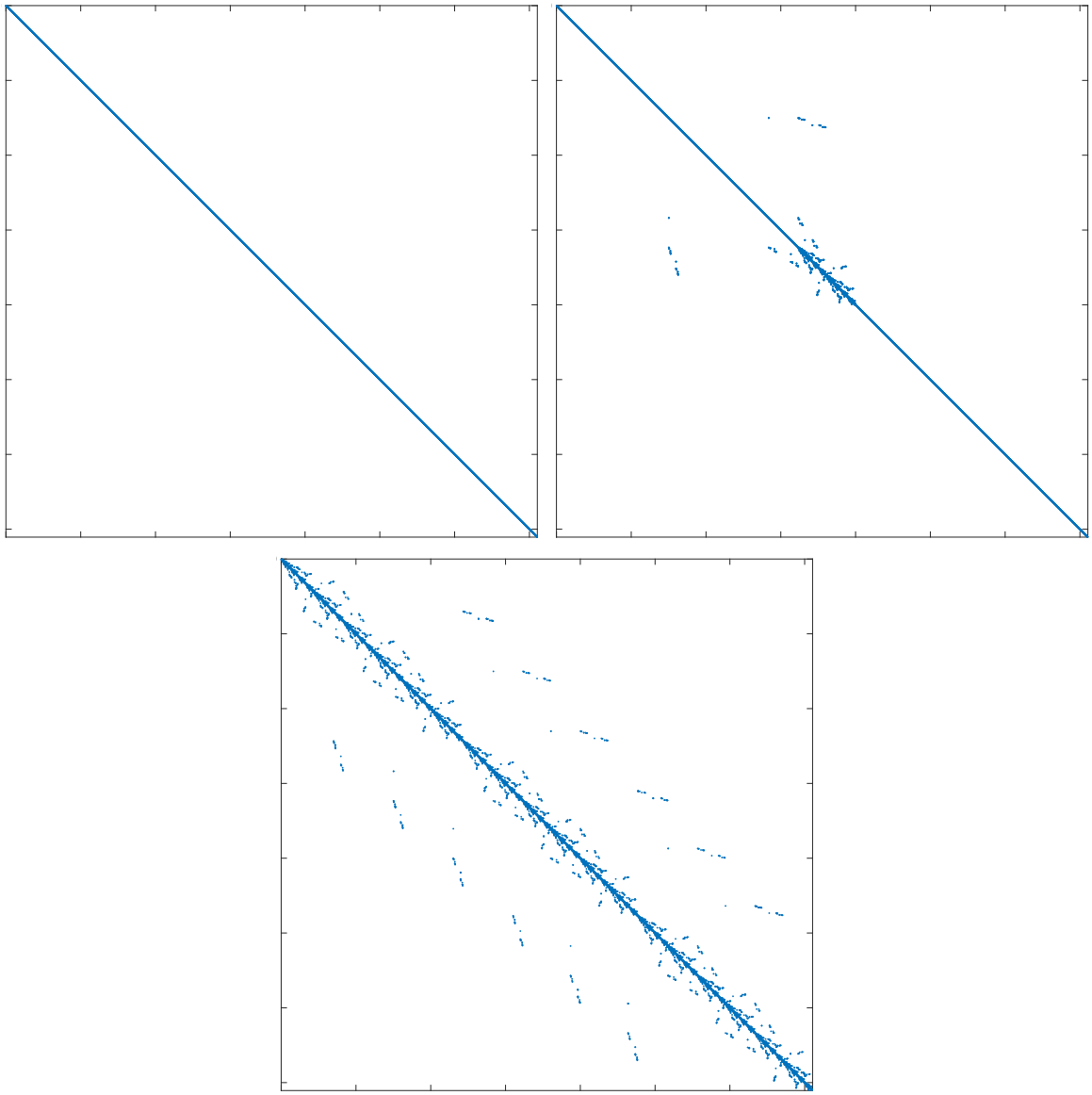

Figure 5.5 | The global matrix $\mathbb{Q}$ for explicit RK2, IMEX RK2 and fully implicit RK2 on Mesh 4 in Fig. (5.1).

Fig. 5.6 and 5.7 respectively show the time evolution of the E_z component at a fixed point in the mesh and the L^2-norm of the error for simulations that are based on Mesh 3 in Fig. 5.1. Fig. 5.8 and Tab. 5.4 are concerned with the numerical convergence of the IMEX-HDG-RK2 method.

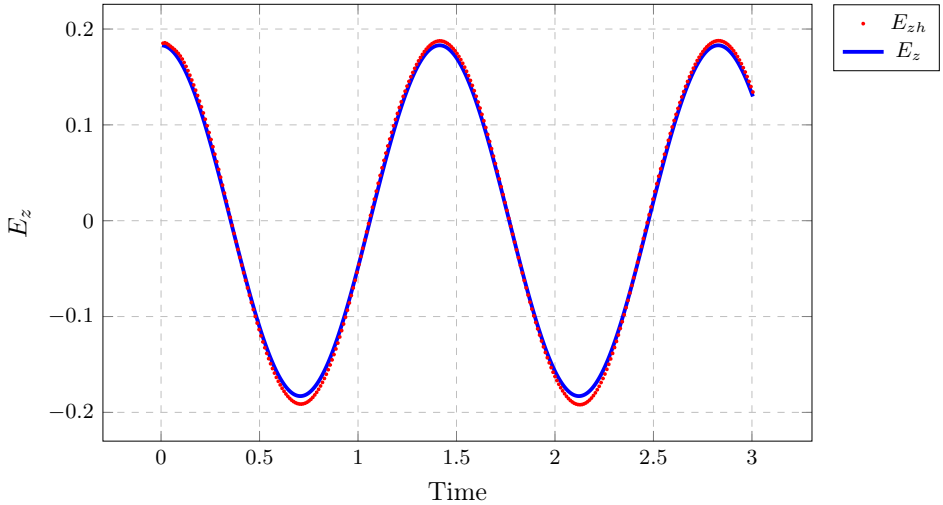

Figure 5.6 | Standing wave in a PEC cavity: IMEX-HDG-RK2 method. Time evolution of the exact and the numerical solution of E_z at a fixed point with a $\mathbb{P}_1$ interpolation using the 3rd mesh of Fig. 5.1

.

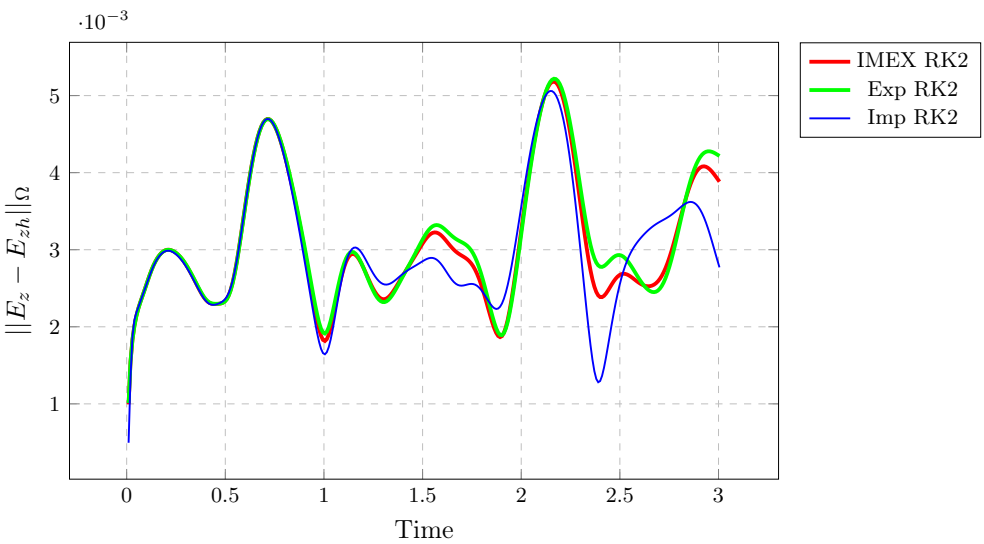

Figure 5.7 | Standing wave in a PEC cavity: IMEX-HDG-RK2 method. Time evolution of the L^2-norm of the error on E_{zh} for a $\mathbb{P}_1$ interpolation.

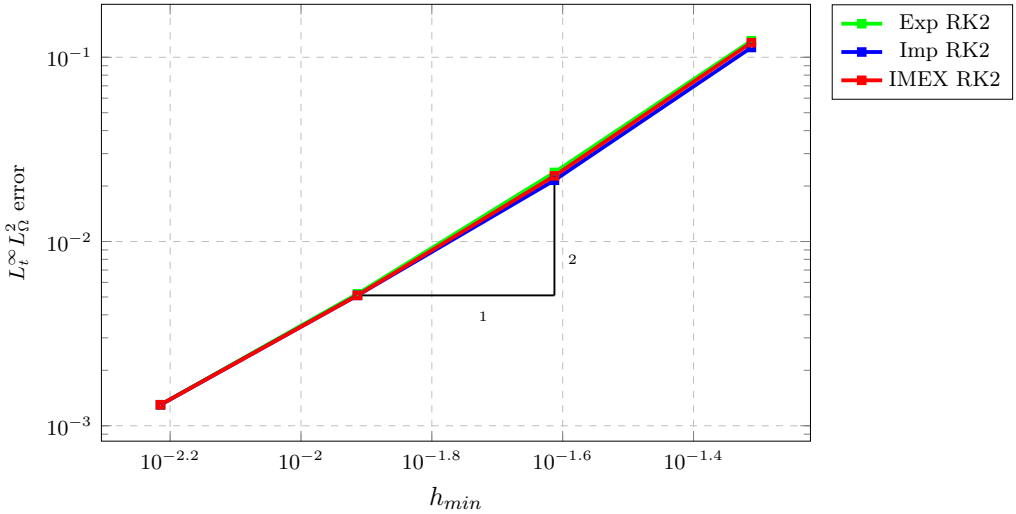

Figure 5.8 | Standing wave in a PEC cavity: IMEX-HDG-RK2 method. Numerical convergence.

P_k	Time scheme	Mesh	h_{min}	$\|\|Ez - Ez_h\|\|_{L_t^\infty L_\Omega^2}$ Error	order
P_1	Explicit RK2	1	4.88e-02	1.23e-01	**-**
		2	2.44e-02	2.37e-02	**2.37**
		3	1.22e-02	5.20e-03	**2.18**
		4	6.10e-03	1.30e-03	**2.00**
	Implicit RK2	1	4.88e-02	1.13e-01	**-**
		2	2.44e-02	2.15e-02	**2.39**
		3	1.22e-02	5.10e-03	**2.07**
		4	6.10e-03	1.30e-03	**2.00**
	IMEX RK2	1	4.88e-02	1.20e-01	**-**
		2	2.44e-02	2.27e-02	**2.40**
		3	1.22e-02	5.10e-03	**2.13**
		4	6.10e-03	1.30e-03	**2.00**

Table 5.4 | Standing wave in a PEC cavity: IMEX-HDG-RK2 method. Maximum L^2-errors and convergence orders.

Tab. 5.5 summarizes a first comparison in terms of CPU time between the three methods while considering a uniform mesh (Mesh 4), a P_1 interpolation and the same time step Δt for the three time stepping schemes. Simulations have been performed with MATLAB on a multi-core computer equipped with Intel(R) Xeon(R) CPU E5-1630 v3 @ 3.70GHz with 32Go of memory. The main

	Explicit RK2	IMEX RK2	Implicit RK2
CPU time	30 mn 11 s	30 mn 37 s	36 mn 23 s

Table 5.5 | Standing wave in a PEC cavity: IMEX-HDG-RK2 method. Computational time in seconds.

two causes for the modification of the CPU time are the time step chosen and the number of non zero elements in the global matrix we are inverting. Firstly, the time step chosen for the fully

explicit and the IMEX RK2 is the same in this case since $h_{\mathcal{T}_h^{CO}} = h$ so the very small modification in the CPU time between the fully explicit and the IMEX RK2 is due to the small modification of the number of non zero elements in the global HDG matrix for the IMEX RK2 time scheme representing the implicit zone in the mesh (see Fig. 5.5). On the other hand we can see a remarkable modification in the number of non zero elements in the global HDG matrix between the latter two time schemes and the fully implicit RK2. The fully implicit RK2 scheme is unconditionally stable so we can use an arbitrary time step to compute the solution, but to maintain the same error level we need to use the time step considered for the IMEX RK2 see Fig. 5.9.

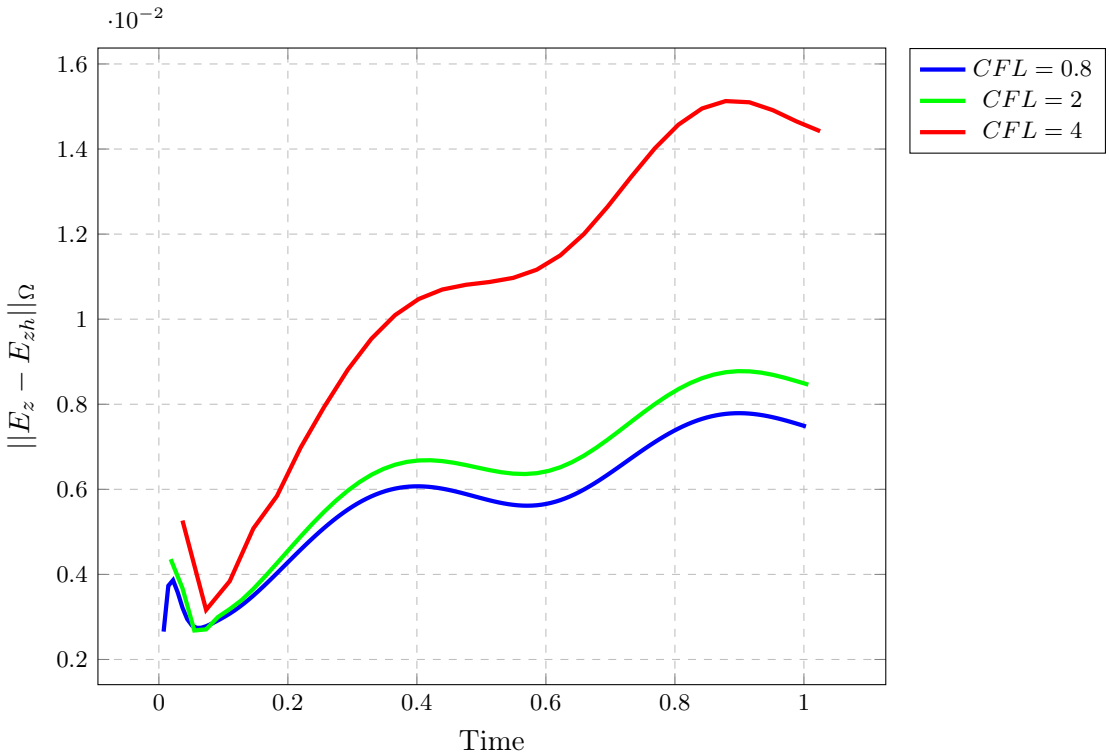

Figure 5.9 | Standing wave in a PEC cavity: IMEX-HDG-RK2 method. Time evolution of the L^2-norm of the error on E_{zh} for a $\mathbb{P}_1$ interpolation and different CFLs for the fully implicit RK2 time scheme.

IMEX-HDG-RK3

The fully discrete IMEX-HDG-RK3 scheme is given by the following steps

$$
\left\{
\begin{array}{rcl}
\mathbb{M}^{exp}\dfrac{\boldsymbol{v}_h^{n,1}-\boldsymbol{v}_h^{n}}{\Delta t}+\mathbb{M}^{imp}\dfrac{\boldsymbol{v}_h^{n,1}-\boldsymbol{v}_h^{n}}{\Delta t} & = & -\alpha\mathbb{D}^{imp}\boldsymbol{v}_h^{n,1}-\alpha\mathbb{C}^{imp}\mathcal{A}_{HDG}\boldsymbol{\Lambda}_h^{n,1},\\
\mathbb{G}\boldsymbol{\Lambda}_h^{n,1} & = & -\mathbb{B}^{exp}\boldsymbol{v}_h^{n,1}-\mathbb{B}^{imp}\boldsymbol{v}_h^{n,1},\\
\mathbb{M}^{exp}\dfrac{\boldsymbol{v}_h^{n,2}-\boldsymbol{v}_h^{n}}{\Delta t}+\mathbb{M}^{imp}\dfrac{\boldsymbol{v}_h^{n,2}-\boldsymbol{v}_h^{n}}{\Delta t} & = & \alpha\mathbb{D}^{imp}\boldsymbol{v}_h^{n,1}+\alpha\mathbb{C}^{imp}\mathcal{A}_{HDG}\boldsymbol{\Lambda}_h^{n,1}\\
 & - & \alpha\mathbb{D}^{imp}\boldsymbol{v}_h^{n,2}-\alpha\mathbb{C}^{imp}\mathcal{A}_{HDG}\boldsymbol{\Lambda}_h^{n,2},\\
\mathbb{G}\boldsymbol{\Lambda}_h^{n,2} & = & -\mathbb{B}^{exp}\boldsymbol{v}_h^{n,2}-\mathbb{B}^{imp}\boldsymbol{v}_h^{n,2},\\
\mathbb{M}^{exp}\dfrac{\boldsymbol{v}_h^{n,3}-\boldsymbol{v}_h^{n}}{\Delta t}+\mathbb{M}^{imp}\dfrac{\boldsymbol{v}_h^{n,3}-\boldsymbol{v}_h^{n}}{\Delta t} & = & -\mathbb{D}^{exp}\boldsymbol{v}_h^{n,2}-\mathbb{C}^{exp}\mathcal{A}_{HDG}\boldsymbol{\Lambda}_h^{n,2}\\
 & - & (1-\alpha)\mathbb{D}^{imp}\boldsymbol{v}_h^{n,2}\\
 & - & (1-\alpha)\mathbb{C}^{imp}\mathcal{A}_{HDG}\boldsymbol{\Lambda}_h^{n,2}\\
 & - & \alpha\mathbb{D}^{imp}\boldsymbol{v}_h^{n,3}-\alpha\mathbb{C}^{imp}\mathcal{A}_{HDG}\boldsymbol{\Lambda}_h^{n,3},\\
\mathbb{G}\boldsymbol{\Lambda}_h^{n,3} & = & -\mathbb{B}^{exp}\boldsymbol{v}_h^{n,3}-\mathbb{B}^{imp}\boldsymbol{v}_h^{n,3},\\
\mathbb{M}^{exp}\dfrac{\boldsymbol{v}_h^{n,4}-\boldsymbol{v}_h^{n}}{\Delta t}+\mathbb{M}^{imp}\dfrac{\boldsymbol{v}_h^{n,4}-\boldsymbol{v}_h^{n}}{\Delta t} & = & -\dfrac{1}{4}\mathbb{D}^{exp}\boldsymbol{v}_h^{n,2}-\dfrac{1}{4}\mathbb{C}^{exp}\mathcal{A}_{HDG}\boldsymbol{\Lambda}_h^{n,2}\\
 & - & \dfrac{1}{4}\mathbb{D}^{exp}\boldsymbol{v}_h^{n,3}-\dfrac{1}{4}\mathbb{C}^{exp}\mathcal{A}_{HDG}\boldsymbol{\Lambda}_h^{n,3}\\
 & - & \beta\mathbb{D}^{imp}\boldsymbol{v}_h^{n,1}-\beta\mathbb{C}^{imp}\mathcal{A}_{HDG}\boldsymbol{\Lambda}_h^{n,1}\\
 & - & \eta\mathbb{D}^{imp}\boldsymbol{v}_h^{n,2}-\eta\mathbb{C}^{imp}\mathcal{A}_{HDG}\boldsymbol{\Lambda}_h^{n,2}\\
 & - & \delta\mathbb{D}^{imp}\boldsymbol{v}_h^{n,3}\\
 & - & \delta\mathbb{C}^{imp}\mathcal{A}_{HDG}\boldsymbol{\Lambda}_h^{n,3}\\
 & - & \alpha\mathbb{D}^{imp}\boldsymbol{v}_h^{n,4}-\alpha\mathbb{C}^{imp}\mathcal{A}_{HDG}\boldsymbol{\Lambda}_h^{n,4},\\
\mathbb{G}\boldsymbol{\Lambda}_h^{n,4} & = & -\mathbb{B}^{exp}\boldsymbol{v}_h^{n,4}-\mathbb{B}^{imp}\boldsymbol{v}_h^{n,4},\\
\mathbb{M}\dfrac{\boldsymbol{v}_h^{n+1}-\boldsymbol{v}_h^{n}}{\Delta t} & = & -\dfrac{1}{6}\mathbb{D}\boldsymbol{v}_h^{n,2}-\dfrac{1}{6}\mathbb{C}\mathcal{A}_{HDG}\boldsymbol{\Lambda}_h^{n,2}\\
 & - & \dfrac{1}{6}\mathbb{D}\boldsymbol{v}_h^{n,3}-\dfrac{1}{6}\mathbb{C}\mathcal{A}_{HDG}\boldsymbol{\Lambda}_h^{n,3}\\
 & - & \dfrac{2}{3}\mathbb{D}\boldsymbol{v}_h^{n,4}-\dfrac{2}{3}\mathbb{C}\mathcal{A}_{HDG}\boldsymbol{\Lambda}_h^{n,4},\\
\mathbb{G}\boldsymbol{\Lambda}_h^{n} & = & -\mathbb{B}\boldsymbol{v}_h^{n},
\end{array}
\right.
\tag{5.25}
$$

where α, η and β are defined in Table 5.2 and $\delta = (\frac{1}{2}-\beta-\eta-\alpha)$. After calculating $\boldsymbol{\Lambda}_h^n$ from the last equation of (5.25), the local problem for $\boldsymbol{v}_h^{n,1}$ is deduced from the first two equations as

- If $i \in \mathcal{CO}$

$$
\begin{array}{rc}
 & \mathbb{M}_{e_i}\dfrac{\boldsymbol{v}_{e_i}^{n,1}-\boldsymbol{v}_{e_i}^{n}}{\Delta t}=0\\
\Rightarrow & \boldsymbol{v}_{e_i}^{n,1}=\boldsymbol{v}_{e_i}^{n}.
\end{array}
\tag{5.26}
$$

- If $j \in \mathcal{FI}$

$$
\begin{aligned}
& \mathbb{M}_{e_j} \frac{\boldsymbol{v}_{e_j}^{n,1} - \boldsymbol{v}_{e_j}^{n}}{\Delta t} = -\alpha \mathbb{D}_{e_j} \boldsymbol{v}_{e_j}^{n,1} - \alpha \mathbb{C}_{e_j} \mathcal{A}_{HDG}^{e_j} \boldsymbol{\Lambda}^{n,1} \\
\Rightarrow \quad & \left(\mathbb{M}_{e_j} + \alpha \Delta t \mathbb{D}_{e_j} \right) \boldsymbol{v}_{e_j}^{n,1} = \mathbb{M}_{e_j} \boldsymbol{v}_{e_j}^{n} - \alpha \Delta t \mathbb{C}_{e_j} \mathcal{A}_{HDG}^{e_j} \boldsymbol{\Lambda}^{n,1} \\
\Rightarrow \quad & \underbrace{\left(\frac{1}{\alpha \Delta t} \mathbb{M}_{e_j} + \mathbb{D}_{e_j} \right)}_{\mathbb{A}_{e_j}} \boldsymbol{v}_{e_j}^{n,1} = \frac{1}{\alpha \Delta t} \mathbb{M}_{e_j} \boldsymbol{v}_{e_j}^{n} - \mathbb{C}_{e_j} \mathcal{A}_{HDG}^{e_j} \boldsymbol{\Lambda}^{n,1} \\
\Rightarrow \quad & \boldsymbol{v}_{e_j}^{n,1} = \mathbb{A}_{e_j}^{-1} \left(\frac{1}{\alpha \Delta t} \mathbb{M}_{e_j} \boldsymbol{v}_{e_j}^{n} - \mathbb{C}_{e_j} \mathcal{A}_{HDG}^{e_j} \boldsymbol{\Lambda}^{n,1} \right).
\end{aligned}
\tag{5.27}
$$

Then, the global problem for $\boldsymbol{\Lambda}_h^{n,1}$ is deduced from the second equation of (5.25) as

$$
\begin{aligned}
\sum_{l=1}^{|\mathcal{T}_h|} \left[\mathcal{A}_{HDG}^{e_l} \right]^T \mathbb{G}_{e_l} \mathcal{A}_{HDG}^{e_l} \boldsymbol{\Lambda}^{n,1} = & - \sum_{i=1}^{|\mathcal{CO}|} \left[\mathcal{A}_{HDG}^{e_i} \right]^T \mathbb{B}_{e_i} \boldsymbol{v}_{e_i}^{n,1} \\
& - \sum_{j=1}^{|\mathcal{FI}|} \left[\mathcal{A}_{HDG}^{e_j} \right]^T \mathbb{B}_{e_j} \boldsymbol{v}_{e_j}^{n,1}.
\end{aligned}
\tag{5.28}
$$

Using (5.26) and (5.27) we can directly deduce that

$$
\mathbb{Q} \boldsymbol{\Lambda}^{n,1} = - \sum_{i=1}^{|\mathcal{CO}|} \left[\mathcal{A}_{HDG}^{e_i} \right]^T \mathbb{B}_{e_i} \boldsymbol{v}_{e_i}^{n} - \frac{1}{\alpha \Delta t} \sum_{j=1}^{|\mathcal{FI}|} \left[\mathcal{A}_{HDG}^{e_j} \right]^T \mathbb{B}_{e_j} \mathbb{A}_{e_j}^{-1} \mathbb{M}_{e_j} \boldsymbol{v}_{e_j}^{n},
\tag{5.29}
$$

while

$$
\mathbb{Q} = \mathbb{G} - \sum_{j=1}^{|\mathcal{FI}|} \left[\mathcal{A}_{HDG}^{e_j} \right]^T \mathbb{B}_{e_j} \mathbb{A}_{e_j}^{-1} \mathbb{C}_{e_j} \mathcal{A}_{HDG}^{e_j}.
\tag{5.30}
$$

The local problem for $\boldsymbol{v}_h^{n,2}$ is deduced from the second two equations as

- If $i \in \mathcal{CO}$

$$
\begin{aligned}
& \mathbb{M}_{e_i} \frac{\boldsymbol{v}_{e_i}^{n,2} - \boldsymbol{v}_{e_i}^{n}}{\Delta t} = 0 \\
\Rightarrow \quad & \boldsymbol{v}_{e_i}^{n,2} = \boldsymbol{v}_{e_i}^{n}.
\end{aligned}
\tag{5.31}
$$

- If $j \in \mathcal{FI}$

$$
\begin{aligned}
\mathbb{M}_{e_j} \frac{\boldsymbol{v}_{e_j}^{n,2} - \boldsymbol{v}_{e_j}^{n}}{\Delta t} &= \alpha \mathbb{D}_{e_j} \boldsymbol{v}_{e_j}^{n,1} + \alpha \mathbb{C}_{e_j} \mathcal{A}_{HDG}^{e_j} \boldsymbol{\Lambda}^{n,1} \\
&- \alpha \mathbb{D}_{e_j} \boldsymbol{v}_{e_j}^{n,2} - \alpha \mathbb{C}_{e_j} \mathcal{A}_{HDG}^{e_j} \boldsymbol{\Lambda}^{n,2} \\
\Rightarrow \quad \mathbb{A}_{e_j} \boldsymbol{v}_{e_j}^{n,2} &= \frac{1}{\alpha \Delta t} \mathbb{M}_{e_j} \boldsymbol{v}_{e_j}^{n} + \mathbb{D}_{e_j} \boldsymbol{v}_{e_j}^{n,1} \\
&+ \mathbb{C}_{e_j} \mathcal{A}_{HDG}^{e_j} \boldsymbol{\Lambda}^{n,1} - \mathbb{C}_{e_j} \mathcal{A}_{HDG}^{e_j} \boldsymbol{\Lambda}^{n,2} \\
\Rightarrow \quad \boldsymbol{v}_{e_j}^{n,2} = \mathbb{A}_{e_j}^{-1} \Bigg(& \frac{1}{\alpha \Delta t} \mathbb{M}_{e_j} \boldsymbol{v}_{e_j}^{n} + \mathbb{D}_{e_j} \boldsymbol{v}_{e_j}^{n,1} + \mathbb{C}_{e_j} \mathcal{A}_{HDG}^{e_j} \boldsymbol{\Lambda}^{n,1} \\
& - \mathbb{C}_{e_j} \mathcal{A}_{HDG}^{e_j} \boldsymbol{\Lambda}^{n,2} \Bigg).
\end{aligned}
\tag{5.32}
$$

Then, the global problem for $\boldsymbol{\Lambda}_h^{n,2}$ is deduced from the fourth equation of (5.25) as

$$\begin{aligned}\sum_{l=1}^{|\mathcal{T}_h|} \left[\mathcal{A}_{HDG}^{e_l}\right]^T \mathbb{G}_{e_l} \mathcal{A}_{HDG}^{e_l} \boldsymbol{\Lambda}^{n,2} = &- \sum_{i=1}^{|\mathcal{CO}|} \left[\mathcal{A}_{HDG}^{e_i}\right]^T \mathbb{B}_{e_i} \boldsymbol{v}_{e_i}^{n,2} \\ &- \sum_{j=1}^{|\mathcal{FI}|} \left[\mathcal{A}_{HDG}^{e_j}\right]^T \mathbb{B}_{e_j} \boldsymbol{v}_{e_j}^{n,2}.\end{aligned} \tag{5.33}$$

Using (5.31) and (5.32) we can directly deduce that

$$\begin{aligned}\mathbb{Q}\boldsymbol{\Lambda}^{n,2} \quad = \quad &- \sum_{i=1}^{|\mathcal{CO}|} \left[\mathcal{A}_{HDG}^{e_i}\right]^T \mathbb{B}_{e_i} \boldsymbol{v}_{e_i}^{n} \\ &- \sum_{j=1}^{|\mathcal{FI}|} \left[\mathcal{A}_{HDG}^{e_j}\right]^T \mathbb{B}_{e_j} \mathbb{A}_{e_j}^{-1} \\ &\left(\frac{1}{\alpha\Delta t}\mathbb{M}_{e_j}\boldsymbol{v}_{e_j}^{n} + \mathbb{D}_{e_j}\boldsymbol{v}_{e_j}^{n,1} + \mathbb{C}_{e_j}\mathcal{A}_{HDG}^{e_j}\boldsymbol{\Lambda}^{n,1}\right).\end{aligned} \tag{5.34}$$

The local problem for $\boldsymbol{v}_h^{n,3}$ is deduced from the third two equations as

- If $i \in \mathcal{CO}$

$$\begin{aligned}\mathbb{M}_{e_i}\frac{\boldsymbol{v}_{e_i}^{n,3} - \boldsymbol{v}_{e_i}^{n}}{\Delta t} &= -\mathbb{D}_{e_j}\boldsymbol{v}_{e_j}^{n,2} - \mathbb{C}_{e_j}\mathcal{A}_{HDG}^{e_j}\boldsymbol{\Lambda}^{n,2} \\ \Rightarrow \quad \boldsymbol{v}_{e_i}^{n,3} &= \boldsymbol{v}_{e_i}^{n} - \Delta t \mathbb{M}_{e_i}^{-1}\left(\mathbb{D}_{e_j}\boldsymbol{v}_{e_j}^{n,2} + \mathbb{C}_{e_j}\mathcal{A}_{HDG}^{e_j}\boldsymbol{\Lambda}^{n,2}\right).\end{aligned} \tag{5.35}$$

- If $j \in \mathcal{FI}$

$$\begin{aligned}\mathbb{M}_{e_j}\frac{\boldsymbol{v}_{e_j}^{n,3} - \boldsymbol{v}_{e_j}^{n}}{\Delta t} \quad &= \quad -(1-\alpha)\mathbb{D}_{e_j}\boldsymbol{v}_{e_j}^{n,2} \\ &\quad -(1-\alpha)\mathbb{C}_{e_j}\mathcal{A}_{HDG}^{e_j}\boldsymbol{\Lambda}^{n,2} \\ &\quad -\alpha\mathbb{D}_{e_j}\boldsymbol{v}_{e_j}^{n,3} - \alpha\mathbb{C}_{e_j}\mathcal{A}_{HDG}^{e_j}\boldsymbol{\Lambda}^{n,3} \\ \Rightarrow \qquad \mathbb{A}_{e_j}\boldsymbol{v}_{e_j}^{n,3} \quad &= \quad \frac{1}{\alpha\Delta t}\mathbb{M}_{e_j}\boldsymbol{v}_{e_j}^{n} - \frac{(1-\alpha)}{\alpha}\mathbb{D}_{e_j}\boldsymbol{v}_{e_j}^{n,2} \\ &\quad -\frac{(1-\alpha)}{\alpha}\mathbb{C}_{e_j}\mathcal{A}_{HDG}^{e_j}\boldsymbol{\Lambda}^{n,2} - \mathbb{C}_{e_j}\mathcal{A}_{HDG}^{e_j}\boldsymbol{\Lambda}^{n,3} \\ \Rightarrow \qquad \boldsymbol{v}_{e_j}^{n,3} \quad &= \quad \mathbb{A}_{e_j}^{-1}\Bigg(\frac{1}{\alpha\Delta t}\mathbb{M}_{e_j}\boldsymbol{v}_{e_j}^{n} - \frac{(1-\alpha)}{\alpha}\mathbb{D}_{e_j}\boldsymbol{v}_{e_j}^{n,2} \\ &\qquad -\frac{(1-\alpha)}{\alpha}\mathbb{C}_{e_j}\mathcal{A}_{HDG}^{e_j}\boldsymbol{\Lambda}^{n,2} \\ &\qquad -\mathbb{C}_{e_j}\mathcal{A}_{HDG}^{e_j}\boldsymbol{\Lambda}^{n,3}\Bigg).\end{aligned} \tag{5.36}$$

Then, the global problem for $\boldsymbol{\Lambda}_h^{n,3}$ is deduced from the sixth equation of (5.25) as

$$\begin{aligned}\sum_{l=1}^{|\mathcal{T}_h|}\left[\mathcal{A}_{HDG}^{e_l}\right]^T\mathbb{G}_{e_l}\mathcal{A}_{HDG}^{e_l}\boldsymbol{\Lambda}^{n,3} = &-\sum_{i=1}^{|\mathcal{CO}|}\left[\mathcal{A}_{HDG}^{e_i}\right]^T\mathbb{B}_{e_i}\boldsymbol{v}_{e_i}^{n,3}\\ &-\sum_{j=1}^{|\mathcal{FI}|}\left[\mathcal{A}_{HDG}^{e_j}\right]^T\mathbb{B}_{e_j}\boldsymbol{v}_{e_j}^{n,3}.\end{aligned} \tag{5.37}$$

Using (5.35) and (5.36) we can directly deduce that

$$\begin{aligned}\mathbb{Q}\boldsymbol{\Lambda}^{n,3} = &-\sum_{i=1}^{|\mathcal{CO}|}\left[\mathcal{A}_{HDG}^{e_i}\right]^T\mathbb{B}_{e_i}\left[\boldsymbol{v}_{e_i}^{n}-\Delta t\mathbb{M}_{e_i}^{-1}\left(\mathbb{D}_{e_j}\boldsymbol{v}_{e_j}^{n,2}+\mathbb{C}_{e_j}\mathcal{A}_{HDG}^{e_j}\boldsymbol{\Lambda}^{n,2}\right)\right]\\ &-\sum_{j=1}^{|\mathcal{FI}|}\left[\mathcal{A}_{HDG}^{e_j}\right]^T\mathbb{B}_{e_j}\mathbb{A}_{e_j}^{-1}\Bigg(\frac{1}{\alpha\Delta t}\mathbb{M}_{e_j}\boldsymbol{v}_{e_j}^{n}-\frac{(1-\alpha)}{\alpha}\mathbb{D}_{e_j}\boldsymbol{v}_{e_j}^{n,2}\\ &\qquad-\frac{(1-\alpha)}{\alpha}\mathbb{C}_{e_j}\mathcal{A}_{HDG}^{e_j}\boldsymbol{\Lambda}^{n,2}\\ &\qquad-\mathbb{C}_{e_j}\mathcal{A}_{HDG}^{e_j}\boldsymbol{\Lambda}^{n,3}\Bigg).\end{aligned} \tag{5.38}$$

The local problem for $\boldsymbol{v}_h^{n,4}$ is deduced from the fourth two equations as

- If $i\in\mathcal{CO}$

$$\begin{aligned}\mathbb{M}_{e_i}\frac{\boldsymbol{v}_{e_i}^{n,4}-\boldsymbol{v}_{e_i}^{n}}{\Delta t} &= -\frac{1}{4}\mathbb{D}_{e_j}\boldsymbol{v}_{e_j}^{n,2}-\frac{1}{4}\mathbb{C}_{e_j}\mathcal{A}_{HDG}^{e_j}\boldsymbol{\Lambda}^{n,2}\\ &\quad-\frac{1}{4}\mathbb{D}_{e_j}\boldsymbol{v}_{e_j}^{n,3}-\frac{1}{4}\mathbb{C}_{e_j}\mathcal{A}_{HDG}^{e_j}\boldsymbol{\Lambda}^{n,3}\\ \Rightarrow\quad \boldsymbol{v}_{e_i}^{n,3} &= \boldsymbol{v}_{e_i}^{n}-\frac{\Delta t}{4}\mathbb{M}_{e_i}^{-1}\Bigg(\mathbb{D}_{e_j}\boldsymbol{v}_{e_j}^{n,2}+\mathbb{C}_{e_j}\mathcal{A}_{HDG}^{e_j}\boldsymbol{\Lambda}^{n,2}+\mathbb{D}_{e_j}\boldsymbol{v}_{e_j}^{n,3}\\ &\qquad+\mathbb{C}_{e_j}\mathcal{A}_{HDG}^{e_j}\boldsymbol{\Lambda}^{n,3}\Bigg)\end{aligned} \tag{5.39}$$

- If $j \in \mathcal{FI}$

$$
\begin{aligned}
\mathbb{M}_{e_j}\frac{\boldsymbol{v}_{e_j}^{n,4}-\boldsymbol{v}_{e_j}^{n}}{\Delta t} &= -\beta\mathbb{D}_{e_j}\boldsymbol{v}_{e_j}^{n,1}-\beta\mathbb{C}_{e_j}\mathcal{A}_{HDG}^{e_j}\boldsymbol{\Lambda}^{n,1}\\
&\quad -\eta\mathbb{D}_{e_j}\boldsymbol{v}_{e_j}^{n,2}-\eta\mathbb{C}_{e_j}\mathcal{A}_{HDG}^{e_j}\boldsymbol{\Lambda}^{n,2}\\
&\quad -\delta\mathbb{D}_{e_j}\boldsymbol{v}_{e_j}^{n,3}-\delta\mathbb{C}_{e_j}\mathcal{A}_{HDG}^{e_j}\boldsymbol{\Lambda}^{n,3}\\
&\quad -\alpha\mathbb{D}_{e_j}\boldsymbol{v}_{e_j}^{n,4}-\alpha\mathbb{C}_{e_j}\mathcal{A}_{HDG}^{e_j}\boldsymbol{\Lambda}^{n,4}\\
\Rightarrow \qquad \mathbb{A}_{e_j}\boldsymbol{v}_{e_j}^{n,4} &= \frac{1}{\alpha\Delta t}\mathbb{M}_{e_j}\boldsymbol{v}_{e_j}^{n}-\frac{\beta}{\alpha}\mathbb{D}_{e_j}\boldsymbol{v}_{e_j}^{n,1}\\
&\quad -\frac{\beta}{\alpha}\mathbb{C}_{e_j}\mathcal{A}_{HDG}^{e_j}\boldsymbol{\Lambda}^{n,1}\\
&\quad -\frac{\eta}{\alpha}\mathbb{D}_{e_j}\boldsymbol{v}_{e_j}^{n,2}-\frac{\eta}{\alpha}\mathbb{C}_{e_j}\mathcal{A}_{HDG}^{e_j}\boldsymbol{\Lambda}^{n,2}\\
&\quad -\frac{\delta}{\alpha}\mathbb{D}_{e_j}\boldsymbol{v}_{e_j}^{n,3}--\frac{\delta}{\alpha}\mathbb{C}_{e_j}\mathcal{A}_{HDG}^{e_j}\boldsymbol{\Lambda}^{n,3}\\
&\quad -\mathbb{C}_{e_j}\mathcal{A}_{HDG}^{e_j}\boldsymbol{\Lambda}^{n,4}\\
\Rightarrow \qquad \boldsymbol{v}_{e_j}^{n,4} &= \mathbb{A}_{e_j}^{-1}\Bigg(\frac{1}{\alpha\Delta t}\mathbb{M}_{e_j}\boldsymbol{v}_{e_j}^{n}-\frac{\beta}{\alpha}\mathbb{D}_{e_j}\boldsymbol{v}_{e_j}^{n,1}\\
&\quad -\frac{\beta}{\alpha}\mathbb{C}_{e_j}\mathcal{A}_{HDG}^{e_j}\boldsymbol{\Lambda}^{n,1}\\
&\quad -\frac{\eta}{\alpha}\mathbb{D}_{e_j}\boldsymbol{v}_{e_j}^{n,2}-\frac{\eta}{\alpha}\mathbb{C}_{e_j}\mathcal{A}_{HDG}^{e_j}\boldsymbol{\Lambda}^{n,2}\\
&\quad -\frac{\delta}{\alpha}\mathbb{D}_{e_j}\boldsymbol{v}_{e_j}^{n,3}-\frac{\delta}{\alpha}\mathbb{C}_{e_j}\mathcal{A}_{HDG}^{e_j}\boldsymbol{\Lambda}^{n,3}\\
&\quad -\mathbb{C}_{e_j}\mathcal{A}_{HDG}^{e_j}\boldsymbol{\Lambda}^{n,4}\Bigg).
\end{aligned}
\tag{5.40}
$$

Then, the global problem for $\boldsymbol{\Lambda}_h^{n,4}$ is deduced from the eighth equation of (5.25) as

$$
\begin{aligned}
\sum_{l=1}^{|\mathcal{T}_h|}\left[\mathcal{A}_{HDG}^{e_l}\right]^T\mathbb{G}_{e_l}\mathcal{A}_{HDG}^{e_l}\boldsymbol{\Lambda}^{n,4} = &-\sum_{i=1}^{|\mathcal{CO}|}\left[\mathcal{A}_{HDG}^{e_i}\right]^T\mathbb{B}_{e_i}\boldsymbol{v}_{e_i}^{n,4}\\
&-\sum_{j=1}^{|\mathcal{FI}|}\left[\mathcal{A}_{HDG}^{e_j}\right]^T\mathbb{B}_{e_j}\boldsymbol{v}_{e_j}^{n,4}.
\end{aligned}
\tag{5.41}
$$

Using (5.39) and (5.40) we can directly deduce that

$$
\begin{aligned}
\mathbb{Q}\boldsymbol{\Lambda}^{n,4} \quad = & -\sum_{i=1}^{|\mathcal{CO}|} \left[\mathcal{A}_{HDG}^{e_i}\right]^T \\
& \mathbb{B}_{e_i}\Bigg[\boldsymbol{\upsilon}_{e_i}^n - \frac{\Delta t}{4}\mathbb{M}_{e_i}^{-1}\Bigg(\mathbb{D}_{e_j}\boldsymbol{\upsilon}_{e_j}^{n,2} + \mathbb{C}_{e_j}\mathcal{A}_{HDG}^{e_j}\boldsymbol{\Lambda}^{n,2} \\
& \qquad + \mathbb{D}_{e_j}\boldsymbol{\upsilon}_{e_j}^{n,3} + \mathbb{C}_{e_j}\mathcal{A}_{HDG}^{e_j}\boldsymbol{\Lambda}^{n,3}\Bigg)\Bigg] \\
& -\sum_{j=1}^{|\mathcal{FI}|} \left[\mathcal{A}_{HDG}^{e_j}\right]^T \mathbb{B}_{e_j}\mathbb{A}_{e_j}^{-1}\Bigg(\frac{1}{\alpha\Delta t}\mathbb{M}_{e_j}\boldsymbol{\upsilon}_{e_j}^n - \frac{\beta}{\alpha}\mathbb{D}_{e_j}\boldsymbol{\upsilon}_{e_j}^{n,1} \\
& \qquad - \frac{\beta}{\alpha}\mathbb{C}_{e_j}\mathcal{A}_{HDG}^{e_j}\boldsymbol{\Lambda}^{n,1} \\
& \qquad - \frac{\eta}{\alpha}\mathbb{D}_{e_j}\boldsymbol{\upsilon}_{e_j}^{n,2} - \frac{\eta}{\alpha}\mathbb{C}_{e_j}\mathcal{A}_{HDG}^{e_j}\boldsymbol{\Lambda}^{n,2} \\
& \qquad - \frac{\delta}{\alpha}\mathbb{D}_{e_j}\boldsymbol{\upsilon}_{e_j}^{n,3} \\
& \qquad - \frac{\delta}{\alpha}\mathbb{C}_{e_j}\mathcal{A}_{HDG}^{e_j}\boldsymbol{\Lambda}^{n,3} \\
& \qquad - \mathbb{C}_{e_j}\mathcal{A}_{HDG}^{e_j}\boldsymbol{\Lambda}^{n,4}\Bigg).
\end{aligned}
\tag{5.42}
$$

To validate that the HDG-IMEX-RK3 is a third order accurate, we must consider a $\mathbb{P}_2$ interpolation since the HDG discretization is of order $k+1$ in space. Tab. 5.6 summarizes a first comparison in terms of CPU time between the three methods while considering a uniform mesh (Mesh 4), a P_2 interpolation and the same time step Δt for the three time stepping schemes. Fig. 5.10 and 5.11 respectively show the time evolution of the E_z component at a fixed point in the mesh and the L^2-norm of the error for simulations that are based on Mesh 4 in Fig. 5.1. Fig. 5.12 and Tab. 5.7 are concerned with the numerical convergence of the IMEX-HDG-RK3 method.

	Explicit RK3	IMEX RK3	Implicit RK3
CPU time	1 h 8 mn	1 h 20 mn	2 h 6 mn

Table 5.6 | Standing wave in a PEC cavity: IMEX-HDG-RK3 method. Computational time in seconds.

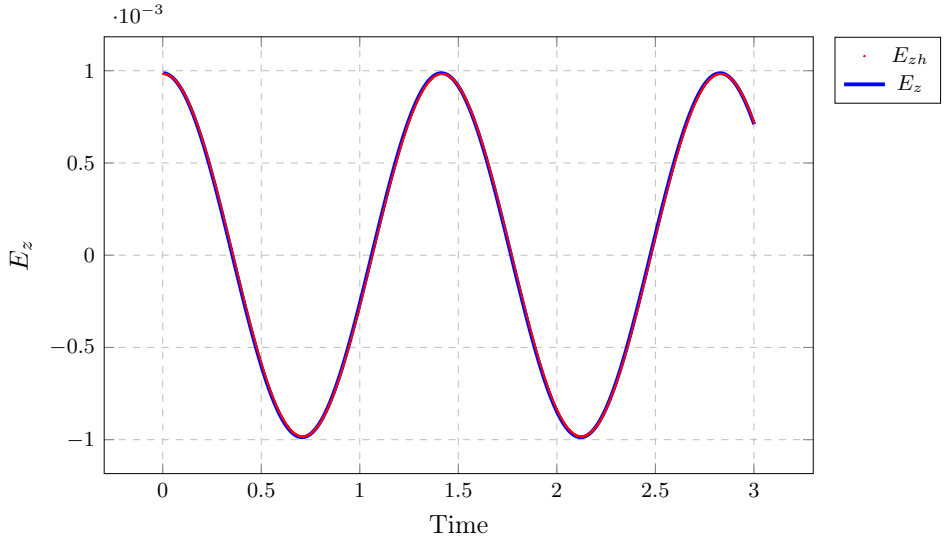

Figure 5.10 | Standing wave in a PEC cavity: IMEX-HDG-RK3 method. Time evolution of the exact and the numerical solution of E_z at a fixed point with a $\mathbb{P}_2$ interpolation using the 4th mesh of Fig. 5.1

.

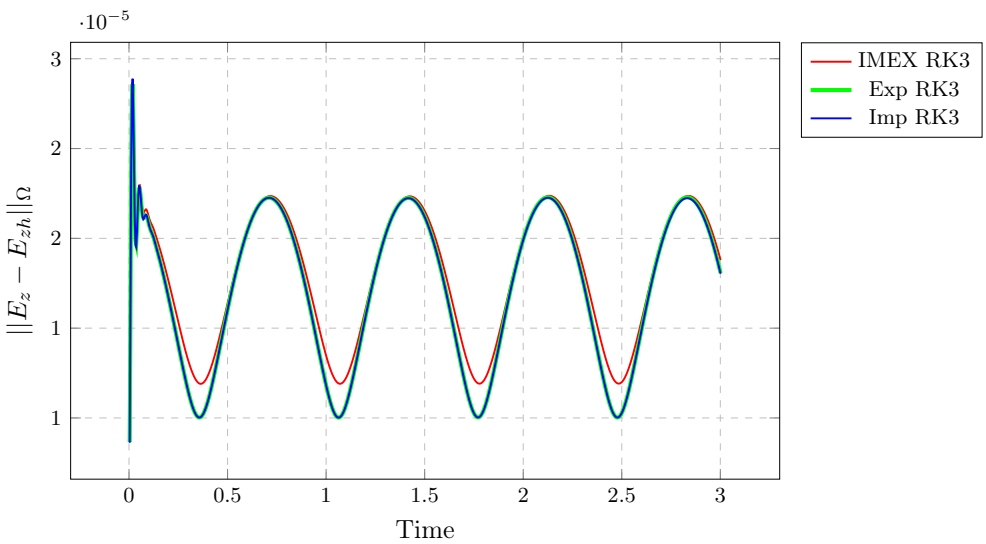

Figure 5.11 | Standing wave in a PEC cavity: IMEX-HDG-RK3 method. Time evolution of the L^2-norm of the error on E_{zh} for a $\mathbb{P}_2$ interpolation.

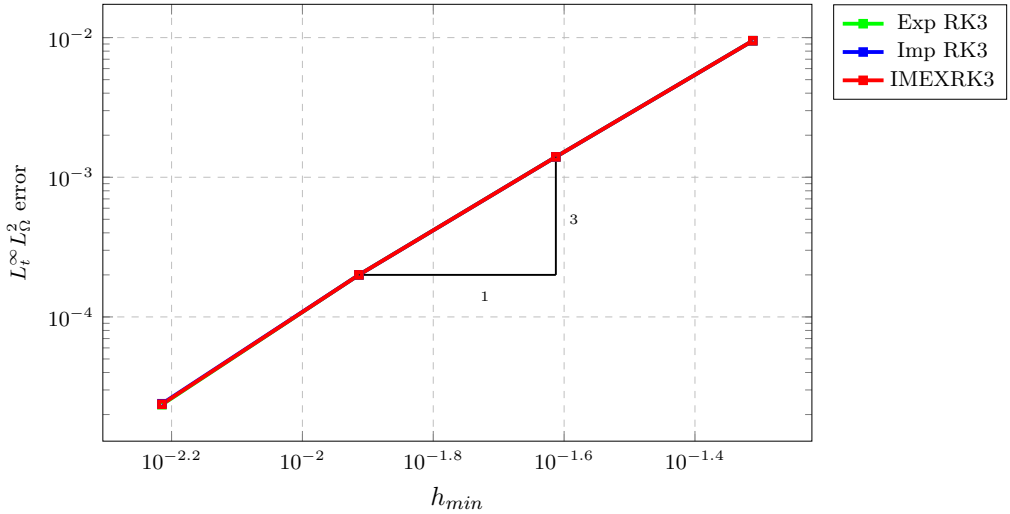

Figure 5.12 | Standing wave in a PEC cavity: IMEX-HDG-RK3 method. Numerical convergence.

P_k	Time scheme	CFL	h_{min}	$\|\|Ez - Ez_h\|\|_{L_t^\infty L_\Omega^2}$ Error	order
P_2	Explicit RK3	0.6	4.88e-02	9.50e-03	**-**
			2.44e-02	1.40e-03	**2.76**
			1.22e-02	2.00e-04	**2.81**
			6.10e-03	2.35e-05	**3.09**
	Implicit RK3	0.6	4.88e-02	9.50e-03	**-**
			2.44e-02	1.40e-03	**2.76**
			1.22e-02	2.00e-04	**2.81**
			6.10e-03	2.39e-05	**3.06**
	IMEX RK3	0.6	4.88e-02	9.50e-03	**-**
			2.44e-02	1.40e-03	**2.76**
			1.22e-02	2.00e-04	**2.81**
			6.10e-03	2.37e-05	**3.07**

Table 5.7 | Standing wave in a PEC cavity: IMEX-HDG-RK3 method. Maximum L^2-errors and convergence orders.

5.4.2 Propagation of a standing wave in a PEC disc sector

We here again consider a model problem for which an analytical solution is available and that consists in the propagation of a standing wave in a PEC disc sector (see [54] for details). The domain of computation is defined by

$$\Omega_\alpha = \{\boldsymbol{x} = (r\cos\theta, r\sin\theta) \in \mathbb{R}^2\,;\, |x_1| \leq 1, |x_2| \leq 1, 0 \leq \theta \leq \frac{\pi}{\alpha}\},$$

with perfectly metallic walls, while $0 < \alpha < \frac{1}{2}$. The electric permittivity and the magnetic permeability are set to the constant vacuum values. By imposing a source current $J(\boldsymbol{x}, t) = \frac{1}{\omega}\left(\omega^2\Phi(\boldsymbol{x}) + \Delta\Phi(\boldsymbol{x})\right)\sin(\omega t)$, the exact time-domain solution is given by

Exact solution

$$\begin{cases} E_z(\boldsymbol{x},t) &= \Phi(\boldsymbol{x})\cos(\omega t), \\ \boldsymbol{H}(\boldsymbol{x},t) &= -\dfrac{1}{\omega}\boldsymbol{\nabla}\times\boldsymbol{\Phi}(\boldsymbol{x})\sin(\omega t), \end{cases} \tag{5.43}$$

with

$$\Phi(\boldsymbol{x}) = \chi(r)J_\alpha(wr)\sin(\alpha\theta),$$

where $\chi \in \mathcal{C}^2(\mathbb{R})$ is a cut-off function such that $\chi = 1$ if $0 \leq r \leq 0.2$, $\chi = 0$ if $r > 0.9$ and χ is polynomial if $0.2 \leq r \leq 0.9$ and J_α is the bessel function. The electromagnetic field is initialized at $t = 0$ as $H_x = H_y = 0$ and

$$E_z(x, y, t = 0) = \Phi(\boldsymbol{x}).$$

We consider this problem for $\alpha = \frac{2}{3}$, which corresponds to a domain meshed first uniformly in Fig. 5.13 (left) and locally refined in Fig. 5.13 (right).

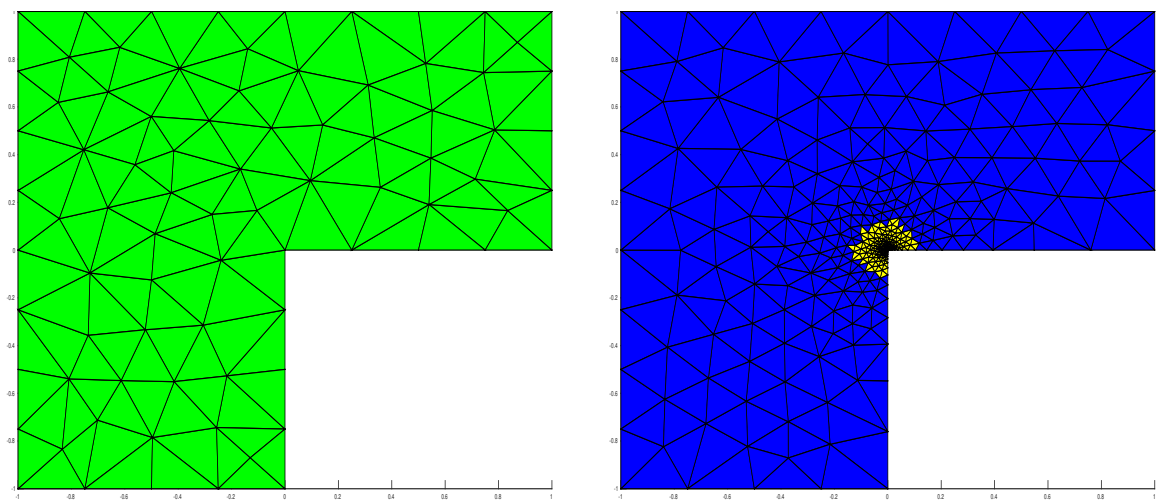

Figure 5.13 | Standing wave in a PEC disc sector. Uniform and locally refined meshes for $\Omega_{\frac{2}{3}}$.

Fig. 5.14 shows the exact solution for E_z and H_x on the locally refined mesh for $\Omega_{\frac{2}{3}}$ at time $t = 1.25$. The solution presents a singularity at the origin, as shown on the bottom image of Fig. 5.14. Therefore, it is necessary to locally refine the mesh in this region to preserve the convergence of the HDG scheme, see Fig. 5.15, 5.16, 5.17 and 5.18. The first two figures show that the approximated solution is much better for a probe point of coordinates $(0.01, 0.01)$ (near to the origin) for the locally refined mesh than the uniform mesh, while the second two figures shows that the global L^2 error $||H_x - H_{xh}||_\Omega$ and $||E_z - E_{zh}||_\Omega$ are also better in the locally refined mesh case.

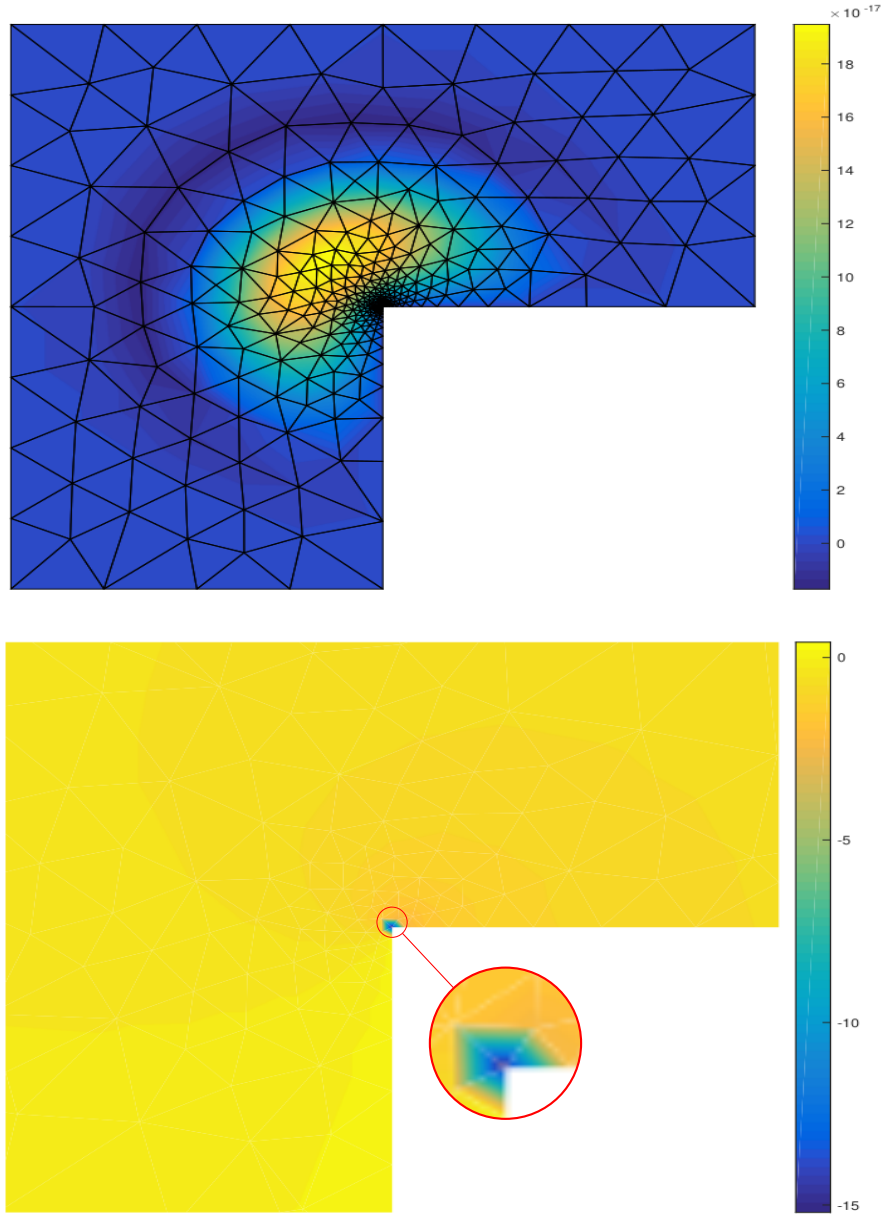

Figure 5.14 | Standing wave in a PEC disc sector. Exact solution for E_z and H_x

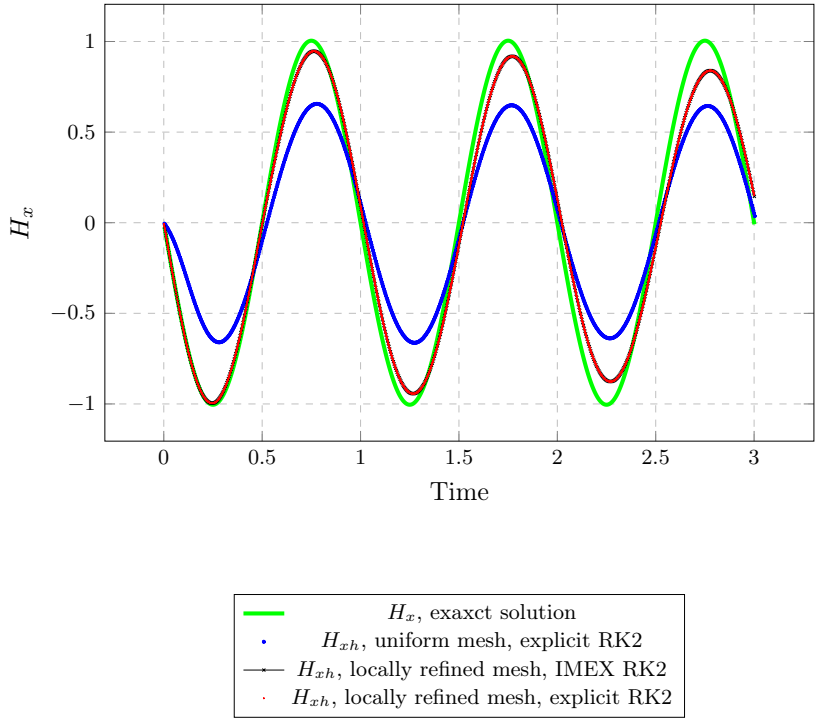

Figure 5.15 | Standing wave in a PEC disc sector. Time evolution of the exact and the numerical solution of H_x at a fixed point $(0.01, 0.01)$ with a $\mathbb{P}_1$ interpolation.

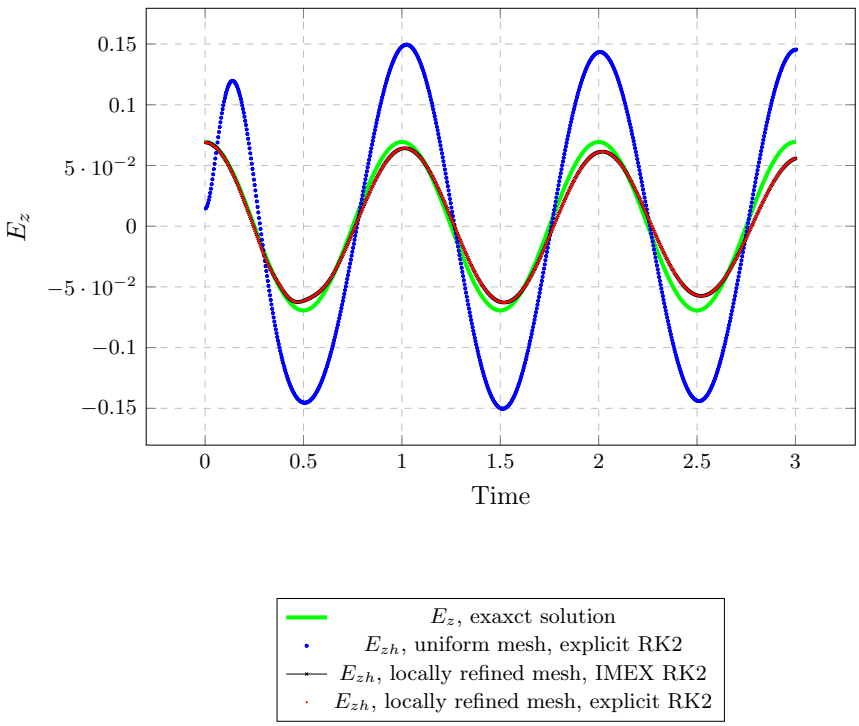

Figure 5.16 | Standing wave in a PEC disc sector. Time evolution of the exact and the numerical solution of E_z at a fixed point $(0.01, 0.01)$ with a $\mathbb{P}_1$ interpolation.

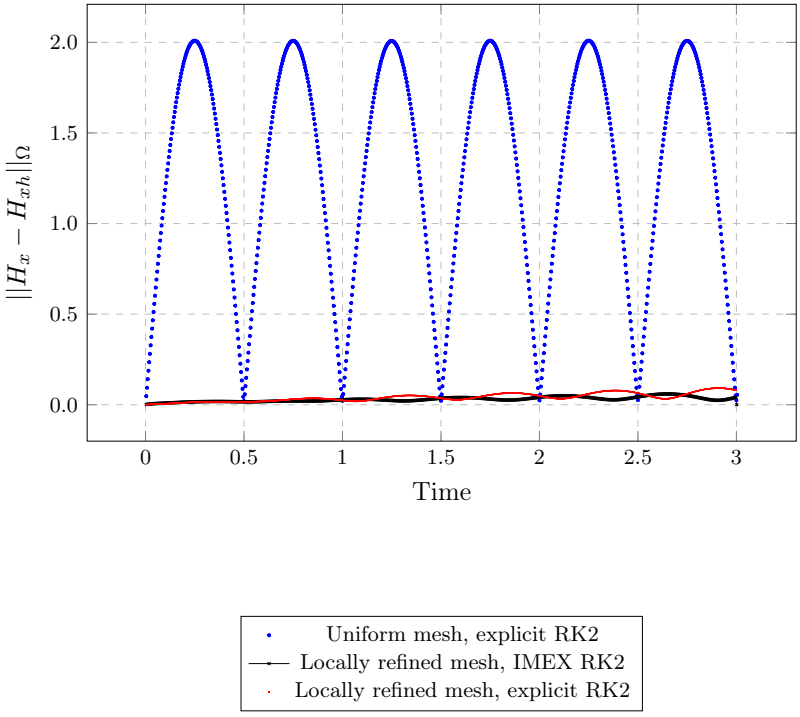

Figure 5.17 | Standing wave in a PEC disc sector. Time evolution of the L^2-norm of the error on H_{xh} with a $\mathbb{P}_1$ interpolation.

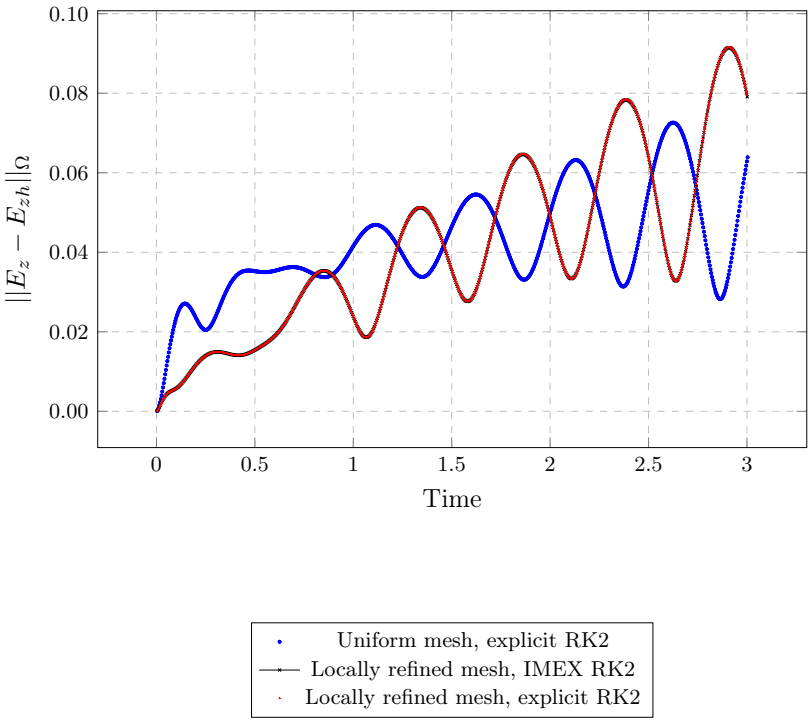

Figure 5.18 | Standing wave in a PEC disc sector. Time evolution of the L^2-norm of the error of E_{zh} with a $\mathbb{P}_1$ interpolation.

The main asset that we can expect from the IMEX HDG method is in terms of computational cost, in comparison to the fully explicit scheme, when using a locally refined mesh. This is due to the fact that the time step insuring the stability will depend only on the smallest element of the coarse mesh unlike the case of fully explicit scheme for which the time step insuring the stability depends on the smallest element in the whole mesh. Let the CFL number be fixed for the totally explicit and the IMEX scheme, so we have

$$CFL = \frac{dt_{imp/exp}}{h_{\mathcal{T}_h^{CO}}} = \frac{dt_{exp}}{h_{\mathcal{T}_h}} \Rightarrow \frac{dt_{imp/exp}}{dt_{exp}} = \frac{h_{\mathcal{T}_h^{CO}}}{h_{\mathcal{T}_h}}. \tag{5.44}$$

The gain in computing time will be affected by the ratio between the smallest element in the coarse mesh and the smallest element in the fine mesh. For the locally refined mesh of Fig. (5.13) right, $h_{\mathcal{T}_h^{CO}} = 4.7 \times 10^{-3}$ and $h_{\mathcal{T}_h} = 1.52 \times 10^{-4}$, and the ratio is almost 31, which implies that the time step used for the IMEX HDG method is 31 times bigger, with the same error level as shown in Fig. 5.19.

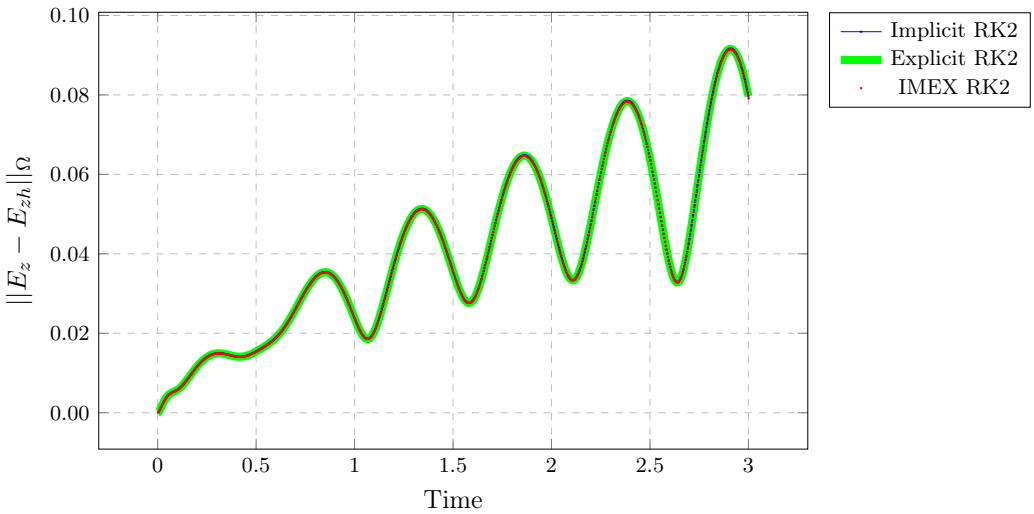

Figure 5.19 | Standing wave in a PEC disc sector. Time evolution of the L^2-norm of the error on E_{zh} with a locally refined mesh and a $\mathbb{P}_1$ interpolation, while $dt_{imp/exp} = dt_{imp} = 3.76 \times 10^{-3}$ and $dt_{exp} = 1.22 \times 10^{-4}$.

Fig. 5.19 shows the error level for the three different time integration schemes, while considering the same time step for the implicit and the IMEX RK2 schemes $\left(dt_{imp/exp} = dt_{imp} = 3.76 \times 10^{-3}\right)$ and a 31 times smaller time step for the explicit RK2 scheme $\left(dt_{exp} = 1.22 \times 10^{-4}\right)$. Note that these time steps are identical for all the results in Fig. 5.15, 5.16, 5.17 and 5.18. In order to improve the gain in time computation between totally implicit and hybrid implicit/explicit RK2, we will consider another locally refined mesh. The first one, considered before, contains 350 elements in the implicit zone and 356 elements in the explicit zone. The HDG matrix to inverse at each time step in this case, contains 12756 non zero elements while it contains 21300 non zero elements in the totally implicit case. The second mesh, which is presented in Fig 5.20, contains 203 elements in the implicit zone while 503 elements are contained in the explicit zone. The HDG matrix to inverse at each time step for the second mesh, contains 9228 non zero elements. It is clear that the computation time to inverse this matrix will be less than the computation time needed for the first mesh, since we have less non zero elements. Note that, decreasing the number of elements in the implicit zone leads to the decrease in the time step preserving the stability, since $h_{\mathcal{T}_h^{CO}}$ is

smaller $\left(h_{\mathcal{T}_h^{CO}} = 1.6 \times 10^{-3},\ dt_{imp/exp} = 1.2 \times 10^{-3}\right)$. In other words, decreasing $h_{\mathcal{T}_h^{CO}}$ leads to the increase of the gain in terms of CPU time between the totally implicit and the IMEX time scheme and to a smaller gain between the totally explicit and the IMEX time scheme. Figure (5.21) shows that there is no difference in error level between the two considered mesh. Tab. 5.8 presents a first comparison in cost between the three methods while considering the two locally refined meshes mentioned above for $\Omega_{\frac{2}{3}}$. Figure (5.22) shows the error level for the third order IMEX HDGTD considered in this work (SSP-LDIRK3), using the second locally refined mesh.

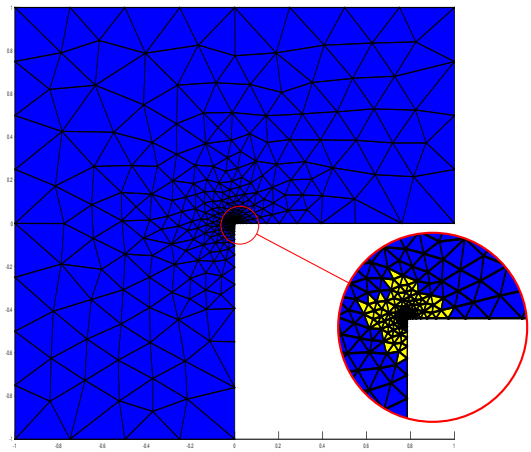

Figure 5.20 | Standing wave in a PEC disc sector. Second locally refined mesh of $\Omega_{\frac{2}{3}}$.

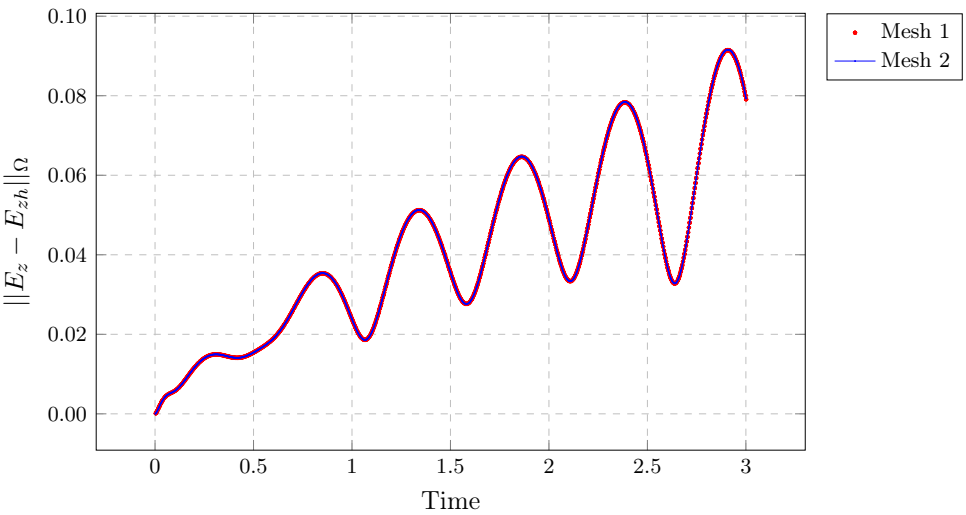

Figure 5.21 | Standing wave in a PEC disc sector. Time evolution of the L^2-norm of the error on E_{zh} with two different locally refined meshes and a $\mathbb{P}_1$ interpolation.

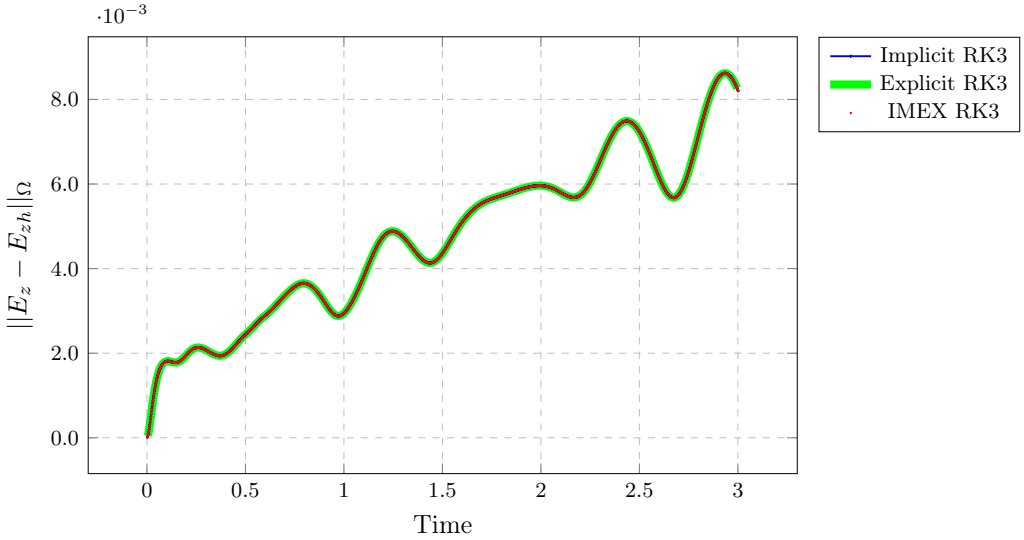

Figure 5.22 | Standing wave in a PEC disc sector. Time evolution of the L^2-norm of the error on E_{zh} with a locally refined mesh and a $\mathbb{P}_2$ interpolation.

	SSP3 (explicit)	SSP-LDIRK3 (IMEX)	LDIRK3 (implicit)
Computational time	28 h 36 mn	5 h 30 mn	6 h 7 mn

Table 5.8 | Standing wave in a PEC disc sector. Computational time for fully explicit, IMEX and the fully implicit RK3 HDG methods.

5.4.3 Propagation of a standing wave in a PEC cavity with $\varepsilon = \varepsilon(\mathbf{x})$

We now consider a model problem for which an analytical solution can be computed. The domain of computation is defined by

$$\Omega = \{(x, y) \in \mathbb{R}^2\,;\, 0 \leq x \leq 1, 0 \leq y \leq 1\},$$

with perfectly metallic walls. We consider the propagation of an eigenmode in a source-free *i.e.* $\boldsymbol{J} = 0$ closed cavity. The electric permittivity is defined as

$$\varepsilon(x, y) = \frac{1}{c^2(x, y)} \begin{cases} 1 & 0 \leq x \leq 1 - h, \\ \dfrac{1}{c^2} & 1 - h \leq x \leq 1, \end{cases} \tag{5.45}$$

while the magnetic permeability is set to the constant vacuum value.

Proposition 2. *The exact time-domain solution is given by*

Exact solution

$$\begin{cases} E_z(x,y,t) &= \psi(x)\sin(\pi y)\cos(\lambda_0 t), \\ H_x(x,y,t) &= -\dfrac{\pi}{\lambda_0}\psi(x)\cos(\pi y)\sin(\lambda_0 t), \\ H_y(x,y,t) &= \dfrac{1}{\lambda_0}\psi'(x)\sin(\pi y)\sin(\lambda_0 t), \end{cases} \tag{5.46}$$

while $\psi'(x) = \dfrac{d}{dx}\psi(x)$, λ_0 *is a constant dependent of* c *(more details in the proof below) and*

$$\psi(x) = \begin{cases} \sin(\alpha_0 x) & 0 \le x \le 1-h, \\ \dfrac{\sin(\alpha_0(1-h))}{\sin(\beta_0 h)}\sin(\beta_0(1-x)) & 1-h \le x \le 1, \end{cases} \tag{5.47}$$

where

$$\alpha_0 = \sqrt{\lambda_0^2 - \pi^2} \text{ and } \beta_0 = \sqrt{\frac{\lambda_0^2}{c^2} - \pi^2}.$$

Proof. The E_z component of the the Maxwell equations described in (2.37) can be reformulated in a second order wave form

$$\frac{1}{c^2(x)}\partial_t^2 E_z(x,y,t) - \Delta E_z(x,y,t) = 0. \tag{5.48}$$

We have a computational domain with perfectly metallic walls so the boundary conditions are

$$E_z(0,y,t) = E_z(1,y,t) = E_z(x,0,t) = E_z(x,1,t) = 0. \tag{5.49}$$

Assuming that

$$E_z(x,y,t) = \phi(x,t)\sin(\pi y),$$

and inserting this expression in (5.48) we obtain

$$\frac{1}{c^2(x)}\partial_t^2\,\phi(x,t)\sin(\pi y) - \partial_x^2\phi(x,t)\sin(\pi y) + \pi^2\phi(x,t)\sin(\pi y) = 0,$$

and

$$\frac{1}{c^2(x)}\partial_t^2\,\phi(x,t) - \partial_x^2\phi(x,t) + \pi^2\phi(x,t) = 0. \tag{5.50}$$

Let us now consider that

$$\phi(x,t) = \psi(x)\cos(\lambda t).$$

Back to (5.50) we obtain

$$-\frac{\lambda^2}{c^2(x)}\psi(x)\cos(\lambda t) - \psi''(x)\cos(\lambda t) + \pi^2\psi(x,t)\cos(\lambda t) = 0,$$

so finally

$$\psi''(x) + \left(\frac{\lambda^2}{c^2(x)} - \pi^2\right)\psi(x) = 0. \tag{5.51}$$

$c(x)$ is ≤ 1 forall $x \in [0,1]$ so we must consider $\lambda > \pi$ to obtain a wave solution. Our goal now is to solve the system below

$$\begin{cases} \psi_1''(x) + \left(\lambda^2 - \pi^2\right)\psi_1(x) & = & 0, & 0 \leq x \leq 1-h \\ \psi_2''(x) + \left(\dfrac{\lambda^2}{c^2} - \pi^2\right)\psi_2(x) & = & 0, & 1-h \leq x \leq 1 \end{cases} \tag{5.52}$$

Let us introduce $\alpha(\lambda) = \sqrt{\lambda^2 - \pi^2}$ and $\beta(\lambda) = \sqrt{\dfrac{\lambda^2}{c^2} - \pi^2}$. The solution of (5.52) can be written as

$$\begin{cases} \psi_1(x) & = & c_1 \cos\left(\alpha(\lambda)x\right) + c_2 \sin\left(\alpha(\lambda)x\right), & 0 \leq x \leq 1-h \\ \psi_2(x) & = & k_1 \cos\left(\beta(\lambda)x\right) + k_2 \sin\left(\beta(\lambda)x\right), & 1-h \leq x \leq 1 \end{cases}$$

Remark 9. The second equation of (5.52) can be written as

$$\psi_2''(1-x) + \left(\frac{\lambda^2}{c^2} - \pi^2\right)\psi_2(1-x) = 0, \quad 0 \leq x \leq h.$$

Let $z(x) = \psi_2(1-x)$ for $0 \leq x \leq h$, we have that $z''(x) = \psi_2''(1-x)$ for $0 \leq x \leq h$, so

$$z''(x) + \left(\frac{\lambda^2}{c^2} - \pi^2\right)z(x) = 0, \quad 0 \leq x \leq h.$$

We can deduce that

$$z(x) = k_1 \cos\left(\beta(\lambda)x\right) + k_2 \sin\left(\beta(\lambda)x\right), \quad 0 \leq x \leq h,$$

which implies that

$$\psi_2(1-x) = k_1 \cos\left(\beta(\lambda)x\right) + k_2 \sin\left(\beta(\lambda)x\right), \quad 0 \leq x \leq h.$$

Finally

$$\psi_2(x) = k_1 \cos\left(\beta(\lambda)(1-x)\right) + k_2 \sin\left(\beta(\lambda)(1-x)\right), \; 1-h \leq x \leq 1.$$

The solution of (5.52) is now written as

$$\begin{cases} \psi_1(x) & = & c_1 \cos\left(\alpha(\lambda)x\right) + c_2 \sin\left(\alpha(\lambda)x\right), & 0 \leq x \leq 1-h \\ \psi_2(x) & = & k_1 \cos\left(\beta(\lambda)(1-x)\right) + k_2 \sin\left(\beta(\lambda)(1-x)\right), & 1-h \leq x \leq 1. \end{cases} \tag{5.53}$$

Our goal now is to find the four constants (c_1, c_2, k_1 and k_2). In order to do that, we will use the boundary conditions, the continuity of $\psi(x)$ and the continuity of $\psi'(x)$. Eq. (5.49) gives us $\psi_1(0) = \psi_2(1) = 0$, so finally

$$c_1 = k_1 = 0.$$

Since $\psi \in \mathcal{C}^0(0,1)$ we have that $\psi_1(1-h) = \psi_2(1-h)$ and

$$c_2 \sin\left((1-h)\alpha(\lambda)\right) - k_2 \sin\left(h\beta(\lambda)\right) = 0.$$

Similary, $\psi \in \mathcal{C}^1(0,1)$ implies that $\psi_1'(1-h) = \psi_2'(1-h)$ and

$$c_2\alpha(\lambda)\cos\left((1-h)\alpha(\lambda)\right) + k_2\beta(\lambda)\cos\left(h\beta(\lambda)\right) = 0.$$

The system of the last two boxed equation can be written in the matrix form as

$$\underbrace{\begin{pmatrix} \sin\Big((1-h)\alpha(\lambda)\Big) & -\sin\left(h\beta(\lambda)\right) \\ \alpha(\lambda)\cos\Big((1-h)\alpha(\lambda)\Big) & \beta(\lambda)\cos(h\beta(\lambda)) \end{pmatrix}}_{\mathcal{A}(\lambda)} \begin{pmatrix} c_2 \\ k_2 \end{pmatrix} = \begin{pmatrix} 0 \\ 0 \end{pmatrix}. \tag{5.54}$$

In order to have a non zero solution for the above system, we must find a λ_0 such that $det_{\mathcal{A}}(\lambda_0) = 0$. We have

$$\begin{aligned}
\det_{\mathcal{A}}(\lambda) &= \beta(\lambda)\sin\left((1-h)\alpha(\lambda)\right)\cos(h\beta(\lambda)) \\
&+ \alpha(\lambda)\sin\left(h\beta(\lambda)\right)\cos\left((1-h)\alpha(\lambda)\right) \\
&= \frac{\beta(\lambda)}{2}\sin\left((1-h)\alpha(\lambda) + h\beta(\lambda)\right) \\
&+ \frac{\beta(\lambda)}{2}\sin\left((1-h)\alpha(\lambda) - h\beta(\lambda)\right) \\
&+ \frac{\alpha(\lambda)}{2}\sin\left((1-h)\alpha(\lambda) + h\beta(\lambda)\right) \\
&- \frac{\alpha(\lambda)}{2}\sin\left((1-h)\alpha(\lambda) - h\beta(\lambda)\right) \\
&= \left(\frac{\beta(\lambda)+\alpha(\lambda)}{2}\right)\sin\left((1-h)\alpha(\lambda) + h\beta(\lambda)\right) \\
&+ \left(\frac{\beta(\lambda)-\alpha(\lambda)}{2}\right)\sin\left((1-h)\alpha(\lambda) - h\beta(\lambda)\right)
\end{aligned}$$

Finally we must find λ_0 such that

$$\begin{aligned}
&\sin\left((1-h)\alpha(\lambda_0) + \beta(\lambda_0)h\right) \\
&= \left(\frac{\alpha(\lambda_0)-\beta(\lambda_0)}{\alpha(\lambda_0)+\beta(\lambda_0)}\right)\sin\left((1-h)\alpha(\lambda_0) - \beta(\lambda_0)h\right).
\end{aligned} \tag{5.55}$$

In summary, for $\lambda = \lambda_0$, the system (5.54) has an infinite number of solutions and we will take $c_2 = 1$ and $k_2 = \dfrac{\sin\left((1-h)\alpha(\lambda_0)\right)}{\sin\left(h\beta(\lambda_0)\right)}$ as a solution verifying the first equation of this system, to obtain

$$\psi(x) = \begin{cases} \sin\left(\alpha_0 x\right) & 0 \le x \le 1-h, \\ \dfrac{\sin\left(\alpha_0(1-h)\right)}{\sin\left(\beta_0 h\right)}\sin\left(\beta_0(1-x)\right) & 1-h \le x \le 1. \end{cases}$$

□

The electromagnetic field is initialized at $t = 0$ as $H_x = H_y = 0$ and

$$E_z(x, y, t = 0) = \psi(x)\sin(\pi y).$$

In the following, we will consider $c = 0.1$, $h = 0.2$, $\lambda_0 = 7.0595$ verifying (5.55), which is found by a bisection method of order 10^{-13} ($\det_{\mathcal{A}}(\lambda_0) = 1.0170 \times 10^{-13}$). The graph of ψ is presented

in Figure (5.23). Fig. 5.24 shows two different meshes for Ω, *i.e.* , a uniform mesh (left) and a locally refined mesh (right). We can see that for $x \geq 0.8$ the wavelength is much smaller than the wavelength before 0.8 so we have to increase the number of mesh elements in the region where $x \geq 0.8$ to better catch the information of the wave. The exact solution for E_z is presented in Fig. 5.25 at time t = T. Figs. 5.26 and 5.27 illustrate the requirement of using a locally refined mesh. Indeed, in Fig. 5.26, we observe that the approximate solution is much better for a probe point of coordinates $(0.9, 0.5)$ (in the region where the wavelength is smaller) for the locally refined mesh than the uniform mesh. In addition, Fig. 5.27, clearly shows that the global L^2 error $||E_z - E_{zh}||_\Omega$ is reduced when using a locally refined mesh.

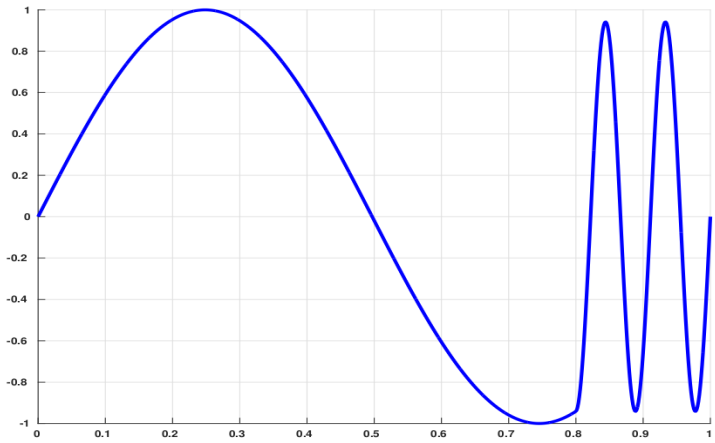

Figure 5.23 | Propagation of a standing wave in a PEC cavity with $\varepsilon = \varepsilon(\mathbf{x})$. Profile of $\psi(x)$ used for the exact solution.

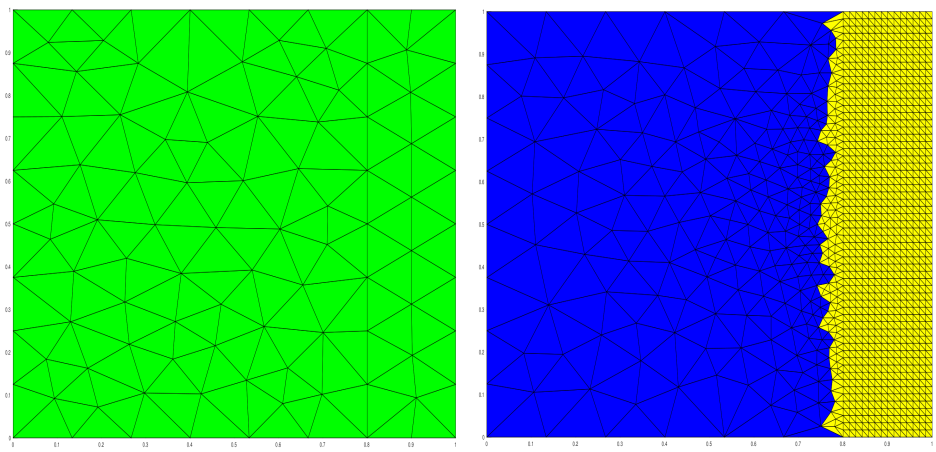

Figure 5.24 | Propagation of a standing wave in a PEC cavity with $\varepsilon = \varepsilon(\mathbf{x})$. Uniform and locally refined meshes for Ω.

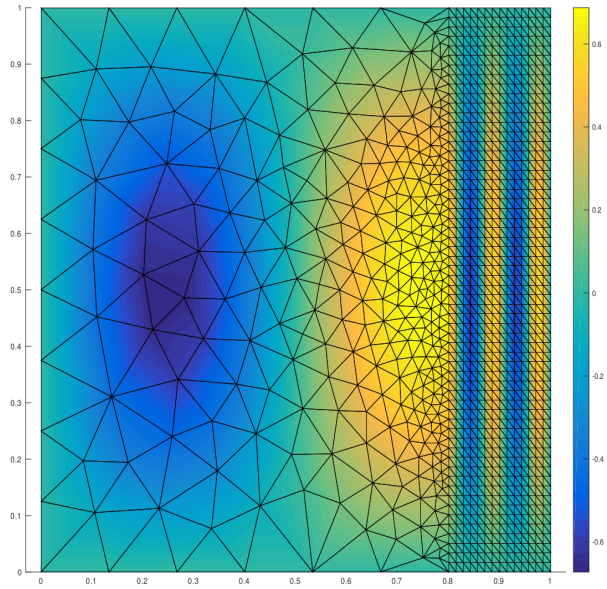

Figure 5.25 | Propagation of a standing wave in a PEC cavity with $\varepsilon = \varepsilon(\mathbf{x})$. Exact solution for E_z on Ω.

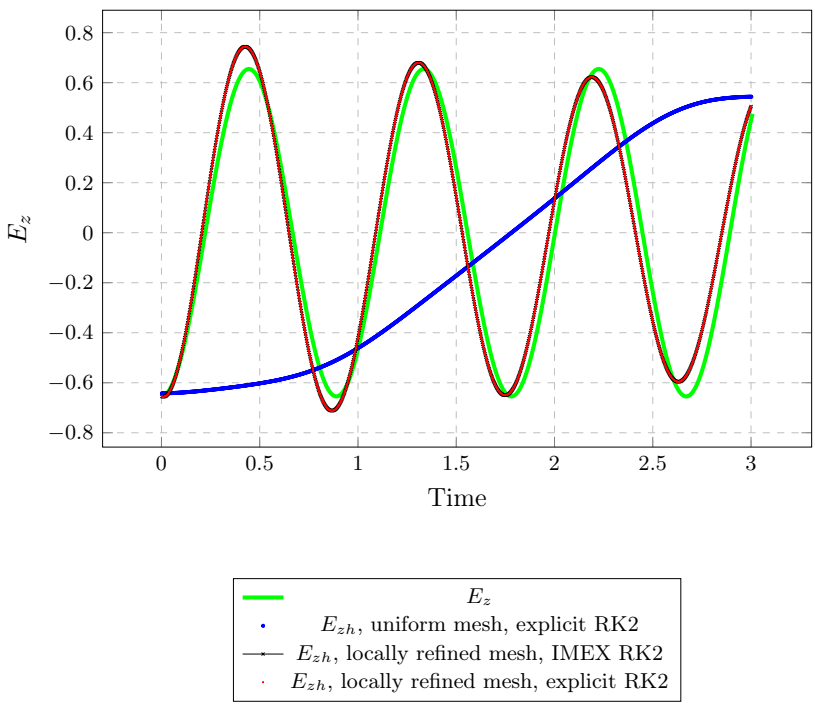

Figure 5.26 | Propagation of a standing wave in a PEC cavity with $\varepsilon = \varepsilon(\mathbf{x})$. Time evolution of the exact and the numerical solution of E_z at a fixed point$(0.9, 0.5)$, with a $\mathbb{P}_1$ interpolation.

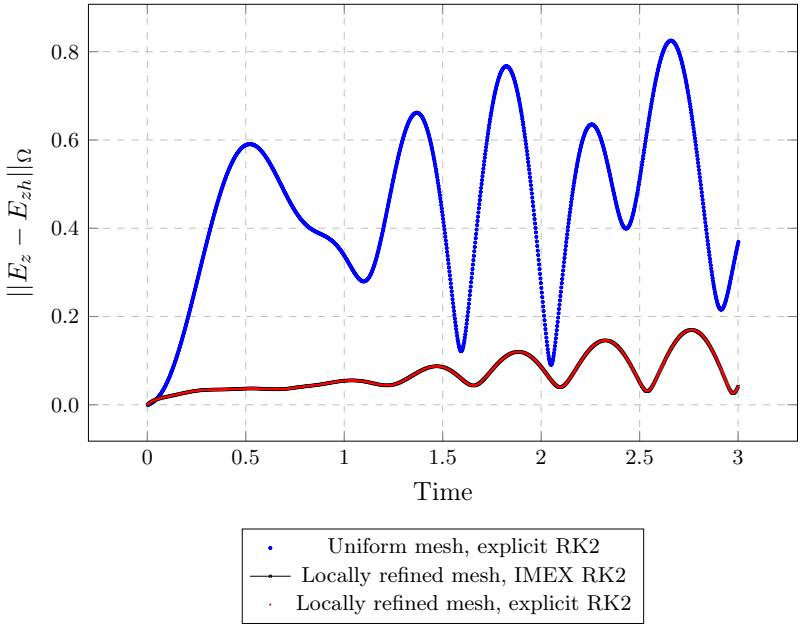

Figure 5.27 | Propagation of a standing wave in a PEC cavity with $\varepsilon = \varepsilon(\mathbf{x})$. Time evolution of the L^2-norm of the error on E_{zh} with a $\mathbb{P}_1$ interpolation.

Here we have $h_{\mathcal{T}_h^{CO}} = 2.90 \times 10^{-3}$ and $h_{\mathcal{T}_h} = 2.13 \times 10^{-4}$ (ratio between them is almost 13.6). Thus, the time step used for the IMEX HDG method is 13.6 times bigger than the one used for the fully explicit HDG method, without affecting the overall accuracy as shown in Fig. 5.28. Note that the time steps used for the implicit and IMEX HDG RK2 methods are the same $\left(dt_{imp/exp} = dt_{imp} = 2.32 \times 10^{-3}\right)$, and $dt_{exp} = 1.7 \times 10^{-4}$ is the time step considered for the fully explicit HDG RK2 method. The implicit zone contains 1864 elements, while 391 elements are contained in the explicit zone. the global HDG matrix to inverse at each time step in this case, contains 58480 non zero elements while it contains 67864 non zero elements in the totally implicit case. Tab. 5.9 presents a comparison in terms of computing cost between the three methods while considering the locally refined mesh for Ω (Fig. 5.25) with a $\mathbb{P}_1$ interpolation. Fig. 5.29 shows the time evolution of the L^2-norm of the error of E_z with the third order SSP-LDIRK3 IMEX HDG method.

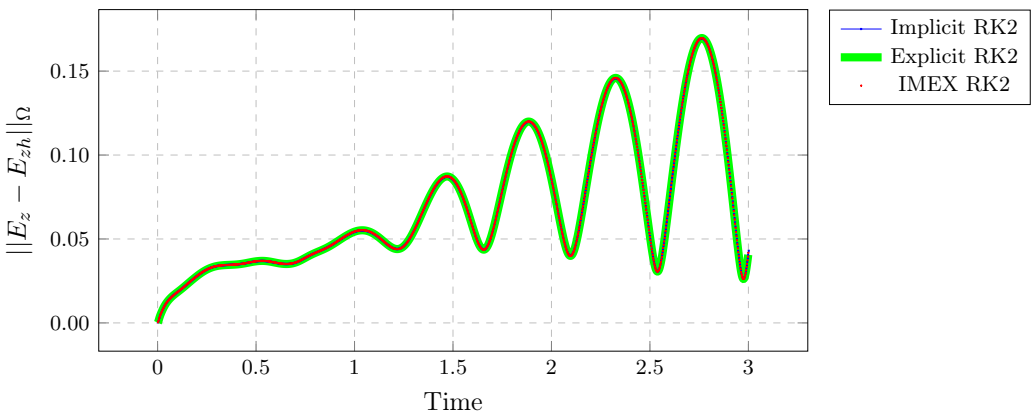

Figure 5.28 | Propagation of a standing wave in a PEC cavity with $\varepsilon = \varepsilon(\mathbf{x})$. Time evolution of the L^2-norm of the error for a $\mathbb{P}_1$ interpolation.

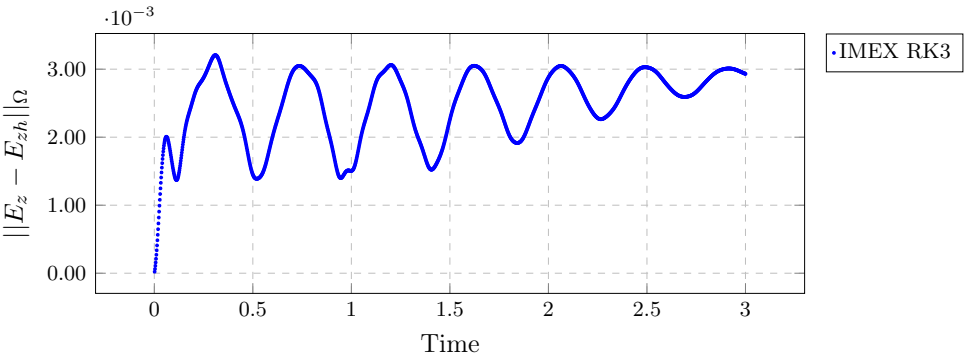

Figure 5.29 | Propagation of a standing wave in a PEC cavity with $\varepsilon = \varepsilon(\mathbf{x})$. Time evolution of the L^2-norm of the error for a $\mathbb{P}_2$ interpolation.

	Explicit RK2	IMEX RK2	Implicit RK2
Computational time	50 h 33 mn	4 h 23 mn	4 h 45 mn

Table 5.9 | Propagation of a standing wave in a PEC cavity with $\varepsilon = \varepsilon(\mathbf{x})$. Computational time for fully explicit, IMEX and fully implicit RK2 HDG methods.

5.4.4 A nano-waveguide problem

This is a prototype problem of a photonic crystal structure in the emerging nanophotonics area [40]. The idea here is to simulate an idealized waveguide device before it has undertaken an optimization procedure to maximize the performance of directional transmission (see [55] for example). The photonic crystal type represents a nano-structuring device encapsulated in a 10.25×10.25 square which is composed of 15 cylindrical holes of radius 0.3125. Here $\mu = 1$ and the value of the permittivity ε corresponds to silicium within the holes ($\varepsilon = 3.14$), silica ($\varepsilon = 1.5$) in the device enclosing the holes, and surrounding air ($\varepsilon = 1$).

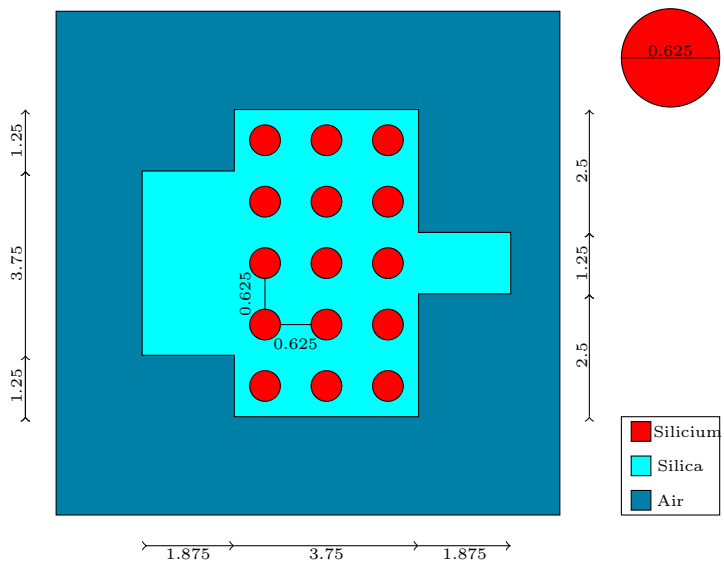

Figure 5.30 | A nano-waveguide problem. The photonic crystal structure.

We use absorbing boundary conditions with an incident plane wave of frequency $0.5\,m^{-1}$ ($\omega = \pi$). We solve the problem for a time period equal $T = 16/\sqrt{2}$. First, we consider the photonic crystal structure presented in Fig. 5.30 with a non locally refinement grid, see Fig. 5.31. This mesh consists of 1830 elements, 285 elements for the 15 silicium holes, 1083 elements for the silica part and the rest for the surrounding air. Fig. 5.32 shows the solution for E_z on the uniform mesh at time $t = 16/\sqrt{2}$ with the explicit RK3 time integration and for a $\mathbb{P}_2$ interpolation. The time step chosen is $\Delta t = 1.26 \times 10^{-2}\,m$.

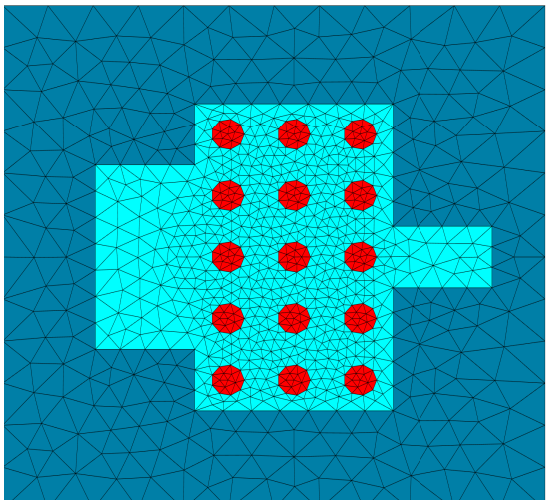

Figure 5.31 | A nano-waveguide problem. A non locally refined grid for the photonic crystal device.

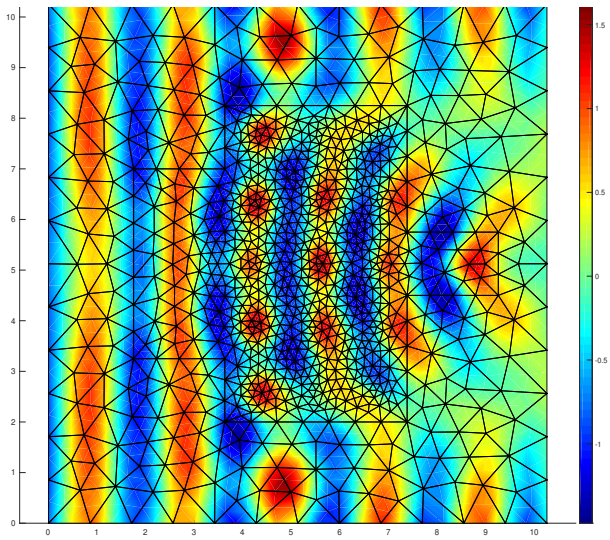

Figure 5.32 | A nano-waveguide problem. The electric field at time $T = 16/\sqrt{2}$ with an explicit RK3 time integration and for a $\mathbb{P}_2$ interpolation.

Then, we consider the same photonic crystal structure, but with a smaller distance ($d = 0.025$) between the holes (see Fig. 5.33 for details). The locally refined mesh considered in Fig. 5.34 consists of 2290 elements, 948 elements for the 15 silicium holes, 1168 elements for the silica part and the rest for the surrounding air. Fig. 5.35 shows the considered implicit zone in yellow (190 elements) and that of the explicit zone in blue (2100 elements). Here we have $h_{\mathcal{T}_h^{CO}} = 1.18 \times 10^{-2}$ and $h_{\mathcal{T}_h} = 3.78 \times 10^{-3}$ (ratio between them is almost 3). Thus, the time step used for the IMEX-HDG-RK3 method is three times bigger than the one used for the fully explicit RK3 HDG method (see (5.44)).

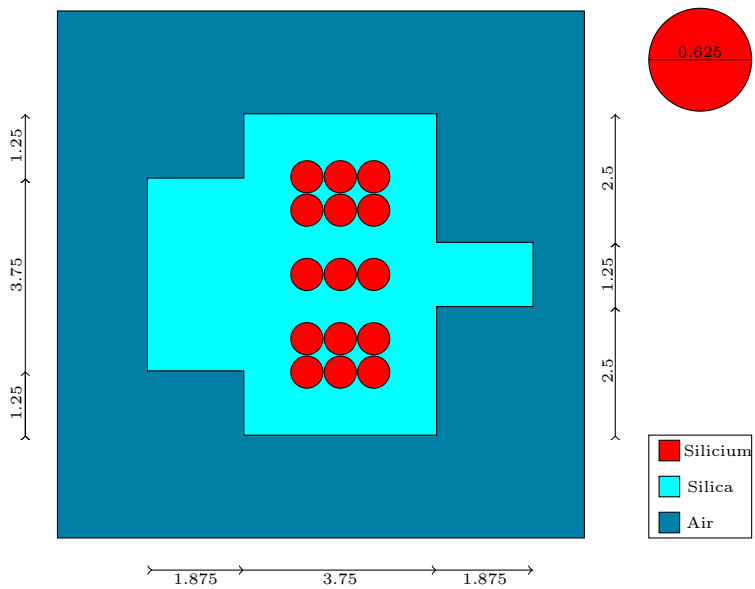

Figure 5.33 | A nano-waveguide problem. The photonic crystal structure.

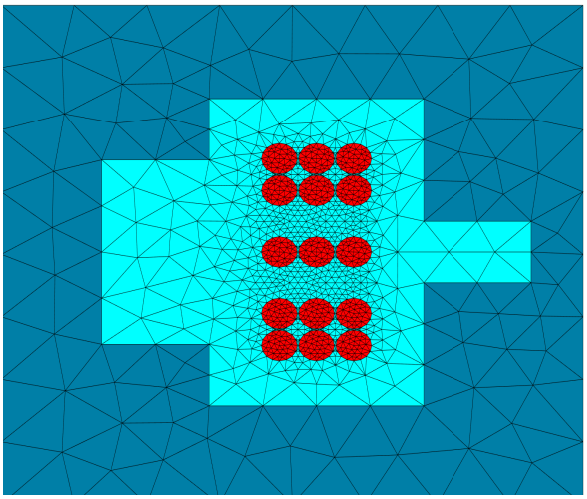

Figure 5.34 | A nano-waveguide problem. Locally refined mesh for the photonic crystal device.

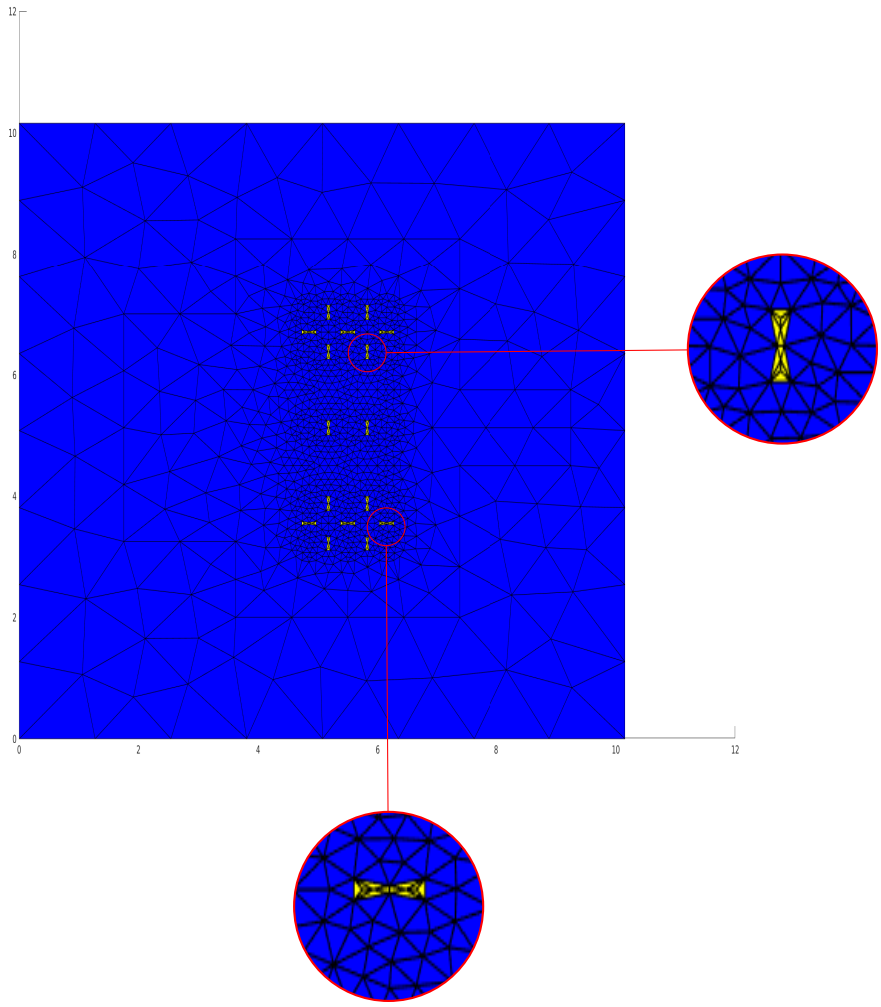

Figure 5.35 | A nano-waveguide problem. $\mathcal{T}_h^{CO}$ and $\mathcal{T}_h^{FI}$ of the locally refined mesh for the photonic crystal device.

Fig. 5.36 shows the difference in sparsity for the global matrix $\mathbb{Q}$ defined in (5.30), between the explicit HDG, implicit HDG and IMEX-HDG-RK3 methods. We can see that, due to the IMEX scheme, we have a block-diagonal matrix corresponding to the degrees of freedom in the coarse part and a sparse matrix in the fine part while it is not the case for the fully implicit scheme. In particular, in comparison with the fully implicit scheme, we have a much cheaper global matrix to inverse at each time step with the IMEX-HDG-RK3 method, the global HDG matrix for the fully implicit RK3 scheme contains 154719 non zero element while that of the IMEX-HDG-RK3 contains 41319 non zero element only. Tab. 5.10 compares the three methods in terms of CPU time while considering the mesh shown in Fig. 5.35, a $\mathbb{P}_2$ interpolation and the same time step for the IMEX and the fully implicit schemes. Fig. 5.37 and 5.38 show that the solution for E_z with the IMEX-HDG-RK3 time integration is similar to the solution E_z with the fully explicit RK3 time scheme on the locally refined mesh (Fig. 5.35) at time $t = T$ and for a $\mathbb{P}_2$ interpolation. The time step chosen for the IMEX-HDG-RK3 is $\Delta t = 7 \times 10^{-3}\, m$, while it is $\Delta t = 2.26 \times 10^{-3}\, m$ for the fully explicit RK3.

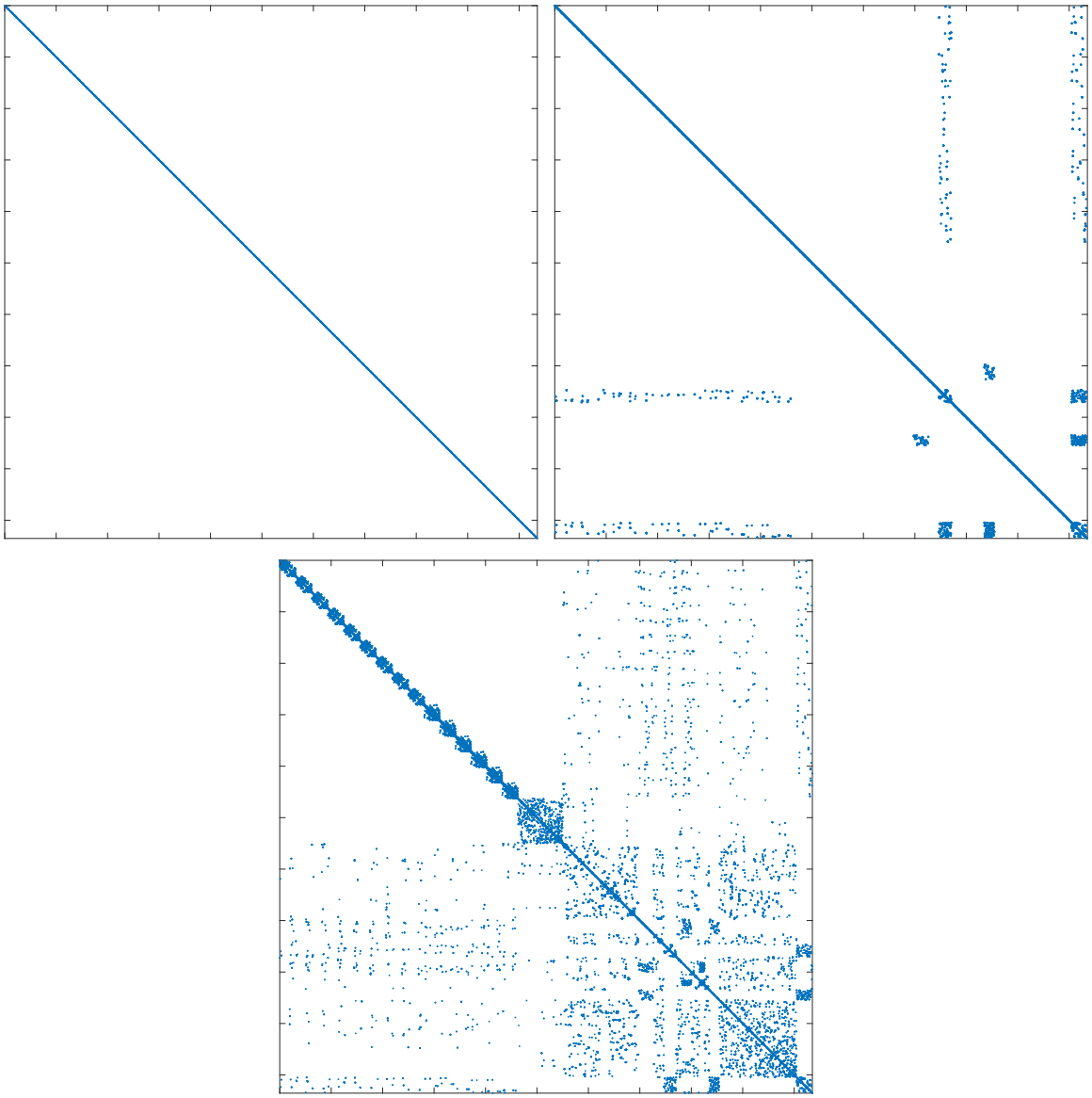

Figure 5.36 | A nano-waveguide problem.The global matrix $\mathbb{Q}$ for explicit RK3, IMEX RK3 and fully implicit RK3 on the mesh presented in Fig. (5.35).

	Explicit RK3	IMEX RK3	Implicit RK3
Computational time	4 h 30 mn	1 h 30 mn	2 h 30 mn

Table 5.10 | A nano-waveguide problem. Computational time for fully explicit, IMEX and fully implicit RK3 HDG methods.

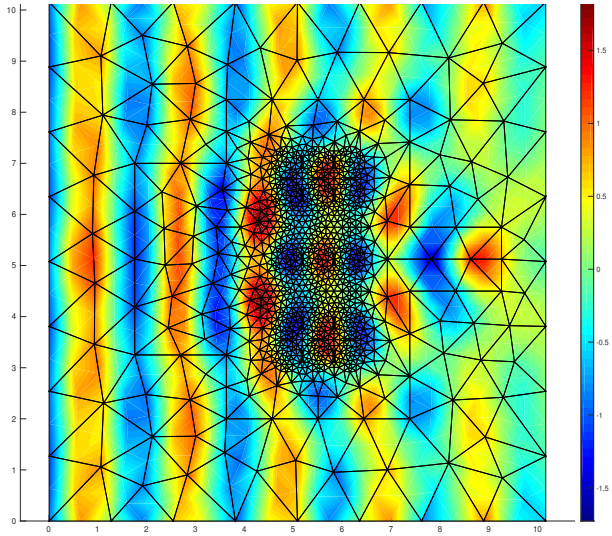

Figure 5.37 | A nano-waveguide problem. The electric field at time $T = 16/\sqrt{2}$ with the IMEX-HDG-RK3 time integration and for a $\mathbb{P}_2$ interpolation with a small distance between the silicium holes.

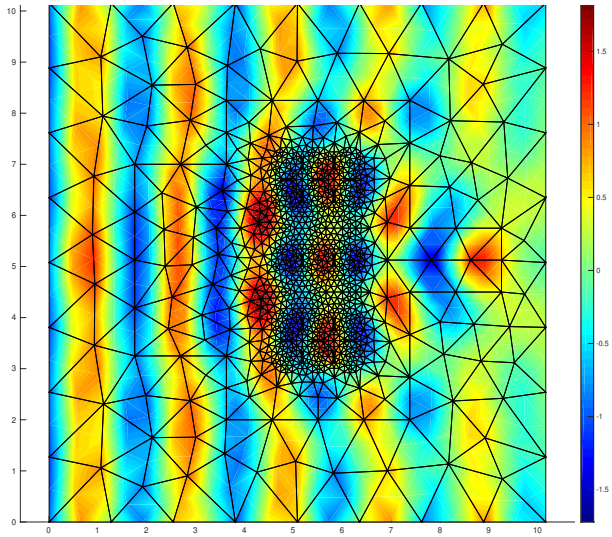

Figure 5.38 | A nano-waveguide problem. The electric field at time $T = 16/\sqrt{2}$ with the fully explicit RK3 time integration and for a $\mathbb{P}_2$ interpolation with a small distance between the silicium holes.

5.5 Conclusion

In this chapter we have presented hybrid implicit/explicit time schemes for the hybridizable discontinuous Galerkin discretization of the time-dependent Maxwell's equations with three different orders. We have proved, in the case of the first and second order, that the stability of these schemes

depends only on the coarse mesh. Then, we have presented several numerical examples: First on a simple test case to validate and study the numerical convergence of these methods. Second, we studied two cases where the analytical solution is irregular. And finally we have presented a physical problem, namely photonic crystal device where we don't have access to an analytical solution. Overall we obtained that this contribution is to be employed as an efficient way of reducing the computational time compared to the fully explicit and implicit schemes without any loss in the accuracy.

6

Outlook

First, the advantages of using HDG methods over those of DG methods in stationary and time-domain problems while using fully implicit schemes were presented. Three sample examples from previous works were explained in detail, and numerical results showed the outperforming of the HDG method over that of the DG method both in the memory requirement and CPU time metrics. Then, a fully explicit HDG method for the 3D time-domain Maxwell equations was formulated and several theoretical proofs were given. The method can be seen as a generalization of the classical DGTD scheme based on upwind fluxes. It coincides with the latter scheme for a particular choice of the stabilization parameter τ introduced in the definition of numerical traces in the HDG framework. The influence of this parameter on the scheme was assessed numerically, and the numerical solutions of Maxwell equations in the case of propagation of a standing wave in a cubic PEC cavity, propagation of a plane wave in a homogeneous domain and scattering of a plane wave by a dielectric sphere were presented in the last section of the chapter 3.
The next chapter contains a full presentation of a postprocessing approach for the fully explicit hybridizable discretization of the time-dependent Maxwell's equations in 3D. This postprocessing technique is inexpensive, and can be computed independently in each mesh element of the mesh, and at every time step of interest. It is thus well adapted to parallel computer architectures. Moreover, it is particularly suited to applications requiring a higher accuracy in localized regions, either in time or space. Numerical examples were presented, both with analytical solutions and in complicated geometries, that indicate that our postprocessing approach improves the convergence rate of the discrete solution in the $H(curl)$-norm by one order. Overall, this contribution is to be employed as an efficient way of reducing the $H(curl)$-norm error of discontinuous Galerkin discretizations.
The final chapter aims at elaborating a hybrid implicit/explicit (IMEX) HDG method for Maxwell's equations. In the first place, the semi-discrete formulation were written in terms of coarse and fine elements and then three IMEX time schemes of different orders were proposed to complete the fully discrete formulation of the method. Several theoretical proofs were given in order to obtain the stability of the method for the first and second order IMEX time integration when combined to the HDG spatial discretization. Numerical results were obtained with a 2D Matlab code on four different numerical cases assessing the convergence, the accuracy and the gain obtained by

the method in terms of CPU time in the cases where the locally refined meshes are a must for the accuracy of the approximated solution.

6.1 Future works

The topics presented in this manuscript call for a number of possible further developments, both from the numerical and the physical point of view. We close this manuscript with a shortlist of these topics:

- Giving a theoretical proof for the $k+1$ convergence order of the postprocessed solution in the $H(curl)$-norm.
- Giving a theoretical proof for the optimal convergence order of the proposed hybrid implicit/explicit HDG schemes. The proofs for the first and second order will be direct application to those done in [30], while for the third order, the proof is more complex.
- Devising an IMEX HDGTD formulation for the system of time-domain Maxwell equations coupled to a generalized dispersion model that can be fitted to describe the behavior of a wide range of metallic nanostructures [56].
- Elaborate a 3D code with the IMEX hybridizable discontinuous Galerkin method to simulate some realistic physical cases.

7

Appendix

This appendix contains a conference paper on the fully explicit HDGTD method for Maxwell's equations [37] and a submitted paper on a postprocessing technique for a discontinuous Galerkin discretization of time-dependent Maxwell's equations.

An Explicit Hybridizable Discontinuous Galerkin Method for the 3D Time-Domain Maxwell Equations

Georges Nehmetallah, Stéphane Lanteri, Stéphane Descombes, and Alexandra Christophe

1 Motivations and Objectives

The DGTD method is nowadays a very popular numerical method in the computational electromagnetics community. A lot of works are mostly concerned with time explicit DGTD methods relying on the use of a single global time step computed so as to ensure stability of the simulation. It is however well known that when combined with an explicit time integration method and in the presence of an unstructured locally refine mesh, a high order DGTD method suffers from a severe time step size restriction. An alternative approach that has been considered in [5, 7, 16] is to use a hybrid explicit-implicit (or locally implicit) time integration strategy. Such a strategy relies on a component splitting deduced from a partitioning of the mesh cells in two sets respectively gathering coarse and fine elements. The computational efficiency of this locally implicit DGTD method depends on the size of the set of fine elements that directly influences the size of the sparse part of the matrix system to be solved at each time. Therefore, an approach for reducing the size of the subsystem of globally coupled (i.e. implicit) unknowns is worth considering if one wants to solve very large-scale problems.

A particularly appealing solution in this context is given by the concept of hybridizable discontinuous Galerkin (HDG) method. The HDG method has been first introduced by Cockbrun et al. in [4] for a model elliptic problem and has been subsequently developed for a variety of PDE systems in continuum mechanics [13]. The essential ingredients of a HDG method are a local Galerkin projection of the underlying system of PDEs at the element level onto spaces of polynomials

G. Nehmetallah (✉) · S. Lanteri · S. Descombes · A. Christophe
Université Côte d'Azur, INRIA, CNRS, LJAD, Sophia-Antipolis Cedex, France
e-mail: georges.nehmetallah@inria.fr; stephane.lanteri@inria.fr; stephane.descombes@univ-cotedazur.fr; alexandra.christophe@inria.fr

S. J. Sherwin et al. (eds.), *Spectral and High Order Methods for Partial Differential Equations ICOSAHOM 2018*, Lecture Notes in Computational Science and Engineering 134, https://doi.org/10.1007/978-3-030-39647-3_41

to parameterize the numerical solution in terms of the numerical trace; a judicious choice of the numerical flux to provide stability and consistency; and a global jump condition that enforces the continuity of the numerical flux to arrive at a global weak formulation in terms of the numerical trace. The HDG methods are fully implicit, high-order accurate and most importantly, they reduce the globally coupled unknowns to the approximate trace of the solution on element boundaries, thereby leading to a significant reduction in the degrees of freedom. HDG methods for the system of time-harmonic Maxwell equations have been proposed in [9, 10, 14]. We have only developed the implicit HDG method for the time-domain Maxwell equations [3]. In view of devising a hybrid explicit-implicit HDG method, a preliminary step is therefore to elaborate on the principles of a fully explicit HDG formulation. It happens that fully explicit HDG methods have been studied recently for the acoustic wave equation by Kronbichler et al. [8] and Stanglmeier et al. [15]. In [15] the authors present a fully explicit, high order accurate in both space and time HDG method. In this paper we outline the formulation of this explicit HDGTD, present numerical results including a preliminary assessment of its superconvergence properties. We adopt a low storage Runge-Kutta scheme [2] for the time integration of the semi-discrete HDG equations. This work is a first step towards the construction of a hybrid explicit-implicit HDG method for time-domain electromagnetics.

2 Problem Statement and Notations

We consider the system of 3D time-domain Maxwell equations on a bounded polyhedral domain $\Omega \subset \mathbb{R}^3$

$$\begin{cases} \varepsilon \partial_t \mathbf{E} - \mathbf{curl}\mathbf{H} = -\mathbf{J}, \text{ in } \Omega \times [0, T], \\ \mu \partial_t \mathbf{H} + \mathbf{curl}\mathbf{E} = 0, \text{ in } \Omega \times [0, T], \end{cases} \tag{1}$$

where the symbol ∂_t denotes a time derivative, $\mathbf{J}$ the current density, T a final time, $\mathbf{E}(\mathbf{x}, t)$ and $\mathbf{H}(\mathbf{x}, t)$ are the electric and magnetic fields. The dielectric permittivity ε and the magnetic permeability μ are varying in space, time-invariant and both positive functions. The boundary of Ω is defined as $\partial\Omega = \Gamma_m \cup \Gamma_a$ with $\Gamma_m \cap \Gamma_a = \emptyset$. The boundary conditions are chosen as

$$\begin{cases} \mathbf{n} \times \mathbf{E} = 0, \text{ on } \Gamma_m \times [0, T], \\ \mathbf{n} \times \mathbf{E} + \mathbf{n} \times (\mathbf{n} \times \mathbf{H}) = \mathbf{n} \times \mathbf{E}^{\text{inc}} + \mathbf{n} \times (\mathbf{n} \times \mathbf{H}^{\text{inc}}) \\ \qquad = \mathbf{g}^{\text{inc}}, \text{ on } \Gamma_a \times [0, T]. \end{cases} \tag{2}$$

Here $\mathbf{n}$ denotes the unit outward normal to $\partial\Omega$ and $(\mathbf{E}^{\text{inc}}, \mathbf{H}^{\text{inc}})$ a given incident field. The first boundary condition is often referred as a metallic boundary condition and is applied on a perfectly conducting surface. The second relation is an absorbing boundary condition and takes here the form of the Silver-Müller condition. It is applied on a surface corresponding to an artificial truncation of a theoretically unbounded propagation domain. Finally, the system is supplemented with initial conditions: $\mathbf{E}_0(\mathbf{x}) = \mathbf{E}(\mathbf{x}, 0)$ and $\mathbf{H}_0(\mathbf{x}) = \mathbf{H}(\mathbf{x}, 0)$. For sake of simplicity, we omit the volume source term $\mathbf{J}$ in what follows.

We introduce now the notations and approximation spaces. We first consider a partition $\mathscr{T}_h$ of $\Omega \subset \mathbb{R}^3$ into a set of tetrahedron. Each non-empty intersection of two elements K^+ and K^- is called an interface. We denote by $\mathscr{F}_h^I$ the union of all interior interfaces of $\mathscr{T}_h$, by $\mathscr{F}_h^B$ the union of all boundary interfaces of $\mathscr{T}_h$, and $\mathscr{F}_h = \mathscr{F}_h^I \cup \mathscr{F}_h^B$. Note that $\partial\mathscr{T}_h$ represents all the interfaces ∂K for all $K \in \mathscr{T}_h$. As a result, an interior interface shared by two elements appears twice in $\partial\mathscr{T}_h$, unlike in $\mathscr{F}_h$ where this interface is evaluated once. For an interface $F \in \mathscr{F}_h^I$, $F = \overline{K}^+ \cap \overline{K}^-$, let $\mathbf{v}^\pm$ be the traces of $\mathbf{v}$ on F from the interior of $K^\pm$. On this interior face, we define mean values as $\{\mathbf{v}\}_F = (\mathbf{v}^+ + \mathbf{v}^-)/2$ and jumps as $[\![\mathbf{v}]\!]_F = \mathbf{n}^+ \times \mathbf{v}^+ + \mathbf{n}^- \times \mathbf{v}^-$ where the unit outward normal vector to K is denoted by $\mathbf{n}^\pm$. For the boundary faces these expressions are modified as $\{\mathbf{v}\}_F = \mathbf{v}^+$ and $[\![\mathbf{v}]\!]_F = \mathbf{n}^+ \times \mathbf{v}^+$ since we assume $\mathbf{v}$ is single-valued on the boundaries. In the following, we introduce the discontinuous finite element spaces and some basic operations on these spaces for later use. Let $\mathbb{P}_{p_K}(K)$ denotes the space of polynomial functions of degree at most p_K on the element $K \in \mathscr{T}_h$. The discontinuous finite element space is introduced as

$$\mathbf{V}_h = \left\{ \mathbf{v} \in \left[L^2(\Omega)\right]^3 \text{ such that } \mathbf{v}|_K \in \left[\mathbb{P}_{p_K}(K)\right]^3, \quad \forall K \in \mathscr{T}_h \right\}, \tag{3}$$

where $L^2(\Omega)$ is the space of square integrable functions on the domain Ω. The functions in $\mathbf{V}_h$ are continuous inside each element and discontinuous across the interfaces between elements. In addition, we introduce a traced finite element space

$$\begin{aligned} \mathbf{M}_h = \Big\{ \boldsymbol{\eta} \in \left[L^2(\mathscr{F}_h)\right]^3 \text{ such that } \boldsymbol{\eta}|_F \in \left[\mathbb{P}_{p_F}(F)\right]^3 \\ \text{and } \left(\boldsymbol{\eta} \cdot \mathbf{n}\right)|_F = 0, \quad \forall F \in \mathscr{F}_h \Big\}. \end{aligned} \tag{4}$$

For two vectorial functions $\mathbf{u}$ and $\mathbf{v}$ in $\left[L^2(D)\right]^3$, we denote $(\mathbf{u}, \mathbf{v})_D = \int_D \mathbf{u} \cdot \mathbf{v}\, \mathrm{d}\mathbf{x}$ provided D is a domain in $\mathbb{R}^3$, and we denote $< \mathbf{u}, \mathbf{v} >_F = \int_F \mathbf{u} \cdot \mathbf{v}\, \mathrm{d}s$ if F is a

two-dimensional face. Accordingly, for the mesh $\mathscr{T}_h$ we have

$$(\cdot,\cdot)_{\mathscr{T}_h} = \sum_{K\in\mathscr{T}_h} (\cdot,\cdot)_K\,, \qquad \langle\cdot,\cdot\rangle_{\partial\mathscr{T}_h} = \sum_{K\in\mathscr{T}_h} \langle\cdot,\cdot\rangle_{\partial K}\,,$$
$$\langle\cdot,\cdot\rangle_{\mathscr{F}_h} = \sum_{F\in\mathscr{F}_h} \langle\cdot,\cdot\rangle_F\,, \qquad \langle\cdot,\cdot\rangle_{\Gamma_a} = \sum_{F\in\mathscr{F}_h\cap\Gamma_a} \langle\cdot,\cdot\rangle_F\,.$$

We set $\mathbf{v}^t = -\mathbf{n}\times(\mathbf{n}\times\mathbf{v})\,,\quad \mathbf{v}^n = \mathbf{n}\,(\mathbf{n}\cdot\mathbf{v})$ where $\mathbf{v}^t$ and $\mathbf{v}^n$ are the tangential and normal components of $\mathbf{v}$ such as $\mathbf{v} = \mathbf{v}^t + \mathbf{v}^n$.

3 Principles and Formulation of the HDG Method

Following the classical DG approach, approximate solutions ($\mathbf{E}_h$,$\mathbf{H}_h$), for all $t \in [0, T]$, are seeked in the space $\mathbf{V}_h \times \mathbf{V}_h$ satisfying for all K in $\mathscr{T}_h$

$$\begin{cases} \left(\varepsilon\partial_t\mathbf{E}_h, \mathbf{v}\right)_K - \left(\mathbf{curl}\mathbf{H}_h, \mathbf{v}\right)_K = 0, \ \forall\mathbf{v}\in\mathbf{V}_h, \\ \left(\mu\partial_t\mathbf{H}_h, \mathbf{v}\right)_K + \left(\mathbf{curl}\mathbf{E}_h, \mathbf{v}\right)_K = 0, \ \forall\mathbf{v}\in\mathbf{V}_h. \end{cases} \tag{5}$$

Applying Green's formula, on both equations of (5) introduces boundary terms which are replaced by numerical traces $\hat{\mathbf{E}}_h$ and $\hat{\mathbf{H}}_h$ in order to ensure the connection between element-wise solutions and global consistency of the discretization. This leads to the global formulation for all $t \in [0, T]$

$$\begin{cases} \left(\varepsilon\partial_t\mathbf{E}_h, \mathbf{v}\right)_K - \left(\mathbf{H}_h, \mathbf{curl}\mathbf{v}\right)_K + \left\langle\hat{\mathbf{H}}_h, \mathbf{n}\times\mathbf{v}\right\rangle_{\partial K} = 0, \ \forall\mathbf{v}\in\mathbf{V}_h, \\ \left(\mu\partial_t\mathbf{H}_h, \mathbf{v}\right)_K + \left(\mathbf{E}_h, \mathbf{curl}\mathbf{v}\right)_K - \left\langle\hat{\mathbf{E}}_h, \mathbf{n}\times\mathbf{v}\right\rangle_{\partial K} = 0, \ \forall\mathbf{v}\in\mathbf{V}_h. \end{cases} \tag{6}$$

It is straightforward to verify that $\mathbf{n}\times\mathbf{v} = \mathbf{n}\times\mathbf{v}^t$ and $<\mathbf{H}, \mathbf{n}\times\mathbf{v}> = -<\mathbf{n}\times\mathbf{H}, \mathbf{v}>$. Therefore, using numerical traces defined in terms of the tangential components $\hat{\mathbf{H}}_h^t$ and $\hat{\mathbf{E}}_h^t$, we can rewrite (6) as

$$\begin{cases} \left(\varepsilon\partial_t\mathbf{E}_h, \mathbf{v}\right)_K - \left(\mathbf{H}_h, \mathbf{curl}\mathbf{v}\right)_K + \left\langle\hat{\mathbf{H}}_h^t, \mathbf{n}\times\mathbf{v}\right\rangle_{\partial K} = 0, \ \forall\mathbf{v}\in\mathbf{V}_h, \\ \left(\mu\partial_t\mathbf{H}_h, \mathbf{v}\right)_K + \left(\mathbf{E}_h, \mathbf{curl}\mathbf{v}\right)_K - \left\langle\hat{\mathbf{E}}_h^t, \mathbf{n}\times\mathbf{v}\right\rangle_{\partial K} = 0, \ \forall\mathbf{v}\in\mathbf{V}_h. \end{cases} \tag{7}$$

The hybrid variable $\boldsymbol{\Lambda}_h$ introduced in the setting of a HDG method [4] is here defined for all the interfaces of $\mathscr{F}_h$ as

$$\boldsymbol{\Lambda}_h := \hat{\mathbf{H}}_h^t, \quad \forall F\in\mathscr{F}_h. \tag{8}$$

We want to determine the fields $\hat{\mathbf{H}}_h^t$ and $\hat{\mathbf{E}}_h^t$ in each element K of $\mathscr{T}_h$ by solving system (7) and assuming that $\boldsymbol{\Lambda}_h$ is known on all the faces of an element K. We consider a numerical trace $\hat{\mathbf{E}}_h^t$ for all K given by

$$\hat{\mathbf{E}}_h^t = \mathbf{E}_h^t + \tau_K \mathbf{n} \times (\boldsymbol{\Lambda}_h - \mathbf{H}_h^t) \text{ on } \partial K, \tag{9}$$

where τ_K is a local stabilization parameter which is assumed to be strictly positive. We recall that $\mathbf{n} \times \mathbf{H}_h^t = \mathbf{n} \times \mathbf{H}_h$. The definitions of the hybrid variable (8) and numerical trace (9) are exactly those adopted in the context of the formulation of HDG methods for the 3D time-harmonic Maxwell equations [10–12, 14].

Following the HDG approach, when the hybrid variable $\boldsymbol{\Lambda}_h$ is known for all the faces of the element K, the electromagnetic field can be determined by solving the local system (7) using (8) and (9).

From now on we will note by g^{inc} the L^2 projection of g^{inc} on $\mathbf{M}_h$. Summing the contributions of (7) over all the elements and enforcing the continuity of the tangential component of $\hat{\mathbf{E}}_h$, we can formulate a problem which is to find $(\mathbf{E}_h, \mathbf{H}_h, \boldsymbol{\Lambda}_h) \in \mathbf{V}_h \times \mathbf{V}_h \times \mathbf{M}_h$ such that for all $t \in [0, T]$

$$\begin{aligned}
\left(\varepsilon \partial_t \mathbf{E}_h, \mathbf{v}\right)_{\mathscr{T}_h} - \left(\mathbf{H}_h, \mathbf{curl}\mathbf{v}\right)_{\mathscr{T}_h} + \left\langle \boldsymbol{\Lambda}_h, \mathbf{n} \times \mathbf{v}\right\rangle_{\partial \mathscr{T}_h} &= 0, \ \forall \mathbf{v} \in \mathbf{V}_h, \\
\left(\mu \partial_t \mathbf{H}_h, \mathbf{v}\right)_{\mathscr{T}_h} + \left(\mathbf{E}_h, \mathbf{curl}\mathbf{v}\right)_{\mathscr{T}_h} - \left\langle \hat{\mathbf{E}}_h^t, \mathbf{n} \times \mathbf{v}\right\rangle_{\partial \mathscr{T}_h} &= 0, \ \forall \mathbf{v} \in \mathbf{V}_h, \\
\left\langle [\![\hat{\mathbf{E}}_h]\!], \boldsymbol{\eta}\right\rangle_{\mathscr{F}_h} - \left\langle \boldsymbol{\Lambda}_h, \boldsymbol{\eta}\right\rangle_{\Gamma_a} - \left\langle \mathbf{g}^{\text{inc}}, \boldsymbol{\eta}\right\rangle_{\Gamma_a} &= 0, \ \forall \boldsymbol{\eta} \in \mathbf{M}_h,
\end{aligned} \tag{10}$$

where the last equation is called the conservativity condition with which we ask the tangential component of $\hat{\mathbf{E}}_h$ to be weakly continuous across any interface between two neighboring elements.

We now reformulate the system with numerical fluxes. We can deduce from the third equation of (10) that

$$\boldsymbol{\Lambda}_h = \begin{cases} \dfrac{1}{\tau_{K^+} + \tau_{K^-}} \left(2 \left\{\tau_K \mathbf{H}_h^t\right\}_F + [\![\mathbf{E}_h^t]\!]_F\right), & \text{if } F \in \mathscr{F}_h^I, \\ \dfrac{1}{\tau_K} \mathbf{n} \times \mathbf{E}_h^t + \mathbf{H}_h^t, & \text{if } F \in \mathscr{F}_h \cap \Gamma_m, \\ \dfrac{1}{\tau_K + 1} \left(\tau_K \mathbf{H}_h^t + \mathbf{n} \times \mathbf{E}_h^t - \mathbf{g}^{\text{inc}}\right). & \text{if } F \in \mathscr{F}_h \cap \Gamma_a. \end{cases} \tag{11}$$

By replacing (11) in (9) we obtain $\hat{\mathbf{E}}_h^t = \hat{\mathbf{E}}_h^{t,+} = \hat{\mathbf{E}}_h^{t,-}$ with

$$\hat{\mathbf{E}}_h^t = \begin{cases} \dfrac{\tau_{K^+}\tau_{K^-}}{\tau_{K^+} + \tau_{K^-}} \left(2 \left\{\dfrac{1}{\tau_K} \mathbf{E}_h^t\right\}_F - [\![\mathbf{H}_h^t]\!]_F\right), & \text{if } F \in \mathscr{F}_h^I, \\ 0, & \text{if } F \in \mathscr{F}_h \cap \Gamma_m, \\ \dfrac{1}{\tau_K + 1} \left(\mathbf{E}_h^t - \tau_K \mathbf{n} \times \mathbf{H}_h^t - \tau_K \mathbf{n} \times \mathbf{g}^{\text{inc}}\right). & \text{if } F \in \mathscr{F}_h \cap \Gamma_a. \end{cases} \tag{12}$$

Thus, the numerical traces (8) and (9) have been reformulated from the conservativity condition. This means that the conservativity condition is now included in the new formulation of the numerical fluxes and can be neglected in the global system of equations. Hence, the local system (6) takes the form of a classical DG formulation, $\forall \mathbf{v} \in \mathbf{V}_h$

$$\begin{cases} \left(\varepsilon \partial_t \mathbf{E}_h, \mathbf{v}\right)_K - \left(\mathbf{H}_h, \mathbf{curl}\mathbf{v}\right)_K + \left\langle \hat{\mathbf{H}}_h^t, \mathbf{n} \times \mathbf{v} \right\rangle_{\partial K} = 0, \\ \left(\mu \partial_t \mathbf{H}_h, \mathbf{v}\right)_K + \left(\mathbf{E}_h, \mathbf{curl}\mathbf{v}\right)_K - \left\langle \hat{\mathbf{E}}_h^t, \mathbf{n} \times \mathbf{v} \right\rangle_{\partial K} = 0. \end{cases} \tag{13}$$

where the numerical fluxes are defined by (11) and (12).

Remark 3 Let $Y_K = \sqrt{\varepsilon_K}/\sqrt{\mu_K}$ be the local admittance associated to cell K and $Z_K = 1/Y_K$ the corresponding local impedance. If we set $\tau_K = Z_K$ in (11) and $1/\tau_K = Y_K$ in (12), the obtained numerical traces coincide with those adopted in the classical upwind flux DGTD method [6].

4 Numerical Results

In order to validate and study the numerical convergence of the proposed HDG method, we consider the propagation of an eigenmode in a closed cavity (Ω is the unit square) with perfectly metallic walls. The frequency of the wave is $f = \sqrt{3}/\sqrt{2}c_0$ where c_0 is the speed of light in vacuum. The electric permittivity and the magnetic permeability are set to the constant vacuum values. The exact time-domaine solution is given in [6].

We start our study by assuming that the penalization parameter τ is equal to 1. In order to insure the stability of the method, numerical CFL conditions are determined for each value of the interpolation order p_K. In our particular case we have ε_K and μ_k are constant $= 1$ $\forall K \in \mathscr{T}_h$, so we have verified that, as we said in Remark 3, for $\tau = 1$, the values of CFL number correspond to the classical upwind flux-based DG method. In Table 1 we summarize the maximum Δt obtained numerically to insure the stability of the scheme

Given these values of Δt max, the L^2-norm of the error is calculated for a uniform tetrahedral mesh with 3072 elements which is constructed from a finite difference grid with $n_x = n_y = n_z = 9$ points, each cell of this grid yielding 6 tetrahedrons. The wave is propagated in the cavity during a physical time $t_{\max}$ corresponding to 8 periods (as shown in Fig. 1). Figure 2 depicts a comparison of

Table 1 Numerically obtained values of Δt max

Interpolation order	$\mathbb{P}_1$	$\mathbb{P}_2$	$\mathbb{P}_3$	$\mathbb{P}_4$
Δt max (s.)	0.32×10^{-9}	0.19×10^{-9}	0.13×10^{-9}	0.94×10^{-10}

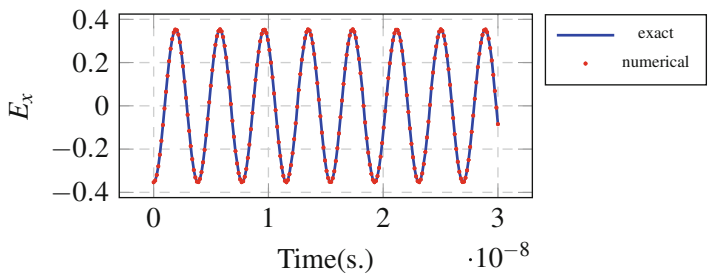

Fig. 1 Time evolution of the exact and the numerical solution of E_x at point $A(0.25, 0.25, 0.25)$ with a $\mathbb{P}_3$ interpolation

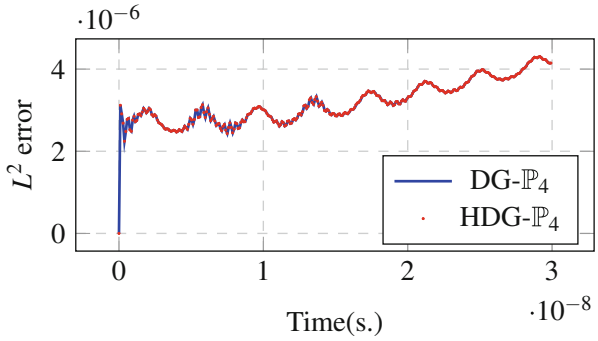

Fig. 2 Time evolution of the L^2-norm of the error for P4

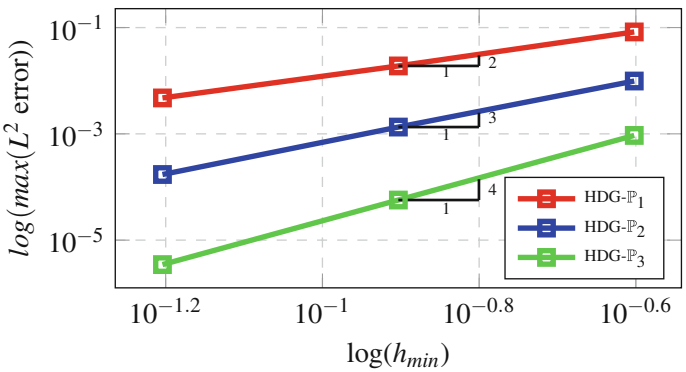

Fig. 3 Numerical convergence order of the time explicit HDG method for $\tau = 1$

the time evolution of the L^2-norm of the error between the solution obtained with an HDG method and a classical upwind flux-based DG method for $p_K = 4$. An optimal convergence with order $p_K + 1$ is obtained as shown in Fig. 3.

Now, we keep the same case than previously and we assess the behavior of the HDG method for various values of the penalization parameter τ. We observe that the time evolution of the electromagnetic energy for any order of interpolation, for different values of the parameter $\tau \neq 1$ and when the Δt used is fixed to the values defined in Table 1, the energy increases in time. In fact, It is necessary to decrease the Δt max for each value of τ to assure the stability (see Table 2 and Fig. 4). For this example, the optimal cost will be for the parameter $\tau = 1$ (having the same cost as an upwind flux for a DG method) otherwise we will spend more time to finish our simulation. On Fig. 5, we show the time evolution of the L^2-error for several values of τ with respect to the maximal time step for the considered parameters. In addition, Table 3 sums up numerical results in term of maximum L^2 errors and convergence rates. It appears that the order of convergence is not affected when the stabilization parameter is varied from 1 (with their associated CFL conditions).

Table 2 Numerically obtained values of the CFL number as a function of the stabilization parameter τ for a $\mathbb{P}1$ interpolation

τ	0.1	1.0	2.0	5.0	10.0
Δt max (s.)	0.31×10^{-10}	3.2×10^{-10}	1.7×10^{-10}	0.66×10^{-10}	0.32×10^{-10}

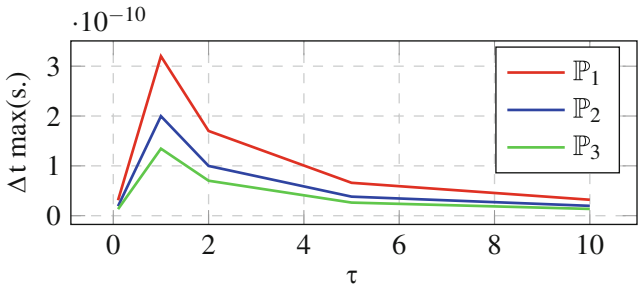

Fig. 4 Variation of the Δt max as a function of τ

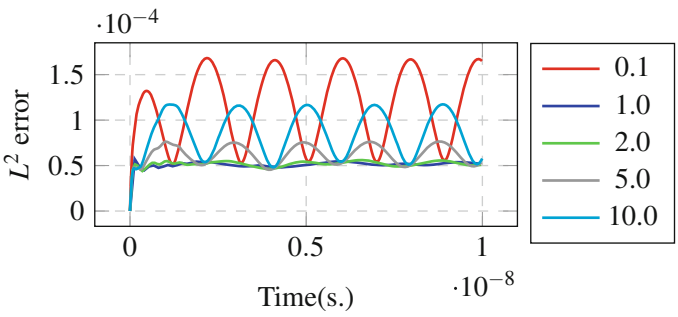

Fig. 5 Time evolution of the L^2-error as a function of τ with a $\mathbb{P}_3$ interpolation

Table 3 Maximum L2-errors and convergence orders

	$\tau = 1.0$					
$1/h$	$\mathbb{P}_1$, $\Delta t = 0.16 \times 10^{-09}$		$\mathbb{P}_2$, $\Delta t = 0.99 \times 10^{-10}$		$\mathbb{P}_3$, $\Delta t = 0.66 \times 10^{-10}$	
1/4	8.29e−02	–	9.87e−03	–	9.34e−04	–
1/8	1.90e−02	2.13	1.34e−03	2.88	5.68e−05	4.04
1/16	4.74e−03	2.00	1.72e−04	2.97	3.46e−06	4.04
	$\tau = 0.1$					
$1/h$	$\mathbb{P}_1$, $\Delta t = 0.16 \times 10^{-10}$		$\mathbb{P}_2$, $\Delta t = 0.96 \times 10^{-11}$		$\mathbb{P}_3$, $\Delta t = 0.66 \times 10^{-11}$	
1/4	2.14e−01	–	1.78e−02	–	2.19e−03	–
1/8	5.46e−02	1.97	2.85e−03	2.65	1.68e−04	3.70
1/16	1.18e−02	2.21	4.06e−04	2.81	1.14e−05	3.88
	$\tau = 10.0$					
$1/h$	$\mathbb{P}_1$, $\Delta t = 0.16 \times 10^{-10}$		$\mathbb{P}_2$, $\Delta t = 0.96 \times 10^{-11}$		$\mathbb{P}_3$, $\Delta t = 0.68 \times 10^{-11}$	
1/4	1.74e−01	–	1.53e−02	–	1.68e−03	–
1/8	4.24e−02	2.04	2.23e−03	2.76	1.17e−04	3.84
1/16	9.4e−03	2.16	3.10e−04	2.87	7.81e−06	3.91

5 Local Postprocessing

We define here, following the ideas of the local postprocessing developed in [1], new approximations for electric and magnetic field and expect that both $\mathbf{E}_h^{n*}$ and $\mathbf{H}_h^{n*}$ converge with order $k+1$ in the $H^{curl}(\mathscr{T}_h)$-norm, whereas $\mathbf{E}_h^n$ and $\mathbf{H}_h^n$ converge with order k in the $H^{curl}(\mathscr{T}_h)$-norm. To postprocess E_h^{n*} we first compute an approximation $(\mathbf{p}_{1,h}^n, \mathbf{p}_{2,h}^n) \in \mathbf{V}(K) \times \mathbf{V}(K)$ to the curl of $\mathbf{E}$, $\mathbf{p}_1(t^n) = \nabla \times \mathbf{E}(t^n)$ and the curl of $\mathbf{H}$, $\mathbf{p}_2(t^n) = \nabla \times \mathbf{H}(t^n)$ by locally solving the below system

$$(\mathbf{p}_{1,h}^n, \mathbf{v})_K = (\mathbf{E}_h^n, \nabla \times \mathbf{v})_K - \langle \hat{\mathbf{E}}_h^{t,n}, \mathbf{n} \times \mathbf{v} \rangle_{\partial K} \quad \forall \mathbf{v} \in \mathbf{V}(K)$$

and,

$$(\mathbf{p}_{2,h}^n, \mathbf{v})_K = (\mathbf{H}_h^n, \nabla \times \mathbf{v})_K - \langle \hat{\mathbf{H}}_h^{t,n}, \mathbf{n} \times \mathbf{v} \rangle_{\partial K} \quad \forall \mathbf{v} \in \mathbf{V}(K)$$

We then find $(\mathbf{E}_h^{n*}, \mathbf{H}_h^{n*}) \in [\mathscr{P}_{k+1}(K)]^3 \times [\mathscr{P}_{k+1}(K)]^3$ such that

$$\begin{cases} (\nabla \times \mathbf{E}_h^{n*}, \nabla \times \mathbf{W})_K = (\mathbf{p}_{h,1}^n, \nabla \times \mathbf{W})_K, & \forall \mathbf{W} \in [\mathscr{P}_{k+1}(K)]^3, \\ (\mathbf{E}_h^{n*}, \nabla Y)_K = (\mathbf{E}_h^n, \nabla Y)_K & \forall Y \in \mathscr{P}_{k+2}(K) \end{cases}$$

and,

$$\begin{cases} (\nabla \times \mathbf{H}_h^{n*}, \nabla \times \mathbf{W})_K = (\mathbf{p}_{h,2}^n, \nabla \times \mathbf{W})_K, & \forall \mathbf{W} \in [\mathscr{P}_{k+1}(K)]^3, \\ (\mathbf{H}_h^{n*}, \nabla Y)_K = (\mathbf{H}_h^n, \nabla Y)_K & \forall Y \in \mathscr{P}_{k+2}(K) \end{cases}$$

It is important to point out that we can compute $\mathbf{E}_h^{n*}$ and $\mathbf{H}_h^{n*}$ at any time step without advancing in time. Hence, the local postprocessing can be performed whenever we need higher accuracy at particular time steps. Numerical results given in Table 4 shows that a second order convergence rate is obtained for the post-processed solution.

6 Conclusion

In this paper we have presented an explicit HDG method to solve the system of Maxwell equations in 3D. The next step is to couple explicit and implicit HDG methods to treat the case of a locally refined mesh.

Table 4 Errors and orders of convergence before and after postprocessing

		$\tau = 1.0$			
		$\|\|E - E_h\|\|_{H_{curl}}$		$\|\|E - E_h^*\|\|_{H_{curl}}$	
P_k	$1/h$	Error	Order	Error	Order
P_1	1/4	9.30e−01	–	6.83e−01	–
	1/6	5.84e−01	1.14	3.10e−01	1.95
	1/8	4.34e−01	1.03	1.67e−01	2.15
P_2	1/4	1.67e−01	–	4.28e−02	–
	1/6	7.46e−02	1.98	1.19e−02	3.16
	1/8	4.29e−02	1.92	4.90e−03	3.06
P_3	1/4	2.30e−02	–	5.00e−03	–
	1/6	7.10e−03	2.90	1.10e−03	3.79
	1/8	3.00e−03	2.99	3.58e−04	3.84

References

1. Abgrall, R., Shu, C.-W.: Handbook of Numerical Methods for Hyperbolic Problems, vol. 17, pp. 190–194. Elsevier/North-Holland, Amsterdam (2016)
2. Carpenter, M.H., Kennedy, C.A.: Fourth-Order 2N-Storage Runge-Kutta Schemes. NASA, Washington (1994)
3. Christophe, A., Descombes, S., Lanteri, S.: An implicit hybridized discontinuous Galerkin method for the 3D time-domain Maxwell equations. Appl. Math. Comput. **319**, 395–408 (2018)
4. Cockburn, B., Gopalakrishnan, J., Lazarov, R.: Unified hybridization of discontinuous Galerkin, mixed, and continuous Galerkin methods for second order elliptic problems. SIAM J. Numer. Anal. **47**, 1319–1365 (2009)
5. Descombes, S., Lanteri, S. Moya, L.: Locally implicit discontinuous Galerkin time domain method for electromagnetic wave propagation in dispersive media applied to numerical dosimetry in biological tissues. SIAM J. Sci. Comput. **38**, A2611–A2633 (2016)
6. Hesthaven, J.S., Warburton, T.: Nodal high-order methods on unstructured grids. I. Time-domain solution of Maxwell's equations. Int. J. Numer. Methods Eng. **181**, 186–221 (2002)
7. Hochbruck, M. Sturm, A.: Error analysis of a second-order locally implicit method for linear Maxwell's equations. SIAM J. Numer. Anal. **54**, 3167–3191 (2016)
8. Kronbichler, M., Schoeder, S., Müller, C., Wall, W.A.: Comparison of implicit and explicit hybridizable discontinuous Galerkin methods for the acoustic wave equation. Int. J. Numer. Methods Eng. **270**, 330–342 (2014)
9. Li, L., Lanteri, S. Perrussel, R.: Numerical investigation of a high order hybridizable discontinuous Galerkin method for 2D time-harmonic Maxwell's equations. COMPEL **2**, 1112–1138 (2013)
10. Li, L., Lanteri, S., Perrussel, R.: A hybridizable discontinuous Galerkin method combined to a Schwarz algorithm for the solution of 3D time-harmonic Maxwell's equations. J. Comput. Phys. **256**, 563–581 (2014)
11. Moya, L.: Temporal convergence of a locally implicit discontinuous Galerkin method for Maxwell's equations. ESAIM Math. Model. Numer. Anal. (M2AN) **46**, 1225–1246 (2012)
12. Moya, L., Descombes, S. Lanteri, S.: Locally implicit time integration strategies in a discontinuous Galerkin method for Maxwell's equations. J. Sci. Comp. **56**, 190–218 (2013)
13. Nguyen, N.C., Peraire, J.: Hybridizable discontinuous Galerkin methods for partial differential equations in continuum mechanics. J. Comput. Phys. **231**, 5955–5988 (2012)
14. Nguyen, N.C., Peraire, J., Cockburn, B.: Hybridizable discontinuous Galerkin methods for the time-harmonic Maxwell's equations. J. Comput. Phys. **231**, 7151–7175 (2011)

15. Stanglmeier, M., Nguyen, N.C., Peraire, J., Cockburn, B.: An explicit hybridizable discontinuous Galerkin method for the acoustic wave equation. Comput. Methods Appl. Mech. Eng. **300**, 748–769 (2016)
16. Verwer, J.G.: Component splitting for semi-discrete Maxwell equations. BIT Numer. Math. **51**, 427–445 (2011)

Noname manuscript No.
(will be inserted by the editor)

A postprocessing technique for a discontinuous Galerkin discretization of time-dependent Maxwell's equations

G. Nehmetallah · T. Chaumont-Frelet · S. Descombes · S. Lanteri

Received: date / Accepted: date

Abstract We present a novel postprocessing technique for a discontinuous Galerkin (DG) discretization of time-dependent Maxwell's equations that we couple with an explicit Runge-Kutta time-marching scheme. The postprocessed electromagnetic field converges one order faster than the unprocessed solution in the $H(\mathrm{curl})$-norm. The proposed approach is local, in the sense that the enhanced solution is computed independently in each cell of the computational mesh, and at each time step of interest. As a result, it is inexpensive to compute, especially if the region of interest is localized, either in time or space. The key ideas behind this postprocessing technique stem from hybridizable discontinuous Galerkin (HDG) methods, which are equivalent to the analyzed DG scheme for specific choices of penalization parameters. We present several numerical experiments that highlight the superconvergence properties of the postprocessed electromagnetic field approximation.

Keywords Time-domain electromagnetics · Maxwell's equations · discontinuous Galerkin method · high-order method · postprocessing

G. Nehmetallah
Université Côte d'Azur, Inria, CNRS, LJAD
2004 Route des Lucioles, BP 93, 06902 Sophia Antipolis Cedex, France
E-mail: georges.nehmetallah@inria.fr

T. Chaumont-Frelet
Université Côte d'Azur, Inria, CNRS, LJAD
2004 Route des Lucioles, BP 93, 06902 Sophia Antipolis Cedex, France
E-mail: theophile.chaumont@inria.fr

S. Descombes
Université Côte d'Azur, Inria, CNRS, LJAD
2004 Route des Lucioles, BP 93, 06902 Sophia Antipolis Cedex, France
E-mail: stephane.descombes@unice.fr

S. Lanteri
Université Côte d'Azur, Inria, CNRS, LJAD
2004 Route des Lucioles, BP 93, 06902 Sophia Antipolis Cedex, France
E-mail: stephane.lanteri@inria.fr

1 Introduction

Maxwell's equations are the most general model of electrodynamic theory [14]. As a result, they are employed in a variety of applications, ranging from telecommunication engineering [17] to nanophotonics [12], to study the propagation of an electromagnetic field and its interaction with structures and matter.

Nowadays, numerical schemes are routinely employed to simulate the propagation of electromagnetic waves by computing approximate solutions to Maxwell's equations [7]. While several approaches, such as finite difference methods [20], are available, we focus here on discontinuous Galerkin methods [11,16,19], which have recently received a lot of attention, due to their great flexibility and ability to handle complex geometries.

Even if currently available computational power allows for useful and realistic simulations, modeling accurately the propagation of electromagnetic fields in complex geometries is still a challenging and very costly task. As a result, numerical schemes are expected to be accurate and robust, but also very efficient and adapted to modern computer architectures.

In the context of finite element methods, postprocessing techniques are an attractive way to improve the accuracy of an already computed discrete approximation. In many cases, these techniques can increase the order of convergence of the method at a very moderate cost. In addition, they often have a "local" nature, which allows for the design of embarrassingly parallel implementations. As a result, postprocessing techniques and superconvergence have attracted a considerable attention in the past decades [2,5,6,13].

In this work, we elaborate a novel postprocessing technique for time-dependent Maxwell's equations. Following [19], Maxwell's equations are discretized with a first-order discontinuous Galerkin method coupled with an explicit Runge-Kutta time-integration scheme [8]. This postprocessing improves the convergence rate in the $H(\mathrm{curl})$-norm by one order. As with similar postprocessing techniques devised in the past, our proposed approach is local, in the sense that the enhanced solution is computed independently in each cell of the computational mesh, and at each time step of interest. This is a key property as (a) it enables the design of highly parallel numerical algorithms, and (b) when the targeted application only requires the knowledge of the electromagnetic field in a limited region of space and/or time, the amount of computations is greatly reduced. Our postprocessing technique is inspired by two recent works, namely, a postprocessing for an explicit HDG discretization of the 2D acoustic wave equation [18], and a postprocessing for a HDG discretization of the 3D time-harmonic Maxwell's equations [1].

We do not carry out the mathematical analysis of the proposed postprocessing but instead, we present a number of numerical experiments highlighting its main features. As a result, our work is organized as follows: in Section 2, we recall the settings and key notations related to Maxwell's equations, discontinuous Galerkin methods, and Runge-Kutta schemes. We describe our

postprocessing in Section 3, and Section 4 presents numerical illustrations of the resulting methodology.

2 Settings

2.1 Maxwell's equations

We consider Maxwell's equations set in a Lipschitz polyhedral domain $\Omega \subset \mathbb{R}^3$ and in a time interval $(0,T)$. Specifically, given $\boldsymbol{J} : (0,T) \times \Omega \to \mathbb{R}^3$, the electromagnetic field $\boldsymbol{E}, \boldsymbol{H} : (0,T) \times \Omega \to \mathbb{R}^3$ satisfies

$$\begin{cases} \varepsilon \partial_t \boldsymbol{E} - \boldsymbol{\nabla} \times \boldsymbol{H} = \boldsymbol{J}, \\ \mu \partial_t \boldsymbol{H} + \boldsymbol{\nabla} \times \boldsymbol{E} = \boldsymbol{0}, \end{cases} \tag{1a}$$

in $(0,T) \times \Omega$, where the functions $\varepsilon, \mu : \Omega \to \mathbb{R}$ respectively represent the electric permittivity and the magnetic permeability of the materials contained in Ω. We assume that $0 < c \leq \varepsilon, \mu \leq C$ a.e. in Ω for fixed constants c and C.

The boundary of Ω is split into two subdomains Γ_{A} and Γ_{P}, and we prescribe the boundary conditions

$$\begin{cases} \boldsymbol{E} \times \boldsymbol{n}_\Omega + \sqrt{\dfrac{\mu}{\varepsilon}} (\boldsymbol{H} \times \boldsymbol{n}_\Omega) \times \boldsymbol{n}_\Omega = \boldsymbol{G} \quad \text{on } (0,T) \times \Gamma_{\mathrm{A}}, \\ \boldsymbol{E} \times \boldsymbol{n}_\Omega = \boldsymbol{0} \quad \text{on } (0,T) \times \Gamma_{\mathrm{P}}, \end{cases} \tag{1b}$$

where $\boldsymbol{n}_\Omega$ denotes the unit vector normal to $\partial\Omega$ pointing outward Ω and $\boldsymbol{G} : (0,T) \times \Gamma_{\mathrm{A}} \to \mathbb{R}^3$ is a tangential load term (i.e. $\boldsymbol{G} \cdot \boldsymbol{n}_\Omega = 0$). The first relation of (1b) is a first-order absorbing boundary condition (ABC) known as the Silver-Muller ABC. It is the simplest form of ABC for Maxwell's equations, and one could alternatively consider higher order ABCs [15] or perfectly matched layers [19]. The second equation in (1b) models the boundary of a perfectly conducting material. Finally, initial conditions are imposed in Ω

$$\begin{cases} \boldsymbol{E}|_{t=0} = \boldsymbol{E}_0, \\ \boldsymbol{H}|_{t=0} = \boldsymbol{H}_0, \end{cases} \tag{1c}$$

where $\boldsymbol{E}_0, \boldsymbol{H}_0 : \Omega \to \mathbb{R}^3$ are given functions.

Classically [4], under the assumption that the data μ, ε, $\boldsymbol{J}$, $\boldsymbol{G}$, $\boldsymbol{E}_0$ and $\boldsymbol{H}_0$ are sufficiently smooth, there exists a unique pair of solution $(\boldsymbol{E}, \boldsymbol{H})$ to (1).

We finally mention that in many applications, $\boldsymbol{G}$ is defined in order to inject an "incident" field in the domain. In this case, we have

$$\boldsymbol{G} := \boldsymbol{E}^{\mathrm{inc}} \times \boldsymbol{n}_\Omega + \sqrt{\frac{\mu}{\varepsilon}} (\boldsymbol{H}^{\mathrm{inc}} \times \boldsymbol{n}_\Omega) \times \boldsymbol{n}_\Omega, \tag{2}$$

where $(\boldsymbol{E}^{\mathrm{inc}}, \boldsymbol{H}^{\mathrm{inc}})$ is a solution to Maxwell's equations in free space. An important example that we will consider in Section 4 is the case where the incident field is a plane wave.

2.2 Mesh and notations

The domain Ω is partitioned into a mesh $\mathcal{T}_h$. We assume that $\mathcal{T}_h$ consists of straight tetrahedral elements K, but hexahedral and/or curved elements could be considered as well. We assume that ε and μ take constant values ε_K and μ_K in each element $K \in \mathcal{T}_h$.

For the sake of simplicity, we restrict our attention to meshes that are conforming in the sense of [10]. Specifically, the intersection $\overline{K}_- \cap \overline{K}_+$ of two distinct elements $K_\pm \in \mathcal{T}_h$ is either a full face, a full edge, or a single vertex of both K_- and K_+. In particular, hanging nodes are not covered by the present analysis. This is not an intrinsic limitation of the method, but this assumption greatly simplifies the forthcoming presentation.

We denote by $\mathcal{F}_h$ the faces of the partition. Recalling that $\mathcal{T}_h$ is conforming, each face $F \in \mathcal{F}_h$ is either the intersection $\partial K_- \cap \partial K_-$ of two elements $K_\pm \in \mathcal{T}_h$, or is contained in the intersection $\partial K \cap \partial\Omega$ of a single element $K \in \mathcal{T}_h$ with the boundary of the domain. We respectively denote by $\mathcal{F}_h^{\mathrm{int}}$, $\mathcal{F}_h^{\mathrm{P}}$ and $\mathcal{F}_h^{\mathrm{A}}$ the set internal faces, and the sets of faces belonging to Γ_{P} and Γ_{A}.

We associate with each face $F \in \mathcal{F}_h$ a unit normal $\boldsymbol{n}_F$, with the convention that $\boldsymbol{n}_F = \boldsymbol{n}_\Omega$ if $F \in \mathcal{F}_h^{\mathrm{P}} \cup \mathcal{F}_h^{\mathrm{A}}$. If $F \in \mathcal{F}_h^{\mathrm{int}}$, the orientation of the normal is arbitrary, but fixed. If $\boldsymbol{v} : \Omega \to \mathbb{R}^3$ is a function admitting well-defined traces on $F \in \mathcal{F}_h$, the notations $[\![\boldsymbol{v}]\!]_F$ and $\{\{\boldsymbol{v}\}\}_F$ denote the "jump" and the "mean" of $\boldsymbol{v}$ on F. If $F \in \mathcal{F}_h^{\mathrm{int}}$ with $F = \partial K_- \cap K_+$, these quantities are defined by

$$[\![\boldsymbol{v}]\!]_F := \boldsymbol{v}_+|_F(\boldsymbol{n}_+ \cdot \boldsymbol{n}_F) + \boldsymbol{v}_-|_F(\boldsymbol{n}_- \cdot \boldsymbol{n}_F), \qquad \{\{\boldsymbol{v}\}\}_F := \frac{1}{2}\left(\boldsymbol{v}_+|_F + \boldsymbol{v}_-|_F\right),$$

where $\boldsymbol{v}_\pm := \boldsymbol{v}|_{K_\pm}$ and $\boldsymbol{n}_\pm$ denotes the unit outward normal to $K_\pm$, while we simply set

$$[\![\boldsymbol{v}]\!]_F := \{\{\boldsymbol{v}\}\}_F := \boldsymbol{v}|_F,$$

if $F \in \mathcal{F}_h^{\mathrm{P}} \cup \mathcal{F}_h^{\mathrm{A}}$.

In the remaining of this work, k is a fixed non-negative integer representing a polynomial degree. For every element $K \in \mathcal{T}_h$, $\mathcal{P}_k(K)$ denotes the set of polynomials defined on K of degree less than or equal k, and $\boldsymbol{\mathcal{P}}_k(K) := (\mathcal{P}_k(K))^3$ denotes the space of vector-valued functions having polynomial components. We finally employ the notation

$$\boldsymbol{\mathcal{P}}_k(\mathcal{T}_h) := \left\{\boldsymbol{v} : \Omega \to \mathbb{R}^3 \mid \boldsymbol{v}|_K \in \boldsymbol{\mathcal{P}}_k(K)\ \forall K \in \mathcal{T}_h\right\},$$

for the space of piecewise polynomial functions. We also employ the notation $\boldsymbol{\mathcal{P}}_k^{\mathrm{t}}(F)$ for the set of vector-valued polynomial functions defined on F that are tangential to F. $\boldsymbol{\mathcal{P}}_k^{\mathrm{t}}(\mathcal{F}_h)$ is then the set of tangential polynomial defined on the skeleton of the mesh that are piecewise in $\boldsymbol{\mathcal{P}}_k^{\mathrm{t}}(F)$.

2.3 The discontinuous Galerkin scheme

We seek the discrete fields as piecewise polynomial functions, namely $\boldsymbol{E}_h, \boldsymbol{H}_h \in \boldsymbol{\mathcal{P}}_k(\mathcal{T}_h)$. Following [3], the first step is to multiply (1a) by two test functions $\boldsymbol{v}$

and $\boldsymbol{w}$, and integrate by parts over each element $K \in \mathcal{T}_h$. We obtain

$$\begin{cases} (\varepsilon \partial_t \boldsymbol{E}_h, \boldsymbol{v})_{\mathcal{T}_h} - (\boldsymbol{H}_h, \boldsymbol{\nabla} \times \boldsymbol{v})_{\mathcal{T}_h} + \langle \widehat{\boldsymbol{H}}_h^{\mathrm{t}}, [\![\boldsymbol{v}]\!] \times \boldsymbol{n} \rangle_{\mathcal{F}_h} = (\boldsymbol{J}, \boldsymbol{v}), \\ (\mu \partial_t \boldsymbol{H}_h, \boldsymbol{w})_{\mathcal{T}_h} + (\boldsymbol{E}_h, \boldsymbol{\nabla} \times \boldsymbol{w})_{\mathcal{T}_h} - \langle \widehat{\boldsymbol{E}}_h^{\mathrm{t}}, [\![\boldsymbol{w}]\!] \times \boldsymbol{n} \rangle_{\mathcal{F}_h} = 0, \end{cases} \tag{3}$$

where $\widehat{\boldsymbol{E}}_h^{\mathrm{t}}, \widehat{\boldsymbol{H}}_h^{\mathrm{t}} \in \boldsymbol{\mathcal{P}}_k^{\mathrm{t}}(\mathcal{F}_h)$ are face-based tangential fields called "numerical fluxes", and

$$\langle \widehat{\boldsymbol{M}}_h^{\mathrm{t}}, [\![\boldsymbol{u}]\!] \times \boldsymbol{n} \rangle_{\mathcal{F}_h} := \sum_{F \in \mathcal{F}_h} \int_F \widehat{\boldsymbol{M}}_h^{\mathrm{t}} \cdot ([\![\boldsymbol{u}]\!]_F \times \boldsymbol{n}_F),$$

for $\boldsymbol{M}_h^{\mathrm{t}} \in \boldsymbol{\mathcal{P}}_k^{\mathrm{t}}(\mathcal{F}_h)$, and $\boldsymbol{u}_h \in \boldsymbol{\mathcal{P}}_k(\mathcal{T}_h)$. We make use of numerical fluxes in the spirit of local DG methods that were originally introduced in [9] for scalar elliptic equations, and later in [16] for Maxwell's equations. We follow [19] to define our numerical fluxes. Specifically, we set $Z_K := \sqrt{\mu_K/\varepsilon_K}$ and $Y_K := 1/Z_K$ for each $K \in \mathcal{T}_h$, and we select

$$\begin{aligned} \widehat{\boldsymbol{E}}_h^{\mathrm{t}}|_F &:= \frac{1}{\{\{Y\}\}} \left(\{\{Y \boldsymbol{E}_h\}\}_F^{\mathrm{t}} + \frac{1}{2} [\![\boldsymbol{H}_h]\!]_F \times \boldsymbol{n} \right), \\ \widehat{\boldsymbol{H}}_h^{\mathrm{t}}|_F &:= \frac{1}{\{\{Z\}\}} \left(\{\{Z \boldsymbol{H}_h\}\}_F^{\mathrm{t}} - \frac{1}{2} [\![\boldsymbol{E}_h]\!]_F \times \boldsymbol{n} \right), \end{aligned}$$

for all $F = \partial K_- \cap \partial K_+ \in \mathcal{F}_h^{\mathrm{int}}$, and

$$\widehat{\boldsymbol{E}}_h^{\mathrm{t}}|_F := \boldsymbol{0} \qquad \widehat{\boldsymbol{H}}_h^{\mathrm{t}}|_F := -Y \boldsymbol{E}_h \times \boldsymbol{n} + \boldsymbol{H}_h^{\mathrm{t}},$$

if $F = \partial K \cap \Gamma_{\mathrm{P}} \in \mathcal{F}_h^{\mathrm{P}}$, and

$$\begin{aligned} \widehat{\boldsymbol{E}}_h^{\mathrm{t}}|_F &:= \frac{1}{2} \left(\boldsymbol{E}_h^{\mathrm{t}} + Z \boldsymbol{H}_h \times \boldsymbol{n} + \boldsymbol{G} \times \boldsymbol{n} \right), \\ \widehat{\boldsymbol{H}}_h^{\mathrm{t}}|_F &:= \frac{Y}{2} \left(Z \boldsymbol{H}_h^{\mathrm{t}} - \boldsymbol{E}_h \times \boldsymbol{n} - \boldsymbol{G} \right), \end{aligned}$$

when $F = \partial K \cap \Gamma_{\mathrm{A}} \in \mathcal{F}_h^{\mathrm{A}}$.

2.4 Time discretization

We can rewrite problem (3) obtained after space discretization as

$$M \dot{U}_h(t) + K U_h(t) = B(t), \quad U_h(0) = U_{h,0} \tag{4}$$

where for each $t \in [0, T]$, the vector $U_h(t)$ contains the coefficients defining $\boldsymbol{E}_h(t)$ and $\boldsymbol{H}_h(t)$ in the nodal basis of $\boldsymbol{\mathcal{P}}_k(\mathcal{T}_h)$, M and K are the usual mass and stiffness matrices associated with (3), and $U_{h,0}$ is the interpolation of the initial conditions in the discretization space.

Classically, the key asset of DG schemes is that the mass matrix is block-diagonal, and hence, easy to invert. Thus, we may safely rewrite (4) as

$$\dot{U}_h(t) = -GU_h(t) + F(t), \quad U_h(0) = U_{h,0}, \tag{5}$$

where $G := M^{-1}K$ and $F(t) := M^{-1}B(t)$. At this point, we recognize in (5) a system of ordinary differential equations that can be discretized with a time marching scheme.

Here, we focus on a low storage Runge-Kutta scheme, usually denoted by LSRK(5,4), presented in [8]. After fixing a time-step Δt, we iteratively construct approximations U_h^n of $U_h(t_n)$, $t_n := n\Delta t$. Specifically, we let $U_h^0 := U_{h,0}$, and for $n \geq 0$, U_h^{n+1} is deduced from U_h^n through the following algorithm

$$\begin{cases} V_h^1 = U_h^n \\ \left.\begin{array}{l} V_h^2 = a_k V_h^2 + \Delta t \left(GV_h^1 + F(t_n + c_k \Delta T)\right) \\ V_h^1 = V_h^1 + b_k V_h^2 \end{array}\right\} \text{ for } \ k = 1, \cdots, 5 \\ U_h^{n+1} = V_h^1, \end{cases}$$

where the coefficients a_k, b_k and c_k are described in Table 1. Then, $\boldsymbol{E}_{h,n}$ and $\boldsymbol{H}_{h,n}$ are the element of $\boldsymbol{\mathcal{P}}_k(\mathcal{T}_h)$ expended on the nodal basis with the coefficients stored in U_h^n.

The above scheme is of particular interest as it is fourth-order accurate with respect to the time step Δt while being memory efficient. Indeed, it only requires the storage of two coefficient vectors in memory.

Classically, as this time integration scheme is explicit, it is stable under a CFL condition linking together the mesh size h and the selected time step Δt. Specifically, given a mesh $\mathcal{T}_h$, we fix the time step by

$$\Delta t := \alpha_k \min_{K \in \mathcal{T}_h} \frac{1}{c_K} \frac{V_K}{A_K} \tag{6}$$

where, $c_K := 1/\sqrt{\varepsilon_K \mu_K}$ is the wave speed in the element K, and V_K and A_K are respectively the volume and the area of K. The constant α_k is selected according to the polynomial degree k. Here, we use the values listed in Table 2, that we obtained after testing the scheme on simple test-cases.

Finally, to ease the discussions in numerical experiments below, we denote by N the number of time steps performed in each simulations.

3 A novel postprocessing

As discussed above, $\boldsymbol{E}_{h,n}$ and $\boldsymbol{H}_{h,n}$ are respectively meant to approximate $\boldsymbol{E}(t_n)$ and $\boldsymbol{H}(t_n)$. The purpose of this section is to introduce postprocessed solutions $\boldsymbol{E}_{h,n}^\star$ and $\boldsymbol{H}_{h,n}^\star$ that are more accurate representations of $\boldsymbol{E}(t_n)$ and $\boldsymbol{H}(t_n)$. This postprocessing is purely local in time, in the sense that the computation of $\boldsymbol{E}_{h,n}^\star$ and $\boldsymbol{H}_{h,n}^\star$ only involves $\boldsymbol{E}_{h,n}$ and $\boldsymbol{H}_{h,n}$. It is also local in

Coeff	Value	Coeff	Value	Coeff	Value
a_1	0	b_1	$\frac{1432997174477}{9575080441755}$	c_1	0
a_2	$-\frac{567301805773}{1357537059087}$	b_2	$\frac{5161836677717}{1361206829357}$	c_2	$\frac{1432997174477}{9575080441755}$
a_3	$-\frac{2404267990393}{2016746695238}$	b_3	$\frac{1720146321549}{2090206949498}$	c_3	$\frac{2526269341429}{6820363962896}$
a_4	$-\frac{3550918686646}{2091501179385}$	b_4	$\frac{3134564353537}{4481467310338}$	c_4	$\frac{2006345519317}{3224310063776}$
a_5	$-\frac{1275806237668}{842570457699}$	b_5	$\frac{2277821191437}{14882151754819}$	c_5	$\frac{2802321613138}{2924317926251}$

Table 1 Values of the coefficients of the LSRK(5,4) scheme.

k	1	2	3	4
α_k	0.70	0.46	0.30	0.21

Table 2 Values of α_k in CFL condition (6).

space as the computation are local to each element $K \in \mathcal{T}_h$. Actually, $\boldsymbol{E}^\star_{h,n}|_K$ (resp. $\boldsymbol{H}^\star_{h,n}|_K$) only depends on $\boldsymbol{E}_{h,n}|_{\widetilde{K}}$ (resp. $\boldsymbol{H}_{h,n}|_{\widetilde{K}}$), where $\widetilde{K}$ is the union of all elements $K' \in \mathcal{T}_h$ sharing (at least) one face with K.

Our approach closely follows previous works. Specifically, similar postprocessing strategies have been derived for the time-harmonic Maxwell's equations [1], as well as time-dependent acoustic wave equation [18]. These works develop in the context of hybridizable discontinuous Galerkin (HDG) methods, but can be easily applied to the DG scheme under consideration, as we depict hereafter.

Our postprocessing hinges on element-wise finite element saddle-point problems. For each element $K \in \mathcal{T}_h$, there exists a unique pair $(\boldsymbol{E}^\star_{h,n}, p) \in \boldsymbol{\mathcal{P}}_{k+1}(K) \times \mathcal{P}_{k+2}(K)/\mathbb{R}$ such that

$$\begin{cases} (\boldsymbol{\nabla} \times \boldsymbol{E}^\star_{h,n}, \boldsymbol{\nabla} \times \boldsymbol{w})_K + (\boldsymbol{\nabla} p, \boldsymbol{w})_K = (\boldsymbol{\nabla} \times \boldsymbol{E}_{h,n}, \boldsymbol{\nabla} \times \boldsymbol{w})_K \\ \qquad\qquad\qquad\qquad + \langle \boldsymbol{E}^{\mathrm{t}}_{h,n} - \widehat{\boldsymbol{E}}^{\mathrm{t}}_{h,n}, \boldsymbol{n} \times \boldsymbol{\nabla} \times \boldsymbol{w} \rangle_{\partial K}, \\ (\boldsymbol{E}^\star_{h,n}, \boldsymbol{\nabla} v)_K = (\boldsymbol{E}_{h,n}, \boldsymbol{\nabla} v)_K, \end{cases}$$

for all $\boldsymbol{w} \in \boldsymbol{\mathcal{P}}_{k+1}(K)$ and $v \in \mathcal{P}_{k+2}(K)/\mathbb{R}$. Similarly, for the magnetic field, there exists a unique pair $(\boldsymbol{H}^\star_{h,n}, q) \in \boldsymbol{\mathcal{P}}_{k+1}(K) \times \mathcal{P}_{k+2}(K)/\mathbb{R}$ such that

$$\begin{cases} (\boldsymbol{\nabla} \times \boldsymbol{H}^\star_{h,n}, \boldsymbol{\nabla} \times \boldsymbol{w})_K + (\boldsymbol{\nabla} q, \boldsymbol{w})_K = (\boldsymbol{\nabla} \times \boldsymbol{H}_{h,n}, \boldsymbol{\nabla} \times \boldsymbol{w})_K \\ \qquad\qquad\qquad\qquad + \langle \boldsymbol{H}^{\mathrm{t}}_{h,n} - \widehat{\boldsymbol{H}}^{\mathrm{t}}_{h,n}, \boldsymbol{n} \times \boldsymbol{\nabla} \times \boldsymbol{w} \rangle_{\partial K}, \\ (\boldsymbol{H}^\star_{h,n}, \boldsymbol{\nabla} v)_K = (\boldsymbol{H}_{h,n}, \boldsymbol{\nabla} v)_K, \end{cases}$$

for all $\boldsymbol{w} \in \boldsymbol{\mathcal{P}}_{k+1}(K)$ and $v \in \mathcal{P}_{k+2}(K)/\mathbb{R}$. $\boldsymbol{E}^\star_{h,n}$ and $\boldsymbol{H}^\star_{h,n}$ are then our postprocessed approximations to $\boldsymbol{E}(t_n)$ and $\boldsymbol{H}(t_n)$.

The left-hand sides of the above definition lead to solve symmetric linear systems of small size. In addition, observing that the left-hand side is actually

the same for the two postprocessing schemes, we deduce that only one matrix factorization is required per element.

The right-hand sides further show that for each $K \in \mathcal{T}_h$, the postprocessed field $\boldsymbol{E}^\star_{h,n}|_K$ only depends on $\boldsymbol{E}_{h,n}|_K$ and the value at the flux $\widehat{\boldsymbol{E}}^{\mathrm{t}}_{h,n}|_F$ on each face $F \in \mathcal{F}_K$. In turn, since the flux is defined using the two elements sharing the face F, we see that $\boldsymbol{E}_{h,n}|_K$ depends on the values taken by $\boldsymbol{E}_{h,n}$ on all the elements K' sharing at least one face with K. A similar comment holds true for $\boldsymbol{H}^\star_{h,n}$.

4 Numerical experiments

4.1 Standing wave in a cavity

We first consider a model problem given by the propagation of standing wave in unit cube $\Omega := (0, L)^3$, $L := 1$ m, with perfectly conducting walls (i.e. $\Gamma_{\mathrm{P}} := \partial\Omega$ and $\Gamma_{\mathrm{A}} := \emptyset$). Specifically, we consider Maxwell's equations (1) with right-hand sides $\boldsymbol{J} := \boldsymbol{0}$, $\boldsymbol{G} := \boldsymbol{0}$ and initial conditions

$$\boldsymbol{E}|_{t=0} := \begin{pmatrix} -\cos(\pi \boldsymbol{x}_1)\sin(\pi \boldsymbol{x}_2)\sin(\pi \boldsymbol{x}_3) \\ 0 \\ \sin(\pi \boldsymbol{x}_1)\sin(\pi \boldsymbol{x}_2)\cos(\pi \boldsymbol{x}_3) \end{pmatrix},$$

and $\boldsymbol{H}|_{t=0} := \boldsymbol{0}$. ε and μ are respectively set to the vacuum values $\varepsilon_0 := (1/36\pi) \times 10^{-9}$ Fm^{-1} and $\mu_0 := 4\pi \times 10^{-7}$ Hm^{-1}, and we select the simulation time $T := 10$ ns. The analytical solution is available, and reads

$$\boldsymbol{E}(t, \boldsymbol{x}) := \cos(\omega t) \begin{pmatrix} -\cos(\pi \boldsymbol{x}_1)\sin(\pi \boldsymbol{x}_2)\sin(\pi \boldsymbol{x}_3) \\ 0 \\ \sin(\pi \boldsymbol{x}_1)\sin(\pi \boldsymbol{x}_2)\cos(\pi \boldsymbol{x}_3) \end{pmatrix},$$

and

$$\boldsymbol{H}(t, \boldsymbol{x}) := \frac{\pi}{\omega}\sin(\omega t) \begin{pmatrix} \sin(\pi \boldsymbol{x}_1)\cos(\pi \boldsymbol{x}_2)\cos(\pi \boldsymbol{x}_3) \\ 2\cos(\pi \boldsymbol{x}_1)\sin(\pi \boldsymbol{x}_2)\cos(\pi \boldsymbol{x}_3) \\ \cos(\pi \boldsymbol{x}_1)\cos(\pi \boldsymbol{x}_2)\sin(\pi \boldsymbol{x}_3) \end{pmatrix},$$

where the angular frequency is given by $\omega := \sqrt{3}\pi c_0/L$, $c_0 := 1/\sqrt{\varepsilon_0\mu_0}$ being the speed of light.

We consider structured meshes $\mathcal{T}_h$ that are obtained by first splitting Ω into $n \times n \times n$ cubes ($n := L/h$), and then splitting each cube into 6 tetrahedra.

Figures 1 and 2 show the behavior of the error for the original and postprocessed discrete solutions with respect to time on a fixed mesh built from a $8 \times 8 \times 8$ Cartesian partition. The time step Δt is selected following CFL condition (6). Both the original and the postprocessed error exhibit an oscillatory behavior, which is typical of this particular test case. The postprocessed solution is about 10 times more accurate than the original one.

Table 3 presents in more detail our results on a series of meshes and for different polynomial degrees. We see that in each case, the curl of the postprocessed solution converges with the expected order, namely $k + 1$.

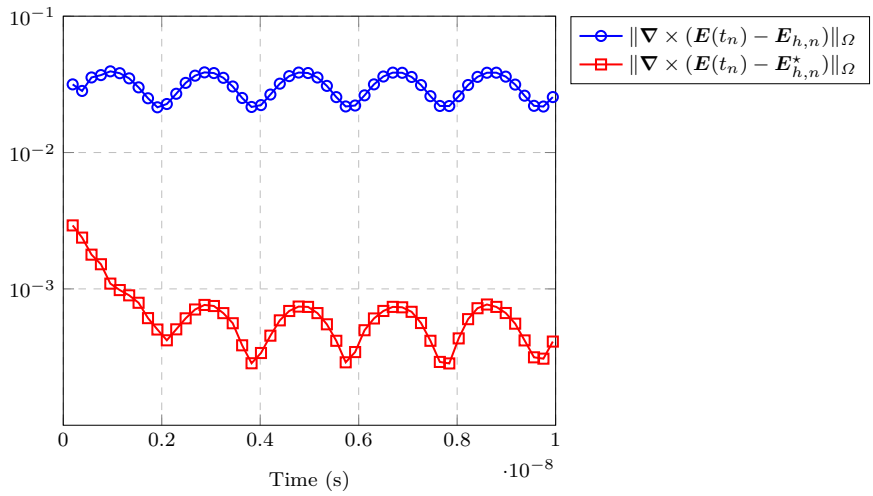

Fig. 1 Standing wave in a cubic cavity: time evolution of the error on the electric field.

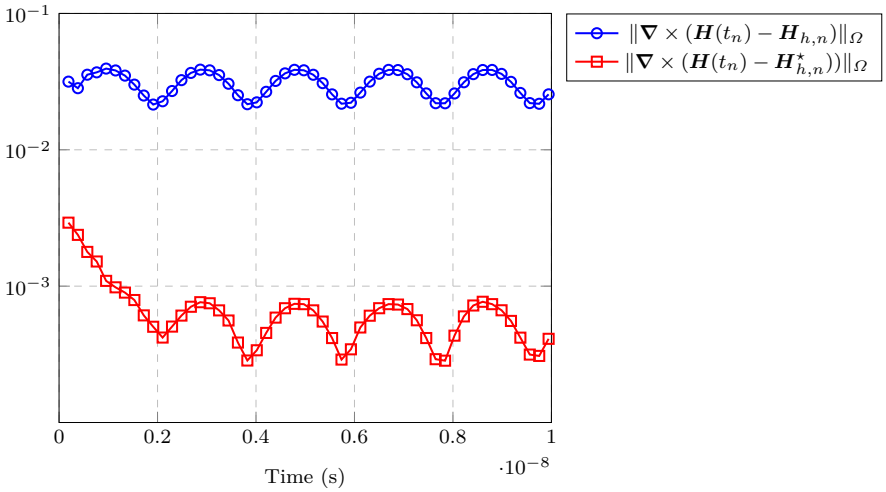

Fig. 2 Standing wave in a cubic cavity: time evolution of the error on the magnetic field.

4.2 Plane wave in free space

We now consider the propagation of a plane wave in free space. Specifically, we consider Maxwell's equations (1) with $\Omega := (0, L)^3$, $L := 1$ m, $\Gamma_{\mathrm{P}} := \emptyset$ and $\Gamma_{\mathrm{A}} := \partial\Omega$. $\boldsymbol{J} := \boldsymbol{0}$, and $\boldsymbol{G}$ is defined by (2) with

$$\boldsymbol{E}^{\mathrm{inc}}(t, \boldsymbol{x}) := \boldsymbol{p} \cos\left(\omega\left(t - \frac{\boldsymbol{d} \cdot \boldsymbol{x}}{c_0}\right)\right), \quad \boldsymbol{H}^{\mathrm{inc}}(t, \boldsymbol{x}) := \sqrt{\frac{\varepsilon_0}{\mu_0}}\boldsymbol{d} \times \boldsymbol{E}^{\mathrm{inc}}(t, \boldsymbol{x}),$$

Table 3 Standing wave in a cubic cavity: numerical convergence.

	h	$\|\boldsymbol{\nabla}\times(\boldsymbol{E}(T)-\boldsymbol{E}_{h,N})\|_\Omega$		$\|\boldsymbol{\nabla}\times(\boldsymbol{E}(T)-\boldsymbol{E}^\star_{h,N})\|_\Omega$	
	1/4	7.99e-01		6.37e-01	
$\mathcal{P}_1$	1/6	4.94e-01	(**eoc 1.19**)	2.69e-01	(**eoc 2.13**)
	1/8	3.65e-01	(**eoc 1.05**)	1.45e-01	(**eoc 2.15**)
	1/4	1.40e-01		3.80e-02	
$\mathcal{P}_2$	1/6	6.55e-02	(**eoc 1.87**)	1.04e-02	(**eoc 3.20**)
	1/8	3.75e-02	(**eoc 1.94**)	4.24e-03	(**eoc 3.12**)
	1/4	2.05e-02		4.32e-03	
$\mathcal{P}_3$	1/6	6.17e-03	(**eoc 2.96**)	9.29e-04	(**eoc 3.74**)
	1/8	2.62e-03	(**eoc 2.98**)	3.09e-04	(**eoc 3.83**)
	h	$\|\boldsymbol{\nabla}\times(\boldsymbol{H}(T)-\boldsymbol{H}_{h,N})\|_\Omega$		$\|\boldsymbol{\nabla}\times(\boldsymbol{H}(T)-\boldsymbol{H}^\star_{h,N})\|_\Omega$	
	1/4	6.17e-01		4.18e-01	
$\mathcal{P}_1$	1/6	3.76e-01	(**eoc 1.22**)	1.80e-01	(**eoc 2.08**)
	1/8	2.70e-01	(**eoc 1.15**)	9.71e-02	(**eoc 2.15**)
	1/4	9.94e-02		2.19e-02	
$\mathcal{P}_2$	1/6	4.68e-02	(**eoc 1.86**)	6.00e-03	(**eoc 3.19**)
	1/8	2.71e-02	(**eoc 1.90**)	2.44e-03	(**eoc 3.13**)
	1/4	1.60e-02		2.46e-03	
$\mathcal{P}_3$	1/6	4.83e-03	(**eoc 2.95**)	5.39e-04	(**eoc 3.74**)
	1/8	2.06e-03	(**eoc 2.96**)	1.82e-04	(**eoc 3.77**)

where $\boldsymbol{p} := (1,0,0)^T$ is the polarization, $\boldsymbol{d} := (0,0,1)^T$ is the direction of propagation and $\omega := 6\pi c_0/L$ is the angular frequency. We impose the initial conditions (1c) with $\boldsymbol{E}_0 := \boldsymbol{E}^{\text{inc}}|_{t=0}$ and $\boldsymbol{H}_0 := \boldsymbol{H}^{\text{inc}}|_{t=0}$. Then, since the medium under consideration is homogeneous, no reflection and/or diffraction occur, and the analytical solution is simply $\boldsymbol{E} = \boldsymbol{E}^{\text{inc}}$ and $\boldsymbol{H} = \boldsymbol{H}^{\text{inc}}$. We select the simulation time $T := 10$ ns. As for the cubic cavity test, we consider structured meshes $\mathcal{T}_h$, that we obtain by first splitting Ω into $n \times n \times n$ cubes ($n := L/h$), and then splitting each cube into 6 tetrahedra. As explained above, the time step is selected using (6). Figures 3 and 4 show the behaviour of the error for the original and postprocessed discrete solutions with respect to time on a fixed mesh based on a $12 \times 12 \times 12$ Cartesian partition. The postprocessed solution is about 5 times more accurate than the original solution. Table 4 presents in more detail our results on a series of meshes and for different polynomial degrees. We see that in each cases, the curl of the postprocessed solution converges with the expected order, namely $k+1$.

4.3 Scattering of a plane wave by a dielectric sphere

We now consider a problem involving a dielectric sphere of radius 0.15 m with $\varepsilon = 2\varepsilon_0$ and $\mu = \mu_0$. The computational domain is bounded by a cube of side 1 m on which the Silver-Muller absorbing condition is applied and the simulation time is $T := 3$ ns. We make use of an unstructured tetrahedral mesh, which

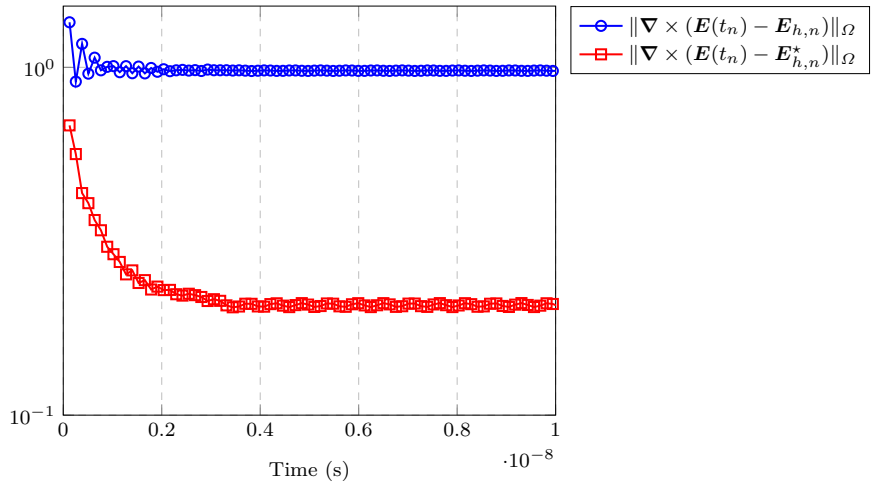

Fig. 3 Plane wave in free space: time evolution of the error on the electric field.

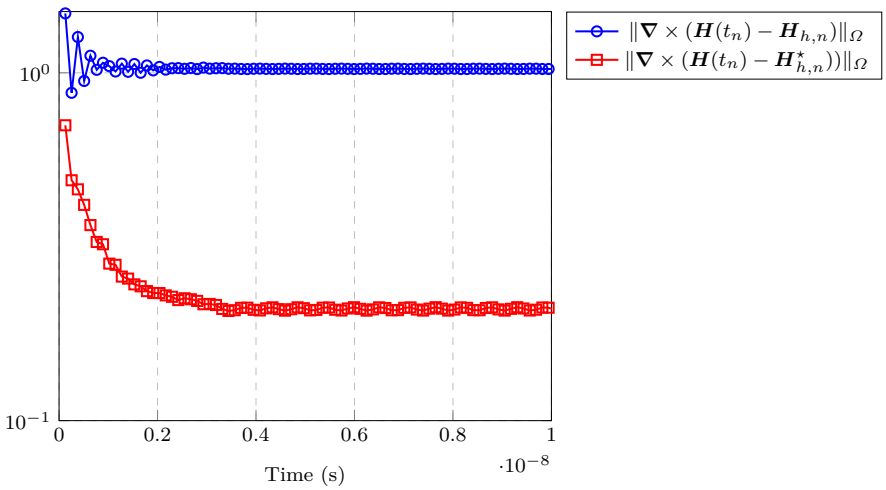

Fig. 4 Plane wave in free space: time evolution of the error on the magnetic field.

consists of 32,602 elements with 565 elements in the sphere and Δt is chosen via (6). The right-hand sides $\boldsymbol{J}$ and $\boldsymbol{G}$ are the same than in Example 4.2, and the initial conditions are taken to be zero. We select $\boldsymbol{\mathcal{P}}_2$ elements, and denote by $(\boldsymbol{E}_h, \boldsymbol{H}_h)$ and $(\boldsymbol{E}^\star_h, \boldsymbol{H}^\star_h)$ the original and postprocessed solutions. As the analytical solution to the problem is unavailable, we compute a reference solution $(\boldsymbol{E}_\mathrm{r}, \boldsymbol{H}_\mathrm{r})$ with $\boldsymbol{\mathcal{P}}_4$ elements on the same mesh and the time step is defined as $\Delta t_\mathrm{r} := \Delta t/3$. Δt_r is chosen as an integral division of Δt to facilitate comparisons. We chose to divide Δt by 3 since, following Table 2, it is the smallest integer for which CFL condition (6) holds true. We refer the reader to Figure 5 for a snapshot of the reference solution.

Table 4 Plane wave in free space: numerical convergence.

	h	$\|\nabla \times (\boldsymbol{E}(T) - \boldsymbol{E}_{h,N})\|_\Omega$		$\|\nabla \times (\boldsymbol{E}(T) - \boldsymbol{E}^\star_{h,N})\|_\Omega$	
$\mathcal{P}_1$	1/8	5.37e-00		6.02e-00	
	1/10	4.38e-00	(**eoc 0.92**)	3.99e-00	(**eoc 1.84**)
	1/12	3.75e-00	(**eoc 0.86**)	2.73e-00	(**eoc 2.08**)
$\mathcal{P}_2$	1/8	1.98e-00		7.92e-01	
	1/10	1.36e-00	(**eoc 1.70**)	3.72e-01	(**eoc 3.38**)
	1/12	9.77e-01	(**eoc 1.81**)	2.08e-01	(**eoc 3.18**)
$\mathcal{P}_3$	1/8	4.63e-01		1.01e-01	
	1/10	2.44e-01	(**eoc 2.88**)	4.25e-02	(**eoc 3.87**)
	1/12	1.43e-01	(**eoc 2.93**)	2.22e-02	(**eoc 3.56**)
	h	$\|\nabla \times (\boldsymbol{H}(T) - \boldsymbol{H}_{h,N})\|_\Omega$		$\|\nabla \times (\boldsymbol{H}(T) - \boldsymbol{H}^\star_{h,N})\|_\Omega$	
$\mathcal{P}_1$	1/8	5.89e-00		6.01e-00	
	1/10	4.68e-00	(**eoc 1.03**)	3.97e-00	(**eoc 1.85**)
	1/12	4.00e-00	(**eoc 0.86**)	2.75e-00	(**eoc 2.03**)
$\mathcal{P}_2$	1/8	2.16e-00		7.60e-01	
	1/10	1.45e-00	(**eoc 1.79**)	3.71e-01	(**eoc 3.21**)
	1/12	1.03e-00	(**eoc 1.89**)	2.11e-01	(**eoc 3.10**)
$\mathcal{P}_3$	1/8	4.87e-01		1.01e-01	
	1/10	2.54e-01	(**eoc 2.93**)	4.32e-02	(**eoc 3.79**)
	1/12	1.48e-01	(**eoc 2.96**)	2.29e-02	(**eoc 3.48**)

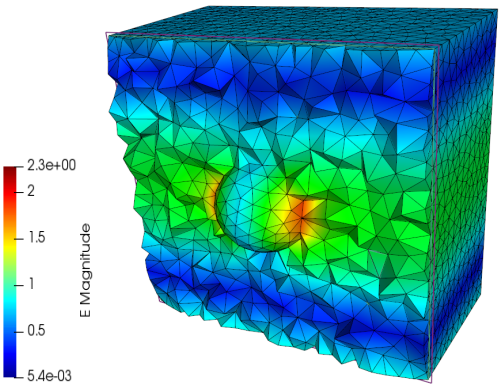

Fig. 5 Representation of $|\boldsymbol{E}_{\mathrm{r}}(T)|$ in the scattering example.

To assess the impact of the postprocessing, we consider a set of evaluation points $\boldsymbol{A}$, and we compute relative errors

$$\mathrm{err}(\boldsymbol{V})^2 = \frac{\sum_{n=1}^N ||\nabla \times (\boldsymbol{V}_{\mathrm{r}}(t_n, \boldsymbol{A}) - \boldsymbol{V}_{h,n}(\boldsymbol{A}))||^2}{\sum_{n=1}^N ||\nabla \times (\boldsymbol{V}_{\mathrm{r}})(t_n, \boldsymbol{A})||^2}$$

and

$$\mathrm{err}^\star(\boldsymbol{V})^2 = \frac{\sum_{n=1}^N ||\nabla \times (\boldsymbol{V}_{\mathrm{r}}(t_n, \boldsymbol{A}) - \boldsymbol{V}^\star_{h,n}(\boldsymbol{A}))||^2}{\sum_{n=1}^N ||\nabla \times (\boldsymbol{V}_{\mathrm{r}})(t_n, \boldsymbol{A})||^2}$$

Table 5 Scattering of a plane wave by a dielectric sphere: L^2 error between the reference solution and the solution with a $\boldsymbol{\mathcal{P}}_2$ interpolation with and without applying the postprocessing.

Point	Field	err	err*
$A_1(0, 0, 0.45)$	$\boldsymbol{E}$	**0.083**	**0.033**
	$\boldsymbol{H}$	**0.103**	**0.048**
$A_2(0.2, -0.3, 0.8)$	$\boldsymbol{E}$	**0.008**	**0.005**
	$\boldsymbol{H}$	**0.008**	**0.006**
$A_3(0.2, -0.3, 0.2)$	$\boldsymbol{E}$	**0.019**	**0.005**
	$\boldsymbol{H}$	**0.020**	**0.006**
$A_4(0.2, 0.3, 0.2)$	$\boldsymbol{E}$	**0.015**	**0.004**
	$\boldsymbol{H}$	**0.017**	**0.005**
$A_5(0.2, 0.3, 0.8)$	$\boldsymbol{E}$	**0.019**	**0.007**
	$\boldsymbol{H}$	**0.027**	**0.007**
$A_6(-0.2, -0.3, 0.8)$	$\boldsymbol{E}$	**0.015**	**0.008**
	$\boldsymbol{H}$	**0.014**	**0.008**
$A_7(-0.2, -0.3, 0.2)$	$\boldsymbol{E}$	**0.027**	**0.008**
	$\boldsymbol{H}$	**0.028**	**0.008**
$A_8(-0.2, 0.3, 0.2)$	$\boldsymbol{E}$	**0.021**	**0.007**
	$\boldsymbol{H}$	**0.024**	**0.007**
$A_9(-0.2, 0.3, 0.8)$	$\boldsymbol{E}$	**0.010**	**0.005**
	$\boldsymbol{H}$	**0.011**	**0.005**

with $\boldsymbol{V} := \boldsymbol{E}$ or $\boldsymbol{H}$. Table 5 shows that our postprocessing approach reduces the error by at least a factor of 2 for the 9 evaluation points that we have selected.

5 Conclusion

In this work we have presented a postprocessing approach for a discontinuous Galerkin discretization of the time-dependent Maxwell's equations in 3D. This postprocessing technique is inexpensive, and can be computed independently in each element of the mesh, and at every time step of interest. It is thus well adapted to parallel computer architectures. Moreover, it is particularly suited to applications requiring a higher accuracy in localized regions, either in time or space. We have presented numerical examples, both with analytical solution and in complicated geometries, that indicate that our postprocessing approach improves the convergence rate of the discrete solution in the $H(\text{curl})$-norm by one order. Overall, this contribution is to be employed as an efficient way of reducing the $H(\text{curl})$-norm error of discontinuous Galerkin discretizations.

References

1. Abgrall, R., Shu, C.: Handbook of numerical methods for hyperbolic problems, vol. 17. Elsevier/North-Holland, Amsterdam (2016)
2. Andreev, A.B., Lazarov, R.D.: Superconvergence of the gradient for quadratic triangular finite elements. Numer. Methods for PDEs **4**, 15–32 (1988)
3. Arnold, D., Brezzi, F., Cockburn, B., Marini, L.: Unified analysis of discontinuous Galerkin, methods for elliptic problems. SIAM J. Numer. Anal. **39**(5), 1749–1779 (2002)
4. Assous, F., Ciarlet, P., Labrunie, S.: Mathematical foundations of computational electromagnetism. Springer (2018)
5. Babuska, I., Strouboulis, T., Upadhyay, C.S., Gangaraj, S.K.: Validation of recipes for the recovery of stresses and derivatives by a computer-based approach. Math. Comput. Mode. **20**, 45 (1994)
6. Babuska, I., Strouboulis, T., Upadhyay, C.S., Gangaraj, S.K.: Computer-based proof of the existence of superconvergence points in the finite element method; superconvergence of the derivatives in finite element solutions of laplaces, poissons and the elasticity equations. Numer. Methods for PDEs **12**, 347–392 (1996)
7. Bondeson, A., Rylander, T., Ingelström, P.: Computational Eelectromagnetics. Springer-Verlag (2013)
8. Carpenter, M., Kennedy, C.: Fourth-order 2N-storage Runge-Kutta schemes. NASA **109112** (1994)
9. Castillo, P., Cockbrn, B., Perugia, I., Schötzau, D.: An a priori error analysis of the local discontinuous Galerkin method for elliptic problems. SIAM J. Numer. Anal. **38**(5), 1676–1706 (2000)
10. Ciarlet, P.: The finite element method for elliptic problems. SIAM (2002)
11. Fezoui, L., Lanteri, S., Lohrengel, S., Piperno, S.: Convergence and stability of a discontinuous Galerkin time-domain method for the 3D heterogeneous Maxwell equations on unstructured meshes. ESAIM Math. Model. Numer. Anal. **39**(6), 1149–1176 (2005)
12. Gaponenko, S.: Introduction to nanophotonics. Cambridge University Press (2010)
13. Goodsell, G., Whiteman, J.R.: A unified treatment of superconvergent recovered gradient functions for piecewise linear finite element approximations. Internat. J. Numer. Methods. Eng. **27**, 469–481 (1989)
14. Griffiths, D.: Introduction to Electrodynamics. Prentice Hall (1999)
15. Hagstrom, T., Lau, S.: Radiation boundary conditions for Maxwell's equations: A review of accurate time-domain formulations. J. Comput. Math. **25**(3), 305–336 (2007)
16. Hesthaven, J., Warburton, T.: Nodal high-order methods on unstructured grids. I. Time-domain solution of Maxwll's equations. J. Comput. Phys. **181**(1), 186–221 (2002)
17. Russer, P.: Electromagnetics, microwave circuit and antenna design for communications engineering. Artech house (2006)
18. Stanglmeier, M., Nguyen, N., Peraire, J., Cockburn, B.: An explicit hybridizable discontinuous Galerkin method for the acoustic wave equation. Comput. Meth. Appl. Mech. Engrg. **300**, 748–769 (2016)
19. Viquerat, J.: Simulation of electromagnetic waves propagation in nano-optics with a high-order discontinuous Galerkin time-domain method. Ph.D. thesis, Université Nice Sophia-Antipolis (2015)
20. Yee, K.: Numerical solution of initial boundary value problems involving Maxwell's equations in isotropic media. IEEE Trans. Antennas Propag. **16**, 302–307 (1966)

Bibliography

[1] J. C. Maxwell, A dynamical theory of the electromagnetic field, Philosophical Transactions of the Royal Society of London 155 (1865) 459–512.

[2] K. Yee, Numerical solution of initial boundary value problems involving Maxwell's equations in isotropic media, IEEE Transactions on Antennas and Propagation 14 (1966) 302 – 307.

[3] R. Holland, L. Simpson, Finite-Difference Analysis of EMP Coupling to Thin Struts and Wires, IEEE Transactions on Electromagnetic Compatibility EMC-23 (2) (1981) 88–97. doi:10.1109/TEMC.1981.303899.

[4] A. C. Cangellaris, C. C. Lin, K. K. Mei, Point-Matched Time Domain Finite Element Methods for Electromagnetic Radiation and Scattering, IEEE Transactions on Antennas and Propagation 35 (10) (1987) 1160–1173. doi:10.1109/TAP.1987.1143981.

[5] C. Fumeaux, D. Baumann, P. Bonnet, R. Vahldieck, Developments of finite-volume techniques for electromagnetic modeling in unstructured meshes, in: 17th Int. Zurich Symp. Electromagn. Compat. 2006, Vol. 2006, 2006, pp. 5–8. doi:10.1109/emczur.2006.214855.

[6] A. Taflove, S. Hagness, Computational electrodynamics: the finite-difference time-domain method - 3rd ed., Artech House Publishers, 2005.

[7] S. Pernet, X. Ferriéres, G. Cohen, High spatial order finite element method to solve Maxwell's equations in time-domain, IEEE Trans. Ant. and Propag. 53 (9) (2006) 2889–2899.

[8] J. Hesthaven, T. Warburton, Nodal high-order methods on unstructured grids. I. Time-domain solution of Maxwell's equations, J. Comput. Phys. 181 (1) (2002) 186–221.

[9] V. Kabakian, V. Shankar, W. Hall, Unstructured grid-based discontinuous Galerkin method for broadband electromagnetic simulations, J. Sci. Comput. 20 (3) (2004) 405–431.

[10] M. Chen, B. Cockburn, F. Reitich, High-order RKDG methods for computational electromagnetics, J. Sci. Comput. 22-23 (2005) 205–226.

[11] B. Cockburn, F. Li, C.-W. Shu, Locally divergence-free discontinuous Galerkin methods for the Maxwell equations, J. Comp. Phys. 194 (2) (2004) 588–610.

[12] L. Fezoui, S. Lanteri, S. Lohrengel, S. Piperno, Convergence and stability of a discontinuous Galerkin time-domain method for the 3D heterogeneous Maxwell equations on unstructured meshes, ESAIM: Math. Model. Numer. Anal. 39 (6) (2005) 1149–1176.

[13] G. Cohen, X. Ferriéres, S. Pernet, A spatial high order hexahedral discontinuous Galerkin method to solve Maxwell's equations in time-domain, J. Comput. Phys. 217 (2) (2006) 340–363.

[14] S. Dosopoulos, J. Lee, Interconnect and lumped elements modeling in interior penalty discontinuous Galerkin time-domain methods, J. Comput. Phys. 229 (2) (2010) 8521–8536.

[15] S. Dosopoulos, J. Lee, Interior penalty discontinuous Galerkin finite element method for the time-dependent first order Maxwell's equations, IEEE Trans. Ant. and Propag. 58 (12) (2010) 4085–4090.

[16] J. Alvarez, L. Angulo, A. Bretones, S. Garcia, A spurious-free discontinuous Galerkin time-domain method for the accurate modeling of microwave filters, IEEE Trans. Microw. Theory Tech. 60 (8) (2012) 2359–2369.

[17] J. Alvarez, L. Angulo, A. Bretones, S. Garcia, 3-D discontinuous Galerkin time-domain method for anisotropic materials, IEEE Ant. Wir. Prop. Lett. 11 (2012) 1182–1185.

[18] B. Z. S. Dosopoulos, J. F. Lee, Non-conformal and parallel discontinuous Galerkin time domain method for Maxwell's equations: EM analysis of IC packages, J. Comput. Phys. 238 (1) (2013) 48–70.

[19] P. Li, L. Jiang, H. Bagci, Cosimulation of electromagnetics-circuit systems exploiting DGTD and MNA, IEEE Trans. Compon. Pack. Manuf. Tech. 4 (6) (2014) 1052–1061.

[20] R. Diehl, K. Busch, J. Niegemann, Comparison of low-storage Runge-Kutta schemes for discontinuous Galerkin time-domain simulations of Maxwell's equations, J. Comp. Theor. Nanosc. 7 (2010) 1572.

[21] S. G. A.Hille, R. Kullock, L. M. Eng, Improving nano-optical simulations through curved elements implemented within the discontinuous Galerkin method computational, J. Comp. Theor. Nanosc. 7 (2010) 1581–1586.

[22] M. König, K. Busch, J. Niegemann, The Discontinuous Galerkin Time-Domain method for Maxwell's equations with anisotropic materials, Photonics and Nanostructures - Fundamentals and Applications 8 (4) (2010) 303–309.

[23] K. Busch, M. König, J. Niegemann, Discontinuous Galerkin methods in nanophotonics, Laser and Photonics Reviews 5 (2011) 1–37.

[24] H. Songoro, M. Vogel, Z. Cendes, Keeping time with Maxwell's equations, IEEE Microw. 11 (2) (2010) 42–49.

[25] J. Diaz, M. Grote, Energy conserving explicit local time-stepping for second-order wave equations, SIAM J. Sci. Comput. 31 (2009) 1985–2014.

[26] M. Grote, M. Mehlin, T. Mitkova, Runge-Kutta-based explicit local time-stepping methods for wave propagation, SIAM J. Sci. Comput. 37 (A774–A775) (2015) 2. doi:10.1137/140958293.

[27] S. Piperno, Symplectic local time stepping in non-dissipative DGTD methods applied to wave propagation problem, ESAIM: Math. Model. Num. Anal. 40 (5) (2006) 815–841.

[28] M. Grote, T. Mitkova, Explicit local time-stepping methods for Maxwel's equations, J. Comp. Appl. Math. 234 (3283–3302) (2010) 12.

[29] A. Taube, M. Dumbser, C. Munz, R. Schneider, A high-order discontinuous Galerkin method with time-accurate local time stepping for the Maxwell equations, Int. J. Numer. Model. 22 (2009) 77–103.

[30] L. Moya, Temporal convergence of a locally implicit discontinuous Galerkin method for Maxwell's equations, ESAIM Math. Model. Numer. Anal. (M2AN) 46 (2012) 1225–1246. doi:10.1051/m2an/2012002.

[31] L. Moya, S. Descombes, S. Lanteri, Locally implicit time integration strategies in a discontinuous Galerkin method for Maxwell's equations, J. Sci. Comp. 56 (1) (2013) 190–218. doi:10.1007/s10915-012-9669-5.

[32] B. Cockburn, J. Gopalakrishnan, R. Lazarov, Unified hybridization of discontinuous Galerkin, mixed, and continuous Galerkin methods for second order elliptic problems, SIAM J. Numer. Anal. 47 (2) (2009) 1319–1365.

[33] N. Nguyen, J. Peraire, Hybridizable discontinuous Galerkin methods for partial differential equations in continuum mechanics, J. Comput. Phys. 231 (18) (2012) 5955–5988.

[34] N. Nguyen, J. Peraire, B. Cockburn, Hybridizable discontinuous Galerkin methods for the time-harmonic Maxwell's equations, J. Comput. Phys. 230 (19) (2011) 7151–7175.

[35] L. Li, S. Lanteri, R. Perrussel, Numerical investigation of a high order hybridizable discontinuous Galerkin method for 2d time-harmonic Maxwell's equations, COMPEL 2 (3) (2013) 1112–1138.

[36] L. Li, S. Lanteri, R. Perrussel, A hybridizable discontinuous Galerkin method combined to a Schwarz algorithm for the solution of 3d time-harmonic Maxwell's equations, J. Comput. Phys. 256 (2014) 563–581.

[37] G. Nehmetallah, S. Lanteri, S. Descombes, A. Christophe, An explicit hybridizable discontinuous galerkin method for the 3d time-domain maxwell equations, in: S. J. Sherwin, D. Moxey, J. Peiró, P. E. Vincent, C. Schwab (Eds.), Spectral and High Order Methods for Partial Differential Equations ICOSAHOM 2018, Springer International Publishing, Cham, 2020, pp. 513–523.

[38] M. Stanglmeier, N. Nguyen, J. Peraire, B. Cockburn, An explicit hybridizable discontinuous Galerkin method for the acoustic wave equation, Comput. Meth. App. Mech. Engrg. 300 (2016) 748–769.

[39] Abgrall, Rémi, Shu, Chi-Wang (Eds.), Handbook of numerical methods for hyperbolic problems, Vol. 17, Elsevier/North-Holland, Amsterdam, 2016.

[40] J. D. Joannopoulos, S. G. Johnson, R. D. Meade (Eds.), Photonics crystals: Molding the flow of light, Princenton University Press, 2008.

[41] D. ARNOLD, F. BREZZI, B. COCKUURN, L. D. MARINI, Unified analysis of discontinuous galerkin methods for elliptic problems, SIAM J. Numer. Anal. 39 (2001) 1749–1779.

[42] L. Li, S. Lanteri, R. Perrussel, A hybridizable discontinuous galerkin method combined to a schwarz algorithm for the solution of 3d time-harmonic maxwell's equation, Journal of Computational Physics 256 (2014) 563–581. doi:10.1016/j.jcp.2013.09.003.

[43] A. Christophe, S. Descombes, S. Lanteri, An implicit hybridized discontinuous Galerkin method for the 3d time-domain Maxwell equations, Appl. Math. Comput. 319 (2017) 395–408. doi:10.1016/j.amc.2017.04.023.

[44] E. Hairer, C. Lubich, M. Roche, The numerical solution of differential algebraic systems by Runge-Kutta methods, Vol. 1409 of Lecture Notes in Mathematics, Springer-Verlag, 1989.

[45] M. Kronbichler, S. Schoeder, C. Muller, W. Wall, Comparison of implicit and explicit hybridizable discontinuous Galerkin methods for the acoustic wave equation, Int. J. Numn. Mth. Engrg. 106 (9) (2015) 712–739. doi:10.1002/nme.5137.

[46] M. Carpenter, C. Kennedy, Fourth-order 2N-storage Runge-Kutta schemes, Tech. Rep. 109112, NASA (1994).

[47] A. Ern, J.-L. Guermond (Eds.), Theory and Practice of Finite Elements, Vol. 159 of Applied Mathematical Science, Springer, 2004.

[48] E. Hairer, G. Wanner, Runge–Kutta Methods, Explicit, Implicit, Springer, 2015, Ch. Scientific Computing, pp. 1282–1285. doi:10.1007/978-3-540-70529-1_144.

[49] J. Williamson, Low-storage Runge-Kutta schemes, J. Comput. Phys. 35 (1980) 48–56.

[50] A. Sturm, Locally implicit time integration for linear Maxwell equations, Ph.D. thesis, Karlsruhe Institute Of Technology (KIT) (2017).

[51] S. Kang, F. X. Giraldo, T. Bui-Thanh, IMEX HDG-DG: A coupled implicit hybridized discontinuous Galerkin and explicit discontinuous Galerkin approach for shallow water systems, Journal of Computational Physics 401 (2020) 109010. doi:10.1016/j.jcp.2019.109010.

[52] S. Boscarino, F. Filbet, G. Russo, High order semi-implicit schemes for time dependent partial differential equations, J. Sci. Comp. 68 (2016) 975–1001. doi:10.1007/s10915-016-0168-y.

[53] M. N'Diaye, On the study and developpement of high-order time integration schemes for ODEs applied to acoustic and electromagnetic wave propagation problems, Ph.D. thesis, Université de Pau et des Pays de l'Adour (2017).
URL https://hal.inria.fr/tel-01808393

[54] T. Chaumont-Frelet, S. Nicaise, High-frequency behaviour of corner singularities in Helmholtz problems, ESAIM: Math. Model. Numer. Anal. 52 (5) (2018) 1803–1845.

[55] C. H. da Silva Santos, M. S. Gonçalves, H. E. Hernández-Figueroa, Designing novel photonic devices by bio-inspired c omputing, IEEE Photonics Technology Letters 22 (15) (2010) 1177–1179.

[56] J. Viquerat, Simulation of electromagnetic waves propagation in nano-optics with a high-order discontinuous Galerkin time-domain method, Theses, Université Nice Sophia Antipolis (Dec. 2015).
URL https://hal.archives-ouvertes.fr/tel-01272010